EX LIBRIS
UNIVERSITATIS
ALBERTENSIS

The Bruce Peel
Special Collections
Library

Digitized by the Internet Archive
in 2025 with funding from
University of Alberta Library

https://archive.org/details/0162012506414

University of Alberta
Library Release Form

Name of Author: Christopher John Anthony Daley

Title of Thesis: Design, Synthesis, and Characterization of New Chiral Ligands and Mechanistic Investigations Into Catalytic Enantioselective Hydrogenation Reactions.

Degree: Doctor of Philosophy

Year this Degree Granted: 2000

Permission is hereby granted to the University of Alberta Library to reproduce single copies of this thesis and to lend or sell such copies for private, scholarly, or scientific research purposes only.

The author reserves all other publication and other rights in association with the copyright in the thesis, and except as herein before provided, neither the thesis nor any substantial portion thereof may be printed or otherwise reproduced in any material form whatever without the author's prior written permission.

University of Alberta

Design, Synthesis, and Characterization of New Chiral Ligands and Mechanistic Investigations Into Catalytic Enantioselective Hydrogenation Reactions.

by

Christopher John Anthony Daley ©

A thesis submitted to the Faculty of Graduate Studies and Research in partial fulfillment of the requirements for the degree of Doctor of Philosophy.

Department of Chemistry

Edmonton, Alberta
Spring, 2000

University of Alberta

Faculty of Graduate Studies and Research

The undersigned certify that they have read, and recommend to the Faculty of Graduate Studies and Research for acceptance, a thesis entitled **Design, Synthesis, and Characterization of New Chiral Ligands and Mechanistic Investigations Into Catalytic Enantioselective Hydrogenation Reactions** submitted by Christopher John Anthony Daley in partial fulfillment of the requirements for the degree of Doctor of Philosophy.

Mom, Dad, and Peggy

Abstract

The ligands (*R*)- and (*S*)-1,2-bis(diphenylphosphino)-2-((diphenylphosphino)-methyl)-1-phenyl propane ((*R*)- and (*S*)-heliphos) were synthesized. The key step was an acid catalyzed diastereoselective Michael addition of diphenylphosphine to di-(1*R*,2*S*,5*R*)-menthyl benzylidenemalonate (**1**) that yields diastereopure products on recrystallization. Tridentate coordination of heliphos was accomplished on reaction with $[Rh(NBD)_2](ClO_4)$ yielding [Rh(heliphos)(NBD)](ClO_4). The crystal structure of [Rh((*R*)-heliphos)(NBD)](ClO_4) (**2**) was determined by X-ray diffraction. Solid state (X-ray) and solution (NMR) studies showed (*R*)-heliphos adopted the predicted locked Λ-helical conformation. The sense of helicity was controlled by the absolute stereochemistry of the stereogenic carbon atom of the ligand. Reaction of heliphos with a number of ruthenium(II) complexes resulted mainly in bidentate coordination. Several synthetic schemes towards the derivatized heliphos ligand Me-heliphos (**3**) were analyzed, as sterics in **3** are proposed to favor tridentate coordination. The synthesis of a key alcohol intermediate $CH_3C(CH(OH)CH_3)(CH_2CO_2CH_3)_2$ (**4**) has essentially finalized the synthesis.

[Ru((*R*)-BINAP)(1-3;5,6-η-C_8H_{11})(MeCN)](BF_4) (**5**) was examined as catalyst precursor in enantioselective hydrogenation reactions. The hydrogenations of α,β-unsaturated acids and esters were performed in model protic (methanol) and aprotic (acetone) solutions to determine the effect of solvent. It was determined that the acids do not undergo reaction in aprotic solvent without added base (e.g. triethylamine). Deuterium labeling studies on the hydrogenations of tiglic acid (**5**), angelic acid (**6**), and

dimethyl itaconate (**7**) further corroborate the mechanisms proposed by Halpern (α,β-unsaturated acids) and Brown (α,β-unsaturated esters).

Studies of the enantioselective hydrogenation of ketones led to the examination of dialkyl 3,3-dimethyloxaloacetate substrates (alkyl = methyl (**10**), *iso*-propyl (**11**), *tert*-butyl (**12**)). The ketones were hydrogenated, under 50 atm of H_2 and at 50 °C, in methanol solution yielding 59% ee (*R*), 69% ee (*R*), 82 % ee (*R*), respectively. Stoichiometric reaction of catalyst with ketones resulted in formation of ruthenium-alkoxide complexes, formed via ketone-hydride insertion, that were isolated and unambiguously characterized (solution NMR) as [Ru((*R*)-BINAP)(alkoxide)(MeCN)](BF_4) (**13**) where alkoxide is from **10**, **11**, or **12**. Results obtained from the stoichiometric hydrogenolysis of **13** indicate that formation of **13** is rapid and reversible prior to the irreversible hydrogenolysis of the ruthenium-oxygen bond. The stereoselectivities of the hydrogenolysis of **13** equals the overall stereoselectivity of the catalytic reaction.

Acknowledgements

I would like to express my gratitude to my supervisor Professor Steven H. Bergens for his advice and teachings throughout my Ph.D. studies, and for providing me with challenging and exciting research projects.

Special thanks to the members of the Bergens group, past and present, in particular Dr. Jason A. Wiles, Christopher E. Lee, and Yiming Yao. Jason has been a source of inspiration and a great friend throughout my Ph.D. studies. Chris has been a great friend, coworker, and camping advisor. I thank Yiming for his friendship as well as his input and chemical knowledge that was helpful in our design and sythesis of heliphos.

I would like to thank all the technical staff in the NMR, MS, Spectral Services, and Elemental Analysis Laboratories, as well as the Glass Shop. I would specifically like to thank Dr. Tom Nakashima, Glen Bigam, Gerdy Aarts, Dr. Bob McDonald, Gerry Streefkerk, Dr. Angie Morales, and Jackie Jorgensen.

During my Ph.D. studies I have participated on a number of intramural sports teams. I would like to thank all the members of those teams for the good times I have had. A special nod to Steve Trepanier for helping organize many of the teams.

Steve Decker, the first person I met here and a great friend. I would like to thank him for the fun times coaching the kids' hockey team and for recruiting a young woman, who ended up becoming my wife, from the University of Waterloo to come to the University of Alberta for a summer job!

Finally, I would like to especially thank my parents, my sisters, and my wife for their unending encouragement over the last five years. It has meant very much to me and I truly appreciate all the support.

Table of Contents

Chapter 1

Introduction 1

Olfactory responses to chiral molecules 1

Action of therapeutic drugs 2

Problems of racemates in drug chemistry 3

Methods of preparing enantiopure molecules 5

Resolution of racemates 5

Separation of enantiomers via crystallization 5

Separation of diastereomers via crystallization 5

Separation of diastereomers via chiral chromatography 6

Kinetically controlled transformations 7

Kinetic resolutions 8

Asymmetric synthesis 9

Stoichiometric asymmetric synthesis 10

Definition and properties of catalysis 11

Enzymatic processes 11

Enantioselective catalysis 12

Objectives of thesis 14

References and Notes 16

Chapter 2

Introduction 21

Features of successful chiral ligands 21

Conformational rigidity 22

Bidentate coordination and C_2 symmetry 22

Chiral C_3-symmetric tris(phosphine) ligands 23

First developments of rigid chiral C_3-symmetric ligands 24

Success in enantioselective catalysis 27

Essential feature of all chiral ligands 28

Conformational control in tripodal C_3-symmetric ligands 28

Heliphos ligand design 29
Reasons for the selection of phosphines as ligand 29
Objective 32
Results and Discussion 32
Synthesis of (*R*)- and (*S*)-heliphos ligands 32
Acid-catalyzed Michael addition reaction studies 32
Physical separation of diastereomers via crystallization 35
Intramolecular phosphine attack 38
Oxidation of phosphine to block intramolecular attack process 38
Reduction of bis(phosphine) phosphine oxide to heliphos 39
Synthesis of [Rh(triphos)(NBD)](ClO_4) 41
Synthesis of [Rh((*R*)-heliphos)(NBD)](ClO_4) 41
[Rh((*R*)-heliphos)(NBD)](ClO_4) solid-state structure analysis 41
[Rh((*R*)-heliphos)(NBD)](ClO_4) solution structure analysis 45
Conclusions 47
Experimental 48
Materials and methods 48
Syntheses of compounds 49
References and Notes 68

Chapter 3

Introduction 73
Arm-dissociation of tripodal ligands in catalysis 73
Group eight catalyst complexes of tripodal ligands 75
Results and Discussion 79
[Rh((*R*)-heliphos)(NBD)](ClO_4) as catalyst 79
Synthesis of η^3-tris(phosphine)-ruthenium(II) complexes 80
Reactions with [Ru(COD)(η^3-allyl)($MeCN)_2$](BF_4) 80
Reactions with [Ru(COD)(η^3-allyl)($CD_2Cl_2)_2$](BF_4) 81
Reactions with $RuCl_2(DMSO)_4$ 82
Molecular model examination of coordinated heliphos ligand 83

Synthesis of Me-heliphos 83
Direct methylation of $C_6H_5CH(PPh_2)CH(CO_2Menth)_2$ 83
Acylation of dialkyl malonate route to Me-heliphos 86
Triol synthetic route to Me-heliphos 88
Catalytic hydrogenation with Ru((*R*)-BINAP)$(NC_5H_5)_2(Cl)_2$ 89
Mesylation of secondary alcohol 90
Conclusions 90
Experimental 91
Materials and methods 91
Reactions and syntheses 91
References and Notes 99

Chapter 4

Introduction 102
[Ru((*R*)-BINAP)(1-3;5,6-η-C_8H_{11})(MeCN)](BF_4) catalyst system 103
Synthesis of [Ru((*R*)-BINAP)(1-3;5,6-η-C_8H_{11})(MeCN)](BF_4) 103
Features of [Ru((*R*)-BINAP)(1-3;5,6-η-C_8H_{11})(MeCN)](BF_4) 103
Objective 104
Results and Discussion 105
Nature of [Ru((*R*)-BINAP)(H)$(MeCN)_n(Sol)_{3-n}$](BF_4) (**2**, Sol = acetone, tetrahydrofuran, or methanol; n = 0-3) 105
Hydrogenation using **2** as catalyst 107
α,β-Unsaturated carboxylic acid or ester substrates 107
Hydrogenation in methanol solution as protic solvent 107
Hydrogenation in acetone solution as aprotic solvent 113
Addition of 1 equivalent of NEt_3 per acid unit 113
Comparison of **2** to reported ruthenium-BINAP catalysts 115
Possible structure of a common catalytic intermediate 117
Role of NEt_3 in catalytic hydrogenations 117
Structure of isolated ruthenium-BINAP-(tiglic acid) complex 118
Allylic alcohol substrate (geraniol) 119

H_2 pressure effect on isomerization versus hydrogenation 119
Ketone substrates 121
Structures of successfully hydrogenated olefin substrates 122
Dimethyl oxaloacetate as ketone substrate 122
Conclusions 123
Experimental 123
Materials and methods 123
Reactions and syntheses 124
References and Notes 136

Chapter 5

Introduction 143
Approaches to catalyst design 143
Most complete ruthenium-bis(phosphine) mechanistic studies reported 144
Objectives 144
Results and Discussion 144
Ruthenium-BINAP catalyzed enantioselective hydrogenation of α,β-unsaturated carboxylic acids and esters 144
Halpern mechanism for hydrogenation of tiglic acid 144
Brown mechanism that counters Halpern's proposed cycle 148
Tiglic acid deuterium labeling studies with [Ru((R)-BINAP)-(1-3;5,6-η-C_8H_{11})(MeCN)](BF_4) (**10**) as catalyst precursor in methanol solution 148
Angelic acid deuterium labeling studies with **10** as catalyst precursor in methanol solution 150
Modified Halpern mechanism proposed for hydrogenation of α,β-unsaturated carboxylic acids 151
Investigation of α,β-unsaturated carboxylate ester hydrogenation using **10** as catalyst precursor corroborating Brown mechanism 155

Mechanistic studies of catalytic hydrogenation of methyl α-acetamidocinnamate using **10** as catalyst precursor 155
Bergens proposed mechanism for catalytic hydrogenation of of methyl α-acetamidocinnamate 156
Deuterium labeling studies on hydrogenation of dimethyl itaconate in methanol solution using **10** as catalyst precursor...... 157
NMR investigation of catalytic hydrogenation 158
Isolation and identification of possible catalytic intermediate...... 158
Conclusions 159
Experimental... 160
Materials and methods... 160
Reactions and syntheses 161
References and Notes.. 167

Chapter 6

Introduction 170
Results and Discussion.. 171
Review of [Ru((*R*)-BINAP)(1-3;5,6-η-C_8H_{11})(MeCN)](BF_4) catalyzed enantioselective hydrogenation reactions 171
Increased enantioselectivity with dimethyl oxaloacetate as ketone substrate 172
Stoichiometric reaction of active catalyst **6** with dimethyl oxaloacetate 172
Examination of non-enolizable ketone 174
Structural characterization of Ru(BINAP)-alkoxide complexes 175
Assignment of substrate signals 175
Absolute configuration about the alkoxy carbon center 177
Stereochemistry about ruthenium metal center 178
Unambiguous characterization of the major Ru(BINAP)-alkoxide diastereomer 180
Assignment of substrate signals 181

Assignment of BINAP signals 182
Substrate-BINAP and BINAP-BINAP correlations (ROESY).......... 184
Low-temperature investigations for pre-insertion complexes 188
Isolated complexes as catalytic intermediates 190
Conclusions 193
Experimental.. 194
Materials and methods.. 194
Reactions and syntheses 194
References and Notes...207

Chapter 7

Conclusions 213
References and Notes...222

List of Tables

Chapter 1

No Tables

Chapter 2

Table 2.1: Catalyst tests for Michael addition of diphenylphosphine to **12**. 34

Table 2.2: Solvent and chiral catalyst screening of Michael addition. 35

Table 2.3: Crystallographic, experimental, and refinement details for 54
(*S*)-**13**.

Table 2.4: Selected interatomic distances of (*S*)-**13**. 55

Table 2.5: Selected interatomic distances of (*S*)-**13**. 56

Table 2.6: Crystallographic, Experimental, and Refinement Details for 60
(*R*)-**17**.

Table 2.7: Selected interatomic distances of (*R*)-**17**. 61

Table 2.8: Selected interatomic distances of (*R*)-**17**. 62

Table 2.9: Crystallographic, Experimental, and Refinement Details for 67
[((*R*)-heliphos)Rh(NBD)](ClO_4)•MeOH ((*R*)-**20**).

Chapter 3

No Tables

Chapter 4

Table 4.1: Hydrogenation of substrates containing an α,β-unsaturated 112
carboxylic acid or ester functionality in methanol solution.

Table 4.2: Hydrogenation of substrates containing an α,β-unsaturated 114
carboxylic acid or ester functionality in acetone solution.

Table 4.3: Comparison of Ru((*R*)-BINAP) catalyst systems. 116

Table 4.4: Hydrogenation of geraniol. 120

Table 4.5: Hydrogenation of simple and functionalized ketones. 122

Chapter 5

Table 5.1: Pattern of deuterium incorporation in tiglic acid hydrogenation catalyzed by **1a** and **10**. 149

Table 5.2: Pattern of deuterium incorporation in angelic acid hydrogenation catalyzed by **10**. 151

Table 5.3: Pattern of deuterium incorporation in hydrogenation of **21**. 158

Chapter 6

Table 6.1: Enantioselective hydrogenation of ketones 7, **9**, and **10**. 180

Table 6.2: Assignment of substrate signals of (*R*)-**11a**. 182

Table 6.3: Hydrogenation of ketones 7, **9**, **10** with ruthenium-alkoxide complexes as catalyst. 191

Table 6.4: Stoichiometric hydrogenation of deuterium labeled ruthenium-alkoxide complexes. 192

Chapter 7

No Tables

List of Figures

Chapter 1

Figure 1.1: Carvone and Aspartame structures. 2

Figure 1.2: Some commercially available drugs. 3

Figure 1.3: Enantiomers of Thalidomide. 4

Figure 1.4: A possible energy-reaction coordinate diagram for kinetically controlled one step reaction forming enantiomeric products from a prochiral substrate. 8

Chapter 2

Figure 2.1: Independent coordination sites in metal complexes. 23

Figure 2.2: Independent coordination sites in C_2- and C_3-symmetric metal complexes. 24

Figure 2.3: Representation of the crystal structure of [Co(L)((*S*)-tan)]-(ClO_4) (L = NCS) reported by Utsuno, excluding the anion. 25

Figure 2.4: Reported chiral tripodal C_3-symmetric ligands. 26

Figure 2.5: Schematic representations of Λ- and Δ-coordinated triphos and of (*R*)-heliphos showing the overlap of phenyl rings in the Δ-(*R*)-conformer. 30

Figure 2.6: Crystal structure of (*S*)-**13**. 36

Figure 2.7: Crystal Structure of (*R*)-**17**. 40

Figure 2.8: ^{31}P NMR of [((*R*)-heliphos)Rh(NBD)](ClO_4) in CD_2Cl_2. 42

Figure 2.9: X-ray crystal structure of [((*R*)-heliphos)Rh(NBD)](ClO_4). 43

Figure 2.10: X-ray crystal structure of [((*R*)-heliphos)Rh(NBD)](ClO_4) showing propeller-like asymmetric array of pendant phenyl rings. 44

Figure 2.11: ^1H NMR of [((*R*)-heliphos)Rh(NBD)](ClO_4) in CD_2Cl_2.. 46

Figure 2.12: Depiction of (*R*)-**20** showing coupling constants. 47

Chapter 3

Figure 3.1: Representation of tridentate and bidentate (arm-dissociated) complexes of triphos, (*R*)-heliphos, and (*R*)-Me-heliphos ruthenium complexes based on molecular models. 84
Figure 3.2: Non-aromatic system for synthesis of trichloride/trimesylate........... 88

Chapter 4

Figure 4.1: *α,β*-Unsaturated acids and esters hydrogenated using **1** as catalyst precursor. 108
Figure 4.2: Allylic alcohol and ketones hydrogenated using **1** as catalyst precursor. 109
Figure 4.3: Net addition of hydrogen to substrates **3a**, **3b**, **4a**, and **4b** occurs through same face in the enantioselective hydrogenations catalyzed by **2**. 110
Figure 4.4: Model structure for a possible common catalytic intermediate........ 117

Chapter 5

Figure 5.1: Assignment of protons for 2-methylbutyric acid............................ 146
Figure 5.2: Structure of angelic acid (**12**). 150
Figure 5.3: Structure of methyl *α*-acetamidocinnamate (**18**)............................ 155
Figure 5.4: Structure of likely catalytic intermediate (**19**) in ruthenium-BINAP catalyzed enantioselective hydrogenation of MAC (**18**). 155
Figure 5.5: NMR characterized major species formed in stoichiometric reaction of **21** with **10**. 159

Chapter 6

Figure 6.1: Substrates hydrogenated in high ee using **1** as catalyst precursor. 172
Figure 6.2: Possible ruthenium complexes formed via stoichiometric Reaction of **6** with **2**. 173

Figure 6.3: Possible structures of major diastereomer (*R*)-**8a** 179

Figure 6.4: Depiction of Ru(BINAP)(MeCN) fragment 183

Figure 6.5: Assignment of quadrant of space about ruthenium center 185

Figure 6.6: Important ROE contacts observed between substrate and BINAP ligand. 186

Figure 6.7: The key ROE contacts that conclusively identified the structure of (*R*)-**11a**. 187

Figure 6.8: Unambiguously characterized structures of (*R*)-**8a**, (*R*)-**11a**, and (*R*)-**12**. 188

Chapter 7

Figure 7.1: Structure of (*R*)-heliphos (**1**) and (*R*)-Me-heliphos (**2**). 213

Figure 7.2: Coordination of (*R*)-heliphos in [Rh((R)-heliphos)(NBD)]-(ClO_4). 214

Figure 7.3: Isolated putative catalytic intermediate in ruthenium-BINAP catalyzed enantioselective hydrogenation of α,β-unsaturated carboxylic acid. 216

Figure 7.4: Possible catalytic intermediates in ruthenium-BINAP catalyzed enantioselective hydrogenation of α,β-unsaturated acids. 217

Figure 7.5: Structures of putative catalytic intermediates (**10a** (major), **11**) in the ruthenium-BINAP catalyzed enantioselective hydrogenation of **9** and **12**, respectively. 218

Figure 7.6: Unambiguously characterized putative catalytic intermediates in ruthenium-BINAP catalyzed enantioselective ketone hydrogenation. 219

List of Schemes

Chapter 1

No Schemes

Chapter 2

Scheme 2.1: Synthesis of diastereopure phosphines (*R*)- and (*S*)-**13**. 33
Scheme 2.2: Synthetic pathway to (*R*)-heliphos. 37
Scheme 2.3: Intramolecular phosphine attack. 38

Chapter 3

Scheme 3.1: Proposed catalytic cycle for achiral Rh(bis(phosphine)) catalyzed hydrogenation of olefins. 74
Scheme 3.2: Proposed catalytic cycle for achiral Rh(tris(phosphine)) catalyzed hydrogenation of olefins (phosphine arm dissociation). 76
Scheme 3.3: Alternate proposed catalytic cycle for achiral Rh(tris(phosphine)) catalyzed hydrogenation of olefins (substrate carbonyl dissociation). 77
Scheme 3.4: Proposed catalytic cycle for achiral Ru(tris(phosphine)) catalyzed hydrogenation of olefins. 78
Scheme 3.5: Proposed synthetic pathway to (*R*)-Me-heliphos based on synthetic pathway utilized in heliphos synthesis. 85
Scheme 3.6: Proposed synthetic pathway to (*R*)-Me-heliphos based on acylation of dialkyl malonate. 87
Scheme 3.7: Proposed synthetic pathway to Me-heliphos via total reduction to triol. 89

Chapter 4

Scheme 4.1: Synthesis of [Ru((*R*)-BINAP)(1-3;5,6-η-C_8H_{11})(MeCN)]-(BF_4) (**1**). 103

Scheme 4.2: Nature of **2** in solution. 106

Scheme 4.3: Reaction scheme describing the competitive hydrogenation versus isomerization in the hydrogenation of geraniol. 120

Chapter 5

Scheme 5.1: Mechanism proposed by Halpern for Ru(bis(phosphine)) catalyzed hydrogenation. 145

Scheme 5.2: Mechanism proposed by Brown for Ru(bis(phosphine)) catalyzed hydrogenation. 147

Scheme 5.3: Proposed general mechanistic pathway for Ru(bis(phosphine)) catalyzed hydrogenation of α,β-unsaturated carboxylic acids. 152

Scheme 5.4: Proposed mechanism to account for deuterium incorporation observed in angelic acid hydrogenation. 153

Scheme 5.5: Another proposed mechanism to account for deuterium incorporation observed in angelic acid hydrogenation. 154

Scheme 5.6: Proposed mechanism by Bergens for the Ru(BINAP) catalyzed hydrogenation of MAC (**18**). 156

Chapter 6

Scheme 6.1: Synthesis of non-enolizable ketone **7** from **2**. 174

Scheme 6.2: ^{13}C APT experiment to determine nature of ketone-hydride insertion. 176

Scheme 6.3: Reaction scheme to determine absolute configuration about alkoxy carbon center. 178

Chapter 7

No Schemes

List of Equations

Chapter 1

Equation 1.1: Reactions of enantiomers with chiral reagents. 9

Equation 1.2: Example of asymmetric synthesis using starting material. 1
with predefined chirality.

Equation 1.3: Example of asymmetric synthesis using achiral starting................ 1
material.

Equation 1.4: First reported example of enantioselective catalysis...................... 1

Chapter 2

Equation 2.1: Example of enantioselective hydrogenation using chiral...............2
tripodal ligand catalyst.

Equation 2.2: Example of enantioselective ring-opening of meso-.......................2
epoxides by trialkyl azides using a chiral tripodal ligand
catalyst.

Chapter 3

Equation 3.1: Reaction of [Ru(COD)(η^3-allyl)(MeCN)$_2$](BF$_4$) and 8
heliphos.

Equation 3.2: Reaction of RuCl$_2$(DMSO)$_4$ and heliphos.....................................8

Chapter 4

Equation 4.1: Displacement of acetonitrile from active catalyst **2** by................ 10
arenes.

Equation 4.2: Reaction of tiglic acid with active catalyst **2**.............................. 11

Chapter 5

No Equations

Chapter 6

No Equations

Chapter 7

Equation 7.1: Reduction of ketone with $RuCl_2((R)\text{-BINAP})(pyridine)_2$ catalyst. 215

List of Abbreviations

Ac	acetate
acac	acetoacetate
APT	attached proton test (^{13}C APT)
BINAP	2,2'-bis(diphenylphosphino)-1,1'-binaphthyl
^{t}Bu	*tert*-butyl
COD	cyclooctadiene
COSY	correlation spectroscopy
de	diastereomeric excess
DMSO	dimethyl sulfoxide
ee	enantiomeric excess
Et	ethyl
GC	gas chromatography
heliphos	1,3-bis(diphenylphosphino)-2-((diphenylphosphino)-methyl)-1-phenyl propane
HETCOR	heteronuclear correlation spectroscopy
HMBC	heteronuclear multiple-bond correlation spectroscopy
HMQC	heteronuclear multiple-quantum coherence spectroscopy
HPLC	high performance liquid chromatography
HRMS	high resolution mass spectrometry
Hz	hertz
MAC	methyl α-acetamidocinnamate
Me	methyl
Menth	menthol
MeOH	methanol
Ms	mesyl
NBD	norbornadiene
NOE	nuclear Overhauser effect
NMR	nuclear magnetic resonance
Ph	phenyl

^{i}Pr	*iso*-propyl
ROESY	rotating frame Overhauser effect spectroscopy
THF	tetrahydrofuran
triphos	1,1,1-tris((diphenylphosphino)methyl)ethane

Chapter 1

Introduction:

Molecular chirality is encountered everywhere in nature. Many living organisms produce only a single enantiomer of a given molecule.[1] The organism's production of enantiopure molecules arises from the inherent chirality of the enzymes that are employed in their formation. The importance of optically active compounds in biological systems is derived in part by the receptor sites with which they interact. These receptor sites, which are themselves chiral, interact differently with the two enantiomeric forms of a given molecule via diastereomeric interactions. The responses produced by these interactions can consequently be significantly different. These molecular recognition sites are found in many biological systems and are often the target of intense investigations in industry, medicine, and academia. The fundamental goal of all such investigations is to understand the structure and reactivity of the recognition and active sites so as to correctly predict and produce a desired consequence upon interaction with specific enantiopure molecules.

Chiral molecules are prevalent in the fields of agrochemicals,[2] flavors,[3] fragrances,[3] and pharmaceuticals.[4] The implications in flavors and fragrances are in the different olfactory responses to enantiomeric forms of a variety of molecules. Consider the forms of the terpene carvone (Figure 1.1): when presented with (*R*)-carvone, one

experiences the odor of spearmint, whereas (*S*)-carvone has the odor of caraway.[5] Enantiomeric molecules often bind to our receptor sites with different effects and can thus be exploited to generate a desired smell in perfumes. In the food additive industry, the development of inexpensive sweet-tasting molecules is pursued. Simple α-amino acids such as the D-(*R*)-enantiomorphs of leucine, phenylalanine, tyrosine, and tryptophan taste sweet while the L-(*S*)-enantiomorphs are bitter.[6] Slight modifications and derivatizations of these α-amino acids can lead to compelling differences in responses. The derivatization of bitter tasting L-phenylalanine with L-aspartic acid, which has no taste, resulted in the formation of the very sweet tasting dipeptide ester called Aspartame (Figure 1.1). Aspartame is approximately 160 times sweeter than sucrose and is a highly successful, low-calorie, sweetener substitute used in a variety of commercial products such as gum and soft drinks.[7] Olfactory responses aside, the effects of absolute configuration in chiral molecules are apparent in drug therapies.

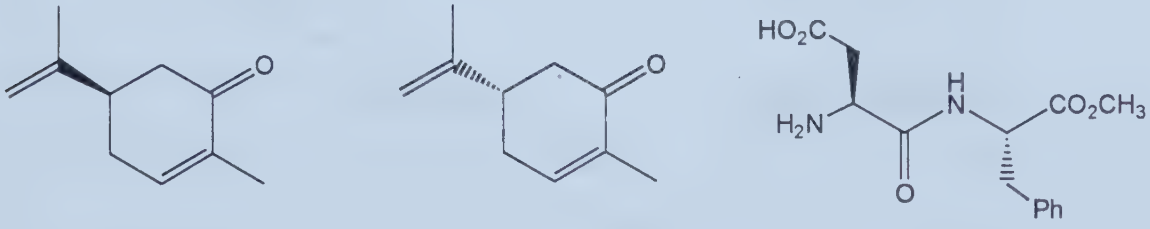

(*R*)-Carvone (*S*)-Carvone Aspartame

Figure 1.1: Enantiomers of carvone and the artificial sweetener Aspartame.

The battle against disease and infection is perhaps the most influential area for chiral molecules. Therapeutic drugs such as anti-tumor agents, anti-histamines, and nonsteroidal analgesics are often chiral molecules. These molecules were developed to interact with the binding sites associated with viruses or bacteria in order to destroy or preferentially bind with them. In doing so, the infectious guests are then unable to

interact with the binding sites and no longer corrupt the host biological system's natural function. Successful designs and syntheses of such drugs have led to many commercially available therapeutic treatments for a variety of afflictions (e.g.: anti-inflammatory: (*S*)-Naproxin and (*S*)-Ibuprofen;[8] anti-viral: (-)-Carbovir,[9] Epivir;[10] attention deficit disorder: (2*R*, 3*R*)-methylphenidate;[11] Figure 1.2). Unfortunately, cases have been documented where drugs have not behaved as designed.

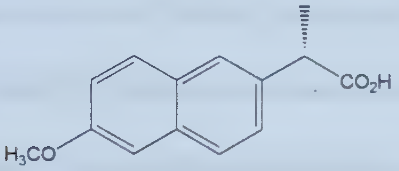

(*S*)-Naproxen

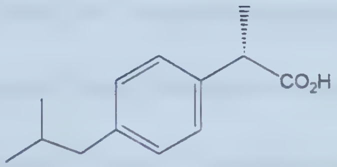

(*S*)-Ibuprofen

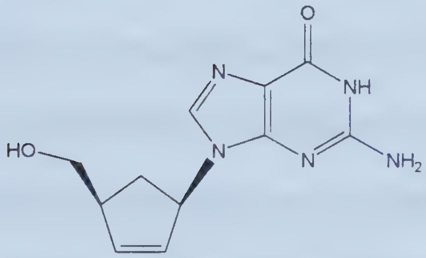

(-)-Carbovir

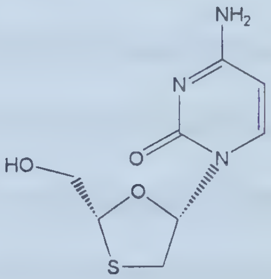

Epivir (Lamivudine)

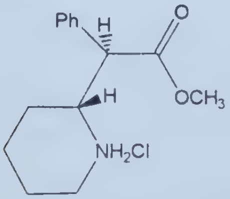

(2*R*,3*R*)-methylphenidate

Figure 1.2: Some commercially available drugs.

In many cases, therapeutic drugs are administered in racemic form. It was believed the active enantiomer of the drug would perform the desired tasks while the other "inactive" enantiomer would simply pass harmlessly through the system. This

[illegible]

[illegible]

[illegible]

[illegible]

ideology was inaccurate, and in some unfortunate instances resulted in dreadful consequences such as the much-publicized case of Thalidomide.[12] In the 1960's, Thalidomide was administered as a racemate to act as a sedative and hypnotic. Its use by pregnant women resulted in a high incidence of fetal deaths, neonatal deaths, and congenital malformations. The teratogenicity has since been attributed to the (*S*)-(-)-enantiomeric form of Thalidimide; the (*R*)-enantiomeric form was the effective drug. This is only one example (Ritalin,[11] Albuterol,[13] and DOPA,[14] are other well-documented examples) in which a commercially available therapeutic drug, delivered as a racemate, has had adverse effects when introduced into a biological system. For these reasons, the introduction of racemic drugs has become increasingly unattractive and policy changes made by regulatory agencies[15] have made it much more difficult for such therapies to be approved. This has expanded to the point where scientists must seriously concern themselves with the effects of any chiral materials that may come in contact, whether by ingestion, adsorption, inhalation, or any other means, with biological systems. As a result, the practical preparation of non-racemic (enantiopure) compounds is of critical importance in the agrochemical, flavors, fragrances, and pharmaceutical industries.

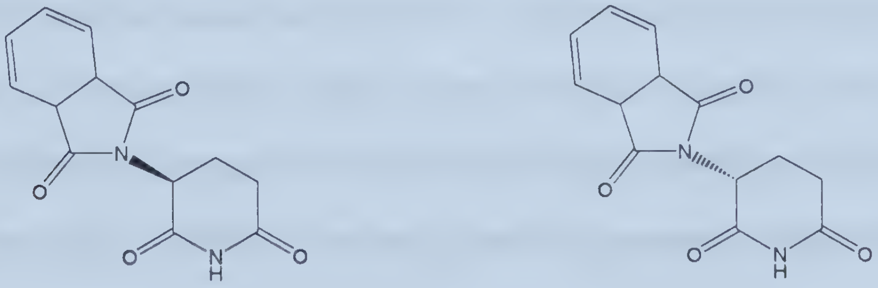

(*S*)-Thalidomide

(*R*)-Thalidomide

Figure 1.3: The enantiomers of Thalidomide (teratogen and effective drug (*S*)- and (*R*)-enantiomers, respectively).

Methods of producing enantiopure compounds.

There are two practical methods available for the production of enantiopure materials: (a) the resolution of racemates and (b) kinetically controlled asymmetric transformations.

Resolution of racemates. The resolution of racemates can be further divided into (a) the physical separation of enantiomers via crystalline forms and (b) the physical separation of diastereomeric derivatives of the enantiomers. The physical separations of enantiomers via crystallization are rare and are generally unpredictable in nature. The first resolution to be documented occurred when Pasteur physically separated the enantiomeric crystals of sodium ammonium tartrate from a racemic mixture.[16] Interestingly, the enantiomer crystal isomorphs of sodium ammonium tartrate only separate below 27 °C and had Pasteur worked in a warmer environment this discovery may not have been made. Another process that has separated enantiomers from a racemic solution is the seeding of the solution by enantiopure crystals of the compound. Under the proper conditions, this has led to the crystallization of the one enantiomer and the retention of the other enantiomer in solution. Isolation of the enantiopure product is then obtained by filtration of the solution. Even in the cases where the above types of physical separation of enantiomers can be accomplished, the techniques are often time consuming and highly laborious in nature. The more commonly utilized separation technique is that of the resolution of enantiomers based upon separation of their diastereomeric derivatives.

Unlike enantiomers, which have identical physical characteristics excluding

optical rotation, diastereomers can have differences in their physical properties. Thus, a mixture of diastereomers may be separated based upon these differences. This technique transforms the racemate, by derivatizing it with another enantiopure molecule, into a 50:50 mixture of diastereomers that is then separated. The most commonly targeted property for separation is the solubility of the resulting diastereomers, but the difference in boiling points, chromatographic retention, and other properties have also been utilized successfully.[17] This technique is still employed but it wastes one enantiomer and requires steps to both derivatize the racemic mixture and to degrade the isolated diastereomer of interest back to the enantiopure molecule. New methods have circumvented the latter two problems by introducing diastereomeric interactions without derivatization.

A further example of a diastereomeric resolution comes from the advent of new technologies in chiral chromatography (HPLC and GC). The development of new chiral columns allows for the separation of enantiomers without further derivatization.[18] The column is made up of an enantiopure support that retains enantiomers of a molecule with differing effectiveness, via diastereomeric interactions, thus producing separation along the length of the column. This technique has been utilized primarily in the determination of the enantiomeric excess (ee) of a reaction mixture but can be used in the preparative separation of racemic mixtures by HPLC. The technique continues to suffer from the waste of one enantiomer, as well as the excessive amounts of solvents required as eluent. Industrial interest is limited due to the excessive cost of scale-up in both the quantity of solvent required and the solvent disposal or recycling processes. The technique, however, has become indispensable as a quick and effective analytical tool in the determination of the enantiomeric excess of a reaction.

Kinetically controlled transformations. Kinetically controlled asymmetric transformations are the most commonly utilized techniques in producing enantiopure compounds. This technique is also the most interesting from a mechanistic viewpoint since diastereomeric transition states or intermediates control the stereochemical course of the reaction. In these processes, the pathways to the products are different but one begins at the same starting point, which is with a prochiral substrate and a chiral reagent. For the simplest one step reactions (Figure 1.4), it is only the free energies of activation ($\Delta G^{\ddagger}$) of the two pathways (forming opposite enantiomers) that differ due to the diastereomeric transition states involved.[19] The asymmetric induction thus depends solely upon the differences in the free energies of activation ($\Delta\Delta G^{\ddagger}$) of the two competing pathways. One could exploit this fundamental difference, in the design and synthesis of chiral reagents that induce a greater difference in the transition state free energies and thus greater differences in free energies of activation. These changes should lead to highly stereoselective reactions. More often than not, reactions are multi-step and the simplified account of asymmetric induction above is not accurate. In multi-step reactions, while the enantioselective step[†] is responsible for the enantioselection of the reaction, the observed ee will still depend on the steps leading up to it. The number of possible reaction sequences is too great to detail here but the interested reader can consult the excellent review by Seeman on the subject.[20] Regardless of the more complex nature of multi-step reactions, the difference in the free energies of activation for the enantioselective step will still affect the enantioselectivity as with a one step reaction.

[†] Enantioselective step is defined as the first irreversible step proceeding through diastereomeric transition states.

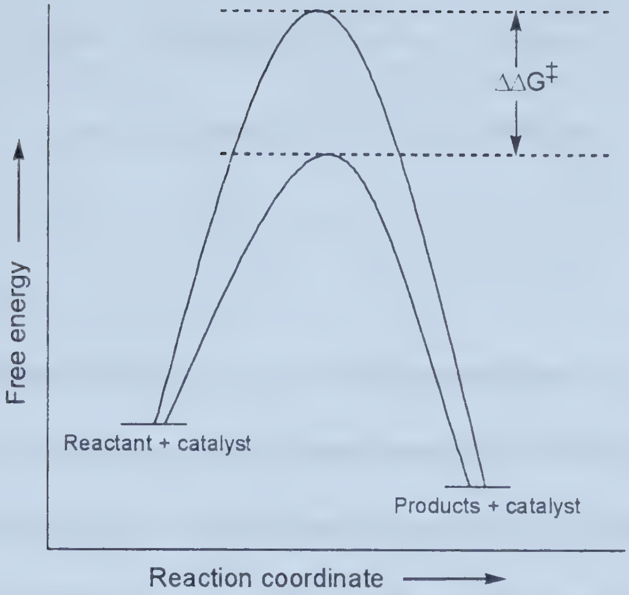

Figure 1.4: A possible energy-reaction coordinate diagram for kinetically controlled one step reaction forming enantiomeric products from prochiral substrate.

Kinetically controlled asymmetric transformations can be further divided into two categories: (a) the process in which there is a preferential reaction of one enantiomer of a racemic substrate with a chiral reagent (kinetic resolutions) and (b) the reaction of prochiral substrates with an achiral reagent to give a chiral product (asymmetric synthesis).

The rates of reaction of enantiomers of a racemic substrate with a chiral reagent are different (Equation 1.1).[21] This difference in rates will preferentially produce reaction with one enantiomer for the above reason. This difference in rates results in a kinetic resolution when the reaction is halted prior to complete consumption of the racemic substrate. If the racemic substrate reacts with chiral reagent, but the reaction is interrupted before it has reached completion, the mixture will be enriched with the product formed from the faster reacting enantiomer. The extreme case of kinetic

$$(-)\text{-Substrate} \quad + \quad R^{*} \longrightarrow [((-)\text{-Subs})(R^{*})]^{\ddagger} \xrightarrow{k_{(-)}} \text{Products}$$

$$(+)\text{-Substrate} \quad + \quad R^{*} \longrightarrow [((+)\text{-Subs})(R^{*})]^{\ddagger} \xrightarrow{k_{(+)}} \text{Products}$$

Equation 1.1

R^{*} = chiral reagent

$$k_{(-)} \neq k_{(+)}$$

resolution is encountered when $k_{(-)}$ is so much greater than $k_{(+)}$, or vice versa, that essentially complete conversion of one enantiomer is achieved without appreciable amounts of reaction with the other enantiomer (Equation 1.1). This technique is highly successful in the production of enantiopure amino acids but overall it is successful in a limited number of cases.[22] Again, this process requires the use of racemate starting materials and therefore the waste of one of the enantiomers remains. The most desirable technique for the production of enantiopure molecules will not waste any of the starting materials or products formed during the transformation. The technique that most closely fits this description is that of asymmetric synthesis defined by Marckwald.

Asymmetric synthesis, also known as stereoselective synthesis, is the most beneficial method for the production of enantiopure materials. Asymmetric synthesis was defined by Marckwald[23] as "those reactions which produce optically active substances from symmetrically constituted (containing either enantiotopic or diastereotopic groups or faces) compounds with the intermediate use of optically active materials but with the exclusion of all analytical processes." It is this definition that will be utilized throughout this thesis. When an asymmetric synthesis is used to discriminate between product enantiomers it is termed an enantioselective synthesis. Unlike processes that begin with racemates, enantioselective synthesis, as defined, converts all the starting

material into one set of stereoisomers. Quantitatively, the extent to which one product enantiomer predominates over the other can vary from the experimentally undetectable to 100%. There are a variety of methods available for asymmetric syntheses. The three common methods are: (a) stoichiometric asymmetric reactions; (b) enzymatic processes; and (c) enantioselective catalytic reactions.

The concept of stoichiometric asymmetric synthesis was clearly outlined in 1894 by Emil Fischer based on his experiments in the conversion of one sugar to its next higher homologue via the cyanohydrin reaction, relating the process directly to the biochemical process for the production of optically active sugars in plants.[24] Although his postulated scheme for the reaction was found to be incorrect, the concept of asymmetric synthesis as Fischer envisaged is still valid today. The simplest of such processes starts with an enantiopure molecule that is then reacted with another molecule that either (a) does not interact with the stereogenic center (Equation 1.2), or (b) directly reacts with the stereogenic center (e.g. S_N2 type reaction). There are numerous reports on these processes showing the products are obtained with either complete retention or inversion of absolute stereochemistry. In these cases the absolute stereochemistry of the desired product was already defined in the starting material. The case often requires that the synthetic chemist generate the first stereogenic center into the molecule.

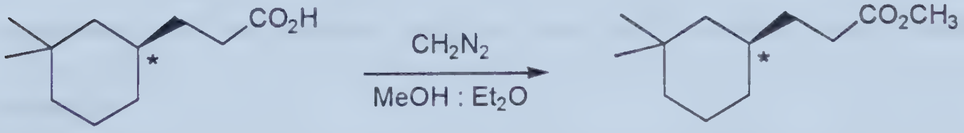

Equation 1.2

This is done by reaction of a prochiral substrate with a chiral reagent leading to the production of the stereogenic center. This chemistry is rich and diverse and several

reviews cite the application of such processes.[22, 25] One example is the reduction of prochiral ketones with chiral trialkylborohydride reagents (Equation 1.3). It remains that one still requires stoichiometric amounts of the chiral reagent. Techniques, however, reducing the chiral reagent required to catalytic amounts were developed.

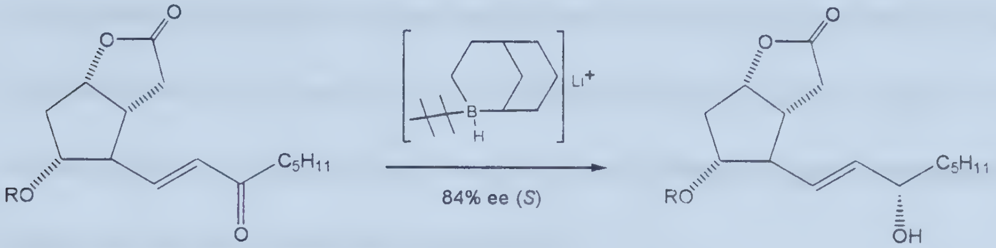

Equation 1.3

A catalyst is defined as "any reagent that can increase the rate of a reaction while not being consumed by the reaction."[26] It is both a reactant and product and thus, by definition, it is not consumed in the reaction. A catalyst cannot displace an equilibrium nor can it make a thermodynamically forbidden reaction allowed. A catalyst provides an alternate reaction pathway in which the activation energy for the process is lower than the non-catalytic process. This lowering of the activation energy leads to the increase in the rate of reaction. Thus catalysis is a purely kinetic phenomenon. The use of chiral catalysts can exploit the differences in activation energies of reaction with prochiral substrates (diastereomeric transition states and/or intermediates) to effect stereoselective reactions. In principle, one can produce millions of chiral molecules as product using only one molecule of chiral catalyst. It is this property that has been exploited successfully in asymmetric catalysis with both enzymatic and transition-metal based catalysts.

Enzymatic processes can be very selective as shown by the 100% selectivity in the formation of natural substances.[1] Biocatalytic methods based on enzyme catalysis, originally limited to the production of natural microbial metabolites, have expanded

greatly in the last decade to encompass synthesis not only of natural and unnatural products of opposite absolute configuration, but of chiral synthons for use in building up new chiral molecules. While enzymes may be "environmentally friendly" as compared to inorganic catalysts, the enzyme-producing cell cultures cannot withstand the rigors of an industrial process and enzyme extracts are often notoriously impure. Regardless, these processes are in widespread use in laboratories and are too great in number to be reviewed here in any significant detail but the interested reader can consult an excellent review on the recent advances in the field.[27]

Transition-metal based catalysts effect stereoselective reactions with high efficiency and they have certain advantages over enzyme based catalysts. Transition-metals promote reactions with a wider variety of substrates, and it is easier to modify the catalyst structure to enhance the rates and stereoselectivities of the reaction. Furthermore: (a) organic transformations can be effected with a level of control ranging from chemoselectivity (discrimination between functional groups), regioselectivity (site selectivity), to stereoselectivity (discrimination between stereoisomeric products); (b) one utilizes only catalytic amounts of a chiral reagent to yield this selectivity; and (c) the chiral catalyst can sometimes be reused. The success is exemplified by the use of chiral transition-metal based catalytic enantioselective reactions in industry.[28]

In attempts to reveal the nature of the interaction of copper salts with diazo esters, Noyori and co-workers serendipitously discovered the first homogeneous transition-metal catalyzed enantioselective reaction. The reaction between styrene and ethyl diazoacetate in the presence of a chiral Schiff base-Cu(II) complex led to the homogeneously catalyzed cyclopropanation of styrene (Equation 1.4).[29] Although the reaction proceeded

with minimal enantioselectivity (10% ee for cis, 6% ee for trans), it began the intense investigation into the use of chiral transition-metal complexes as catalysts for asymmetric organic reactions. Early milestones in the field were achieved with the bis(phosphine)-Rh(I) catalyzed hydrogenation of dehydro amino acids[30] and the phosphine-nickel aided olefin codimerization.[31] Today the field has expanded and evolved to encompass a wide variety of chiral catalysts and reactions to which they can be applied. High enantioselectivities are now found in reactions such as the Sharpless epoxidation, hydrometalation of unsaturated compounds, vicinal hydroxylation of olefins, hydrovinylations, hydroformylations, cyclopropanations, olefin isomerizations, propylene oligomerization, organometallic addition to aldehydes, allylic alkylations, organic halide-organometallic coupling, aldol-type reactions, and ene reactions.[22, 25b, 32]

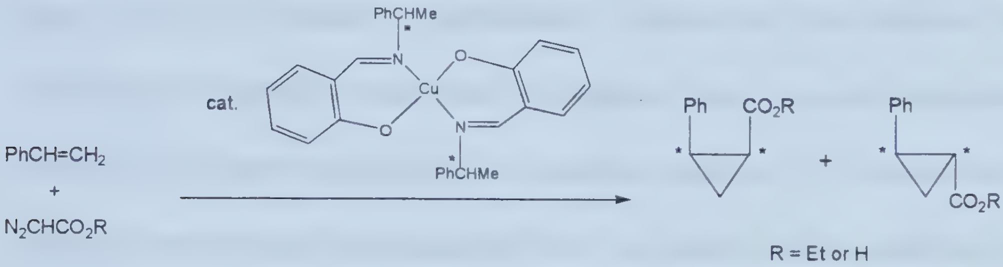

Equation 1.4

The development of new catalyst systems for such reactions, however, has been pursued primarily in an empirical fashion. This methodology of catalyst development has been utilized, as little mechanistic understanding of the catalytic cycles is known. Even with the thousands of reports on transition-metal catalyzed asymmetric reactions there are only a limited number of systems that have been studied to investigate their mechanism[22, 25b] and only a few identifications of possible catalytic intermediates have been observed. The most complete mechanistic studies of hydrogenation reactions are those of Halpern on the rhodium-bis(phosphine) catalyzed enantioselective

hydrogenation of methyl α-acetamidocinnamate.[33] Due to the lack of both the mechanistic details and the structural nature of catalytic intermediates, well-defined principles for the transmission of chirality from the chiral catalyst to the substrate are unknown. A more efficient design of catalysts would be achieved if detailed knowledge of the structural and electronic features of catalytic intermediates of existing catalytic cycles could be obtained. Furthermore, discovering the inherent nature of the enantioselective catalytic reactions investigated may provide information as to the development of new enantioselective catalytic reactions. For the above reasons, it is necessary that in-depth investigations into the nature of the catalysts, chiral ligands, catalytic intermediates, and the overall reaction pathways are to be performed.

The objectives of this work were to develop new catalysts to further investigate their structure and function in enantioselective catalysis reactions. In one effort, the design and synthesis of a new chiral *pseudo*-C_3-symmetric tris(phosphine) ligand for use as a possible chiral auxiliary in catalysis was performed. The design deviates from the popularity of C_2-symmetric bidentate ligands in an effort to further optimize and improve on the chiral recognition (or enantioselectivity) at the metal center.

In another effort, the investigation of a catalyst system, previously designed in the Bergens laboratories, was performed. The comparison of the efficiency of the newly developed [Ru((*R*)-BINAP)(C_8H_{11})(MeCN)](BF_4) system to those of the other reported ruthenium-BINAP systems in enantioselective hydrogenation reactions was undertaken. Its apparent similarities in successful enantioselective hydrogenation reactions led to its use in the investigation into the mechanisms of reaction involved in a variety of enantioselective catalytic hydrogenation reactions (hydrogenation of α,β-unsaturated

carboxylic acids, α,β-unsaturated esters, and ketones). The objective of this work was to determine, in general, the origins of enantioselection in enantioselective hydrogenation reactions using the highly successful ruthenium-BINAP system as catalyst.

References and Notes:

(1) Voet, D.; Voet, J. D. *Biochemistry*: 2nd ed; John Wiley & Sons: New York, 1995; Chapter 12.

(2) (a) *Chirality in Agrochemicals*: Kurihara, N.; Miyamoto, J. Eds.; John Wiley & Sons: New York, 1998. (b) Crosby, J. *Pestic. Sci.* **1996**, *46*, 11. (c) Ramos Tombo, G. M.; Bellus, D. *Angew. Chem. Int. Ed. Eng.* **1991**, *30*, 1193-1215.

(3) (a) Fráter, G.; Bajgrowicz, J. A.; Kraft, P. *Tetrahedron* **1998**, *54*, 7633-7703. (b) Bauer, K.; Garbe, D.; Surburg, H. *Common Fragrance and Flavor Materials*: 2nd ed; VCH Publishers: New York, 1990.

(4) (a) Burk, M. J.; Gross, M. F.; Harper, T. G. P.; Kalberg, C. S.; Lee, J. R.; Martinez, J. P. *Pure Appl. Chem.* **1996**, *68*, 37-41. (b) Schmid, R.; Broger, E. A.; Cereghetti, M.; Crameri, Y.; Foricher, J.; Lalonde, M.; Müller, R. K.; Scalone, M.; Schoettel, G.; Zutter, U. *Pure Appl. Chem.* **1996**, *68*, 131-138. (c) Chan, A. S. C.; Laneman, S. A.; Miller, R. E. In *Selectivity in Catalysis*: Davis, M. E.; Suib, S. L. Eds.; Advances in Chemistry Series 517; American Chemical Society: Washington, 1993; Chapter 2.

(5) (a) Russel, G. F.; Hills, J. I. *Science* **1971**, *173*, 1043. (b) Friedman, L.; Miller, J. G. *Science* **1971**, *172*, 1044.

(6) Coppola, G. M.; Schuster, H. F. *Asymmetric Synthesis: Construction of Chiral Molecules Using Amino Acids*: John Wiley & Sons: New York, 1987; pp. 1-2.

(7) Ojima, I.; Clos, N.; Bastos, C. *Tetrahedron* **1989**, *45*, 6901-6939.

(8) Chan, A. S. C. *Chemtech* **1993**, *23*, 46-51, and references cited within.

(9) (a) Vince, R.; Hua, M. *J. Med. Chem.* **1990**, *33*, 17, and references cited within. (b) Vince, R.; Hua, M. *US Pat.* 4 950 758, **1990**. (c) Vince, R.; Hua, M. *US Pat.* 5 233 041, **1993**.

(10) Soudeyns, H.; Yao, X.-J.; Belleau, B.; Kraus, J.-L.; Nguyen-Ba, N.; Spira, B.; Wainberg, M. A. *Antimicrob. Agents Chemother.* **1991**, *35*, 1386.

(11) *Chem. Eng. News* 21 September 1998; p. 28, and references cited within.

(12) Blaschke, G.; Kraft, H. P.; Fickentscher, K.; Köhler, F. *Arzneim.-Forsch./Drug. Res.* **1979**, *29*, 1640.

(13) Spitzer, W. O. *New Engl. J. Med.* **1992**, *326*, 501-506.

(14) Hyneck, M.; Dent, J.; Hook, J. In *Chirality in Drug Design and Synthesis*: Brown, C. Ed.; Academic Press: Toronto, 1990; Chapter 1, and references cited within.

(15) (a) Stinson, S. C. *Chem. & Eng. News* **1992**, *70*, 46. (c) Borman, S. *Chem. & Eng. News* **1990**, *68*, 9.

(16) Pasteur, L. *Ann. Chim. et phys.* **1848**, *24*, 442.

(17) Raban, M.; Mislow, K. In *Topics in Stereochemistry*: Eliel, E.; Allinger, N. Eds.; Interscience Publishers: New York, 1967; pp. 199-230.

(18) (a) Beesley, T. E.; Scott, R. A. W. *Chiral Chromatography*: John Wiley & Sons: New York, 1999. (b) *Chiral Separations: Applications and Technology*: Ahuja, S., Ed.; American Chemical Society: Washington, 1996. (c*) Practical Approach to Chiral Separations by Liquid Chromatography*: Subramanian, G. Ed.; John Wiley & Sons: New York, 1994.

(19) Morrison, J. D.; Mosher, H. S. *Asymmetric Organic Reactions*: Prentice-Hall, Inc.: New Jersey, 1971; pp. 28-31.

(20) Seeman, J. I. *Chem. Rev.* **1983**, *83*, 84-134.

(21) (a) Kitamura, M.; Tokunaga, M.; Noyori, R. *J. Am. Chem. Soc.* **1993**, *115*, 144-152. (b) Ref 19, pp. 30-35.

(22) Noyori, R. *Asymmetric Catalysis in Organic Synthesis*: John Wiley & Sons, Inc.: New York, 1994; Chapter 1, and references cited within.

(23) Marckwald, W. *Ber.* **1904**, *37*, 1368-1370.

(24) Fischer, E. *Ber.* **1894**, *27*, 3189-3232.

(25) (a) *Reductions in Organic Chemistry*: Abdel-Magid, A. F. Ed.; Advances in Chemistry Series 641; American Chemical Society: Washington, 1996; and references sited within. (b) *Catalytic Asymmetric Synthesis*: Ojima, I. Ed.; VCH Publishers: New York, 1993; and references cited within. (c) Ojima, I.; Clos, N.; Bastos, C. *Tetrahedron* **1989**, *45*, 6901-6939.

(26) Kotz, J. C.; Purcell, K. F. *Chemistry and Chemical Reactivity*: CBS College Publishing: New York, 1987; pp. 503.

(27) Santaniello, E.; Ferraboschi, P.; Grisenti, P.; Manzocchi, A. *Chem. Rev.* **1992**, *92*, 1071-1140.

(28) *Chirality in Industry*: Collins, A. N.; Sheldrake, G. N.; Crosby, J. Eds.; John Wiley & Sons: New York, 1997.

(29) Nozaki, H.; Moriuti, S.; Takaya, H.; Noyori, R. *Tettrahedron Lett.* **1966**, *43*, 5239-5244.

(30) (a) Dang, T. P.; Kagan, H. B. *J. Chem. Soc., Chem. Commun.* **1971**, 481. (b) Knowles, W. S.; Sabacky, M. J.; Vineyard, B. D. *J. Chem. Soc., Chem. Commun.* **1972**, 10-11.

(31) (a) Bogdanović, B. *Angew. Chem. Int. Ed. Engl.* **1973**, *12*, 954. (b) Bogdanović, B.; Henc, B.; Meister, B.; Pauling, H.; Wilke, G. *Angew. Chem. Int. Ed. Engl.* **1972**, *11*, 1023.

(32) Parshall, G.; Ittel, S. D. In *Homogeneous Catalysis: The Applications and Chemistry of Soluble Transition-Metal Complexes*: 2nd ed.; John Wiley & Sons, Inc.: New York, 1992; and references cited within.

(33) (a) Halpern, J. *Pure. Appl. Chem.* **1983**, *55*, 99-106. (b) Halpern, J. *Science* **1982**, *217*, 401-407. This reaction has been most heavily investigated and other references should be consulted. Spectroscopic detection and characterization and X-ray characterization of possible intermediates: (c) McCulloch, B.; Halpern, J.; Thompson, M. R.; Landis, C. R. *Organometallics* **1990**, *9*, 1392-1395. (d) Brown, J. M.; Murrer, B. A. *J. Chem. Soc., Perkin Trans. 2* **1982**, 489-497. (e) Chan, A. S. C.; Pluth, J. J. Halpern, J. *J. Am. Chem. Soc.* **1980**, *102*, 5952-5954. (f) Brown, J. M.; Chaloner, P. A. *J. Am. Chem. Soc.* **1980**, *102*, 3040-3048. (g) Chan, A. C. S.; Halpern, J. *J. Am. Chem. Soc.* **1980**, *102*, 838-840. (h) Brown, J. M.; Chaloner, P. A. *J. Chem. Soc., Chem. Commun.* **1980**, 344-346. (i) Chan, A. C. S.; Pluth, J. J.; Halpern, J. *Inorg. Chim. Acta* **1979**, *37*, L477-L479. (j) Brown, J. M.; Chaloner, P.A. *J. Chem. Soc., Chem. Commun.* **1979**, 613-615. (k) Brown, J. M.; Chaloner, P. A. *Tetrahedron Lett.* **1978**, 1877-1880. (l) Brown, J. M.; Chaloner, P. A. *J. Chem. Soc., Chem. Commun.* **1978**, 321-322. Deuterium labeling studies: (m) Detellier, C.; Gelbrard, G.; Kagan, H. B. *J. Am. Chem. Soc.* **1978**, *100*, 7556-7561. (n) Koenig, K. E.; Knowles, W. S. *J. Am. Chem. Soc.* **1978**, *100*, 7561-7564. Mechanism of interconversion of intermediates: (o) Kless, A.; Börner, A.; Heller,

D.; Selke, R. *Organometallics* **1997**, *16*, 2096-2100. (p) Bircher, H.; Bender, B. R.; von Philipsborn, W. *Magn. Res. Chem.* **1993**, *31*, 293-298. (q) Kadyrov, R.; Freier, T.; Heller, D.; Michalik, M.; Selke, R. *J. Chem. Soc., Chem. Commun.* **1995**, 1746-1746. (r) Brown, J. M.; Chaloner, P. A.; Morris, G. A. *J. Chem. Soc., Perkin Trans. 2* **1987**, 1583-1588. (s) Brown, J. M.; Chaloner, P. A.; Morris, G. A. *J. Chem. Soc., Chem. Commun.* **1983**, 664-666. Kinetic measurements: (t) Chinn, M. S.; Eisenberg, R. *J. Am. Chem. Soc.* **1992**, *114*, 1908-1909. (u) Landis, C. R.; Halpern, J. *J. Am. Chem. Soc.* **1987**, *109*, 1746-1754. Theoretical calculations: (v) Giovannetti, J. S.; Kelly, C. M.; Landis, C. R. *J. Am. Chem. Soc.* **1993**, *115*, 4040-4057. (w) Bosnich, B. *Pure Appl. Chem.* **1990**, *62*, 1131-1134. (x) Bogdan, P. L.; Irwin, J. J.; Bosnich, B. *Organometallics* **1989**, *8*, 1450-1453.

Chapter 2

(*R*)- and (*S*)-1,3-Bis(diphenylphosphino)-2-((diphenylphosphino)methyl)-1-phenyl propane ((*R*)- and (*S*)-heliphos): Solid-State and Solution Conformations of a Chiral, Tripodal Tris(phosphine) Ligand That Is Restrained to One Helical Conformation upon Coordination to a Rhodium(I) Metal Center[†]

Introduction:

The development of chiral auxiliaries for use in asymmetric catalysis is of considerable importance to the economic production of chiral molecules. Whether it be a simple modification of an existing ligand or a new design altogether, the search for ligands that yield increased selectivity is essential to the success of metal catalyzed asymmetric synthesis. It remains that the progress in catalyst development has been empirical in nature rather than through well-defined systematic design and synthesis. Comparisons of successful chiral ligands, however, revealed a number of features that most, if not all, these systems possessed. It is believed that these features are essential components of chiral auxiliaries to ensure high enantioselection in catalysis reactions.[1] These features are (a) conformational rigidity, (b) bidentate or higher coordination, and (c) the possession of C_2 symmetry.

[†] A version of this chapter has been published. *Organometallics* **1997**, *16*, 1890-1896.

The stipulation for conformational rigidity stems from the steric interactions between the chiral ligand and the bonded substrate. A conformationally fluxional ligand could adjust the orientation of its ancillary groups away from the coordinated substrate should undesirable steric interactions occur between the two. This steric relaxation would reduce the overall free energy of the transition state and could therefore reduce the degree of difference in free energies between other diastereomeric transition states formed ($\Delta\Delta G^\circ$ = small). The result of such stabilizations would likely be poor selectivity for the catalytic reaction in question. Another component of fluxionality is that the net asymmetric induction of a ligand is the weighted average of each conformation it adopts in a diastereomeric catalyst-substrate complex. Therefore, the more conformations available, the lower the net asymmetric induction. Conformational rigidity would not allow for either to occur, thus enhancing the difference in free energies of the diastereomeric transition states ($\Delta\Delta G^\circ$ = large) and increasing the overall selectivity of the catalytic reaction.

The latter two features, bidentate coordination and C_2 symmetry, were proposed as criteria for successful ligands because of conditions they impose on the remaining coordination sites, the active sites, on the catalyst. The coordination of C_2-symmetric bidentate ligands reduces the number of possible competing diastereomeric transition states. In a square planar complex, coordination of a C_2-symmetric bidentate ligand leaves two coordination sites available about the metal. The remaining sites are interrelated by the C_2-axis of symmetry thus making them equivalent (Figure 2.1). In octahedral environments, the C_2-symmetric bidentate ligand reduces the number of independent coordination sites to two (Figure 2.1). In each case, the number of possible

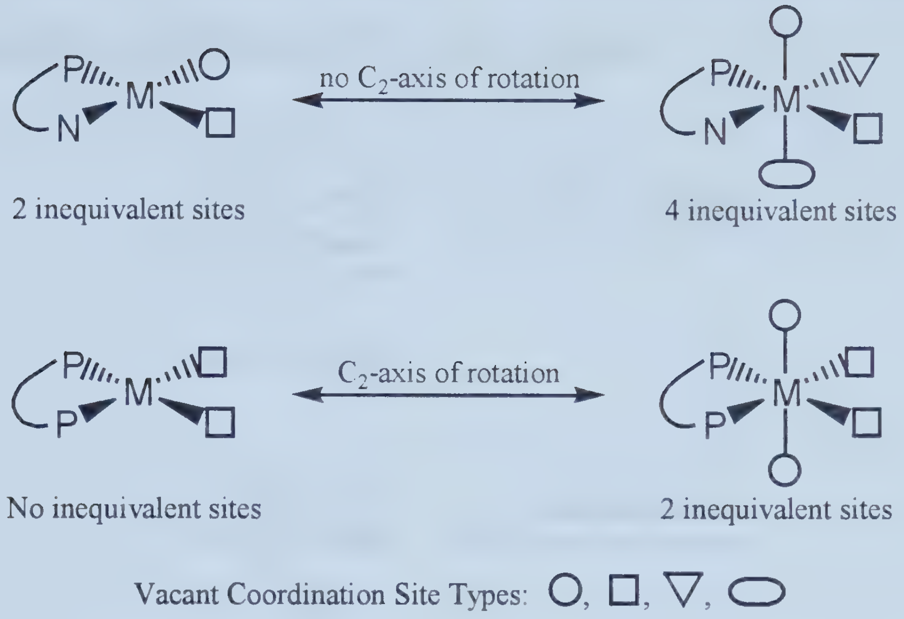
P
M
N
no C_2-axis of rotation
2 inequivalent sites
4 inequivalent sites
C_2-axis of rotation
No inequivalent sites
2 inequivalent sites
Vacant Coordination Site Types:

Figure 2.1: Coordination sites of non symmetric and of C_2-symmetric metal species.

diastereomers is less than that of a complex containing either chiral monodentate or non-symmetric polydentate ligands. With the number of diastereomeric intermediates reduced, one also reduces the number of possible competing reaction pathways, thus increasing the likelihood of high enantioselection. On the basis of these arguments, it follows that these ideas can be expanded to include higher symmetry ligands, namely those possessing a three-fold axis of rotation (C_3 symmetry) to obtain even higher enantioselection.

The simplest C_3-symmetric system is a tridentate ligand. Coordination of C_3-symmetric tridentate ligands to an octahedral metal center reduces the number of different diastereomeric coordination sites from two for C_2-symmetric bidentate ligands (five for chiral monodentate ligands), to one (Figure 2.2). With only one type of coordination site remaining, achieving higher stereoselection in asymmetric catalytic

reactions is expected to be greater. Further, if a sterically rigid ligand is utilized, the stereoselection of the system should be even further enhanced.

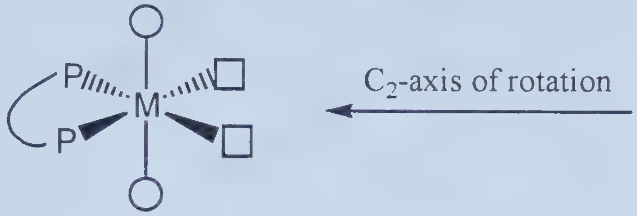

2 inequivalent sites

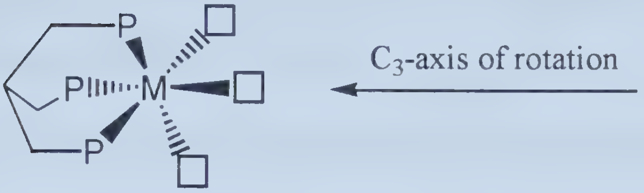

all equivalent sites

Figure 2.2: Coordination sites of C_2-symmetric and C_3-symmetric metal species.

The first development towards sterically rigid C_3-symmetric ligands was the tetradentate nitrogen ligand $N(CH_2CH_2NMe_2)_2(C(H)(Me)(CH_2NMe_2))$ (***S*-tan**) developed by Utsuno.[2] Although tetradentate, the ligand possessed *pseudo*-C_3 symmetry upon coordination to cobalt in the complex [Co(MeCN)(***S*-tan**)](ClO_4) (Figure 2.3). All the five-membered chelate rings (C-N-Co-N-C) adopted λ conformations. It is believed that this configuration is adopted because of the preference by the backbone methyl group (Me_1) to be in an equatorial position of the five membered ring. If the methyl group were in an axial orientation, it would suffer from steric interactions with the backbone of the ligand. In the equatorial position, significant steric interactions are not encountered. Had the absolute stereochemistry about the stereogenic carbon atom been in the *R*-configuration, the rings would have all adopted δ configurations for the same reasons.

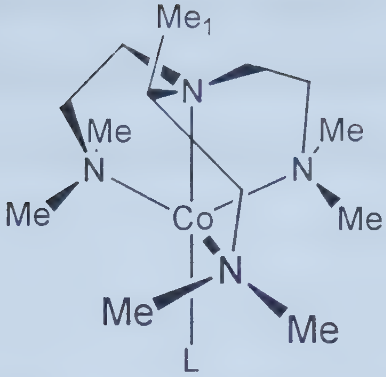

Figure 2.3: Representation of the crystal structure of [Co(L)((S)-tan)](ClO_4) (L = NCS) reported by Utsuno, excluding the anion.

Similar ligands have since been developed by the groups of Canary[3] and Nugent.[4] In all cases, it is believed that the backbone substituent controls the steric rigidity of the system. Furthermore, the backbone substituent has a preference for the equatorial position in ethylenediamine and diethylenediphosphine complexes.[5] In these described systems, the stereogenic center is in the backbone of the ligand. A second type of ligand is known, in which the stereogenic center(s) is located in the ancillary groups on the coordinating atoms (e.g. nitrogen, oxygen, and phosphorus).

The development of C_3-symmetric (or *pseudo*-C_3-symmetric) ligand systems containing the stereogenic center(s) in the ancillary groups of the coordinating atoms came right on the heels of Utsumo's work with ***S*-tan**. The first system was reported by Brunner[6] with *R*-(+)-trisiminphos (**1**; Figure 2.4), followed by Moberg's[7] trispyridine ligands (**2**), Tolman's[8] chiral analogs of the well-known tris(pyrazolyl)hydroborate[9] system (**3**), Burk's[10] tripodal tris(phosphine) systems (**4**, **5**), Venanzi's[11] (*R*,*R*,*R*)-Siliphos (**6**), Huttner's[12] chiral analogs of the well-established tris(phosphine) triphos[13] system ($MeC(CH_2P(R)(Ph))_3$, where R = Ph for triphos) (**7**), Mayer's[14] chiral tris(phosphine)

[illegible]

[illegible]

[illegible]

cyclohexane system (**8**), and Knochel's[15] chiral tripodal triol system (**9**). The stereogenic centers in **8** and **9** are in the backbone. The number of chiral C_3-symmetric or *pseudo*-C_3-symmetric tripodal ligands is limited as compared to those of chiral bidentate ligands.

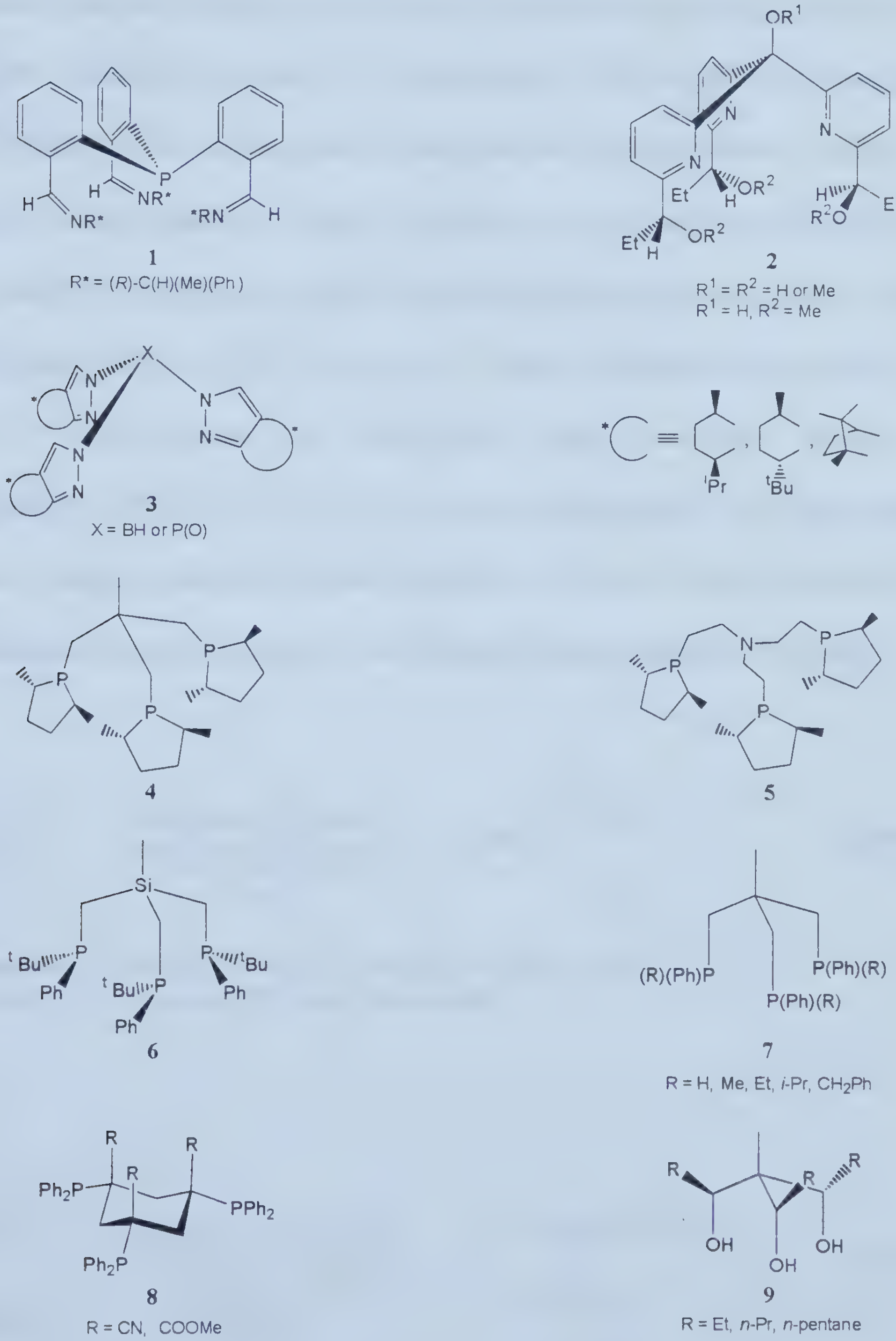

1
R* = (*R*)-C(H)(Me)(Ph)

2
$R^1 = R^2$ = H or Me
R^1 = H, R^2 = Me

3
X = BH or P(O)

4

5

6

7
R = H, Me, Et, *i*-Pr, CH_2Ph

8
R = CN, COOMe

9
R = Et, *n*-Pr, *n*-pentane

Figure 2.4: Reported chiral C_3-symmetric ligands.

In general, the development of C_3-symmetric ligands has been hindered by a lack of high enantioselection achieved with the earlier systems in asymmetric catalysis. However, the recent work of both Burk[10] and Nugent[4] has shown that high enantioselectivities can be obtained with chiral C_3-symmetric systems (Equations 2.1 and 2.2). Burk utilized the ligand **4** in conjunction with rhodium as the catalyst, [(**4**)Rh(COD)](SbF_6), for the catalytic enantioselective hydrogenation of olefins. The enantioselective hydrogenation of methyl *α*-acetamidocinnamate and dimethyl itaconate both proceeded to completion yielding *N*-acetylphenylalanine (89% ee (*R*)) and dimethyl methylsuccinate (95% ee (*S*)), respectively. Nugent investigated the catalytic ring-opening of meso-epoxides by trialkylsilyl azides. When catalyzed by $[((\mathbf{10})Zr(OH))_2\bullet{}^tBuOH]_n$ (**10** = (+)-(*S*,*S*,*S*)-trisisopropanolamine), the ring-opening of cyclohexane oxide by trialkylsilyl azides yielded up to 93% ee. With these results came renewed interest in the development of well-defined chiral C_3-symmetric ligands.

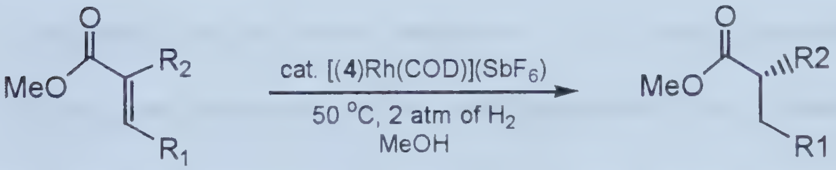

Equation 2.1

α-methyl acetamidocinnamate: R_1 = Ph, R_2 = N(H)C(O)Me (89% ee (*R*))
Dimethyl itaconate: R_1 = H, R_2 = CH_2CO_2Me (95 % ee (*S*))

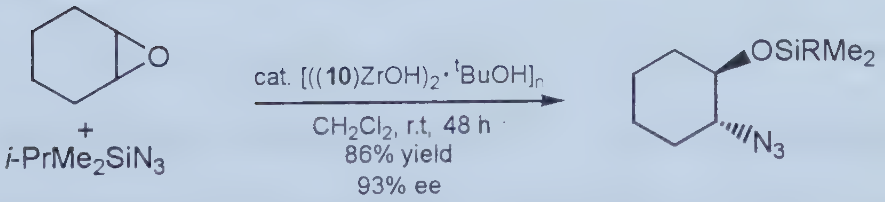

Equation 2.2

An essential component of asymmetric induction for many enantioselective catalytic systems is the conformation of the chiral ligand's framework. More specifically, it is the conformational array of pendent groups projecting towards the labile solvento or free sites (active sites) of the metal that is essential. It is this asymmetric environment that is believed to contribute to the enantioselection of the system. As has been shown, many of the ligands have frameworks that are themselves chiral, and dictate the absolute spatial configuration of the pendent groups near the active sites on the catalyst. Therefore, control over the framework conformations would greatly facilitate the understanding of the origins of enantioselection in these systems.

As demonstrated earlier, approaches used to control conformational fluxionality have included use of rigid ligand frameworks (type I)[16] and use of derivatives of fluxional parent frameworks that are biased toward one conformer (type II).[17] Interestingly, experimental studies of the solution framework conformation(s) of type II chiral ligands are limited in number[18] and have rarely been applied to chiral tripodal tris(phosphines). Considering the few chiral analogues of 1,1,1-tris((diphenylphosphino)methyl)-ethane (triphos), and structurally related tris(phosphines), there remained an element of chirality that had not been directly controlled - the helical conformations they adopt upon coordination to metal centers.[19, 20] The goal of this work was to design and synthesize a new chiral tripodal C_3-symmetric tris(phosphine) ligand (heliphos) with control over the helical conformation it adopts upon coordination to metal centers.

Figure 2.5 shows a model of the left (Λ)- and right (Δ)-handed helical conformations of coordinated triphos. The Λ- and Δ-conformations are enantiomers and it is expected that interconversion between them is facile in most metal complexes.

Figure 2.5 also shows a model of the left (Λ)- and right (Δ)-handed helical conformations of coordinated (*R*)-1,3-bis(diphenylphosphino)-2-((diphenylphosphino)methyl)-1-phenylpropane ((*R*)-heliphos). The Λ- and Δ-conformations would be enantiomers in the absence of the phenyl substituent on the framework (as in triphos). Further observation shows that the phenyl rings of the phosphine groups are held in chiral spatial arrangements of opposite absolute configuration by Λ- and Δ-(*R*)-heliphos. For Λ- and Δ-(*R*)-heliphos, one phenyl ring of each phosphine group is disposed roughly in the plane defined by the phosphorus atoms (equatorial), and the other projects towards an active site on the metal center (axial). Interconversion between the Λ- and Δ-conformations causes the equatorial and axial phenyl rings to exchange orientations, thereby inverting the asymmetric environment of the active sites on the catalyst (Figure 2.5).

Ligand Design. Ball and stick molecular models (HGS) of coordinated (*R*)-heliphos show that severe steric repulsions exist between the phenyl ring on the framework and the equatorial phenyl ring of the *syn*-phosphine group in Δ-(*R*)-heliphos (Figure 2.5). Although the magnitude of this interaction has not been calculated, molecular models show that these phenyl rings physically overlap in the Δ-configuration. This steric interaction is absent in the Λ-configuration. Conversely, models show that similar severe steric interactions occur in Λ-(*S*)-heliphos but are absent in Δ-(*S*)-heliphos. It is proposed that these steric repulsions dictate the conformations of (*R*)- and (*S*)-heliphos, locking them into the less strained Λ-(*R*) and Δ-(*S*) conformers respectively. The selection of phosphines as the coordinating moieties for the ligand system is based

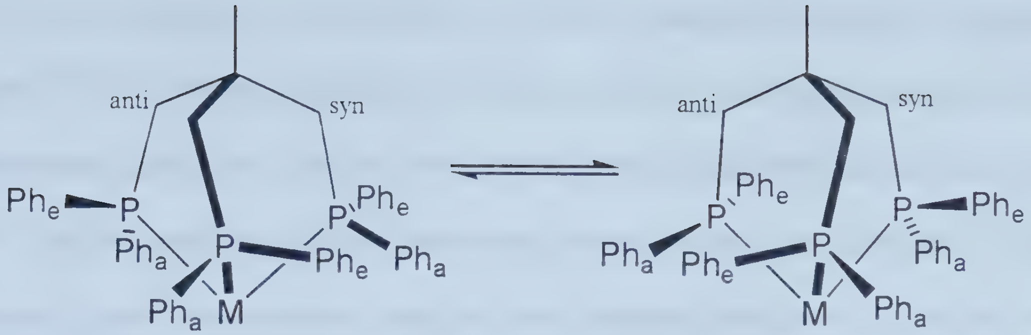
anti
syn
$\mathrm{Ph_e}$
P
$\mathrm{Ph_a}$
M
anti
syn
$\mathrm{Ph_e}$
P
$\mathrm{Ph_a}$
M

Λ-(*R*)-triphos Δ-(*R*)-triphos

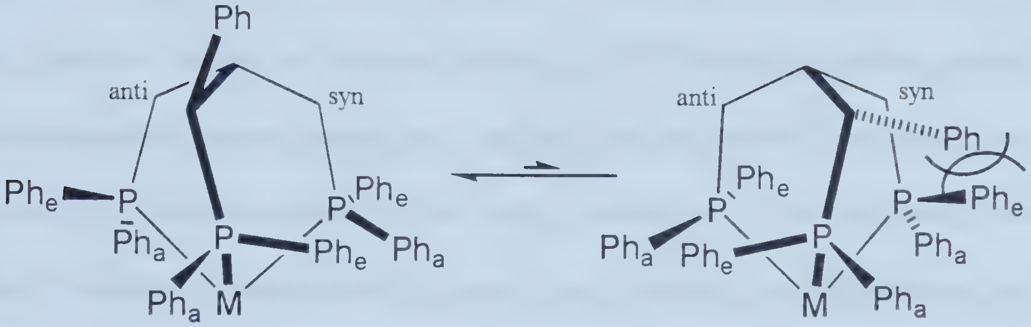
Ph
anti
syn
$\mathrm{Ph_e}$
P
$\mathrm{Ph_a}$
M
anti
syn
Ph
$\mathrm{Ph_e}$
P
$\mathrm{Ph_a}$
M

Λ-(*R*)-heliphos Δ-(*R*)-heliphos

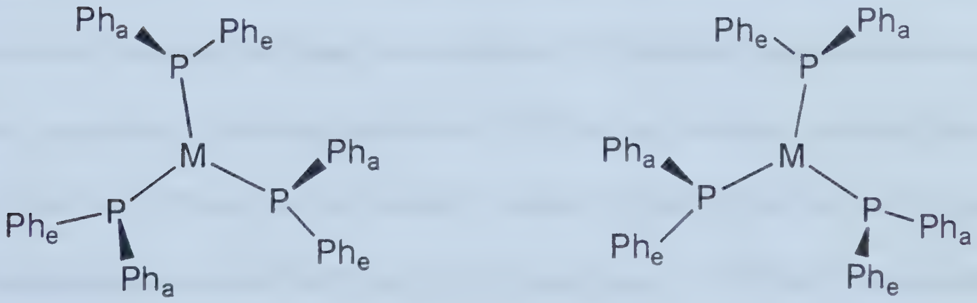
$\mathrm{Ph_a}$
$\mathrm{Ph_e}$
P
M
$\mathrm{Ph_a}$
$\mathrm{Ph_e}$
P
M

Λ-(*R*)-heliphos Δ-(*R*)-heliphos

Figure 2.5: Schematic representations of Λ- and Δ-coordinated triphos and of (*R*)-heliphos showing the overlap of phenyl rings in the Δ-(*R*)-heliphos conformer. The chiral spatial arrangements of equatorial (e) and axial (a) phenyl rings as viewed from the perspective of the active sites on the metal center for Λ- and Δ-coordinated (*R*)-heliphos are also depicted at the bottom of the figure.

[illegible]

on three considerations: (a) the success of chiral phosphine ligands in asymmetric catalysis,[13g, 13h, 21] (b) the availability of a large variety of phosphines, and (c) the ability to probe the ligand, and thus the environment about the catalyst metal center, by ^{31}P NMR. The first consideration has been amply demonstrated in the literature. The most successful ligands in asymmetric catalysis have contained phosphines. The most notable example is the C_2-symmetric BINAP ligand that has been a very successful catalyst ligand in a variety of enantioselective reactions.[22] Phosphines are the most widely used ligating moieties, whether as systems containing solely phosphine ligating groups or in tandem with other ligating groups (e.g. nitrogen, oxygen, sulfur). Secondly, there are a large number of phosphines that can be easily synthesized. The availability of a large number of different substituents (e.g. alkyl, aryl, halogen, oxygen) allows for wide variation in the steric size of the phosphines resulting in the ability to modify the catalyst system with ease. These phosphines can be utilized to probe the steric effects of a catalyst system, between the ligand and substrate. Furthermore, one can also change the electronic properties of the phosphines with differing substituents, allowing for a probe into the electronic effects on the catalyst systems. Finally, the use of phosphines is highly desirable due to the NMR activity of phosphorus. ^{1}H NMR can be utilized to analyze many systems, but little information about the catalyst can be discerned due to the saturation of the spectrum from the excessive amounts of substrate used. The advantage of ^{31}P NMR is that the metal complex can be examined throughout the course of a reaction, without spectral saturation from the substrate. Therefore, the phosphines can also act as good probes into the nature of the catalyst system.

The ultimate objective is to investigate the use of heliphos in asymmetric catalysis. In this chapter, the syntheses of the chiral tris(phosphine) ligands (*R*)- and (*S*)-1,3-bis(diphenylphosphino)-2-((diphenylphosphino)methyl)-1-phenylpropane ((*R*)- and (*S*)-heliphos) as well as their adopted helical conformations (solid-state and solution) upon coordination to rhodium in [Rh((*R*)-heliphos)(NBD)](ClO_4) are discussed.

Results and Discussion:

Synthesis of (*R*)- and (*S*)-heliphos. The ligands (*R*)- and (*S*)-heliphos were prepared according to Schemes 2.1 and 2.2. Di-(1*R*,2*S*,5*R*)-(-)-menthyl malonate (**11**) was synthesized via sodium catalyzed transesterification of dimethyl malonate. Knovenegal condensation of di-(1*R*,2*S*,5*R*)-(-)-menthyl malonate with benzaldehyde in methylene chloride solution yielded di-(1*R*,2*S*,5*R*)-(-)-menthyl benzylidenemalonate (**12**). **12** was obtained as a crystalline solid in 89.5% yield after crystallization. The product **12** was then converted into the diastereomers of **13** by reaction with diphenylphosphine and use of an acid catalyst. This acid-catalyzed, diastereoselective Michael addition of diphenylphosphine to **12** is the most notable feature in the synthetic pathway to (*R*)- and (*S*)-heliphos.

Studies were carried out to determine the optimum conditions for achieving high diastereoselectivity of the product. To determine whether a catalyst, acid or base, would increase the rate of reaction, NMR scale reactions were carried out at ambient temperature in chloroform-*d* with two chiral acids (D-camphoric acid and D-

camphorsulfonic acid), one chiral base (sparteine), one non-chiral acid (*p*-toluenesulfonic acid), and one without added catalyst. The acid catalyzed reactions were the most efficient (Table 2.1). Both the base catalyzed (~ 5%) and non-catalyzed (no reaction) reactions were too slow to be considered further. The acid catalyzed reaction was then investigated with camphorsulfonic acid, dibenzoyl-L-tartaric acid, and L-lactic acid as catalysts in chloroform-*d*, methylene chloride-d_2, and benzene-d_6 (Table 2.2). No

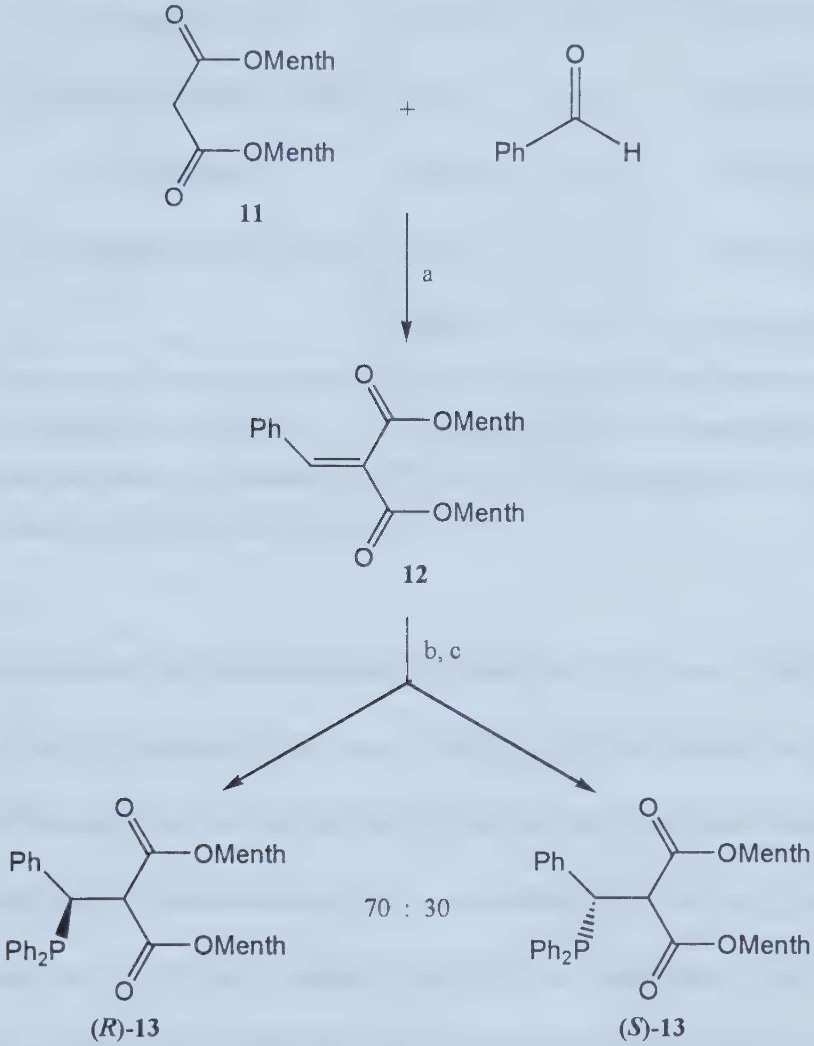
OMenth
OMenth
11
+
Ph
H
a
Ph
OMenth
OMenth
12
b, c
Ph
Ph2P
OMenth
OMenth
(R)-13
70 : 30
Ph
Ph2P
OMenth
OMenth
(S)-13

a) CH_3COOH (20%), piperidine (4%), C_6H_6, 130°C, 24 h. b) $HPPh_2$, *p*-TsOH (2.5 mol %), CH_2Cl_2, 25°C, 72 h. c) fractional crystallization toluene:MeOH (1:10).

Scheme 2.1: Synthesis of diastereopure phosphines (*R*)- and (*S*)-13.

Table 2.1: Catalyst tests for Michael addition to 12.[a]

Sample	Catalyst	Solvent	Time	% Conversion[b] (de)[c]
1[d]	D-Camphoric Acid	$CDCl_3$	4 h	~ 17% (20 %)
2	D-Camphorsulfonic Acid	$CDCl_3$	4 h	~ 50% (32 %)
3	Sparteine	$CDCl_3$	4 h	~ 5% (12 %)
4	*p*-Toluenesulfonic Acid	$CDCl_3$	4 h	~ 45% (30 %)
5	___	$CDCl_3$	4 h	No reaction

[a] All reactions performed in NMR tubes: 5.34×10^{-5} mol of **12**, 5.61×10^{-5} mol $HPPh_2$, 0.6 mL $CDCl_3$, ambient temperature. [b] Determined by ^{31}P NMR. [c] De = diastereoselectivity. [d] D-Camphoric acid did not dissolve well in $CDCl_3$.

appreciable enhancement of diastereoselectivity was detected using chiral acids versus using the non-chiral *p*-toluenesulfonic acid. Further, the best solvent for reaction was found to be methylene chloride. As the chiral acids investigated gave similar reactivity and diastereoselectivity to achiral acids, their use as catalyst would be a waste of chiral material. Reaction of **12** and diphenylphosphine in methylene chloride with *p*-toluenesulfonic acid as catalyst yielded the diastereomeric products of **13** in a quantitative yield with a 40% diastereomeric excess (de).

Table 2.2: Solvent and chiral catalyst screening of Michael addition to 12.[a]

Sample	Catalyst	Solvent[b]	Time	% Conversion[c] (de)
1	Camphorsulfonic Acid	$CDCl_3$	4 h	~ 50% (36%)
2	Camphorsulfonic Acid	CD_2Cl_2	4 h	~ 55% (36%)
3	Camphorsulfonic Acid	C_6D_6	4 h	~ 25% (36%)
4	Dibenzoyl-L-Tartaric Acid	$CDCl_3$	4 h	~ 40% (36%)
5	Dibenzoyl-L-Tartaric Acid	CD_2Cl_2	4 h	~ 45% (36%)
6	Dibenzoyl-L-Tartaric Acid	C_6D_6	4 h	~ 40% (42%)
7	L-Lactic Acid	$CDCl_3$	4 h	~ 30% (36%)
8	L-Lactic Acid	CD_2Cl_2	4 h	~ 35% (36%)
9	L-Lactic Acid	C_6D_6	4 h	~ 30% (42%)

[a] All reactions performed in NMR tubes: **12** (5.34×10^{-5} mol), $HPPh_2$ (5.61×10^{-5} mol), and 0.6 mL $CDCl_3$ at 25°C. [b] All C_6D_6 reactions were sonicated for 30 min to dissolve catalysts. [c] Determined by ^{31}P NMR. The extent of reaction was measured before reaction went to completion to compare the activities of catalysts.

Separation of the diastereomers of **13** was easily performed by fractional crystallization from toluene/methanol solution. Slow recrystallization of the separated diastereomers led to X-ray quality crystals and the solid-state structure of the minor diastereomer was determined and is shown in Figure 2.6. The X-ray analysis provided the unambiguous identification of the absolute configuration about C(2) as the *S* configuration. The minor diastereomeric product formed was therefore **(*S*)-13** and the major product was **(*R*)-13**. It must be noted that in most cases, the production of enantiopure phosphine ligands has required the resolution of racemates. While several

methods of resolution have been developed, they are laborious in nature and often require the use of stoichiometric amounts of chiral metal complexes, which are very expensive, as the resolving agent.[23] Here, the synthetic pathway has led to the development of a scheme that can be utilized in the preparation of a variety of enantiopure phosphines with ease.

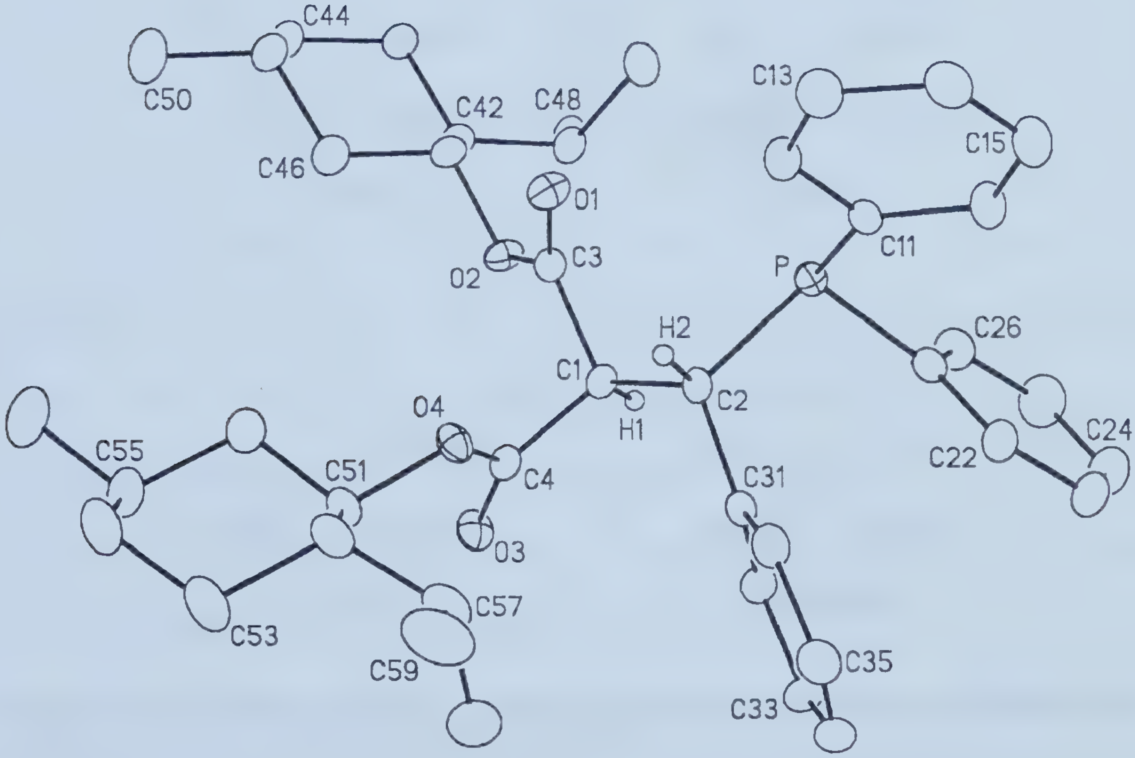
C44
C50
C42
C48
C13
C46
C15
O1
C3
C11
O2
P
H2
C26
C1
O4
C2
H1
C24
C55
C51
C4
C31
C22
O3
C57
C35
C53
C59
C33

Figure 2.6: Perspective view of (*S*)-13 showing the atom labeling scheme. Non-hydrogen atoms are represented by Gaussian ellipses at the 20% probability level. Hydrogen atoms[27] H(1) and H(2) are shown with arbitrarily small thermal parameters, all other hydrogens are not shown.

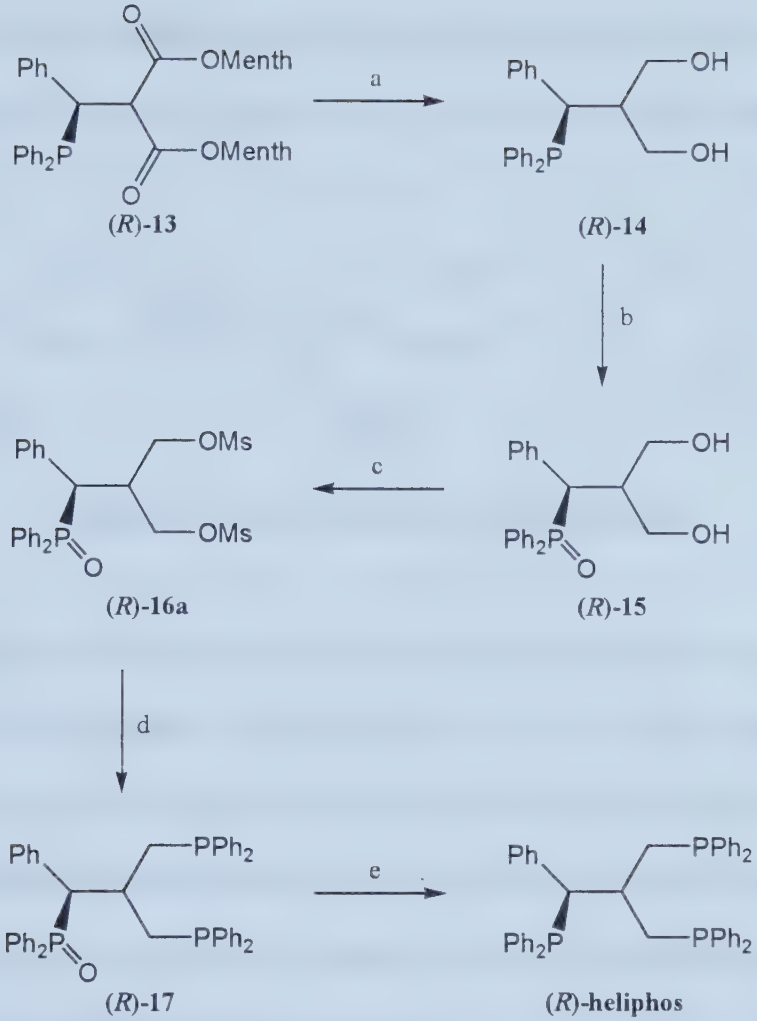
Ph
Ph2P
OMenth
OMenth
(R)-13
a
Ph
Ph2P
OH
OH
(R)-14
b
Ph
Ph2P
O
OH
OH
(R)-15
c
Ph
Ph2P
O
OMs
OMs
(R)-16a
d
Ph
Ph2P
O
PPh2
PPh2
(R)-17
e
Ph
Ph2P
PPh2
PPh2
(R)-heliphos

a) $LiAlH_4$, Et_2O. b) 10% H_2O_2, CH_2Cl_2. c) NEt_3, CH_2Cl_2, CH_3SO_2Cl, -35°C to r.t. d) KH, $HPPh_2$, THF, -10°C to r.t. e) Glass bomb, N(*n*-Bu)$_3$, $SiHCl_3$, 140°C, 96 h.

Scheme 2.2: Synthetic pathway to (*R*)-heliphos. (*S*)-heliphos is prepared by starting with (*S*)-13.

The remaining steps in the synthesis of heliphos were carried out with both (***R***)-**13** and (***S***)-**13** being used independently of each other (Scheme 2.2). The pure diastereomer of **13** was reduced with lithium aluminum hydride to produce the phosphine-diol **14**. Attempts to directly react **14** with two equivalents of mesyl chloride in the presence of

[illegible]

[illegible]

[illegible]

triethylamine did not produce the expected product **16b**. Instead, ^1H and ^{31}P NMR analysis of the reaction suggested that **18** had formed via intramolecular attack of the phosphine of **16b**, displacing a mesyl group, and forming cyclic compounds like **18** (Scheme 2.3).

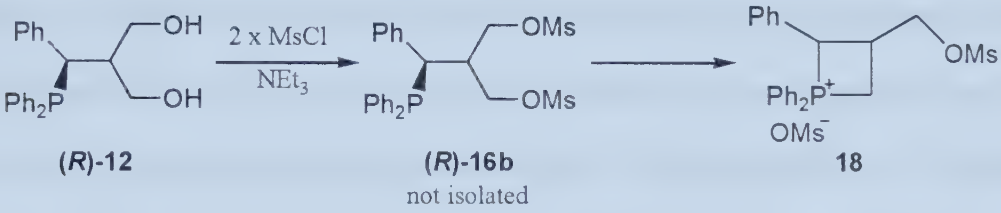

Scheme 2.3: Intramolecular phosphine attack.

The decision to oxidize **14** to the phosphine oxide **15** was made with the anticipation that the phosphine would no longer have a free electron pair available to displace either mesyl group upon formation of **16a**. The phosphine diol **14** was oxidized with 10% hydrogen peroxide to produce the (phosphine oxide)-diol (**15**) in 89% yield. Reaction of **15** with two equivalents of mesyl chloride in the presence of triethylamine produced the desired dimesylate **16a** in 86% yield.

The formation of **17** by displacement of the mesyl groups with diphenylphosphine was performed by inverse addition of **16a** to potassium diphenylphosphide, avoiding intramolecular displacement of a mesyl group. The preliminary synthesis of **17** used a 10% molar excess of potassium hydride to ensure complete formation of potassium diphenylphosphide from diphenylphosphine. However, ^{31}P NMR analysis of the product, in methylene chloride-d_2 solution containing (*R*)-(+)-1,1'-bi-2-naphthol, determined that the resultant bis(phosphine) **17** had been partially racemized (~20%). The addition of the (*R*)-(+)-1,1'-bi-2-naphthol forms diastereomeric salts with **17** that are distinguishable by

their ^{31}P NMR chemical shifts. The use of excess potassium hydride left unreacted hydride in the reaction mixture with **16a** and **17**. It is likely that this excess hydride source deprotonates the acidic benzylic proton (α-methylene proton of phosphine) of **16a** and/or **17** thus causing the partial racemization of the product. The racemization of **17** was averted by using an excess of **12** and diphenylphosphine to potassium hydride (1:1:0.95), ensuring that no excess free hydride, or strong base, was present in solution. Confirmation of the enantiopurity was obtained by the ^{31}P NMR analysis of **17** with (*R*)-(+)-1,1'-bi-2-naphthol, as well as with the X-ray solid-state structure determination. X-ray analysis of the product obtained from reaction of **(*R*)-16a** unambiguously assigned the bis(phosphine)-mono(phosphine oxide) product **17** as being in the *R* absolute configuration at C(1) as expected (Figure 2.7).

Finally, enantiomerically pure heliphos was obtained by reducing **17** with trichlorosilane in the presence of tributylamine at 140 °C over four days in a sealed pressure reactor. The optical purity of (*R*)-heliphos was determined upon oxidation to (*R*)-heliphos tris(phosphine oxide) followed by addition of six equivalents of (*R*)-(+)-1,1'-bi-2-naphthol in chloroform-*d* resulting in three peaks in the ^{31}P NMR spectrum. Addition of (*S*)-heliphos tris(phosphine oxide) resulted in three new peaks, indicating that (*S*)-heliphos was absent from the (*R*)-heliphos reaction mixture. The optical purity of (*S*)-heliphos was determined in an analogous manner.

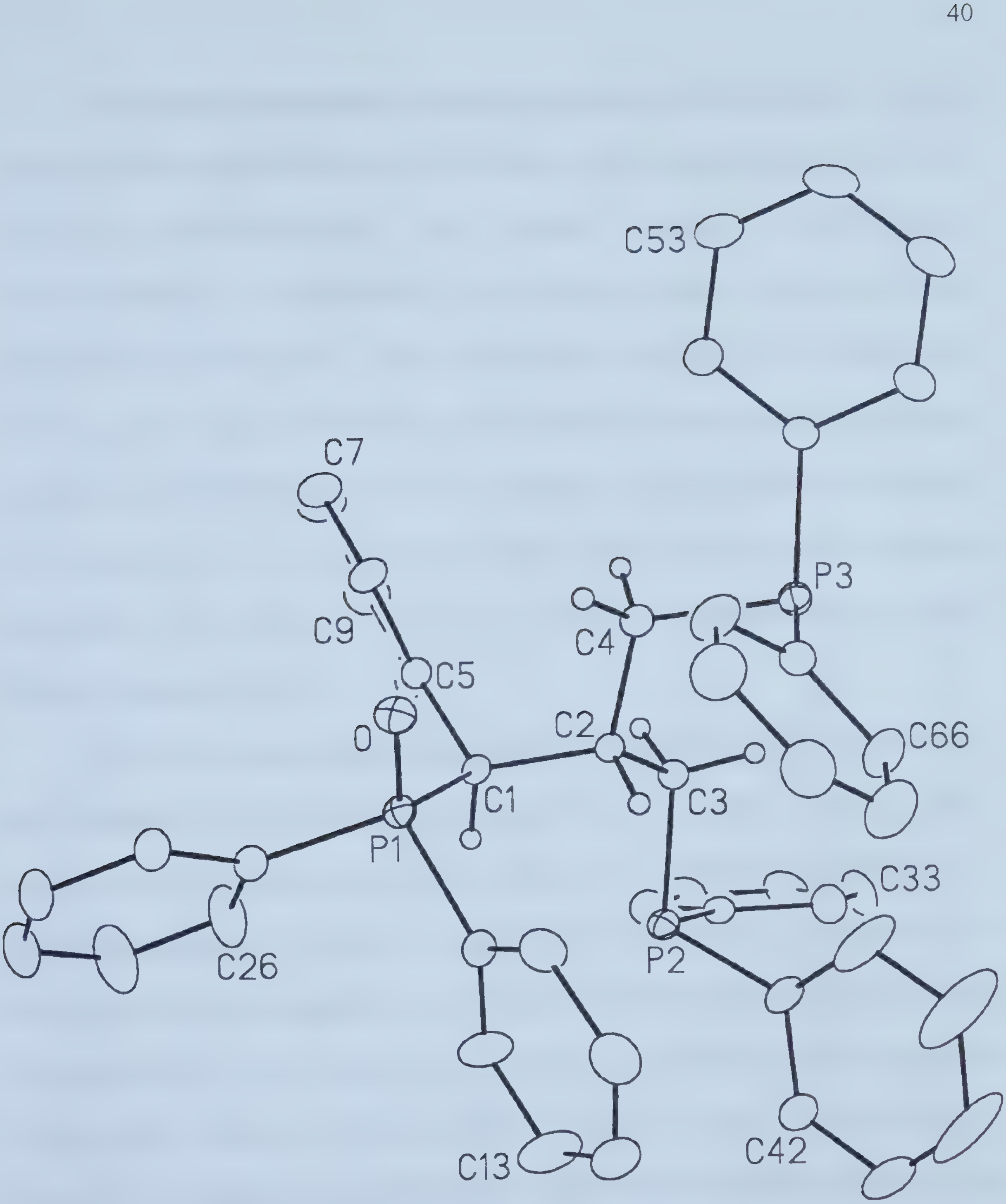
C53
C7
P3
C9
C4
C5
C2
C66
O
C1
C3
P1
C33
C26
P2
C13
C42

Figure 2.7: Perspective view of (*R*)-$C_6H_5CH[P(O)Ph_2]CH(CH_2PPh_2)_2$ ((*R*)-17) showing the atom labeling scheme. Non-hydrogen atoms are represented by Gaussian ellipses at the 20% probability level. Hydrogen atoms[27] are shown with arbitrarily small thermal parameters for the aliphatic (C(1), C(2), C(3), C(4)), and are not shown for the phenyl groups.

Rhodium(I) norbornadiene complexes of triphos and (*R*)-heliphos. The Rh(I) complex [Rh(triphos)(NBD)](ClO_4) (**19**) was prepared as a model complex by reaction of triphos with [Rh$(NBD)_2$](ClO_4). The methylene protons of Λ- and Δ-triphos ($CH_3C(CH_2PPh_2)_3$) are diastereotopic, and exchange magnetic environments upon interconversion between the Λ- and Δ-conformations (Figure 2.5). To determine if interconversion between coordinated Λ- and Δ-triphos was rapid, the ^{1}H NMR spectrum of [Rh(triphos)(NBD)](ClO_4) at -80 °C in methylene chloride-d_2 solution was recorded. The signals could not be separated for the diastereotopic methylene protons indicating that interconversion between Λ- and Δ-triphos was rapid on the NMR time-scale even at the low temperature of -80 °C.

The Rh(I) complex [Rh((*R*)-heliphos)(NBD)](ClO_4) ((*R*)-**20**) was prepared by the slow addition of (*R*)-heliphos to [Rh$(NBD)_2$](ClO_4) in methylene chloride solution. Coordination of the three phosphines was confirmed by ^{31}P NMR analysis (Figure 2.8). All three phosphines were shifted downfield from "free" heliphos, as expected upon coordination, and each phosphorus was coupled to the rhodium metal center and both the other phosphines, which can only occur with tridentate coordination. Slow evaporation of methanolic solutions of (*R*)-**20** yielded X-ray quality crystals that were used to determine the solid-state structure shown in Figure 2.9. The framework of (*R*)-**20** adopted the predicted Λ-configuration in the solid-state, with the Rh-P-C(methylene)-C(10) torsional angles ranging from 35.1(7)° through 27.9(6)°. These values are comparable to those for other coordinated triphos-type ligands.[20] The distances (in Å) between the plane containing the phosphorus atoms and the *ipso*-carbons of the axial

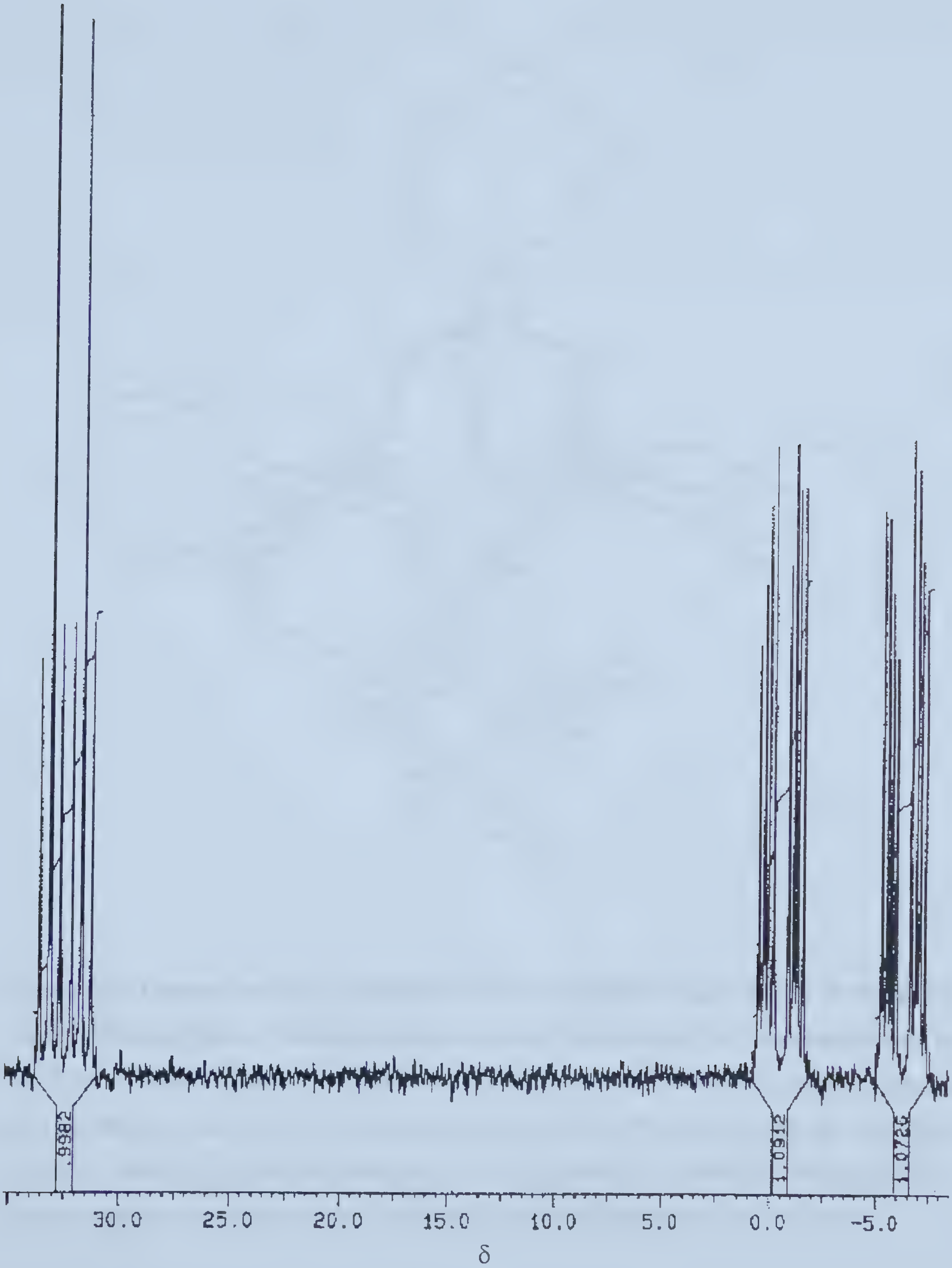

Figure 2.8: $^{31}P\{^1H\}$ NMR of [Rh((*R*)-heliphos)(NBD)](ClO_4) (methylene chloride-d_2).

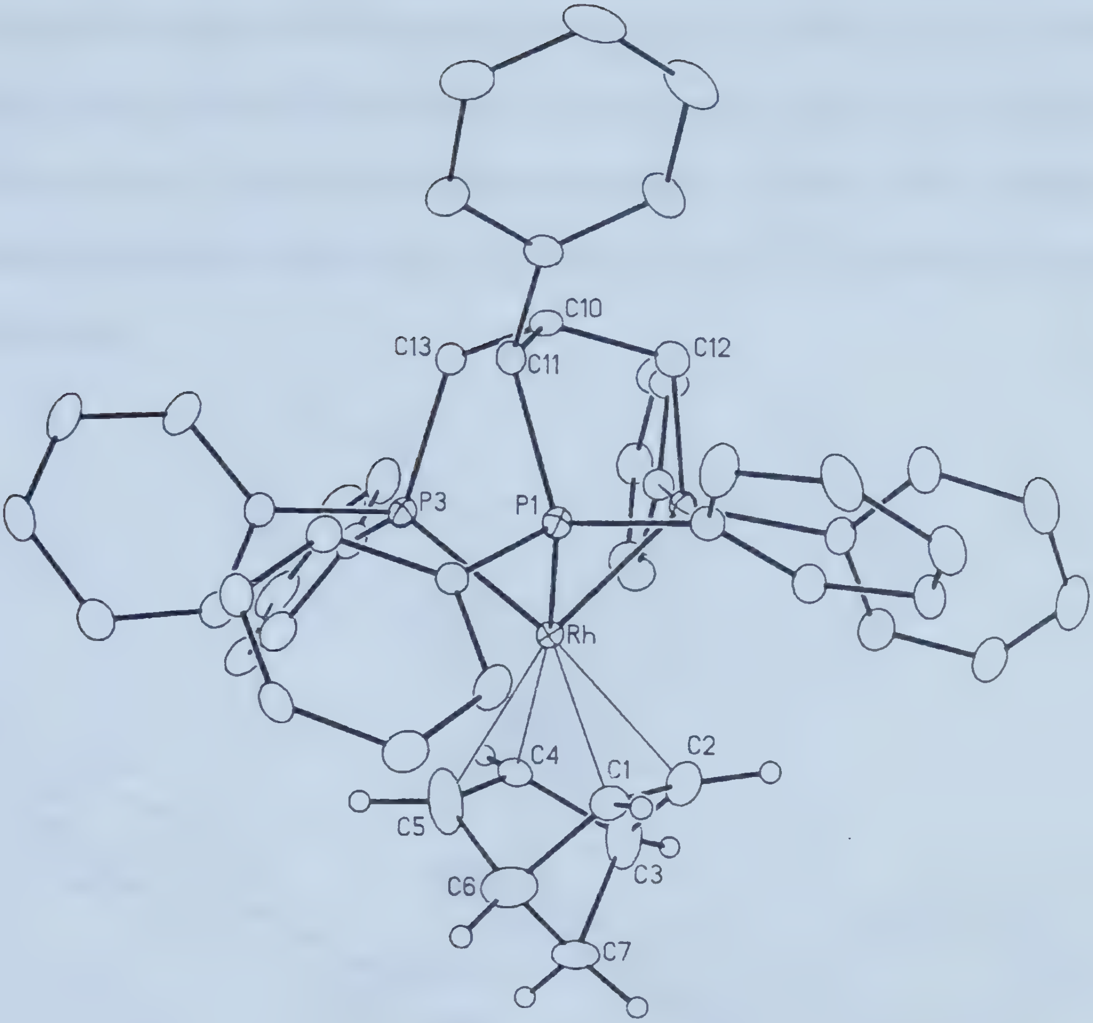

Figure 2.9: Perspective view of [Rh((*R*)-heliphos)(NBD)](ClO_4) ((*R*)-20) showing the atom labeling scheme. Non-hydrogen atoms are represented by Gausiian ellipses at the 20% probability level. Selected bond lengths (Å) and torsional angles (degrees) are as follows; Rh-P(1), 2.352(2); Rh-P(2), 2.376(2); Rh-P(3), 2.308(2); Rh-C(1), 2.216(7); Rh-C(2), 2.254(10); Rh-C(4), 2.177(7); Rh-C(5), 2.260(13); Rh-P(1)-C(11)-C(10), -30.6(6); Rh-P(2)-C(12)-C(10), -35.1(7); Rh-P(3)-C(13)-C(10), -27.9(6).

[illegible]

phenyl rings are 0.474(8) (C(31)), 0.372(9) (C(61)), and 0.415(9) (C(81)). The corresponding distances for the equatorial phenyl rings are -0.21(8) (C(41)), -0.168(9) (C(61)), and -0.107(8) (C(71)) (inclinations towards the ligand framework are assigned a negative value). Figure 2.10 shows the propeller-like asymmetric array of pendent phenyl rings around the rhodium center, with alternating axial and equatorial orientations as designed.

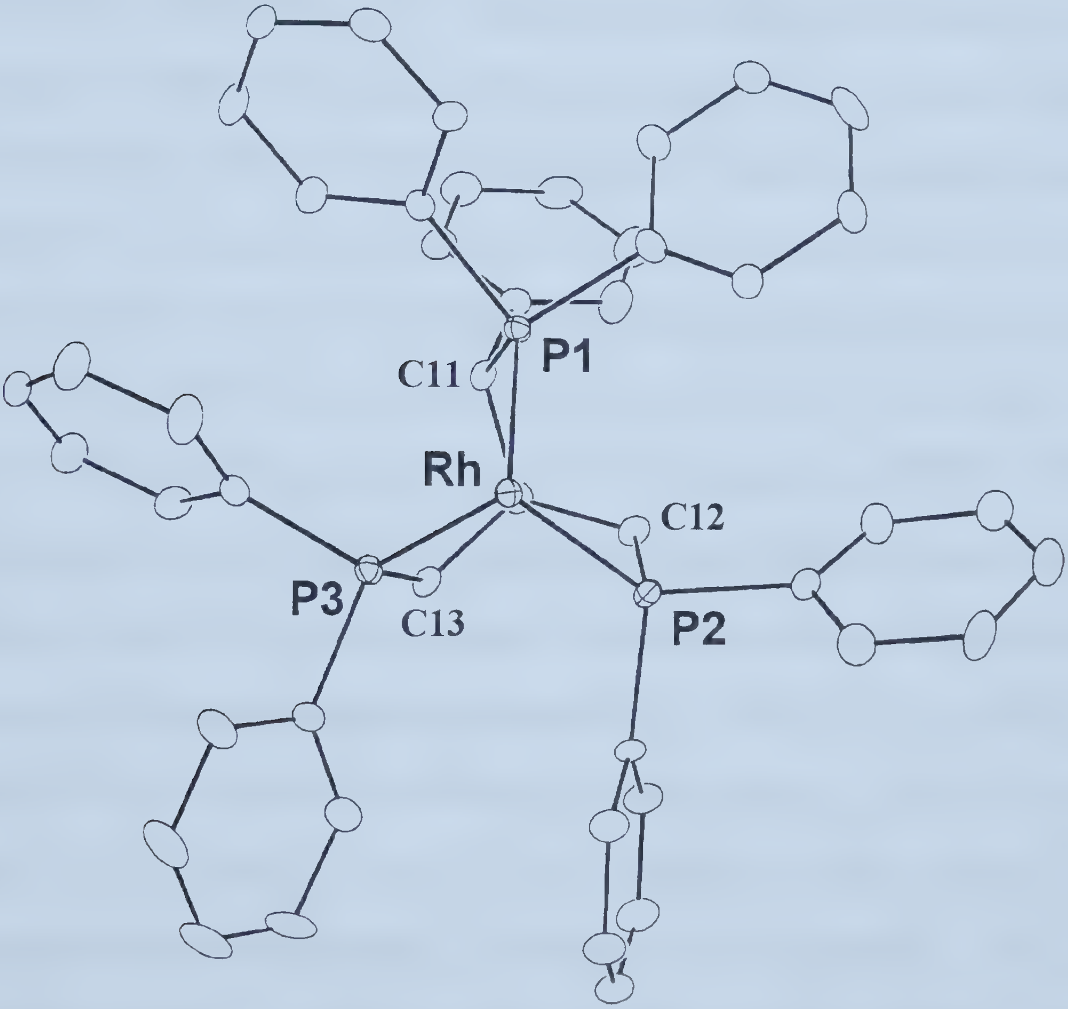

Figure 2.10: Perspective view of [Rh((*R*)-heliphos)(NBD)](ClO_4) ((*R*)-20) showing the arrangement of phenyl groups as viewed by the active sites on the metal (NBD is omitted for clarity). Non-hydrogen atoms are represented by Gaussian ellipses at the 20% probability level.

It is likely that the framework of $[Rh((R)\text{-heliphos})(NBD)](ClO_4)$ strongly favors the Λ-conformer in solution for two reasons. First, the pro-*S* (assuming replacement by a phenyl ring) protons at C(12) and C(13) of Λ-(*R*)-heliphos are oriented towards an adjacent arm's equatorial phenyl ring. This orientation is similar to that of the framework phenyl ring in the unfavored Δ-(*R*)-heliphos (Figure 2.5). For both C(12) and C(13),[24] the ^1H NMR signal for the pro-*S* proton was shifted upfield from the pro-*R* by approximately 0.9 ppm (Figure 2.11). This difference in chemical shift was likely caused by ring current effects of the equatorial phenyl group and indicated that interconversion with appreciable amounts of Δ-(*R*)-**17** did not occur. Second, the coupling constants between the apical proton (at C(10)) and the two pro-*R* methylene protons (at C(12) and C(13)) were approximately 7 Hz, while those with the three pro-*S* methylene protons (at C(11), C(12), and C(13)) were approximately 0 Hz (Figure 2.12). According to the Karplus relationship,[25] a coupling constant of 0 Hz corresponds to $H^{\alpha(C(10))}$ - $H^{\beta(\text{pro-}S)}$ dihedral angles of approximately 90°. These angles are supported by those obtained from molecular models (90°), and the calculated[26] hydrogen atom positions in the crystal structure of Λ-$[Rh((R)\text{-heliphos})(NBD)](ClO_4)$ ($H^{\alpha(C(10))}$ - $H^{\beta(\text{pro-}S)(C(11))} = 87°$, $H^{\alpha(C(10))}$ - $H^{\beta(\text{pro-}S)(C(12))} = 82°$, $H^{\alpha(C(10))}$ - $H^{\beta(\text{pro-}S)(C(13))} = 75°$). For comparison, it is noted that the signals for the methylene protons in the published ^1H NMR spectrum of $[Fe(CH(CH_2PPh_2)_3)(NCCH_3)_3](BPh_4)_2$ coincided at room temperature, and the corresponding $H^{\alpha(\text{apical})}$ - $H^{\beta(\text{methylene})}$ coupling constants were approximately 4 Hz.[20b] These data show that the framework of $[Fe(CH(CH_2PPh_2)_3)(NCCH_3)_3](BPh_4)_2$ is conformationally fluxional and that 4 Hz is the averaged coupling constant of the two environments.

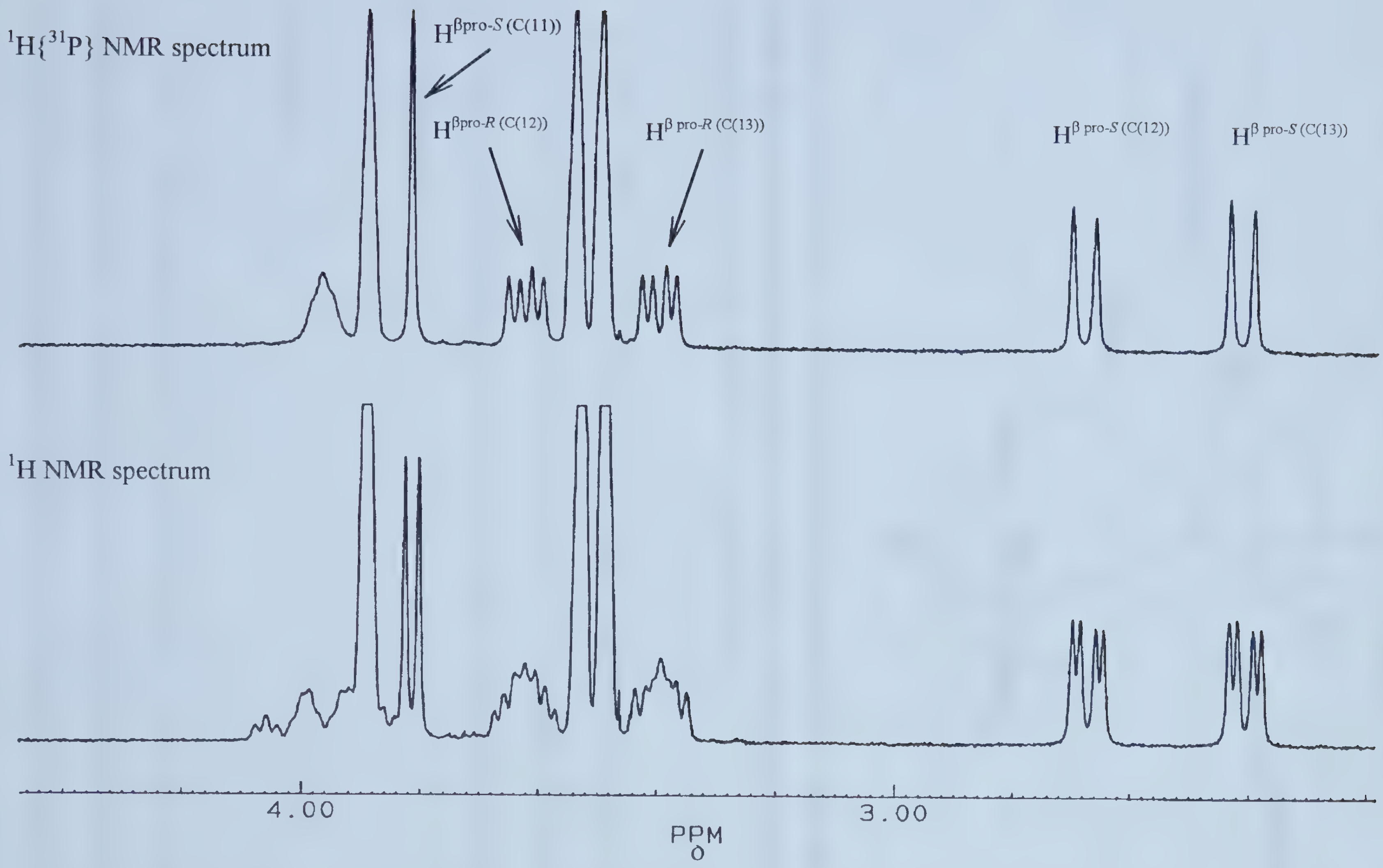

Figure 2.11: Expanded region of ^1H NMR spectrum of [Rh((*R*)-heliphos)(NBD)](ClO_4) in methylene chloride-d_2.

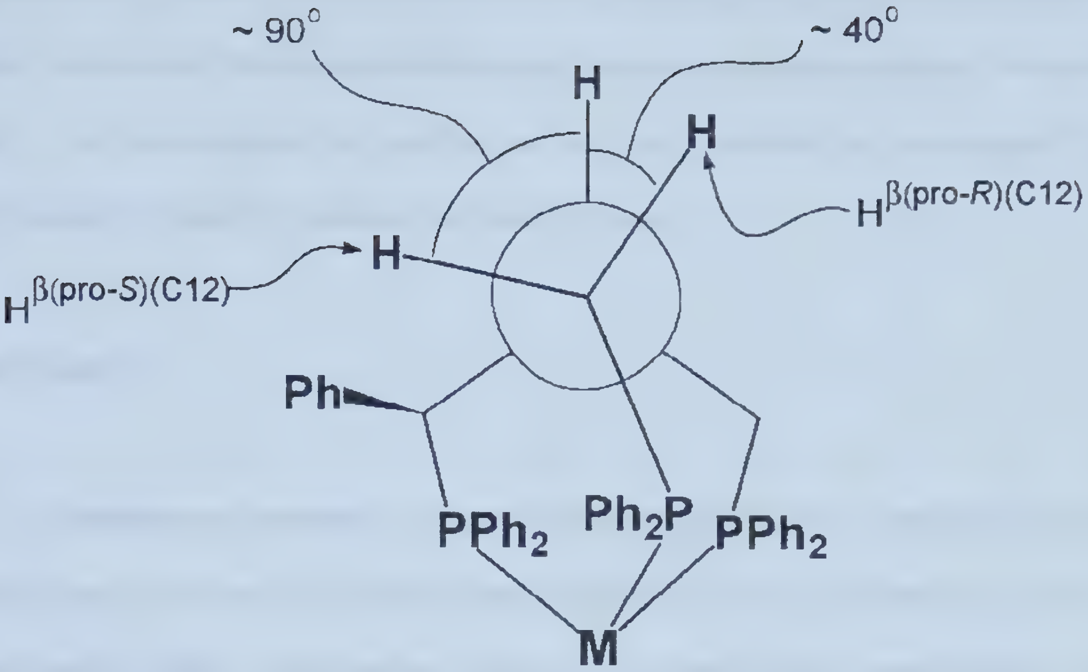
~ 90°
~ 40°
H
H
$H^{\beta(\text{pro-}R)(C12)}$
$H^{\beta(\text{pro-}S)(C12)}$
H
Ph
PPh$_2$
Ph$_2$P
PPh$_2$
M

Figure 2.12: Depiction of coordinated (*R*)-heliphos in (*R*)-20 (M = Rh) showing the angles between the apical proton (H(10)) and the pro-*S* and pro-*R* protons of the phosphine arms (specifically $H^{\beta(\text{pro-}S)(C(12))}$ and $H^{\beta(\text{pro-}R(C(12))}$).

The NMR studies could not exclude a rapid equilibrium with small amounts of the Δ-, or some intermediate conformer in solution. It is unlikely, however, that the severe steric repulsions predicted by models of Δ-[Rh((*R*)-heliphos)(NBD)](ClO$_4$) would allow its formation.

Conclusions:

The chiral tris(phosphines) (*R*)- and (*S*)-heliphos were easily prepared in enantiomerically pure form. It appears that the predicted locked helical conformations of (*R*)- and (*S*)-heliphos in [Rh(heliphos)(NBD)](ClO$_4$) were adopted in both the solution

and solid-state. Further, the asymmetric array of pendent phenyl rings around the metal center contains axial phenyl groups that project towards the spatial domains of the active sites. The determination of whether or not this projection is enantiogenic[27] in enantioselective catalytic reactions must be investigated.

Experimental:

Materials and methods. The solvents *n*-hexane (K, Ph_2CO), methylene chloride (CaH_2), tetrahydrofuran (K, Ph_2CO), diethyl ether (K, Ph_2CO), toluene (K, Ph_2CO), triethylamine (CaH_2), tributylamine (CaH_2), and xylenes (CaH_2) were distilled from drying agents under argon gas, except methanol which was deoxygenated by bubbling with argon gas or dinitrogen gas for 1 h. The argon and dinitrogen gases were passed through a bed of Drierite drying agent. Unless stated otherwise, commercial reagents were used without further purification and all operations were performed under an inert atmosphere of argon or dinitrogen gas. Dr. Robert McDonald performed all solid-state structure determinations.

All ^{1}H, ^{13}C, and ^{31}P NMR spectra were measured with a Bruker AM-400 NMR spectrometer operating at 400.13 MHz, 100.61 MHz, and 161.97 MHz respectively. ^{1}H and ^{13}C NMR chemical shifts are reported in parts per million (δ) relative to tetramethylsilane using the solvent as an internal reference. ^{31}P NMR chemical shifts are reported in parts per million (δ) relative to an 85% H_3PO_4 external reference. Mass spectra were measured using Kratos MS50 or AEI MS9 mass spectrometers. Microanalyses were performed at the University of Alberta Microanalysis Laboratory.

Optical rotations were measured with a Perkin-Elmer 241 polarimeter at 589 nm (sodium D line) using 1.0 dm cells. Specific rotations, $[\alpha]_D$, are reported in degrees per decimeter at 25 °C, and the concentration (c) is given in grams per 100 mL. Melting points were measured with a Gallenkamp capillary melting point apparatus and are uncorrected.

$CH_2(C(O)OMenth)_2$, 11 (Menth = (1*R*, 2*S*, 5*R*)-(-)-menthol). In air, (1*R*, 2*S*, 5*R*)-(-)-menthol (155.14 g, 1.05 mol) was transferred to a 500 mL 3-neck flask. The flask was flushed with Ar then heated to 100 °C to melt the menthol. Once melted, small slices of sodium metal were added (0.389 g, 16.9 mmol), the solution was stirred until all the sodium had reacted and was in solution. Once the solution became homogeneous, dimethyl malonate (28.4 mL, 0.248 mol) was added via syringe. The solution was heated to 145 °C and stirred for 1 h. The solution was cooled to room temperature. The flask had a distillation head, condenser, and vacuum take-off flask placed over the center neck. The flask was placed under reduced pressure and heated to 120 °C to distill off the unreacted menthol. The remaining residue was dissolved in toluene (~300 mL) and transferred to a 1 L separatory funnel. The solution was washed with 1N HCl (2 x 50 mL) until acidic to litmus. The aqueous layer was discarded and the organic layer was then washed with saturated $NaHCO_3$ (100 mL) and saturated NaCl (100 mL). The organic layer was then stirred over $MgSO_4$, filtered, and concentrated under reduced pressure. The solid was recrystallized from methanol to afford **11** as pure white needle-shaped crystals in 72.8% yield (68.72 g). NMR data correspond to those previously reported.[28]

$C_6H_5CH{=}C(C(O)OMenth)_2$, 12 (Menth = (1*R*, 2*S*, 5*R*)-(-)-menthol). In air, **11** (33.102 g, 87.1 mmol), dissolved in benzene (120 mL), was sequentially treated with acetic acid (1.0 mL, 17.4 mmol), piperidine (0.35 mL, 3.5 mmol), and benzaldehyde (10.0 mL, 95.8 mmol) in an azeotropic distillation apparatus. The mixture was refluxed at 120 °C for 1.5 h, then at 130 °C for an additional 24 h. The solution was then cooled to room temperature, benzene (100 mL) was added, and the resultant yellow-red solution was washed with 1 N HCl (2 x 100 mL), saturated $NaHCO_3$ (100 mL), and saturated NaCl (150 mL). The organic layer was dried over Na_2SO_4, filtered, and concentrated under reduced pressure affording a yellow-white solid. The solid was recrystallized from methanol to afford **12** as pure white needle-shaped crystals in 89.5 % yield (36.53 g): m.p 103-104 °C; ^{1}H NMR ($CDCl_3$): δ 0.70-0.95 (m, 21 H), 1.05 (m, 3 H), 1.39 (m, 2 H), 1.50 (m, 2 H), 1.67 (br, 4 H), 1.81 (quint-d, J = 6.9, 2.6 Hz , 1 H), 1.92 (quint-d, J = 6.9, 2.6 Hz, 1 H), 2.07 (br d, J = 12.0 Hz, 1 H), 2.13 (br d, J = 12.0 Hz, 1 H), 4.85 (ddd, J = 24.4, 10.9, 4.4 Hz, 2 H), 7.25-7.40 (br, 3 H), 7.48 (m, 2 H), 7.68 (s, 1 H); ^{13}C NMR ($CDCl_3$): δ 15.87, 16.13, 20.81, 20.90, 22.00, 22.03, 22.91, 23.19, 25.35, 25.97, 31.32, 31.39, 34.07, 34.30, 40.22, 40.86, 46.70, 47.25, 75.39, 75.53, 127.31, 128.56, 129.40, 130.21, 133.02, 141.02, 163.59, 166.32. HRMS (EI). Calcd for $C_{30}H_{44}O_4$: 468.3240. Found: 468.3224. Anal. Calcd for $C_{30}H_{44}O_4$: C, 76.94; H, 9.47. Found: C, 76.79; H, 9.62.

$C_6H_5CH(PPh_2)CH(C(O)OMenth)_2$, (*R*)-13 and (*S*)-13. A solution of **12** (10 g, 21.3 mmol), *p*-toluenesulfonic acid monohydrate (0.10 g, 0.53 mmol), and diphenylphosphine (4.05 g, 21.8 mmol) in methylene chloride (100 mL) was stirred at

room temperature for 72 h. The solution was stirred over $NaHCO_3$ (1 g) for 2 h, filtered, washed with toluene (3 x 10 mL), and concentrated under reduced pressure to afford a white solid in 100% yield (13.97 g). The solid was determined to be a mixture of both ***(R)*-13** and ***(S)*-13** in a 70 : 30 ratio. The solid was dissolved in toluene (20 mL) and methanol was added (300 mL) under reflux. White needle-like crystals of ***(R)*-13** crystallized overnight and were isolated by filtration and washed with cold methanol (20 mL, 0 °C). The filtrate was concentrated under reduced pressure affording a white solid which was dissolved in boiling methanol (300 mL) and concentrated to 200 mL for crystallization. Solid cube-like crystals of (*S*)-**13** were isolated by filtration and washed with cold methanol (20 mL, 0 °C). The filtrate was concentrated (~1/2 volume) and fractional crystallization afforded more (*R*)-**13** and (*S*)-**13**. The combined portions of (*R*)-**13** were recrystallized from toluene and methanol (1 : 20) affording white needle-like crystals of (*R*)-**13** in 80.1% yield (7.83 g): m.p 96 °C (oxidized); ^1H NMR (400 MHz, $CDCl_3$, 25 °C): δ 0.41 (d, J = 6.9 Hz, 3 H), 0.62 (q, 1 H), 0.70-0.80 (m, 10 H), 0.83-1.10 (m, 10 H), 1.18-1.35 (m, 2 H), 1.42-1.63 (m, 6 H), 1.69 (m, 2 H), 1.91 (m, 2 H), 3.94 (dd, $J_{H\text{-}H}$ = 12.1 Hz, $J_{P\text{-}H}$ = 6.3 Hz, 1 H), 4.39 (d, J = 12.1 Hz, 1 H), 4.45 (td, J = 4.4 Hz, 10.9 Hz, 1 H), 4.80 (td, J = 4.4 Hz, 10.9 Hz, 1 H), 6.68 (d, J = 7.2 Hz, 2 H), 6.91-7.03 (m, 3 H), 7.04-7.09 (m, 2 H), 7.13-7.18 (m, 2 H), 7.25-7.36 (m, 4 H), 7.55 (m, 2 H); ^{13}C NMR (400 MHz, $CDCl_3$, 25 °C): δ 15.69, 15.98, 20.84, 20.94, 21.98, 22.06, 22.93, 23.09, 25.50, 25.67, 31.20, 31.45, 34.12, 34.27, 40.05, 40.51, 44.93 (d, $J_{P\text{-}C}$ = 21.6 Hz), 46.60, 47.06, 56.73 (d, $J_{P\text{-}C}$ = 31.8 Hz), 75.38, 75.91, 126.20, 127.54, 127.82, 127.90, 128.21, 128.26, 128.36, 128.73, 129.42, 132.65, 132.82, 134.04 (d, $J_{P\text{-}C}$ = 14.8 Hz), 135.52, 135.75, 135.88 (d, $J_{P\text{-}C}$ = 14.8 Hz), 137.59, 166.93 (d, $J_{P\text{-}C}$ = 19.2 Hz), 167.78.; ^{31}P NMR

(400 MHz, $CDCl_3$, 25 °C): δ 4.36 (s). HRMS (EI). Calcd for $C_{42}H_{55}O_4P$: 654.3838. Found: 654.3838. Anal. Calcd for $C_{42}H_{55}O_4P$: C, 77.03; H, 8.47. Found: C, 77.04; H, 8.73. The combined portions of (*S*)-**13** were recrystallized from pure methanol affording solid white cubes of (*S*)-**13** in 63.9% yield (2.68 g): m.p 95 °C (oxidized); ^1H NMR (400 MHz, $CDCl_3$, 25 °C): δ 0.45 (d, J = 5.9 Hz, 3 H), 0.65-1.00 (m, 20 H), 1.08 (m, 1 H), 1.25 (m, 2 H), 1.35 -1.65 (m, 6 H), 1.70 (m, 2 H), 2.08 (m, 2 H), 3.92(dd, $J_{H\text{-}H}$ = 11.8 Hz, $J_{P\text{-}H}$ = 8.7 Hz, 1 H), 4.39 (d, J = 11.8 Hz, 1 H), 4.51(td, J = 4.4, 10.9 Hz, 1 H), 4.80 (td, J = 4.4, 10.9 Hz, 1 H), 6.64 (d, J = 7.3 Hz, 2 H), 6.95-7.10 (m, 5 H), 7.15 (m, 2 H), 7.25-7.36 (m, 4 H), 7.55 (m, 2 H); ^{13}C NMR (400 MHz, $CDCl_3$, 25 °C): δ 15.74, 16.49, 20.92, 21.88, 22.06, 22.92, 23.43, 25.33, 26.19, 31.20, 31.38, 34.10, 34.30, 40.26, 40.42, 45.13 (d, $J_{P\text{-}C}$ = 23.3 Hz), 46.64, 46.97, 56.43 (d, $J_{P\text{-}C}$ = 32.1 Hz), 75.29, 75.97, 126.23, 127.58, 127.81, 127.89, 128.12, 128.22, 128.27, 128.60, 128.62, 129.61, 132.38, 132.55, 133.64 (d, $J_{P\text{-}C}$ = 16.3 Hz), 135.79, 136.02, 136.52(d, $J_{P\text{-}C}$ = 15.4 Hz), 137.51, 167.21 (d, $J_{P\text{-}C}$ = 19.5 Hz), 167.81; ^{31}P NMR (400 MHz, $CDCl_3$, 25 °C): δ 7.92 (s). HRMS (EI). Calcd for $C_{42}H_{55}O_4P$: 654.3838. Found: 654.3878. Anal. Calcd for $C_{42}H_{55}O_4P$: C, 77.09; H, 8.47. Found: C, 76.99; H, 8.47.

Crystallographic analysis of (*S*)-$C_6H_5CH(PPh_2)CH(C(O)OMenth)_2$, (*S*)-13. Suitable crystals for X-ray diffraction study were obtained by slow evaporation of methanol solutions of (*S*)-$C_6H_5CH(PPh_2)CH(C(O)OMenth)_2$ under a stream of argon gas. The crystal system was monoclinic, and the space group $P2_1$ (No. 4), which was consistent with an enantiomerically pure compound. Crystal data, details of data

collection, and structure solution and refinement are outlined in Table 2.3. Selected bond distances and angles are outlined in Table 2.4 and Table 2.5.

(*R*)- and (*S*)-$C_6H_5CH[P(O)Ph_2]CH(CH_2OH)_2$, (*R*)- and (*S*)-15. To a stirred mixture of $LiAlH_4$ (1.08 g, 28.46 mmol) and ether (100 mL) was added dropwise a solution of (*R*)-**13** (6.50 g, 9.47 mmol) in ether (100 mL) at 0 °C over 10 min. The dropping funnel was rinsed with ether (50 mL), the reaction mixture was stirred for 20 min at 0 °C, and then for an hour at room temperature. The $LiAlH_4$ was neutralized by the dropwise addition of 1.1 mL of deoxygenated distilled water, 1.1 mL of deoxygenated 10% NaOH solution at 0 °C, and 3.3 mL of deoxygenated distilled water at room temperature. The mixture was stirred for 30 min, filtered, washed with methylene chloride (3 x 100 mL), and concentrated under reduced pressure yielding a white solid. The solid was recrystallized from toluene (100 mL) affording white crystals of the phosphine-diol ((*R*)-**14**). The phosphine-diol was dissolved in methylene chloride (400 mL, undistilled) and oxidized by adding a solution of 10% H_2O_2 (35 mL). The reaction mixture was stirred for 5 min and then washed with a solution of saturated $Na_2S_2O_3$ (50 mL) until the excess H_2O_2 was neutralized (negative result with saturated solution of KI). The organic layer was dried over Na_2SO_4, filtered, and concentrated under reduced pressure affording (*R*)-**15** in 77.3% yield (2.68 g), as a white powder. Further purification was unnecessary: ^1H NMR (400 MHz, $CDCl_3$, 25 °C): δ 2.48 (m, 1 H), 3.25 (m, 2 H), 3.50 (dd, J = 4.9, 10.7 Hz, 1 H), 3.60 (dd, J = 11.8, 8.1 Hz, 1 H), 4.29 (dd, $J_{P\text{-}H}$ = 9.9 Hz, $J_{H\text{-}H}$ = 3.5 Hz, 1 H), 7.10-7.35 (m, 6 H), 7.40-7.60(m, 7 H), 7.92 (m, 2 H); ^{13}C NMR (400 MHz, $CDCl_3$, 25 °C): δ 44.06, 44.75, 60.52, 61.33 ($J_{P\text{-}C}$ = 11.8 Hz), 127.35,

Table 2.3: Crystallographic, experimental, and refinement details for (*S*)-$C_6H_5CH(PPh_2)CH(C(O)OMenth)_2$ ((*S*)-13).

Formula	$C_{42}H_{55}O_4P$
Formula weight	654.83
Crystal dimensions (mm)	0.46 x 0.41 x 0.40
Crystal system	Monoclinic
space group	$P2_1$ (No. 4)
unit cell parameters[a]	
a (Å), b (Å), c (Å)	9.2079 (3), 19.4353 (8), 11.3381 (4)
β (deg), V (Å^3), Z	107.336 (3), 1936.87 (12), 2
ρ_{calcd} (g cm^{-3}), μ (mm^{-1})	1.223, 0.920
Diffractometer	Siemens P4/RA
Radiation (λ [Å])	graphite-monochromated Cu Kα (1.54178)
Temperature (°C)	–60
scan type	θ–2θ
data collection 2θ limit (deg)	115.0
total data collected	5717 ($-10 \le h \le 10$, $-20 \le k \le 19$, $-11 \le l \le 11$)[c]
Independent reflections	5177
Number of observations (*NO*)	4923 ($F_o^2 \ge 2\sigma(F_o^2)$)
Structure solution method	direct methods (SHELXS–86[c])
Refinement method	full-matrix least-squares on F^2 (*SHELXL–93*[d])
Absorption correction method	semi-empirical (ψ scans)
range of transmission factors	0.7129–0.6129
data/restraints/parameters	5177 [$F_o^2 \ge -3\sigma(F_o^2)$] / 0 / 424
Flack absolute structure parameter[e]	0.00 (2)
Goodness-of-fit (*S*)[f]	1.074 [$F_o^2 \ge -3\sigma(F_o^2)$]
final *R* indices[g]	
$F_o^2 > 2\sigma(F_o^2)$	$R_1 = 0.0347$, $wR_2 = 0.0844$
all data	$R_1 = 0.0375$, $wR_2 = 0.0869$
Largest difference peak and hole	0.229 and –0.170 e Å^{-3}

[a] Obtained from least-squares refinement of 48 reflections with $52.0° < 2\theta < 57.4°$. [b] Data were collected from Friedel-opposite quadrants with indices of the form ($+h$ $-k$ $\pm l$) and ($-h$ $+k$ $\pm l$). [c] Sheldrick, G. M. *Acta Crystallogr.* **1990**, *A46*, 467–473. [d] Sheldrick, G. M. *SHELXL-93*. Program for crystal structure determination. University of Göttingen, Germany, 1993. Refinement on F_o^2 for all reflections except for 1 having $F_o^2 > -3\sigma(F_o^2)$. Weighted *R*-factors wR_2 and all goodnesses of fit *S* are based on F_o^2; conventional *R*-factors R_1 are based on F_o, with $F_o$set to zero for negative F_o^2. The observed criterion of $F_o^2 > 2\sigma(F_o^2)$ is used only for calculating R_1, and is not relevant to the choice of reflections for refinement. *R*-factors based on $F_o^2$are statistically about twice as large as those based on F_o, and *R*-factors based on ALL data will be even larger. [e] Flack, H. D. *Acta Crystallogr.* **1983**, *A39*, 876–881. The Flack parameter will refine to a value near zero if the structure is in the correct configuration and will refine to a value near one for the inverted configuration. [f] $S = [\Sigma w(F_o^2 - F_c^2)^2/(n-p)]^{1/2}$ (n = number of data; p = number of parameters varied; $w = [\sigma^2(F_o^2) + (0.0303P)^2 + 0.8272P]^{-1}$ where $P = [\mathrm{Max}(F_o^2, 0) + 2F_c^2]/3$). [g] $R_1 = \Sigma||F_o| - |F_c||/\Sigma|F_o|$; $wR_2 = [\Sigma w(F_o^2 - F_c^2)^2/\Sigma w(F_o^4)]^{1/2}$.

Table 2.4: Selected interatomic distances (Å) for (*S*)-$C_6H_5CH(PPh_2)CH$-$(C(O)OMenth)_2$ ((*S*)-13).

Atom1	Atom2	Distance
P	C2	1.903(2)
P	C11	1.836(2)
P	C21	1.831(3)
O1	C3	1.204(3)
O2	C3	1.337(3)
O2	C41	1.467(3)
O3	C4	1.203(3)
O4	C4	1.336(3)
O4	C51	1.467(3)
C1	C2	1.539(3)
C1	C3	1.519(3)
C1	C4	1.515(3)
C2	C31	1.508(3)
C11	C12	1.384(3)
C11	C16	1.385(3)
C12	C13	1.385(4)
C13	C14	1.373(4)
C14	C15	1.368(4)
C15	C16	1.380(4)
C21	C22	1.396(4)
C21	C26	1.388(4)
C22	C23	1.375(4)
C23	C24	1.374(4)
C24	C25	1.358(5)
C25	C26	1.390(4)
C31	C32	1.388(3)
C31	C36	1.389(3)
C32	C33	1.386(4)
C33	C34	1.380(4)
C34	C35	1.376(5)
C35	C36	1.382(4)
C41	C42	1.513(3)
C41	C46	1.510(4)
C42	C43	1.528(3)
C42	C47	1.543(4)
C43	C44	1.521(4)
C44	C45	1.520(4)
C45	C46	1.521(4)
C45	C50	1.514(4)
C47	C48	1.518(4)
C47	C49	1.515(4)
C51	C52	1.525(4)
C51	C56	1.516(4)
C52	C53	1.532(4)
C52	C57	1.526(4)
C53	C54	1.516(5)
C54	C55	1.529(5)
C55	C56	1.529(4)
C55	C60	1.527(5)
C57	C58	1.519(4)
C57	C59	1.530(4)

Table 2.5: Selected interatomic angles (deg) for (*S*)-$C_6H_5CH(PPh_2)CH$-$(C(O)OMenth)_2$ ((*S*)-13).

Atom1	Atom2	Atom3	Angle	Atom1	Atom2	Atom3	Angle
C2	P	C11	100.66(10)	C31	C32	C33	120.8(3)
C2	P	C21	105.77(11)	C32	C33	C34	119.8(3)
C11	P	C21	103.77(11)	C33	C34	C35	120.0(3)
C3	O2	C41	117.5(2)	C34	C35	C36	120.2(3)
C4	O4	C51	117.4(2)	C31	C36	C35	120.7(3)
C2	C1	C3	110.8(2)	O2	C41	C42	107.2(2)
C2	C1	C4	113.3(2)	O2	C41	C46	109.5(2)
C3	C1	C4	105.9(2)	C42	C41	C46	113.0(2)
P	C2	C1	107.86(14)	C41	C42	C43	107.9(2)
P	C2	C31	115.46(15)	C41	C42	C47	113.4(2)
C1	C2	C31	113.5(2)	C43	C42	C47	114.3(2)
O1	C3	O2	124.7(2)	C42	C43	C44	112.3(2)
O1	C3	C1	125.2(2)	C43	C44	C45	112.7(2)
O2	C3	C1	110.1(2)	C44	C45	C46	109.5(2)
O3	C4	O4	124.9(2)	C44	C45	C50	111.4(2)
O3	C4	C1	124.2(2)	C46	C45	C50	111.8(3)
O4	C4	C1	110.9(2)	C41	C46	C45	111.5(2)
P	C11	C12	118.1(2)	C42	C47	C48	110.8(2)
P	C11	C16	124.2(2)	C42	C47	C49	113.6(2)
C12	C11	C16	117.1(2)	C48	C47	C49	111.4(3)
C11	C12	C13	121.5(2)	O4	C51	C52	108.0(2)
C12	C13	C14	120.1(3)	O4	C51	C56	107.8(2)
C13	C14	C15	119.3(3)	C52	C51	C56	113.4(2)
C14	C15	C16	120.5(3)	C51	C52	C53	106.4(2)
C11	C16	C15	121.5(3)	C51	C52	C57	113.3(2)
P	C21	C22	126.0(2)	C53	C52	C57	115.0(3)
P	C21	C26	116.5(2)	C52	C53	C54	112.2(3)
C22	C21	C26	117.4(2)	C53	C54	C55	113.2(3)
C21	C22	C23	121.3(2)	C54	C55	C56	108.9(3)
C22	C23	C24	120.0(3)	C54	C55	C60	112.5(3)
C23	C24	C25	120.2(3)	C56	C55	C60	111.6(3)
C24	C25	C26	120.3(3)	C51	C56	C55	110.4(3)
C21	C26	C25	120.8(3)	C52	C57	C58	113.9(2)
C2	C31	C32	122.2(2)	C52	C57	C59	112.0(3)
C2	C31	C36	119.3(2)	C58	C57	C59	110.3(3)
C32	C31	C36	118.5(2)				

128.14, 128.25, 128 41, 128.82, 128.94, 130.92, 131.04, 131.23, 131.31, 131.36, 131.92, 132.11, 132.91 (J_{P-C} = 3.1 Hz); ^{31}P NMR (400 MHz, $CDCl_3$, 25 °C): δ 37.48. CIMS. (Carrier gas NH_3). Calcd for $C_{22}H_{23}O_3P$: 366.3972. Found: 367.4 (M+H), 368.3 (M+2H), 369.4 (M+3H). Anal. Calcd for $C_{22}H_{23}O_3P$: C, 72.12; H, 6.33. Found: C, 72.17; H, 6.11. **(*S*)-15** was obtained by the same method.

(*R*)- and (*S*)-$C_6H_5CH[P(O)Ph_2]CH(CH_2OMs)_2$, (*R*)- and (*S*)-16a. To a - 35 °C methylene chloride (250 mL) solution of (*R*)-**15** (2.50 g, 6.82 mmol) and dry triethylamine (2.85 mL, 20.5 mmol) was added a solution of methanesulfonyl chloride (1.31 mL, 16.9 mmol) in dry methylene chloride (15 mL) over 10 min. The mixture was allowed to warm to room temperature over 1 h, and then stirred for an additional 45 min. In air, the reaction flask was placed in an ice bath and the solution was quenched by the addition of crushed ice (25 g), followed by cold water (25 g) with vigorous stirring. The ice bath was removed, and the solution stirred until the ice melted. The organic layer was separated, and the aqueous layer back-extracted with methylene chloride (50 mL). The combined organic layers were sequentially washed with cold water (2 x 60 mL), cold saturated $NaHCO_3$ (2 x 100 mL), and cold brine (2 x 60 mL). The organic layer was dried over Na_2SO_4, filtered, and concentrated under reduced pressure to afford a light-yellow solid. The solid was recrystallized from methanol (10 mL) at -10 °C overnight affording white crystals of (*R*)-**16a** in 86.1% yield (3.07 g): m.p 142-143 °C; ^{1}H NMR (400 MHz, $CDCl_3$, 25 °C): δ 2.80 (s, 3 H), 2.80 (s, 3 H), 2.95 (m, 1 H), 3.87 (m, 2 H), 4.15 (d, J = 6.1 Hz, 2 H), 4.85 (dd, J_{P-H} = 10.7 Hz, J_{H-H} = 2.9 Hz, 1 H), 7.00-7.30 (m, 6 H), 7.30-7.60 (m, 7 H), 7.95 (m, 2 H); ^{13}C NMR (400 MHz, $CDCl_3$, 25 °C): δ 36.98,

37.07, 39.19, 43.38 (d, $J_{P\text{-}C}$ = 67.6 Hz), 67.56 (m), 128.07, 128.15, 128.26, 128.96, 129.13, 129.25, 130.37, 130.43, 130.65, 130.74, 130.95, 131.04, 131.48, 131.95, 132.27, 132.35 (br); ^{31}P NMR (400 MHz, $CDCl_3$, 25 °C): δ 31.72. Anal. Calcd for $C_{24}H_{27}O_7P_2$: C, 55.16; H, 5.21. Found: C, 54.93; H, 5.27. (*S*)-**16a** was obtained by the same method.

(*R*)- and (*S*)-$C_6H_5CH[P(O)Ph_2]CH(CH_2PPh_2)_2$, (*R*)- and (*S*)-17. Potassium hydride (3.25 g, 28.5 mmol, 35% mineral oil dispersion) was washed with THF (3 x 30 mL) then suspended in THF (100 mL). Diphenylphosphine (6.23 g, 33.5 mmol) was added dropwise resulting in a red solution. (*R*)-**16a** (2.50 g, 4.78 mmol) was added at -10 °C in one portion as a powder. Stirring was continued at -10 °C for 20 min, then at room temperature for an additional 40 min. The reaction was quenched by the addition of deoxygenated saturated NH_4Cl (10 mL). The mixture was stirred until the organic layer became clear (20 min) and a white precipitate remained. The organic layer was filtered from the white precipitate and the precipitate was washed with THF (2 x 20 mL). The combined organic fractions were then dried over deoxygenated $MgSO_4$, filtered, and concentrated under reduced pressure in a warm water bath. The resulting oil was sonicated in the presence of hexanes (30 mL) leaving a white powder and clear solution. The mixture was filtered, the solid washed with hexanes (2 x 30 mL), and dried under reduced pressure. The solid was recrystallized from methanol affording white crystals of (*R*)-**17** in 81.7% yield (2.57 g): m.p 211-212 °C; $[\alpha]_D$ = -91.74° (toluene, *c* 0.5047); ^{1}H NMR (400 MHz, $CDCl_3$, 25 °C): δ 1.70 (m, 2 H), 2.21 (br, 1 H), 3.10 (br, 1 H), 3.80 (m, 1 H), 4.68 (m, 1 H), 7.00-7.40 (m, 29 H), 7.56 (m, 4 H), 7.71 (br, 2 H); ^{13}C NMR (400 MHz, $CDCl_3$, 25 °C): δ 32.45 (m), 32.85 (m, two carbons overlapped), 46.95 (ddd, $J_{P\text{-}C}$ =

70.2, 10.9, 7.3 Hz), 125.38, 127.29, 128.03, 128.14, 128.23, 128.31, 128.39, 128.47, 128.54, 128.88, 129.11, 130.76, 130.84, 130.97, 131.09, 131.17, 131.56, 131.99, 132.07, 132.13, 132.20, 132.31, 132.38, 132.69 (d, $J_{P\text{-}C}$ = 29.8 Hz), 133.49, 133.68, 133.73 (d, $J_{P\text{-}C}$ = 10.7 Hz), 134.24, 134.45, 136.28 (d, $J_{P\text{-}C}$=11.1 Hz), 136.73 (d, $J_{P\text{-}C}$ = 13.6 Hz), 138.71 (d, $J_{P\text{-}C}$ = 9.1 Hz), 139.25 (d, $J_{P\text{-}C}$ = 10.3 Hz); ^{31}P NMR (400 MHz, $CDCl_3$, 25 °C): δ 32.62, -20.99, -23.97. HRMS (EI). Calcd for $C_{46}H_{41}OP_3$: 702.2371. Found: 702.2372. Anal. Calcd for $C_{46}H_{41}OP_3$: C, 78.68; H, 5.88. Found: C, 78.37; H, 5.93. (*S*)-**17** was obtained by the same method. $[\alpha]_D$ = +91.93° (toluene, *c* 0.5058).

Crystallographic analysis of (*R*)-$C_6H_5CH[P(O)Ph_2]CH(CH_2PPh_2)_2$, (*R*)-17. Suitable crystals for X-ray diffraction study were obtained by slow evaporation of methanol solutions of (*R*)-$C_6H_5CH[P(O)Ph_2]CH(CH_2PPh_2)_2$ under a stream of argon gas. The crystal system was monoclinic, and the space group $P2_1$ (No. 4), which was consistent with an enantiomerically pure compound. Crystal data, details of data collection, structure solution, and refinement are outlined in Table 2.6. Selected bond distances and angles are outlined in Table 2.7 and Table 2.8.

(*R*)- and (*S*)-$C_6H_5CH(PPh_2)CH(CH_2PPh_2)_2$, (*R*)- and (*S*)-heliphos. A high pressure reactor was charged with a solution of (*R*)-**17** (2.50 g, 3.56 mmol) in distilled *p*-xylene (20 mL). The reactor was placed in an ice-water bath. Distilled *n*-tributyl amine (5.04 mL, 21.2 mmol) and trichlorosilane (1.80 mL, 17.8 mmol) were added, and the reactor was sealed. The reaction mixture was warmed to room temperature and then heated at 140 °C for 96 h. The reactor was cooled to room temperature, and the reaction

Table 2.6: Crystallographic, experimental, and refinement details for (*R*)-$C_6H_5CH[P(O)Ph_2]CH(CH_2PPh_2)_2$ ((*R*)-17).

Formula	$C_{46}H_{41}OP_3$
Formula weight	702.70
Crystal dimensions (mm)	0.24 x 0.20 x 0.18
Crystal system	Monoclinic
space group	$P2_1$ (No. 4)
unit cell parameters[a]	
a (Å), b (Å), c (Å)	9.5092 (7), 18.8928 (9), 10.9129 (6)
β (deg), V (Å^3), Z	99.074 (5), 1936.0 (2), 2
ρ_{calcd} (g cm^{-3}), μ (mm^{-1})	1.205, 1.664
Diffractometer	Siemens P4/RA
Radiation (λ [Å])	graphite-monochromated Cu Kα (1.54178)
Temperature (°C)	–60
scan type	θ–2θ
data collection 2θ limit (deg)	115.0
total data collected	5574 ($-10 \le h \le 10$, $-20 \le k \le 19$, $-11 \le l \le 11$)[b]
Independent reflections	5043
Number of observations (*NO*)	4601 ($F_o^2 \ge 2\sigma(F_o^2)$)
Structure solution method	direct methods (SHELXS–86[c])
Refinement method	full-matrix least-squares on F^2 (*SHELXL–93*[d])
Absorption correction method	Gaussian integration (face-indexed)
range of transmission factors	0.7781–0.7179
data/restraints/parameters	5042 [$F_o^2 \ge -3\sigma(F_o^2)$] / 0 / 451
Flack absolute structure parameter[e]	0.00 (2)
Goodness-of-fit (*S*)[f]	1.074 [$F_o^2 \ge -3\sigma(F_o^2)$]
final *R* indices[g]	
$F_o^2 > 2\sigma(F_o^2)$	$R_1 = 0.0398$, $wR_2 = 0.0843$
all data	$R_1 = 0.0467$, $wR_2 = 0.0899$
Largest difference peak and hole	0.133 and –0.162 e Å^{-3}

[a] Obtained from least-squares refinement of 47 reflections with $55.0° < 2\theta < 58.1°$. [b] Data were collected from Friedel-opposite quadrants with indices of the form ($+h$ $-k$ $\pm l$) and ($-h$ $+k$ $\pm l$). [c] Sheldrick, G. M. *Acta Crystallogr.* **1990**, *A46*, 467–473. [d] Sheldrick, G. M. *SHELXL-93*. Program for crystal structure determination. University of Göttingen, Germany, 1993. Refinement on F_o^2 for all reflections except for 1 having $F_o^2 > -3\sigma(F_o^2)$. Weighted *R*-factors wR_2 and all goodnesses of fit *S* are based on F_o^2; conventional *R*-factors R_1 are based on F_o, with $F_o$set to zero for negative F_o^2. The observed criterion of $F_o^2 > 2\sigma(F_o^2)$ is used only for calculating R_1, and is not relevant to the choice of reflections for refinement. *R*-factors based on $F_o^2$are statistically about twice as large as those based on F_o, and *R*-factors based on ALL data will be even larger. [e] Flack, H. D. *Acta Crystallogr.* **1983**, *A39*, 876–881. The Flack parameter will refine to a value near zero if the structure is in the correct configuration and will refine to a value near one for the inverted configuration. [f] $S = [\Sigma w(F_o^2 - F_c^2)^2/(n-p)]^{1/2}$ (n = number of data; p = number of parameters varied; $w = [\sigma^2(F_o^2) + (0.0303P)^2 + 0.8272P]^{-1}$ where $P = [\text{Max}(F_o^2, 0) + 2F_c^2]/3$). [g] $R_1 = \Sigma||F_o| - |F_c||/\Sigma|F_o|$; $wR_2 = [\Sigma w(F_o^2 - F_c^2)^2/\Sigma w(F_o^4)]^{1/2}$.

Table 2.7: Selected interatomic distances (Å) for (*R*)-$C_6H_5CH[P(O)Ph_2]CH$-$(CH_2PPh_2)_2$ ((*R*)-17).

Atom1	Atom2	Distance
P1	O	1.485(2)
P1	C1	1.825(3)
P1	C11	1.801(4)
P1	C21	1.807(4)
P2	C3	1.846(3)
P2	C31	1.834(3)
P2	C41	1.826(4)
P3	C4	1.843(4)
P3	C51	1.841(4)
P3	C61	1.837(4)
C1	C2	1.562(5)
C1	C5	1.530(5)
C2	C3	1.543(4)
C2	C4	1.540(5)
C5	C6	1.390(5)
C5	C10	1.382(5)
C6	C7	1.384(5)
C7	C8	1.361(6)
C8	C9	1.366(6)
C9	C10	1.380(6)
C11	C12	1.387(5)
C11	C16	1.377(6)
C12	C13	1.361(6)
C13	C14	1.351(8)
C14	C15	1.385(8)
C15	C16	1.407(7)
C21	C22	1.376(5)
C21	C26	1.379(5)
C22	C23	1.377(6)
C23	C24	1.356(6)
C24	C25	1.355(6)
C25	C26	1.385(6)
C31	C32	1.388(5)
C31	C36	1.383(5)
C32	C33	1.387(6)
C33	C34	1.378(6)
C34	C35	1.363(6)
C35	C36	1.388(5)
C41	C42	1.396(5)
C41	C46	1.361(7)
C42	C43	1.369(6)
C43	C44	1.355(8)
C44	C45	1.366(9)
C45	C46	1.391(7)
C51	C52	1.370(5)
C51	C56	1.370(5)
C52	C53	1.388(6)
C53	C54	1.343(7)
C54	C55	1.367(7)
C55	C56	1.373(6)
C61	C62	1.381(5)
C61	C66	1.388(5)
C62	C63	1.368(6)
C63	C64	1.359(7)
C64	C65	1.371(7)
C65	C66	1.383(6)

Table 2.8: Selected interatomic angles (deg) for (*R*)-$C_6H_5CH[P(O)Ph_2]CH(CH_2PPh_2)_2$ ((*R*)-17).

Atom1	Atom2	Atom3	Angle	Atom1	Atom2	Atom3	Angle
O	P1	C1	115.74(14)	C22	C21	C26	117.0(4)
O	P1	C11	112.1(2)	C21	C22	C23	121.4(4)
O	P1	C21	112.9(2)	C22	C23	C24	120.6(4)
C1	P1	C11	103.9(2)	C23	C24	C25	119.4(5)
C1	P1	C21	106.1(2)	C24	C25	C26	120.3(5)
C11	P1	C21	105.2(2)	C21	C26	C25	121.2(4)
C3	P2	C31	100.11(15)	P2	C31	C32	123.3(3)
C3	P2	C41	103.8(2)	P2	C31	C36	118.5(3)
C31	P2	C41	101.3(2)	C32	C31	C36	118.2(3)
C4	P3	C51	101.3(2)	C31	C32	C33	120.7(4)
C4	P3	C61	101.7(2)	C32	C33	C34	120.3(4)
C51	P3	C61	101.2(2)	C33	C34	C35	119.4(4)
P1	C1	C2	111.3(2)	C34	C35	C36	120.8(4)
P1	C1	C5	113.5(2)	C31	C36	C35	120.6(4)
C2	C1	C5	113.7(3)	P2	C41	C42	116.8(3)
C1	C2	C3	110.2(3)	P2	C41	C46	125.8(3)
C1	C2	C4	112.0(3)	C42	C41	C46	117.5(4)
C3	C2	C4	111.5(3)	C41	C42	C43	122.4(5)
P2	C3	C2	113.6(2)	C42	C43	C44	118.6(5)
P3	C4	C2	112.9(2)	C43	C44	C45	121.0(5)
C1	C5	C6	121.9(3)	C44	C45	C46	119.9(7)
C1	C5	C10	120.0(3)	C41	C46	C45	120.6(5)
C6	C5	C10	118.0(3)	P3	C51	C52	125.9(3)
C5	C6	C7	120.4(4)	P3	C51	C56	116.2(3)
C6	C7	C8	120.4(4)	C52	C51	C56	117.8(4)
C7	C8	C9	120.1(4)	C51	C52	C53	120.7(4)
C8	C9	C10	120.0(4)	C52	C53	C54	120.5(5)
C5	C10	C9	121.1(4)	C53	C54	C55	119.5(4)
P1	C11	C12	122.7(3)	C54	C55	C56	120.2(5)
P1	C11	C16	118.6(3)	C51	C56	C55	121.2(4)
C12	C11	C16	118.6(4)	P3	C61	C62	123.9(3)
C11	C12	C13	121.7(5)	P3	C61	C66	118.3(3)
C12	C13	C14	119.6(5)	C62	C61	C66	117.8(4)
C13	C14	C15	121.5(5)	C61	C62	C63	120.7(4)
C14	C15	C16	118.5(5)	C62	C63	C64	121.8(4)
C11	C16	C15	120.0(5)	C63	C64	C65	118.4(5)
P1	C21	C22	117.1(3)	C64	C65	C66	120.8(5)

mixture treated with 30% deoxygenated aqueous NaOH (50 mL). The reaction mixture was stirred at 60 °C for 1.5 h until both layers became transparent. The layers were separated and the aqueous layer was back-extracted with toluene (2 x 25 mL). The combined organic layers were washed sequentially with 30 % deoxygenated aqueous NaOH (50 mL), deoxygenated distilled water (50 mL), 0.1 N HCl (75 mL), and deoxygenated distilled water (50 mL). The organic layer was dried over Na_2SO_4, filtered, and concentrated under reduced pressure. The remaining white solid was dried under reduced pressure for an additional 1 h then recrystallized from methanol affording white cube shaped crystals of (*R*)-**heliphos** in 82.0% yield (2.00 g): m.p 140-141 °C ; $[\alpha]_D = -71.74°$ (toluene, *c* 1.0174); ^1H NMR (400 MHz, $CDCl_3$, 25 °C): δ 1.80 (br, 3 H), 2.99 (br, 1 H), 3.26 (br, 1 H), 4.59 (br, 1 H), 6.90- 7.60 (m, 35 H); ^{13}C NMR (400 MHz, $CDCl_3$, 25 °C): δ 31.48 (m), 32.11 (m), 33.51 (m), 47.20 (dd, $J_{P\text{-}C}$ = 8.5, 9.4 Hz), 126.64, 127.82, 127.89, 128.14, 128.14, 128.38, 128.44 (br), 128.83, 131.29, 131.38, 132.06, 132.15, 132.23, 132.33, 133.53, 133.72, 133.85, 134.05, 134.22, 136.44 (d, $J_{P\text{-}C}$ = 14.3 Hz), 137.01(d, $J_{P\text{-}C}$ = 4.9 Hz), 137.14 (d, $J_{P\text{-}C}$ = 3.2 Hz), 137.39 (d, $J_{P\text{-}C}$ = 14.1 Hz), 137.96 (d, $J_{P\text{-}C}$ = 9.2 Hz), 139.54 (d, $J_{P\text{-}C}$ = 10.9 Hz); ^{31}P NMR (400 MHz, $CDCl_3$, 25 °C): δ -12.23, -21.72, -24.08. HRMS (EI). Calcd for $C_{46}H_{41}P_3$: 686.2421. Found: 686.2437. Anal. Calcd for $C_{46}H_{41}P_3$: C, 80.51; H, 6.02. Found: C, 80.68; H, 6.09. (*S*)-**heliphos** was obtained by the same method. $[\alpha]_D = +72.50°$ (toluene, *c* 0.5310).

Optical purity of (*R*)-heliphos. Crystallized (*R*)-heliphos was oxidized to the corresponding trioxide following the same experimental procedure used to oxidize (*R*)-**14** to (*R*)-**15**. A mixture of (*R*)-heliphos trioxide and 6 equivalents of optically pure (*R*)-(+)-

1,1'-bi-2-naphthol was dissolved in $CDCl_3$. ^{31}P NMR (400 MHz, C_6D_6, 25 °C): δ 35.51, -21.45, -23.88.

[Rh((*R*)-heliphos)(NBD)](ClO_4), (*R*)-20. A stirred solution of [Rh(NBD)$_2$]-(ClO_4) (98.5 mg, 0.25 mmol) in methylene chloride (1.0 mL) at 0 °C was slowly treated with a solution of (*R*)-**heliphos** (0.1752 g, 0.25 mmol) in methylene chloride (1.0 mL). The yellow-red reaction mixture was stirred at room temperature for 1 h. The solution was concentrated under reduced pressure and the resulting orange solid was washed with hexanes (3 x 5 mL). The solid was crystallized from methanol affording red-orange crystals of [Rh((*R*)-heliphos)(NBD)](ClO_4) in 88.2% yield (216 mg): $[\alpha]_D$ = +127.18° (toluene, *c* 0.5032); ^1H NMR (400 MHz, CD_2Cl_2, 25 °C): δ 1.41 (br, 2 H), 2.37 (dd, J = 5.3, 16.2 Hz, 1 H), 2.67 (dd, J = 4.9, 15.2 Hz , 1 H), 3.35 (m, 1 H), 3.55 (m, 5 H), 3.81 (d, J = 9.0 Hz, 1 H), 3.87 (br, 3 H), 6.27 (m, 2 H), 6.70 (m, 8 H), 7.00-7.35 (m, 15 H), 7.50 (br, 5 H), 7.12 (m, 3 H), 7.85 (m, 2 H); $^1H\{^{31}P\}$ NMR (400 MHz, CD_2Cl_2:$CDCl_3$ = 1:1, 25 °C): δ 1.44 (br, 2 H), 2.42 (d, $^2J_{H\text{-}H}$ = 16.2 Hz, 1 $H^{\beta pro\text{-}S\,(C(13))}$), 2.68 (d, $2J_{H\text{-}H}$ = 15.6 Hz , 1 $H^{\beta pro\text{-}S\,(C(12))}$), 3.40 (dd, $^2J_{H\text{-}H}$ = 16.2 Hz, $^3J_{H\text{-}H}$ = 7.0 Hz, 1 $H^{\beta pro\text{-}R\,(C(13))}$), 3.49 (br, 2 H), 3.53 (br, 2 H), 3.63 (dd, $^2J_{H\text{-}H}$ = 15.6 Hz, $^3J_{H\text{-}H}$ = 7.6 Hz, 1 $H^{\beta pro\text{-}R\,(C(12))}$), 3.82 (s, 1 $H^{\beta pro\text{-}S\,(C(11))}$), 3.89 (br, 2 H), 3.98(br, 1H), 6.28 (d, 2 H), 6.70 (m, 8 H), 7.00-7.35 (m, 15 H), 7.50 (br, 5 H), 7.12 (m, 3 H), 7.85 (d, 2 H); ^{13}C NMR (400 MHz, CD_2Cl_2, 25 °C): δ 25.26 (t, $J_{P\text{-}C}$ = 17.2 Hz), 27.12 (dd, $J_{P\text{-}C}$ = 12.6, 20.4 Hz), 37.83 (br), 44.27 (t, $J_{P\text{-}C}$ = 13.47 Hz), 46.67, 46.91(br), 47.42 (m), 61.82, 127.75, 127.86, 128.16, 128.61, 128.71, 129.05, 129.14, 129.53, 129.55, 129.64, 130.01, 130.10, 130.46, 130.70, 130.77, 130.88, 130.99, 131.48, 131.52, 131.59, 131.64, 132.25, 132.32, 132.43, 134.45 (d, $J_{P\text{-}C}$ = 5.4

Hz), 134.78 (d, $J_{P\text{-}C}$ = 5.4 Hz), 136.27, 136.59, 136.70, 136.83, 137.03 (d, $J_{P\text{-}C}$ = 10.8 Hz), 139.95 (d, $J_{P\text{-}C}$ = 8.9 Hz); ^{31}P NMR (400 MHz, CD_2Cl_2, 25 °C): δ -7.23 (ddd, $J_{P\text{-}Rh}$ = 111.6, $J_{P\text{-}P}$ = 19.3, 35.9 Hz), 0.765 (ddd, $J_{P\text{-}Rh}$ = 113.9, $J_{P\text{-}P}$ = 19.3, 36.7 Hz) (*pseudo*-dt, $J_{P\text{-}Rh}$ = 116.7, $J_{P\text{-}P}$ = 36.7, 35.9 Hz). Anal. Calcd for $C_{53}H_{49}P_3RhClO_4$: C, 64.89; H, 5.04. Found: C, 64.89; H, 5.08. [Rh((*S*)-heliphos)(NBD)](ClO_4) (**(*S*)-8**) was obtained by the same method. [α]$_D$ = -128.64° (toluene, *c* 0.4975).

Crystallographic analysis of [Rh((*R*)-heliphos)(NBD)](ClO$_4$)•MeOH, (*R*)-20. Suitable crystals for X-ray diffraction study were obtained by slow evaporation of methanol solutions of [Rh((*R*)-heliphos)(NBD)](ClO_4) under a stream of argon gas. The crystal system was monoclinic, and the space group $P2_1$ (No. 4), which was consistent with an enantiomerically pure compound. Crystal data, details of data collection, and structure solution and refinement are outlined in Table 2.9. Selected bond distances and angles are outlined in Results and Discussion section of text.

[Rh(triphos)(NBD)](ClO$_4$), (19). A stirred solution of [Rh(NBD)$_2$](ClO_4) (48.4 mg, 0.125 mmol) in methylene chloride (2.0 mL) at 0 °C was slowly treated with a solution of triphos (78.2 mg, 0.125 mmol, Aldrich) in methylene chloride (1.0 mL). The yellow-red reaction mixture was stirred at room temperature for 1 h. The solution was concentrated under reduced pressure and the resulting orange solid was washed with hexanes (3 x 10 mL). The solid was used without further purification. ^{1}H NMR (CD_2Cl_2): δ 1.46 (s, 2 H), 1.59 (q, 3 H), 2.42 (dd, 6 H, C*H*$_2$CH$_3$), 3.61 (br s, 4H), 3.88 (br s, 2H), 6.89 - 7.25 (m, 24 H), 7.28 - 7.41 (t, 6 H); ^{31}P NMR (CD_2Cl_2): δ -9.59 (d, $J_{P\text{-}Rh}$ =

113.7 Hz); ^{1}H NMR (400 MHz, CD_2Cl_2, -80 °C): δ 1.38 (s, 2 H), 1.50 (br s, 3 H), 2.29 (br s, 6 H, CH_2CH_3), 3.46 (br s, 4H), 3.90 (br s, 2H), 6.92 - 7.02 (br s, 12 H), 7.09 (t, 12 H), 7.28 (t, 6 H); ^{31}P NMR (400 MHz, C D_2Cl_2, -80 °C): δ 8.99 (d, $J_{P\text{-}Rh}$ = 113.7 Hz).

Table 2.9: Crystallographic, experimental, and refinement details for [((*R*)-heliphos)Rh(NBD)](ClO_4)•MeOH ((*R*)-20).

Formula	$C_{54}H_{53}ClO_5P_3Rh$
Formula weight	1012.23
Crystal dimensions (mm)	0.32 x 0.25 x 0.24
Crystal system	Monoclinic
space group	$P2_1$ (No. 4)
unit cell parameters[a]	
a (Å), b (Å), c (Å)	9.5295 (9), 18.307 (2), 13.564 (2)
β (deg), V (Å^3), Z	99.362 (13), 2334.9 (5), 2
ρ_{calcd} (g cm^{-3}), μ (mm^{-1})	1.441, 0.575
Diffractometer	Enraf-Nonius CAD4
Radiation (λ [Å])	graphite-monochromated Mo Kα (0.710 73)
Temperature (°C)	–50
scan type	θ–2θ
data collection 2θ limit (deg)	50.0
total data collected	8826 ($-10 \leq h \leq 10$, $-20 \leq k \leq 19$, $-11 \leq l \leq 11$)[b]
Independent reflections	8169
Number of observations (*NO*)	7116 ($F_o^2 \geq 2\sigma(F_o^2)$)
Structure solution method	direct methods/fragment search (DIRDIF–94[c])
Refinement method	full-matrix least-squares on F^2 (*SHELXL–93*[d])
Absorption correction method	DIFABS
range of transmission factors	1.258–0.840
data/restraints/parameters	8169 [$F_o^2 \geq -3\sigma(F_o^2)$] / 0 / 579
Flack absolute structure parameter[e]	-0.06 (4)
Goodness-of-fit (*S*)[f]	1.054 [$F_o^2 \geq -3\sigma(F_o^2)$]
final *R* indices[g]	
$F_o^2 > 2\sigma(F_o^2)$	$R_1 = 0.0579$, $wR_2 = 0.1567$
all data	$R_1 = 0.0706$, $wR_2 = 0.1715$
Largest difference peak and hole	+1.488 and –0.987 e Å^{-3}

[a] Obtained from least-squares refinement of 47 reflections with 20.2° < 2θ < 25.4°. [b] Data were collected from Friedel-opposite quadrants with indices of the form ($+h$ $-k$ $\pm l$) and ($-h$ $+k$ $\pm l$). [c] Beurskens, P. T.; Admiraal, G.; Beurskens, G.; Bosman, W. P.; de Gelder, R.; Israel, R.; Smits, J. M. M. The DIRDIF-94 Program System; Crystallography Laboratory, University of Nijmegen, The Netherlands, 1994. [d] Sheldrick, G. M. *SHELXL-93*. Program for crystal structure determination. University of Göttingen, Germany, 1993. Refinement on F_o^2 for all reflections except for 1 having $F_o^2 > -3\sigma(F_o^2)$. Weighted *R*-factors wR_2 and all goodnesses of fit *S* are based on F_o^2; conventional *R*-factors R_1 are based on F_o, with $F_o$set to zero for negative F_o^2. The observed criterion of $F_o^2 > 2\sigma(F_o^2)$ is used only for calculating R_1, and is not relevant to the choice of reflections for refinement. *R*-factors based on $F_o^2$are statistically about twice as large as those based on F_o, and *R*-factors based on ALL data will be even larger. [e] Flack, H. D. *Acta Crystallogr.* **1983**, *A39*, 876–881. The Flack parameter will refine to a value near zero if the structure is in the correct configuration and will refine to a value near one for the inverted configuration. [f] $S = [\Sigma w(F_o^2 - F_c^2)^2/(n-p)]^{1/2}$ (n = number of data; p = number of parameters varied; $w = [\sigma^2(F_o^2) + (0.0303P)^2 + 0.8272P]^{-1}$ where $P = [\mathrm{Max}(F_o^2, 0) + 2F_c^2]/3$). [g] $R_1 = \Sigma||F_o| - |F_c||/\Sigma|F_o|$; $wR_2 = [\Sigma w(F_o^2 - F_c^2)^2/\Sigma w(F_o^4)]^{1/2}$.

References and Notes

(1) (a) Whitesell, J. K. *Chem. Rev.* **1989**, *89*, 1581. (b) Brunner, H. *Angew. Chem. Int. Ed. Engl.* **1983**, *22*, 897-1012.

(2) (a) Utsuno, S.; Miyamae, H.; Horikoshi, S.; Endo, I. *Inorg. Chem.* **1985**, *24*, 1348-1354. (b) Endo, I.; Horikoshi, S.; Utsuno, S. *J. Chem. Soc., Chem. Commun.* **1981**, 296-297.

(3) Canary, J. W.; Allen, C. S.; Castagnetto, J. M.; Wang, Y. *J. Am. Chem. Soc.* **1995**, *117*, 8484-8485.

(4) (a) Nugent, W. A.; Harlow, R. L. *J. Am. Chem. Soc.* **1994**, *116*, 6142-6148. (b) Nugent, W. A.; RajanBabu, T. V.; Burk, M. J. *Science* **1993**, *259*, 479. (c) Nugent, W. A. *J. Am. Chem. Soc.* **1992**, *114*, 2768-2769.

(5) Brunner, H. *Angew. Chem. Int. Ed. Engl.* **1983**, *22*, 897-1012.

(6) Brunner, H.; Rahman, A. F. M. M. *Chem. Ber.* **1984**, *117*, 710.

(7) Adolfsson, H.; Wärnmark, K.; Moberg, C. *J. Chem. Soc., Chem. Commun.* **1992**, 1054-1055.

(8) (a) Cloux, D. D.; Tokar, C. J.; Osama, M.; Houser, R. P.; Keyes, M.; Tolman, W. B. *Organometallics* **1994**, *13*, 2856. (b) LeCloux, D. D.; Tolman, W. B. *J. Am. Chem. Soc.* **1993**, *115*, 1153-1154. (c) Tokar, C. J.; Kettler, P. B.; Tolman, W. B. *Organometallics* **1992**, *11*, 2738.

(9) Trofimenko, S. *Chem. Rev.* **1993**, *93*, 943-980.

(10) Burk, M. J.; Harlow, R. L. *Angew. Chem. Int. Ed. Engl.* **1990**, *29*, 1462.

(11) Ward, T. R.; Venanzi, L. M.; Albinati, A.; Lianza, F.; Gerfin, T.; Gramlich, V.; Tombo, G. M. R. *Helv. Chim. Acta* **1991**, *74*, 983.

(12) Walter, O.; Klein, T.; Huttner, G.; Zsolnai, L. *Z. Naturforsch.* **1995**, *50b*, 729.

(13) (a) Bianchini, C.; Meli, A. *J. Chem. Soc., Dalton Trans.* **1996**, 801. (b) Bianchini, C.; Herrera, V.; Jimenez, M. V.; Meli, A.; Sanchez-Delgado, R.; Vizza, F. *J. Am. Chem. Soc.* **1995**, *117*, 8567-8575. (c) Ma, S.; Venanzi, L. M. *Tetrahedron Lett.* **1993**, *34*, 8071. (d) Sernau, V.; Huttner, G.; Fritz, M.; Zsolnai, L.; Walker, O. *J. Organomet. Chem.* **1993**, *458*, 63. (e) Bianchini, C.; Meli, A.; Peruzzini, M.; Vizza, F.; Frediani, P.; Ramirez, J. A. *Organometallics* **1990**, *9*, 226.

(14) (a) Mayer, H. A.; Stößel, P.; Fawzi, R.; Steimann, M. *J. Organomet. Chem.* **1995**, *492*, C1-C3. (b) Mayer, H. A.; Stößel, P.; Fawzi, R.; Steimann, M. *Chem. Ber.* **1995**, *128*, 719-723.

(15) (a) Lütjens, H.; Wahl, G.; Möller, F.; Knochel, P.; Sundermeyer, J. *Organometallics* **1997**, *16*, 5869-5878. (b) Lütjens, H.; Knochel, P. *Tetrahedron: Asymmetry* **1994**, *5*, 1161-1162.

(16) For representative examples see the following. Bis(phosphines): (a) Fu, T. Y.; Liu, Z.; Scheffer, J. R.; Trotter, J. *Tetrahedron Lett.* **1994**, *35*, 7593. (b) Brunner, H. *J. Organomet. Chem.* **1986**, *300*, 39. (c) Miyashita, A.; Takaya, H.; Souchi, T.; Noyori, R. *Tetrahedron* **1984**, *40*, 1245. Nitrogen donor atoms: (d) Fritschi, H.; Leutenegger, U.; Siegmann, K.; Pfaltz, A.; Keller, W.; Kratky, Ch. *Helv. Chim. Acta* **1988**, *71*, 1541. (e) Helmchen, G.; Krotz, A.; Ganz, K.-T.; Hannen, D. *Syn Lett* **1991**, 257. Oxygen donor atoms: (f) Maruoka, K.; Itoh, T.; Araki, Y.;

Shirasaka, T.; Yamamoto, H. *Bull. Chem. Soc. Jpn.* **1988**, *61*, 2975. For recent extensive reviews on enantioselective catalysis see the following: (g) Noyori, R. *Asymmetric Catalysis In Organic Synthesis*; Wiley Interscience, John Wiley and Sons: New York, 1994. (h) *Catalytic Asymmetric Synthesis*; Ojima, I., Ed.; VCH Publishers: New York, 1993.

(17) For representative examples see the following. Bis(phosphines): (a) Burns, C. J.; Martin, C. A.; Sharpless, K. B. *J. Org. Chem.* **1989**, *54*, 2826. (b) Vineyard, B. D.; Knowles, W. S.; Sabacky, M. J.; Bachman, G. L.; Weinkauft, D. J. *J. Am. Chem. Soc.* **1977**, *99*, 5946. (c) Fryzuk, M. D.; Bosnich, B. *J. Am. Chem. Soc.* **1977**, *99*, 6262. (d) Kagan, H. B.; Dang, T.-P. *J. Am. Chem. Soc.* **1972**, *94*, 6429. Oxygen donor atoms: (e) Seebach, D.; Behrendt, L.; Felix, D. *Angew. Chem. Int. Ed. Engl.* **1991**, *30*, 1321, and reviews in references 13g and 13h.

(18) For examples see the following: (a) Beyreuther, S.; Hunger, J.; Zsolnai, L. *Chem. Ber.* **1996**, *129*, 745. (b) Brown, M. J.; Guiry, P. J.; Price, D. W. *Tetrahedron: Asymmetry* **1994**, *5*, 561. (c) Giovannetti, J. S.; Kelly, C. M.; Landis, C. R. *J. Am. Chem. Soc.* **1993**, *115*, 4040. (d) Brown, M. B.; Maddox, P. J. *J. Chem. Soc. Chem. Commun.* **1987**, 1276. (e) Alcock, N. W.; Brown, J. M.; Derome, A. E.; Lucy, A. R. *J. Chem. Soc. Chem. Commun.* **1985**, 575. (f) Brunner, H.; Beier, P.; Riepl, G. *Organometallics* **1985**, *4*, 1732. (g) Brown, J. M.; Chaloner, P. A. *J. Am. Chem. Soc.* **1978**, *100*, 4307.

(19) (a) Heidel, H.; Huttner, G.; Zsolnai, L. *Z. Naturforsch.* **1995**, *50 b*, 729. (b) Seitz, T.; Muth, A.; Huttner, G. *Z. Naturforsch.* **1994**, *50 b*, 1045. (c) Heidel, H.; Huttner, G.; Helmchen, G. *Z. Naturforsch.* **1993**, *48 b*, 1681. (d) Walter, O.;

Klein, T.; Huttner, G.; Zsolnai, L. *J. Organomet. Chem.* **1993**, *458*, 63. (e) Ward, T. R.; Venanzi, L. M.; Albinati, A.; Lianza, F.; Gerfin, T.; Gramlich, V.; Tombo, G. M. R. *Helv. Chim. Acta* **1991**, *74*, 983. (f) Reference 10.

(20) (a) Heidel, H.; Scherer, J.; Asam, A.; Huttner, G.; Walter, O.; Zsolnai, L. *Chem. Ber.* **1995**, *128*, 293. (b) Janssen, B. C.; Sernau, V.; Huttner, G.; Asam, A.; Walter, O.; Buchner, M.; Zsolnai, L. *Chem. Ber.* **1995**, *128*, 63. (c) Janssen, B. C.; Asam, A.; Huttner, G.; Sernau, V.; Zsolnai, L. *Chem. Ber.* **1994**, *127*, 501. (d) Seitz, Th.; Muth, A.; Huttner, G.; Klein, Th.; Walter, O.; Fritz, M.; Zsolnai, L. *J. Organomet. Chem.* **1994**, *469*, 155. (e) Muth, A.; Walter, O.; Huttner, G.; Asam, A.; Zsolnai, L.; Emmerich, C. *J. Organomet. Chem.* **1994**, *468*, 149, and references cited therein.

(21) (a) Mayer, H. A.; Kaska, W. C. *Chem. Rev.* **1994**, *94*, 1239-1272. (b) Noyori, R. *Asymmetric Catalysis in Organic Synthesis*: John Wiley & Sons, Inc.: New York, 1994. (c) Ojima, I.; Clos, N.; Bastos, C. *Tetrahedron* **1989**, *45*, 6901-6939. (d) Brunner, H. *J. Organomet. Chem.* **1986**, *300*, 39-56. (e) Pidcock, A.; McAuliffe, C. A. *Transition Metal Complexes of Phosphorus, Arsenic, and Antimony Ligands*: John Wiley & Sons; New York, 1973.

(22) Some examples of success with BINAP as ligand: (a) Kumobayashi, H. *Recl. Trav. Chim. Pays-Bas* **1996**, *115*, 201-210. (b) Noyori, R. *Acta Chemica Scandinavica* **1996**, *50*, 380-390. (c) Akutagawa, S. *Appl. Cat. A* **1995**, *128*, 171-207.

(23) Wilen, S. H.; Collet, A.; Jacques, J. *Tetrahedron* **1977**, *33*, 2725-2736.

(24) The signals for all framework protons were unambiguously assigned on the basis of chemical shifts, COSY, and NOE experiments.

(25) Karplus, M. J. *J. Am. Chem. Soc.* **1963**, *85*, 2870.

(26) Positions were calculated assuming idealized sp^3 geometries about the carbon atoms of the framework.

(27) Enantiogenic is defined as the components of chirality responsible for the enantioselection during an enantioselective reaction.

(28) Rule, G. R.; Harrower, J. *J. Chem. Soc.* **1930**, 2319.

(29) Schlenk, T. G.; Downes, J. M.; Milne, C. R. C.; Mackenzie, P. B.; Boucher, H.; Whelan, J.; Bosnich, B. *Inorg. Chem.* **1985**, *24*, 2334.

Chapter 3

Metal Complexes of Heliphos: Arm Dissociation.

Introduction:

The coordination of tripodal ligands is well documented.[1] The closest analog to the heliphos ligand is triphos ($CH_3C(CH_2PPh_2)_3$). Triphos is known to coordinate to several different metal centers,[2] the complexes of which have found applications in a number of stoichiometric and catalytic reactions. When utilized in catalysis, it had been found that phosphine arm dissociation could occur. Some group nine metal tricoordinate triphos complexes of cobalt, rhodium, and iridium show arm dissociation at ambient temperature as identified by the characterization of η^2-triphos complexes.[3]

Such arm dissociation may be necessary in the catalytic hydrogenation of olefin or carbonyl compounds, with $M(\eta^2\text{-bis(phosphine)})^+$ (**1**, M = Rh, Ir) complexes as catalyst (Scheme 3.1). The nonchiral catalytic cycle shown is based on the accepted mechanism proposed by Halpern for the enantioselective hydrogenation of methyl α-acetamidocinnamate (**5**), with rhodium-bis(phosphine) catalysts.[4] In general, the prochiral substrates that yield the greatest enantioselectivity have bidentate or greater coordination. Considering such reactions, one begins with a catalyst species with the metal in the +1 oxidation state (**1**). This reacts with the incoming substrate

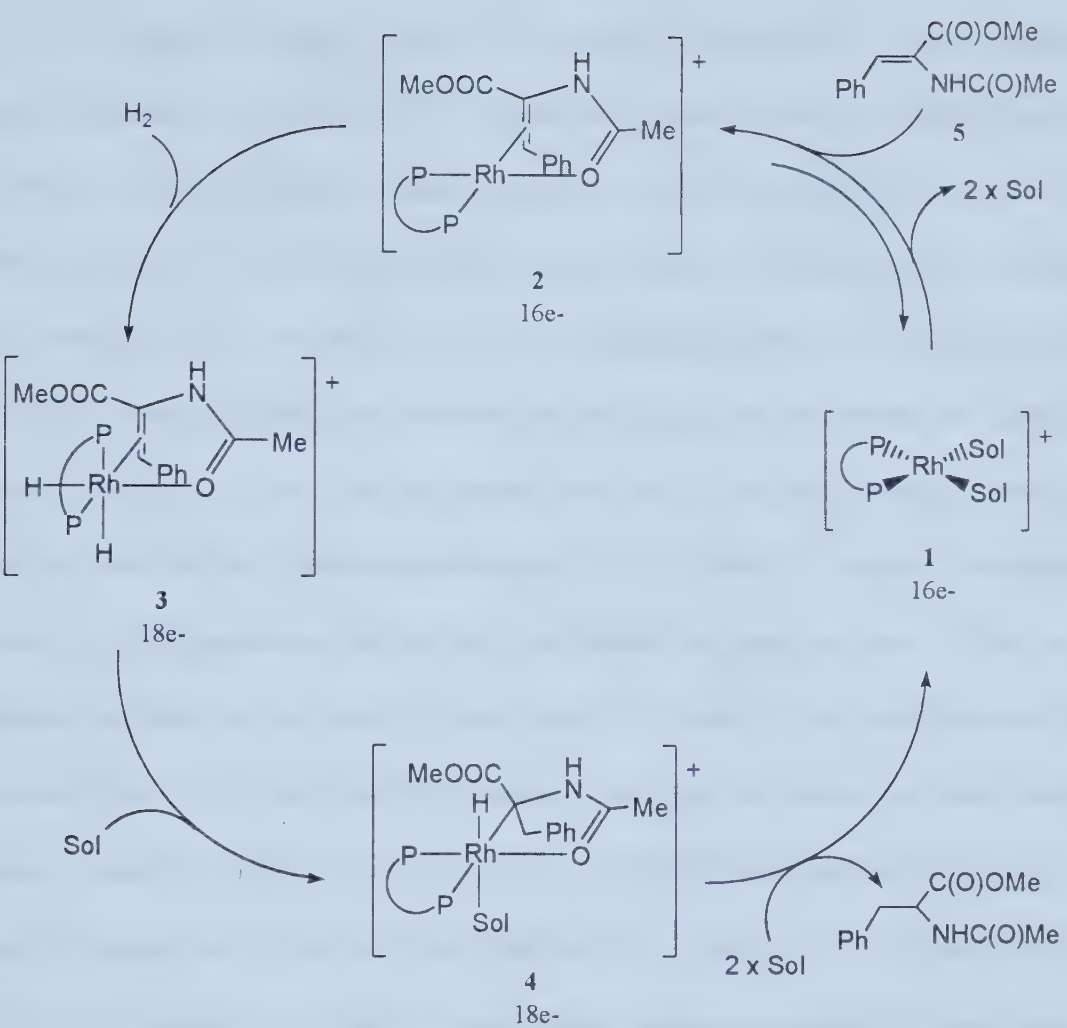
H2
MeOOC
H
N
Me
Ph
O
P
Rh
P
+
2
16e-
C(O)OMe
Ph
NHC(O)Me
5
2 x Sol
3
18e-
1
16e-
Sol
4
18e-
2 x Sol

Scheme 3.1: Catalytic cycle of the achiral Rh(bis(phosphine)) catalyzed hydrogenation of olefins based on Halpern mechanism.[4]

forming the coordination complex **2** displacing the solvent from **1**. The coordination species **2** would then react with dihydrogen gas, forming the 18e$^-$ M(H)$_2$(η^2-bis(phosphine)) complex **3**. The complex **3** would undergo insertion of the C=C bond into the rhodium-hydride bond forming the 18e$^-$ species **4**. Finally, a reductive elimination of **4** results in the expulsion of the hydrogenation product and reforms the active catalyst species **1** thus completing the catalytic cycle.

Considering the same catalytic cycle and extrapolating it with tridentate phosphine ligands, one may run into a problem at the activation of dihydrogen gas (Scheme 3.2). The coordinated substrate species **7** is a five coordinate 18e$^-$ species. The oxidative addition of dihydrogen gas to **7** would require the formation of an unlikely seven coordinate, 20e$^-$ species **8**. It is more reasonable that, prior to the oxidative addition of dihydrogen, arm dissociation occurs resulting in an unsaturated 16e$^-$ species **9**. Oxidative addition of dihydrogen gas would form **10** that can then undergo insertion of the olefin bond into the rhodium-hydride bond (**11**), followed by reductive elimination releasing the hydrogenation product and completing the catalytic cycle. The loss of tridentate coordination may result in poor transfer of chirality and could explain poor enantioselection. It is also possible, however, that the mechanism deviates from the proposed Halpern mechanism and that prior to dihydrogen gas activation there is carbonyl dissociation of the substrate leading to a stable 18e$^-$ η^3-triphos dihydrido complex (**12**) (Scheme 3.3). Then **12** could undergo oxidative addition of dihydrogen gas forming **13**. Complex **13** could undergo insertion to form **11**, followed by reductive elimination to yield the desired hydrogenation product and regenerate the active catalyst (**6**). Under these circumstances, one may still expect to achieve high enantioselectivities.

Going to the group eight metals as catalyst complexes may avoid phosphine arm dissociation entirely (Scheme 3.4). This scheme is an extrapolation based on the accepted mechanistic investigation of the Ru((*R*)-BINAP)(OAc)$_2$ catalyzed enantioselective hydrogenation of tiglic acid (**18**) reported primarily by Halpern[5] and subsequently confirmed by Takaya,[6] Achiwa,[7] and Chan.[8] The hydrogenation is believed to occur with heterolytic cleavage of dihydrogen gas, resulting in the formation

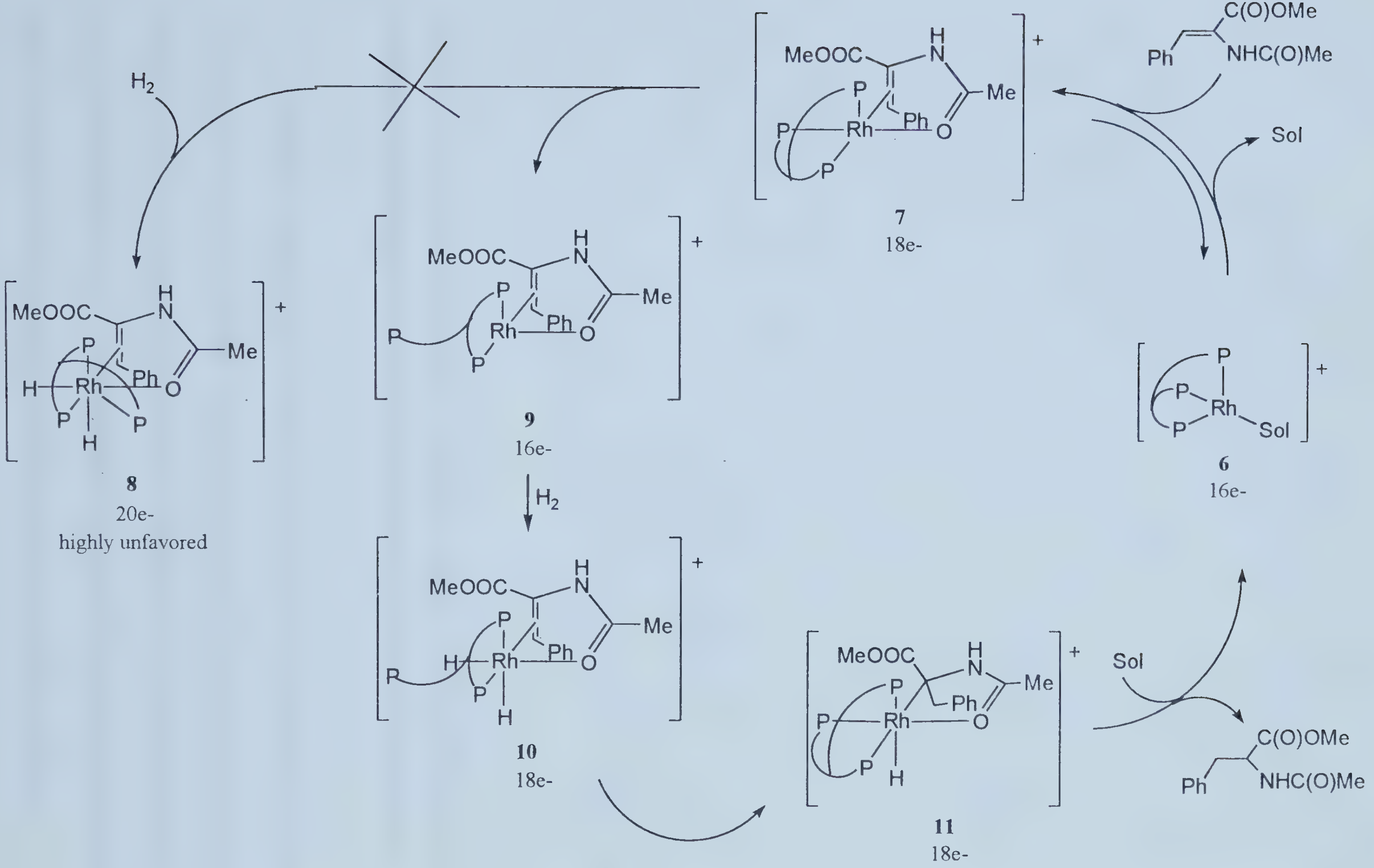
C(O)OMe
Ph
NHC(O)Me
Sol
MeOOC
H
N
Me
P
Rh
Ph
O
+
7
18e-
6
16e-
H2
9
16e-
H2
10
18e-
8
20e-
highly unfavored
11
18e-
C(O)OMe
Ph
NHC(O)Me
Sol

Scheme 3.2: Proposed catalytic cycle for achiral Rh(tris(phosphine) catalyzed hydrogenation of olefins (arm dissociation).

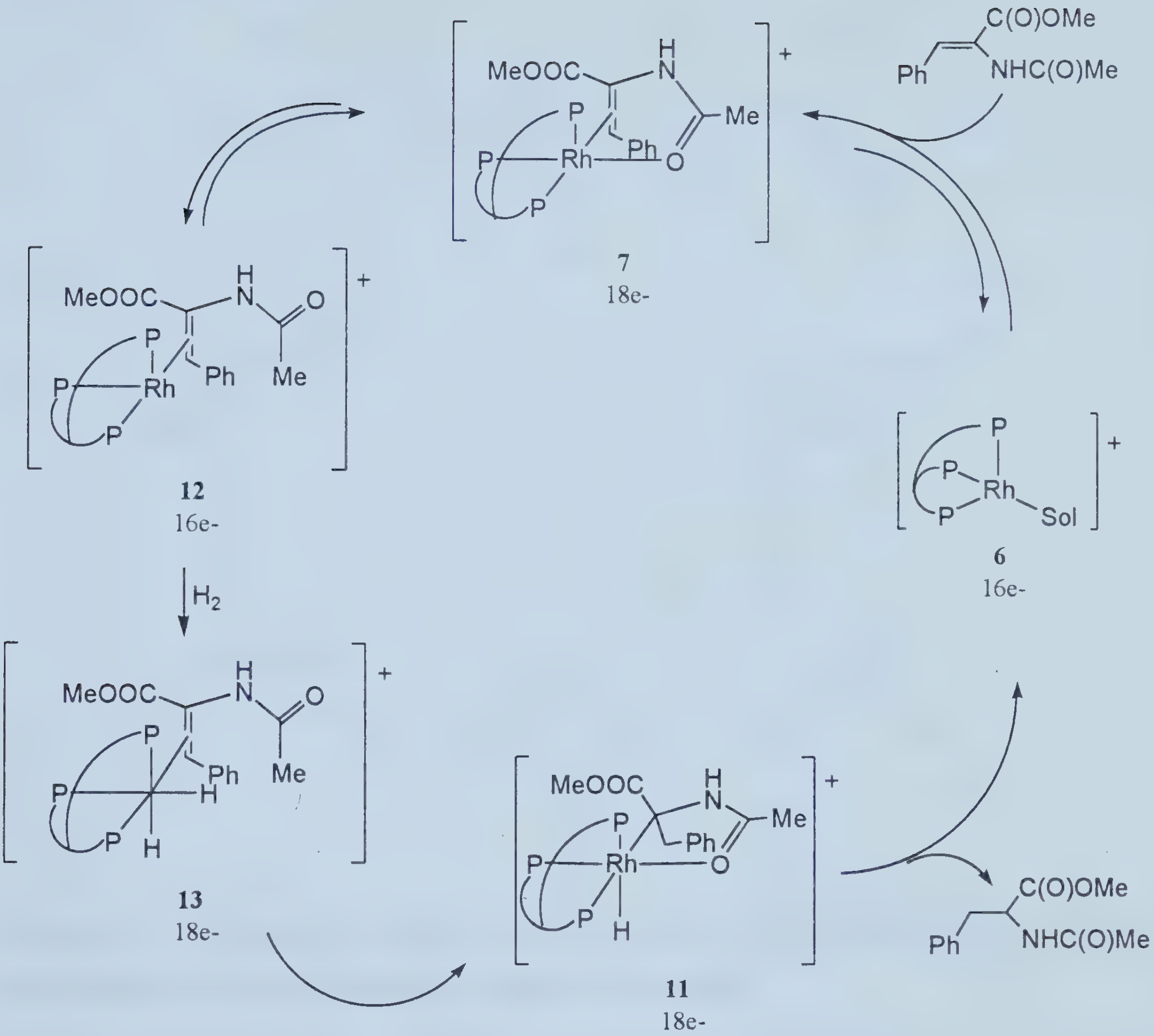

Scheme 3.3: Alternate proposed achiral catalytic cycle for Rh(tris(phosphine)) catalyzed hydrogenation of olefins with substrate carbonyl dissociation.

of a ruthenium monohydride species (**16**) that would be capable of coordinating a bidentate substrate, the hydride, and the three arms of the ligand without requiring arm-dissociation in the process. Thus at no time would the C_3 symmetry be removed, yielding higher enantioselectivities. This mechanism is believed to be a reasonable postulate as no highly unstable species are encountered throughout the catalytic pathway.

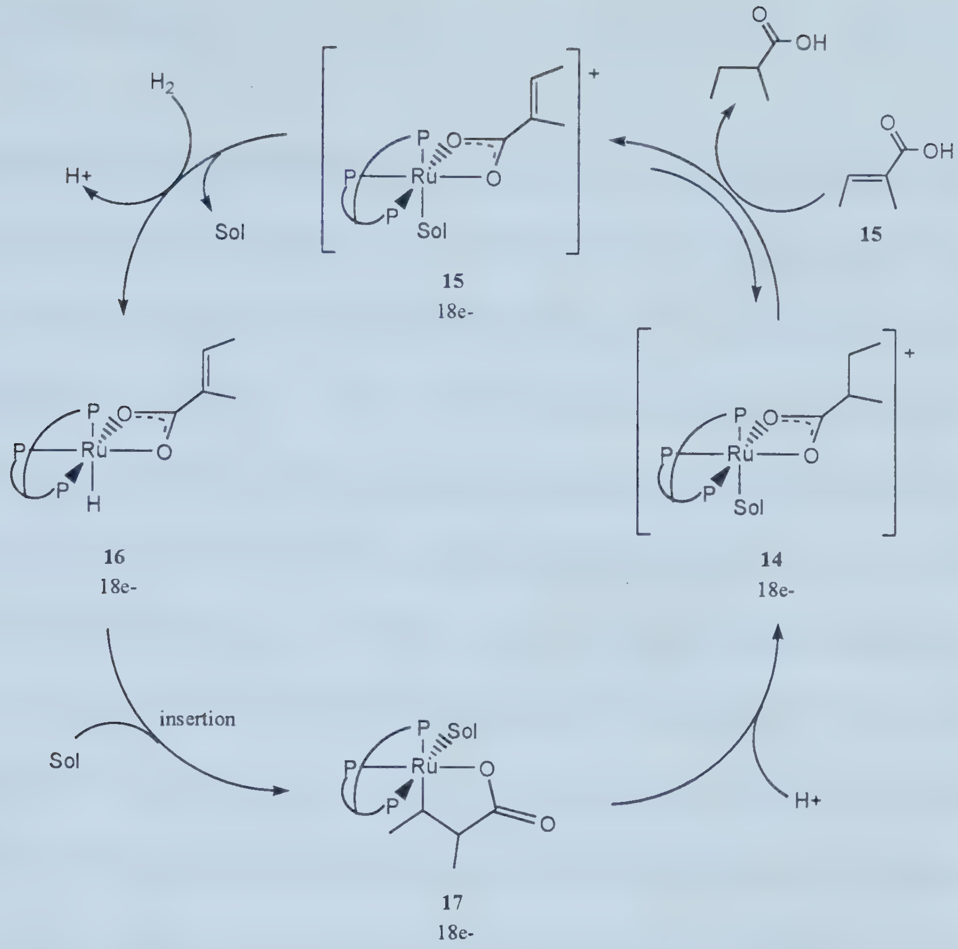

Scheme 3.4: Proposed catalytic cycle for achiral Ru(tris(phosphine)) catalyzed hydrogenation of olefins based on Halpern mechanism.[5]

The examination of [((*R*)-heliphos)Rh(NBD)](ClO$_4$) complex for use as catalyst in enantioselective hydrogenation reactions is reported. The synthesis of η^3-phosphine-ruthenium(II) complexes (η^3-phosphine = heliphos and derivatives) as catalysts in enantioselective hydrogenation reactions and the investigation of the proposed theory of complete coordination versus arm dissociation of η^3-phosphine-ruthenium(II) catalyst complexes is reported in the following section.

Results and Discussion:

[Rh((*R*)-heliphos)(NBD)](ClO_4) as catalyst. The investigations of [Rh((*R*)-heliphos)(NBD)](ClO_4) as catalyst in the enantioselective hydrogenation of the olefin substrate methyl α-acetamidocinnamate (**5**, 4 atm H_2, 25 °C, methanol) yielded poor enantioselectivity (~12% ee).[9] It is noted that, in the successful enantioselective hydrogenation of the olefins methyl α-acetamidocinnamate and dimethyl itaconate (89% ee (*R*) and 95% ee (*S*) respectively) using [(**18**)Rh(COD)](SbF_6) (**18** = $C(CH_2P(-CHCH_3CH_2CH_2C(H)(CH_3)-)_3)$ as catalyst, it was reported that higher temperatures were required as compared to other rhodium-(bis(phosphine)) systems (50 °C versus ambient temperatures).[10] This observation has led to the proposal that the tripodal ligand, as suggested by the catalytic cycle, undergoes phosphine arm dissociation forming an η^2-tris(phosphine) complex. For the case with [Rh((*R*)-heliphos)(NBD)](ClO_4) as catalyst, while elevated temperatures were not required, it is likely that similar arm dissociation of the heliphos ligand occurred. It appears that in both cases, the reactions may follow the proposed Halpern mechanism where arm dissociation of the tris(phosphine) ligand is favored over carbonyl dissociation of the substrate. Furthermore, it is not surprising that poor enantioselectivities were observed with [Rh((*R*)-heliphos)(NBD)](ClO_4) as catalyst as the symmetry of η^3-heliphos was likely destroyed by phosphine arm dissociation. Investigations of other rhodium systems were not performed as syntheses of η^3-heliphos-ruthenium(II) complexes were examined as alternative systems where arm dissociation was postulated as not occurring in enantioselective hydrogenation reactions (Scheme 3.4).

Synthesis of η^3-tris(phosphine)-ruthenium(II) complexes. Attempts at the synthesis of a ruthenium(II) complex with all three phosphines of heliphos coordinated began with the reaction of heliphos with $[Ru(COD)(\eta^3\text{-allyl})(MeCN)_2](BF_4)$ (**19**) in methylene chloride solution (Equation 3.1). **19** has been used to produce $[Ru((R)\text{-BINAP})(1\text{-}3;5,6\text{-}\eta\text{-}C_8H_{11})(MeCN)](BF_4)$ (**20**), a catalyst species developed in the Bergens laboratories, which, when reacted with dihydrogen gas, yields the well-defined ruthenium monohydride species $[Ru((R)\text{-BINAP})(H)(Sol)_{3\text{-}n}(MeCN)_n](BF_4)$ (**21**; Sol = acetone, MeOH, or THF; n = 0-3).[11] Reaction occurred between **19** and (*R*)-heliphos, but tripodal product was not obtained. The ^1H NMR analysis indicated that the displacement of COD had occurred to generate a complex mixture of products. ^{31}P NMR analysis confirmed the presence of two major products (40% and 30%) along with a number of other minor products. The ^{31}P NMR of the major products indicated that only two of the phosphines of heliphos had coordinated to the ruthenium, the third remained unattached. This assignment was based on the observed chemical shifts and coupling constants each of the phosphines had in the ^{31}P NMR investigation of the products. Each of the major products had two ^{31}P signals shifted downfield (at approximately δ 50 and δ 23) compared to any of the free heliphos (δ -12.23, -21.72, and -24.08), and the signals were each doublets ($^3J_{P\text{-}P} \approx 47$ Hz) indicating coordination to the ruthenium center. The third ^{31}P NMR signal of each product (approximately δ -15) was not shifted significantly from those of free heliphos and it had no couplings to any other phosphines, indicating non-coordination. It was believed that competitive coordination was occurring between the final phosphine arm and the free acetonitrile released upon tridentate coordination of the

heliphos ligand. In order to remove this ligand competition, a different synthetic route to achieving tripodal coordination was undertaken.

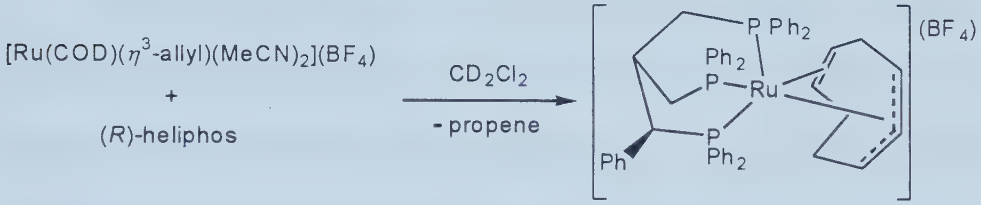

Equation 3.1

The starting material $[Ru(COD)(\eta^3\text{-allyl})(MeCN)_2](BF_4)$ (**19**) was synthesized from the reaction of $Ru(COD)(\eta^3\text{-allyl})_2$ complex with one equivalent of $HBF_4 \bullet OEt_2$ in acetonitrile solution. In order to remove the acetonitrile from solution, the synthesis was carried out in methylene chloride solution and the product immediately reacted[†] with heliphos. ^1H NMR analysis of the product indicate that COD was not displaced but rather the η^3-allyl group was displaced as propene.[††] ^{31}P NMR analysis at -40 °C showed the presence of a compound that indicated coordination of all three phosphines of heliphos did occur. Again, this assignment was based on the chemical shifts and coupling constants of the observed ^{31}P signals. All three signals (δ 42.0, 15.2, and -2.7) were shifted downfield from free heliphos as expected. As well, each signal was observed as either a doublet of doublets or as an apparent triplet, indicating $^2J_{P\text{-}P}$ coupling, which can only occur upon coordination of all three phosphines to ruthenium. However, the amount of tripodal coordination complex observed was only 30% of the product mixture, and unfortunately, all attempts to isolate the desired product were unsuccessful. A completed structural characterization of the tripodal ruthenium complex

---

[†] The complex $[Ru(COD)(\eta^3\text{-allyl})(MeCN)_2](BF_4)$ is very thermally sensitive but is somewhat stabilized by the strongly coordinating MeCN ligands. In the absence of MeCN, the product is too unstable to isolate.

[††] Similar observations made in the reaction of (*R*)-BINAP with $Ru(COD)(\eta^3\text{-allyl})_2$ producing $[Ru((R)\text{-}BINAP)(1\text{-}3;5,6\text{-}\eta\text{-}C_8H_{11})(MeCN)](BF_4)$.

could not be obtained, but it is thought that a likely structure is that of the type portrayed in Equation 3.1.

In attempts to obtain a better system where no acetonitrile was present to compete with tridentate chelation and where the tripodal ruthenium complex could be isolated, the synthesis of $RuCl_2(DMSO)_4$ (**22**) was performed. Venanzi had reported that reaction of **22** with the triphos ligand ($CH_3C(CH_2PPh_2)_3$) (**23**) yielded the tridentate coordinated dimeric complex $[Ru_2(\eta^3\text{-}Cl)_3(\mathbf{23})_2](Cl)$ (Equation 3.2).[12] Reaction of heliphos with **22** in toluene yielded a ^{31}P NMR spectrum showing two major products (A 48% and B 40%). However, the ^{31}P NMR analysis indicated that both species were again bidentate in nature with one phosphine arm uncoordinated (A; δ 53.5 ppm (d, $^3J_{P\text{-}P}$ = 53.0 Hz), 50.4 ppm (d, $^3J_{P\text{-}P}$ = 53.0 Hz), and -13.7 ppm (br s): B; δ 36.2 ppm (d, $^3J_{P\text{-}P}$ = 43.5 Hz), 31.8 (d, $^3J_{P\text{-}P}$ = 43.5 Hz), and -13.7 ppm (br s)). Venanzi did report that when trying to coordinate the similar, more bulky ligand, $CH_3C(CH_2AsPh_2)_3$ (**24**), incomplete coordination occurred. Complete coordination was obtained upon reaction of the product mixture with methanol in methylene chloride solution. Reaction of the heliphos product under similar conditions did not afford the desired tridentate coordination. The ^{31}P NMR analysis indicated no change in structure as all chemical shifts and coupling constants remained identical. A number of other attempts to achieve tridentate coordination of

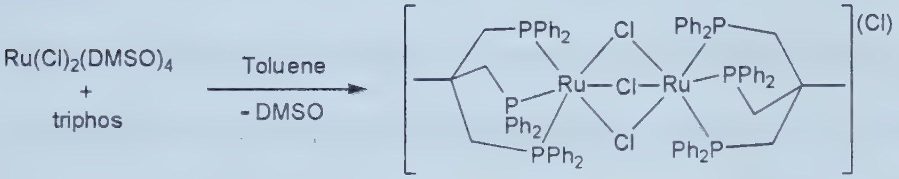

Equation 3.2

heliphos to a ruthenium(II) metal center were carried out in the Bergens laboratories without success.[9]

Reexamination of the structure of η^3-coordinated heliphos by molecular models suggested that phosphine arm dissociation, or rather non-coordination, may be due to excessive steric interactions around the metal that would be alleviated by arm dissociation. The ligand triphos has a methyl group on the central carbon and molecular models suggest that should arm dissociation occur, followed by rotation of the backbone C-P bond, the steric interaction between the diphenylphosphino group and the methyl group would be severe (Figure 3.1). For these reasons, coordination to the metal center is expected to be favored. Molecular models of the heliphos complex suggest that there would be little steric interaction between the dissociated phosphine arm and the apical hydrogen on the central carbon of the backbone (Figure 3.1). Therefore, attempts were made to derivatize heliphos to form a similar neopentyl unit as triphos, yielding similar steric interactions thus favoring coordination to the metal center (Figure 3.1).

Synthesis of Me-heliphos. The strategy was to modify the existing synthetic pathway utilized in the synthesis of heliphos (Scheme 3.5). Initial attempts focussed on ways to derivatize the enantiopure diastereomer ((*R*)-**25**) by performing a proton abstraction from the malonate center followed by methylation with methyl iodide to form (*R*)-**26**. All attempts to achieve the desired reaction by this scheme resulted in no *C*-methylation at the correct carbon center.[13] This result is due to the proton on the α-carbon from the phosphine (also a benzylic proton) being more acidic than the malonate

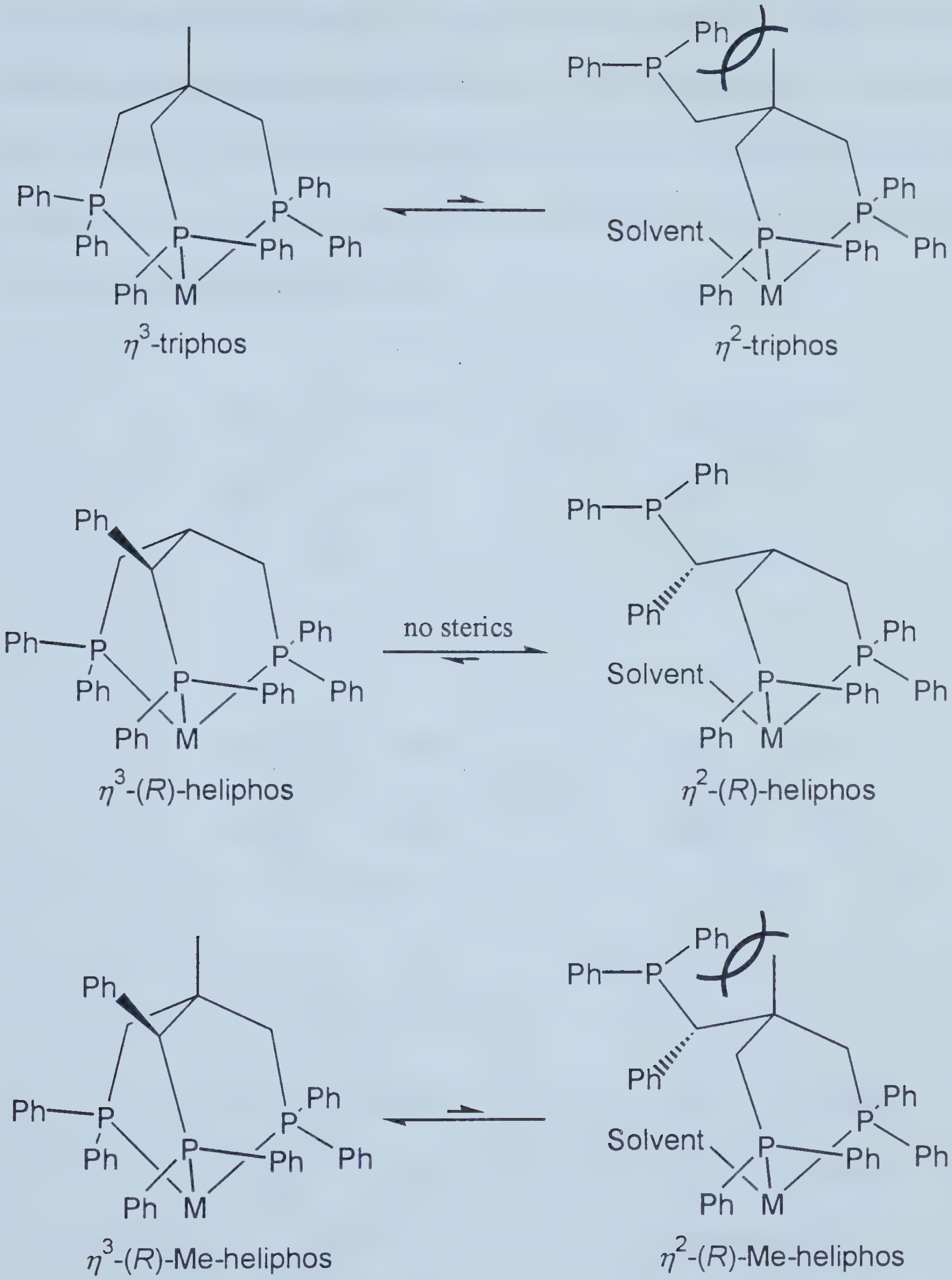
Ph
Ph—P
Ph
P
Ph
P
Ph
Ph
Ph
M
η3-triphos
Solvent
η2-triphos
no sterics
η3-(R)-heliphos
η2-(R)-heliphos
η3-(R)-Me-heliphos
η2-(R)-Me-heliphos

Figure 3.1: Representation of tridentates and bidentate (arm dissociated) complexes of triphos, (*R*)-heliphos, and (*R*)-Me-heliphos ruthenium complexes based on molecular models.

proton. The acidity of this center was observed in the synthesis of heliphos, where excess potassium hydride caused partial racemization of the bis(phosphine) mono(phosphine oxide) product.[14] Further, it is likely that the sheer bulk of **25** created too much steric congestion about the carbon center, to allow methyl iodide to approach. New synthetic routes were devised for these reasons.

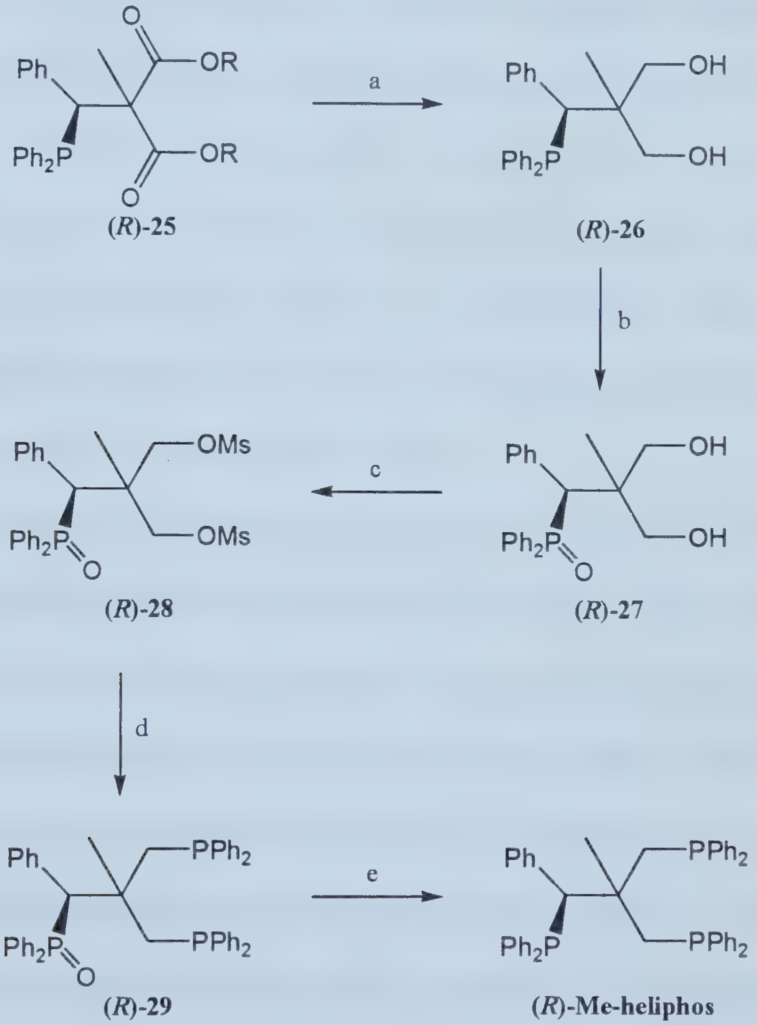
Ph
Ph₂P
OR
OR
(*R*)-25
a
Ph
Ph₂P
OH
OH
(*R*)-26
b
Ph
Ph₂P
O
OH
OH
(*R*)-27
c
Ph
Ph₂P
O
OMs
OMs
(*R*)-28
d
Ph
Ph₂P
O
PPh₂
PPh₂
(*R*)-29
e
Ph
Ph₂P
PPh₂
PPh₂
(*R*)-Me-heliphos

a) $LiAlH_4$, Et_2O. b) 10% H_2O_2, CH_2Cl_2. c) NEt_3, CH_2Cl_2, CH_3SO_2Cl. d) KH, $HPPh_2$, THF, -10°C to r.t. e) Glass bomb, $N(n\text{-}Bu)_3$, $SiHCl_3$, 140°C, 96 h.

Scheme 3.5: Proposed synthetic pathway to (*R*)-Me-heliphos based on synthetic pathway utilized in heliphos synthesis. (*S*)-Me-heliphos would be prepared by starting with (*S*)-11.

Another synthetic route tested began with the use of dialkyl malonate as starting material (Scheme 3.6). The approach was to acylate the malonate, methylate the product **31** to form the neopentyl unit complex **32**, and then to convert the product to Me-heliphos. By acylating the dialkyl malonate, there remains a single carbon acidic site in the product and it is at the desired position for *C*-methylation. It is expected that competition from *O*-alkylation will arise with bulky alkylating agents resulting in enolate products.[15] The use of methyl iodide, a small methylating agent, was expected to favor the *C*-alkylation. Further, the acyl group is located in the position where a diphenylphosphino group is required and, in principle, it can be converted by reduction to the corresponding secondary alcohol, followed by mesylation, and displacement of the mesyl group by diphenylphosphide. From there, the synthesis would follow the same synthetic pathway utilized in converting **25** to heliphos.

Use of the single-step malonate acylation procedure with stoichiometric amounts of magnesium dichloride developed by Rathke[16] was reported to give equal or higher yields of product than other acylating procedures. Reaction of di-(1*R*,2*S*,5*R*)-(-)-menthyl malonate under these conditions did not yield any acylated product. Diethyl malonate underwent acylation with benzoyl chloride as reported and yielded **31** in 84 % yield after distillation. The diethyl acylmalonate **31** has an acidic enolic proton and is shown, by ^{1}H NMR, to favor its enol form in chloroform (20:80; keto:enol). The corresponding anion of **31** is expected to be a rather weak nucleophile due to the stabilization from both ester functionalities and the strong enol stability. Furthermore, *C*-alkylation is expected to be difficult due to the low nucleophilicity of the carbon center, competition from *O*-alkylation of enolate, and the overall crowded steric environment about the carbon

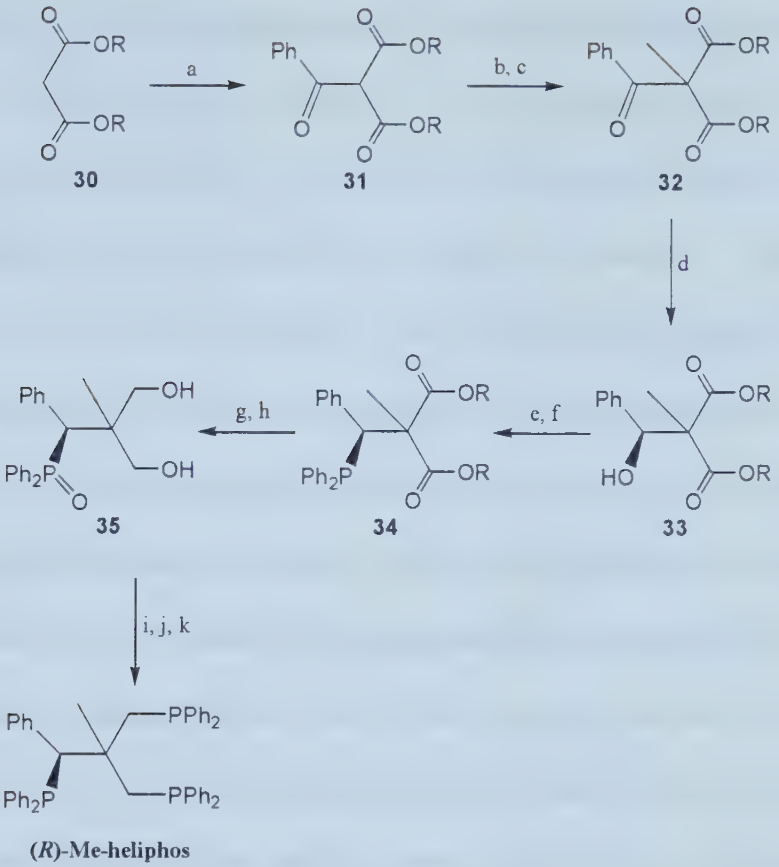

a) $C_6H_5C(O)Cl$, $MgCl_2$, CH_2Cl_2. b) $[(n\text{-Bu})_4N](HSO_4)$, 2 NaOH, $CHCl_3$. c) CH_3I, $CHCl_3$. d) $NaBH_4$, EtOH. e) NEt_3, CH_2Cl_2, CH_3SO_2Cl. f) KH, $HPPh_2$, THF, -10°C to r.t. g) $LiAlH_4$, Et_2O. h) 10% H_2O_2, CH_2Cl_2. i) NEt_3, CH_2Cl_2, CH_3SO_2Cl. j) KH, $HPPh_2$, THF, -10°C to r.t. k) Glass bomb, $N(n\text{-Bu})_3$, $SiHCl_3$, 140°C.

Scheme 3.6: Proposed synthetic pathway to (*R*)-Me-heliphos based on acylation of dialkyl malonate.

center. Brändström and Junggren[15] reported the successful methylation of such compounds by forming tetrabutylammonium salts of the compounds, dissolving them in chloroform and adding methyl iodide. Addition of bulkier alkyl iodides results in excessive amounts of *O*-alkylation and thus this method is practical only for the methyl addition reaction. The reaction proceeded to yield the methyl derivative **32** as a clear colorless liquid in 68% overall yield after distillation. Reduction of **32** with sodium borohydride, however, did not afford the alcohol product **33**. The ^1H NMR analysis

showed the presence of a diethyl methylmalonate, thus degradation of the product **33** or of **32** had occurred, likely via retro acylation. The identification of the degradation benzyl product was not determined. Attempts to hydrosilylate **32** with Wilkinson's Catalyst, $Rh(PPh_3)_3Cl$, at 90 °C over 48 h yielded no reaction. The catalytic hydrogenation of **32** was then performed, with $[Rh((R)\text{-BINAP})(NBD)](ClO_4)$ as catalyst, in methanol for 20 h at 100 atm of H_2 and 60 °C. ^{1}H NMR analysis showed that reaction had occurred, but the resulting product was not the expected alcohol but rather the degraded product diethyl methylmalonate. All attempts at reducing the ketone group of **32** to the secondary alcohol resulted in the degradation of the product or in no reaction.

The difficulty in reducing **32** led to the synthetic approach shown in Scheme 3.7. The total reduction of **32** with lithium aluminum hydride yielded the expected triol **36** in 70% yield. The derivatization of the triol **36** to the trihalide **37** or the trimesylate **38** using reported procedures were unsuccessful resulting in no reaction, decomposition, or partial reaction yielding several products. The formation of trihalides and trimesylates of $CH_3C(CH_2X)_3$ (X = Cl, Br, I, OMs), while difficult, have been reported.[17] It was thought that, in the case of **36**, perhaps the presence of the phenyl group caused unwanted electronic or steric effects that hindered reaction; thus, the methyl analog **39** (Figure 3.2) was made. The synthesis of the **39** and **40** were performed in an analogous manner to the synthesis of **32** only with acetyl chloride replacing benzoyl chloride as starting material. Unfortunately, attempts to reduce **40** resulted in degradation to dimethyl methylmalonate.

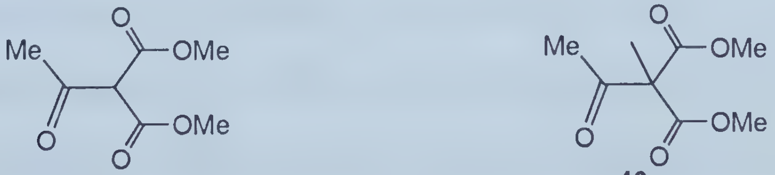

39 **40**

Figure 3.2: Non-aromatic system for synthesis of trichloride/trimesylate.

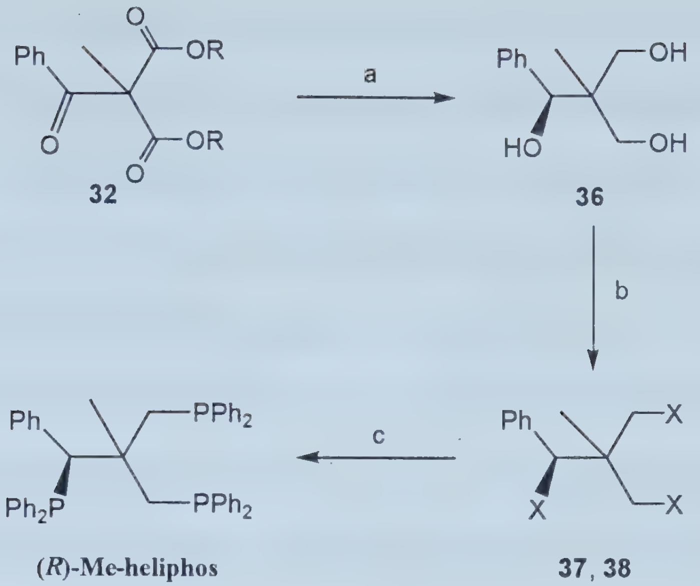

a) $LiAlH_4$, Et_2O. b) NEt_3, THF, $SOCl_2$ for X = Cl; NEt_3, CH_2Cl_2, CH_3SO_2Cl for X = OMs. c) 2 KH, 2 $HPPh_2$, THF, -10°C to r.t.

Scheme 3.7: Proposed synthetic pathway to (*R*)-Me-heliphos via reduction to a triol.

While new synthetic pathways were being devised to afford the desired Me-heliphos, the Bergens group developed a new catalyst system. The catalytic enantioselective hydrogenation of **40** was performed using the new catalyst, Ru((*R*)-BINAP)(pyridine)$_2$(Cl)$_2$, in the presence of four equivalents of aqueous HCl, in methanol solution for 20 h under 90 atm of H_2 and 60 °C in an unsealed sample vial. Once cooled, the bomb was depressurized and it was found that much of the reaction solution was outside of the sample vial. ^{1}H NMR analysis of the solution outside the vial indicated that degradation had occurred once again. The contents of the vial, however, were found to contain the desired alcohol $CH_3C(H)(OH)C(CH_3)(CO_2CH_3)_2$ (**41**) with no starting material or degradation product present. Upon repeating the reaction under the same conditions, only in a sealed vial, it was found that all the product had degraded as before. After several variations on the reaction, it was determined that the cause of the

degradation was the protic solvent in which the reactions were carried out. In an open vial, the methanol is displaced from the reaction and complete hydrogenation is observed without degradation. Reexamination of the attempted reductions of **32** revealed that all failed reductions occurred in reactions where protic solvents were utilized. Regardless, the desired alcohol (**41**) was then derivatized to the mesylate.

Reaction of **41** with triethylamine and methanesulfonyl chloride in methylene chloride solution yielded the desired mesylate product **42** in 90% yield by ^{1}H NMR. All further steps, the displacement of the mesyl group by diphenylphosphide, reduction of the esters, mesylation, etc. remain to be completed.

Conclusions:

Although the total synthesis of the desired compound is incomplete, the heart of the synthetic problem has been resolved. The completion of the synthesis should be routine in nature since the remaining steps have all been successfully performed in the syntheses of heliphos and other heliphos derivatives.[14] Upon completion of the synthesis of Me-heliphos, its coordination to ruthenium metal centers must be examined to determine if the proposed steric interaction between the added methyl group and that of the uncoordinated phosphine arm will favor tridentate coordination.

Experimental:

Materials and methods. The solvents methylene chloride (CaH_2), tetrahydrofuran (K, Ph_2CO), diethyl ether (K, Ph_2CO), toluene (K, Ph_2CO), triethylamine (CaH_2), and methanol (MgOMe) were distilled from drying agents under argon gas. The argon and dinitrogen gases were passed through a bed of Drierite drying agent. Unless stated otherwise, commercial reagents were used without further purification and all operations were performed under an inert atmosphere of argon or dinitrogen gas.

All ^1H, ^{13}C, and ^{31}P NMR spectra were measured with a Bruker AM-200 or AM-400 NMR spectrometer. ^1H and ^{13}C NMR chemical shifts are reported in parts per million (δ) relative to tetramethylsilane using the solvent as an internal reference. ^{31}P NMR chemical shifts are reported in parts per million (δ) relative to an 85% H_3PO_4 external reference. All ^{13}C and ^{31}P NMR spectra are ^1H decoupled unless stated otherwise. Mass spectra were measured using Kratos MS50 or AEI MS9 mass spectrometers. Microanalyses were performed at the University of Alberta Microanalysis Laboratory. The compounds [Ru(COD)(η^2-allyl)(MeCN)$_2$](BF$_4$),[11] RuCl$_2$(DMSO)$_4$,[12] **31**,[15] and **39**,[15] were synthesized via literature procedures.

Reaction of (*R*)-heliphos with [Ru(COD)(η^3-allyl)(MeCN)$_2$](BF$_4$). In air, (*R*)-heliphos (16.4 mg, 2.39 x 10^{-5} mol) and [Ru(COD)(η^3-allyl)(MeCN)$_2$](BF$_4$) (10.0 mg, 2.39 x 10^{-5} mol) were transferred to an NMR tube. The tube was sealed with a septum and then purged with Ar to remove all traces of oxygen. Once under Ar atmosphere, CD_2Cl_2 (0.6 mL) was transferred to the tube via gas-tight syringe. The NMR tube was

then shaken vigorously for 10 min and then analyzed by ^{1}H and ^{31}P NMR. Examination of the ^{1}H NMR showed the displacement of cyclooctadiene (COD) had occurred. ^{31}P NMR analysis indicated several products but the two major products (A ~40% and B ~30%) were found to be bidentate coordination of (*R*)-heliphos. ^{31}P NMR of major products (CD_2Cl_2, 25°C): δ 50.8 (d, $^{2}J_{P\text{-}P}$ = 46.0 Hz, 1P, A), 49.8 (d, $^{2}J_{P\text{-}P}$ = 47.5 Hz, 1P, B), 24.0 (d, $^{2}J_{P\text{-}P}$ = 47.5 Hz, 1P, B), 23.2 (d, $^{2}J_{P\text{-}P}$ = 46.0 Hz, 1P, A), -15.5 (s, 1P, A or B), -15.6 (s, 1P, A or B).

Addition of (*R*)-heliphos to the reaction of Ru(COD)(η^3-allyl)$_2$ with HBF$_4$•OEt$_2$. To a small Schlenk flask was transferred Ru(COD)(η^2-allyl) (10.0 mg, 3.4 x 10^{-5} mol). The flask was placed under vacuum and then the atmosphere replaced with Ar (x 3) to remove traces of oxygen. To this was transferred THF (1.0 mL) to dissolve the compound. To the stirred solution was added 1 equiv of HBF_4•OEt_2 and the solution was then stirred for 5 min. The solution was placed under vacuum to remove the solvent and then dissolved in CD_2Cl_2 (0.6 mL). The solution was transferred to an NMR tube containing (*R*)-heliphos (23.4 mg, 3.4 x 10^{-5} mol). The tube was shaken vigorously and then analyzed by ^{1}H and ^{31}P NMR. The room temperature spectra were very broad therefore they were re-recorded at -40 °C. ^{31}P NMR analysis indicated the presence of a compound (~ 30%) with all 3 arms of heliphos coordinated to the ruthenium center. Attempts to isolate this species from the reaction solution were unsuccessful. ^{31}P NMR of tripodal complex (CD_2Cl_2, -40°C): δ 42.0 (dd, $^{2}J_{P\text{-}P}$ = 30.5 Hz, $^{2}J_{P\text{-}P}$ = 38.5 Hz, 1P), 15.2 (apparent t, $^{2}J_{P\text{-}P}$ = 38.5 Hz, 1P), -2.7 (dd, $^{2}J_{P\text{-}P}$ = 30.5 Hz, $^{2}J_{P\text{-}P}$ = 38.5 Hz, 1P).

Attempted synthesis of [Ru_2((*R*)-heliphos)$_2$(η^2-Cl)$_3$](Cl). In air, $RuCl_2(DMSO)_4$ (22.3 mg, 4.60 x 10^{-4} mol) was transferred to a 50 mL flask and the flask was fitted with a condenser and gas-inlet adapter. The system was flushed with dinitrogen gas for 30 min. To a separate Schlenk tube was transferred (*R*)-heliphos (29.9 mg, 4.35 x 10^{-4} mol). The tube was sealed with a septum and placed under high vacuum and refilled with dinitrogen gas (x 3). To the flask containing $RuCl_2(DMSO)_4$, was transferred toluene (4.0 mL) via gas-tight syringe. The solution was stirred at 75 °C for 10 min then the (*R*)-heliphos was transferred over to the flask with toluene (2.0 mL) via canula. The solution was then stirred at 110 °C for 20 h. The flask was cooled to ambient temperature and the solvent was removed under reduced pressure yielding a yellow solid product. The sample was then further dried at 40 °C for 2 h under high vacuum and then analyzed by ^{31}P NMR and indicated presence of two compounds (**A**:**B**; 53:47). ^{31}P NMR (81.0 MHz, CD_2Cl_2): δ -11.2 (br s and s, 2P, 1P of **A** and 1P of **B**, overlapped), 33.1 (d, 1P, $^2J_{P\text{-}P}$ = 43 Hz, **B**), 37.9 (d, 1P, $^2J_{P\text{-}P}$ = 43 Hz, **B**), 52.0 (d, 1P, $^2J_{P\text{-}P}$ = 52 Hz, **A**), 55.1 (d, 1P, $^2J_{P\text{-}P}$ = 52 Hz, **A**). Addition of CD_3OD (1:1 with CD_2Cl_2) to the NMR tube with vigorous shaking did not change the spectrum. Anal. Calcd for $[C_{46}H_{41}P_3RuCl_2]_2$: C, 64.34; H, 4.81; S, 0; Cl, 8.26. Found: C, 59.24; H, 5.30; S, 5.58; Cl, 7.24. Anal. Calcd for Ru(η^2-(*R*)-heliphos)$(DMSO)_2(Cl)_2$: C, 59.17; H, 5.26; S, 6.32; Cl, 7.00.

$C_6H_5C(O)C(CH_3)(CO_2CH_2CH_3)_2$ (32). In air, **31** (5.9346 g, 2.25 x 10^{-2} mol) was transferred to a 250 mL flask along with $CHCl_3$ (25 mL) and the solution was stirred for 5 min. To the solution was added an aqueous solution (25 mL) of NaOH (1.7977 g,

4.49×10^{-2} mol) and n-Bu_4NHSO_4 (7.6275 g, 2.25×10^{-2} mol) over 2 min. The solution was stirred for 2 h and then it was transferred to a separatory funnel. The organic layer was separated and the aqueous layer back-extracted with $CHCl_3$ (2 x 15 mL). The organic layers were combined then the solvent was removed under reduced pressure. The solid residue was then recrystallized in EtOAc (9.1638 g, 80.7% yield). The solid (6.8938 g, 1.36×10^{-2} mol) was then transferred to a 100 mL flask and dissolved in $CHCl_3$ (50 mL). To the stirred solution was added CH_3I (2.7 mL, 4.21×10^{-2} mol). The solution was stirred for 1.5 h then the solvent was removed under reduced pressure yielding a yellow-white slurry. The solid was then recrystallized with Et_2O (2.85 g, 75.1% yield). ^1H NMR (200.1 MHz, $CDCl_3$): δ 1.19 (t, 3H, $C_6H_5C(O)C(CH_3)$-$(CO_2CH_2C\mathit{H}_3)_2$), 1.85 (s, 3H, $C_6H_5C(O)C(C\mathit{H}_3)(CO_2CH_2CH_3)_2$), 4.26 (q, 4H, $C_6H_5C(O)C(CH_3)(CO_2C\mathit{H}_2CH_3)_2$), 7.35 - 7.55 (m, 3H, $C_6\mathit{H}_5C(O)C(CH_3)(CO_2CH_2CH_3)_2$), 7.85 (m, 2H, $C_6\mathit{H}_5C(O)C(CH_3)$-$(CO_2CH_2CH_3)_2$). **39** was prepared in a similar manner (67.5% yield). ^1H NMR (400.1 MHz, $CDCl_3$): δ 1.61 (s, 3H, $C\mathit{H}_3C(O)C(CH_3)(CO_2CH_3)_2$), 2.28 (s, 3H, $CH_3C(O)C(C\mathit{H}_3)(CO_2CH_3)_2$), 3.79 (s, 6H, $CH_3C(O)C(CH_3)(CO_2C\mathit{H}_3)_2$).

$CH_3(C(H)(C_6H_5)(OH))(CH_2OH)_2$ (36). In air, $LiAlH_4$ (19.989 g, 5.24×10^{-1} mol) was transferred to a 3-necked flask and a dropping funnel, gas-inlet adapter, and septa were placed on the flask. The system was placed under vacuum, heated, and refilled with argon gas. To the flask was added Et_2O (150 mL) via canula. The ketodiester **32** (9.725 g, 3.49×10^{-2} mol) was transferred to the dropping funnel along with Et_2O (100 mL). The flask was placed in a 0 °C bath and the **32**/Et_2O solution was

added dropwise over 30 min. The solution was then stirred for 30 min at 0 °C and then for a further 3.5 h at ambient temperature. The $LiAlH_4$ was neutralized by the dropwise addition of deoxygenated distilled water (20.0 mL) at 0 °C, deoxygenated 10% NaOH solution (20.0 mL) at 0 °C, and deoxygenated distilled water at room temperature (60.0 mL). The mixture was stirred for 30 min, filtered, the solid washed with CH_2Cl_2 (3 x 100 mL), and concentrated under reduced pressure yielding a white solid (3.99 g, 58.2% yield). ^1H NMR (400.1 MHz, acetone-d_6): δ 0.7 (s, 3H,$\mathit{CH_3}C(C(H)(C_6H_5)(OH))(CH_2OH)_2$), 3.40 (dd, 1H, $CH_3C(C(H)(C_6H_5)(OH))(C\mathit{H_2}OH)_2$), 3.50 (dd, 1H, $CH_3C(C(H)(C_6H_5)(OH))(C\mathit{H_2}OH)_2$), 3.58 (dd, 1H, $CH_3C(C(H)(C_6H_5)(OH))(C\mathit{H_2}OH)_2$), 3.74 (dd, 1H, $CH_3C(C(H)(C_6H_5)(OH))(C\mathit{H_2}OH)_2$), 3.85 (dd, 1H, $CH_3C(C(H)(C_6H_5)(OH))(CH_2O\mathit{H})_2$), 3.98 (‘t’, 1H, $CH_3C(C(H)(C_6H_5)(OH))(CH_2O\mathit{H})_2$), 4.62 (d, 1H, $CH_3C(C(H)(C_6H_5)(O\mathit{H}))(CH_2OH)_2$), 4.92 (d, 1H, $CH_3C(C(\mathit{H})(C_6H_5)(OH))(CH_2OH)_2$), 7.22 (m, 1H, $CH_3C(C(H)(C_6\mathit{H_5})(OH))(CH_2OH)_2$), 7.31 (t, 2H, $CH_3C(C(H)(C_6\mathit{H_5})(OH))(CH_2OH)_2$), 7.41 (d, 2H, $CH_3C(C(H)(C_6\mathit{H_5})(OH))(CH_2OH)_2$). ^{13}C (100.6 MHz, acetone-d_6): δ 12.2 (1C, $CH_3\mathit{C}(C(H)(C_6H_5)(OH))(CH_2OH)_2$), 15.3 (1C, $\mathit{C}H_3C(C(H)(C_6H_5)(OH))(CH_2OH)_2$), 67.3 (1C, $CH_3C(C(H)(C_6H_5)(OH))(\mathit{C}H_2OH)_2$), 67.4 (1C, $CH_3C(C(H)(C_6H_5)(OH))(\mathit{C}H_2OH)_2$), 77.2 (1C, $CH_3C(\mathit{C}(H)(C_6H_5)(OH))(CH_2OH)_2$), 127.6 (1C, $CH_3C(C(H)(\mathit{C_6}H_5)(OH))(CH_2OH)_2$), 128.1 (2C, $CH_3C(C(H)(\mathit{C_6}H_5)(OH))(CH_2OH)_2$), 128.5 (2C, $CH_3C(C(H)(\mathit{C_6}H_5)(OH))(CH_2OH)_2$), 143.5 (1C, $CH_3C(C(H)(\mathit{C_6}H_5)(OH))(CH_2OH)_2$).

($CH_3C(O)C(CH_3)(CO_2CH_3)_2$ (40). In air, **39** (12.50 g, 7.18 x 10^{-2} mol), K_2CO_3 (9.92 g, 7.18 x 10^{-2} mol), and acetone (200 mL) were transferred to a 250 mL flask. A

condenser and gas-inlet adapter were added and the system flushed with argon gas for 30 min. To the stirred solution was added CH_3I (18 mL, 2.87×10^{-1} mol). The reaction was stirred under reflux (40 °C) for 16 h. The solution was cooled to room temperature and the solvent removed under reduced pressure. The remaining solid/liquid had CH_2Cl_2 (25 mL) added and the heterogeneous solution, was passed through an alumina column (10 cm high, 0.5 cm diameter). The column was washed with CH_2Cl_2 (100 mL) to ensure all product was passed through the column. The solvent was then removed under reduced pressure yielding a clear-pale yellow liquid (11.8 g, 87.5% yield). ^1H NMR (400.1 MHz, $CDCl_3$): δ 1.62 (s, 3H, $(CH_3C(O)C(\mathit{CH}_3)(CO_2CH_3)_2)$), 2.28 (s, 3H, $(\mathit{CH}_3C(O)C(CH_3)$-$(CO_2CH_3)_2)$), 3.79 (s, 6H, $(CH_3C(O)C(CH_3)(CO_2\mathit{CH}_3)_2)$).

$CH_3C(H)(OH)C(CH_3)(CO_2CH_3)_2$ (41). Ru((*R*)-BINAP)$(Cl)_2(C_5H_5N)_2$ (20.7 mg, 2.17×10^{-5} mol) was transferred to a 20 mL sample vial and the vial was sealed with a septum. The vial was then flushed for 20 min with argon gas to remove all traces of oxygen. Once deoxygenated, methanol (5.0 mL) was added via gas-tight syringe. To the solution was added 4 equiv of 2 N HCl (44 μL, 8.69×10^{-5} mol). The solution was stirred for 5 min then **40** (0.409 g, 2.17×10^{-3} mol) in methanol (5.0 mL) was transferred via canula. The sample vial was placed in a glove bag, the septum removed, and the vial placed in a steel bomb. The bomb was then sealed, removed from the glove bag, flushed (x 3) with dihydrogen gas, then pressurized to 1225 psig. The bomb was then placed in a preheated 60 °C bath and stirred for 24 h. The bomb was cooled to ambient temperature, depressurized, and opened to the atmosphere. The solution was both in the sample vial, orange solution, and outside the vial, clear and colorless. The solutions were placed

under reduced pressure to remove solvent and then analyzed by ^{1}H NMR. The solution outside the vial was shown to contain dimethyl methylmalonate as the product. The solution inside the vial was shown to be that of **41** (100% yield by ^{1}H NMR). ^{1}H NMR (400.1 MHz, $CDCl_3$): δ 1.11 (d, 3H, $^{3}J_{H\text{-}H}$ = 6.5 Hz, $\mathit{CH_3}C(H)(OH)C(CH_3)(CO_2CH_3)_2$), 1.39 (s, 3H, $CH_3C(H)(OH)C(\mathit{CH_3})(CO_2CH_3)_2$), 2.99 (br s, 1H, $CH_3C(H)(O\mathit{H})C(CH_3)$-$(CO_2CH_3)_2$), 3.72 (s, 3H, $CH_3C(H)(OH)C(CH_3)(CO_2\mathit{CH_3})_2$), 3.74 (s, 3H, $CH_3C(H)$-$(OH)C(CH_3)(CO_2\mathit{CH_3})_2$), 4.31 (q, 1H, $^{3}J_{H\text{-}H}$ = 6.5 Hz, $CH_3C(\mathit{H})(OH)C(CH_3)(CO_2CH_3)_2$).

$CH_3C(H)(OSO_2CH_3)C(CH_3)(CO_2CH_3)_2$ (42). To a 250 mL three-necked flask was transferred **41** (0.502 g, 2.63 x 10^{-3} mol) and a dropping funnel was added. The was flushed with argon gas to remove all traces of oxygen. To the purged system, CH_2Cl_2 (~80 mL) was added at -60 °C. To the cooled solution was added NEt_3 (0.55 mL, 3.94 x 10^{-3} mol) via gas-tight syringe. To the dropping funnel was added methanesulfonyl chloride (0.23 mL, 2.89 x 10^{-3} mol) and CH_2Cl_2 (10 mL). The solution was added dropwise over 10 min while the flask was kept at -40 °C. The solution was allowed to warm to ambient temperature over 1 h and then stirred for a further 4.5 h. The solution was then quenched with added crushed ice (~18 g) and distilled water (18.0 mL) and stirred for 30 min. The solution was then transferred to a separatory funnel and the organic layer was separated. The aqueous layer was back-extracted with CH_2Cl_2 (3 x 40 mL). The organic layers were combined in the separatory funnel and washed sequentially with distilled water (2 x 50 mL, -10 °C), saturated $NaHCO_3$ solution (2 x 50 mL, -10 °C), and saturated NaCl solution (2 x 50 mL, -10 °C). The organic layers were then stirred over $MgSO_4$ for 16 h. The solution was filtered, the solid washed with

CH_2Cl_2 (4 x 50 mL), and the solvent removed under reduced pressure yielding a clear, pale yellow liquid (0.635 g, 90.0% yield). ^{1}H NMR (400.1 MHz, $CDCl_3$): δ 1.46 (d, 3H, $^3J_{H-H}$ = 7.0 Hz, $CH_3C(H)(OSO_2CH_3)C(CH_3)(CO_2CH_3)_2$), 1.48 (s, 3H, $CH_3C(H)$-$(OSO_2CH_3)C(CH_3)(CO_2CH_3)_2$), 3.02 (s, 3H, $CH_3C(H)(OSO_2CH_3)C(CH_3)$-$(CO_2CH_3)_2$), 3.78 (s, 3H, $CH_3C(H)(OSO_2CH_3)C(CH_3)(CO_2CH_3)_2$), 3.80 (s, 3H, $CH_3C(H)(OSO_2CH_3)$-$C(CH_3)(CO_2CH_3)_2$), 5.42 (q, 1H, $^3J_{H-H}$ = 7.0 Hz, $CH_3C(H)(OSO_2CH_3)C(CH_3)$-$(CO_2CH_3)_2$).

References and Notes:

(1) Some representative examples: (a) Lütjens, H.; Wahl, G.; Möller, F.; Knochel, P.; Sundermeyer, J. *Organometallics* **1997**, *16*, 5869-5878. (b) Bianchini, C.; Meli, A. *J. Chem. Soc., Dalton Trans.* **1996**, 801. (a) Adolfsson, H.; Wärnmark, K.; Moberg, C. *J. Chem. Soc., Chem. Commun.* **1992**, 1054. (b) Trofimenko, S. *Chem. Rev.* **1993**, *93*, 943. (c) Walter, O.; Klein, T.; Huttner, G.; Zsolnai, L. *Z. Naturforsch.* **1995**, *50b*, 729. (d) Bianchini, C.; Herrera, V.; Jimenez, M. V.; Meli, A.; Sanchez-Delgado, R.; Vizza, F. *J. Am. Chem. Soc.* **1995**, *117*, 8567-8575. (e) Mayer, H. A.; Stößel, P.; Fawzi, R.; Steimann, M. *J. Organomet. Chem.* **1995**, *492*, C1-C3. (f) Mayer, H. A.; Stößel, P.; Fawzi, R.; Steimann, M. *Chem. Ber.* **1995**, *128*, 719-723. (g) Lütjens, H.; Knochel, P. *Tetrahedron: Asymmetry* **1994**, *5*, 1161-1162. (h) Ma, S.; Venanzi, L. M. *Tetrahedron Lett.* **1993**, *34*, 8071. (i) Sernau, V.; Huttner, G.; Fritz, M.; Zsolnai, L.; Walker, O. *J. Organomet. Chem.* **1993**, *458*, 63. (j) Ward, T. R.; Venanzi, L. M.; Albinati, A.; Lianza, F.; Gerfin, T.; Gramlich, V.; Tombo, G. M. R. *Helv. Chim. Acta* **1991**, *74*, 983. (k) Burk, M. J.; Harlow, R. L. *Angew. Chem. Int. Ed. Engl.* **1990**, *29*, 1462. (l) Bianchini, C.; Meli, A.; Peruzzini, M.; Vizza, F.; Frediani, P.; Ramirèz, J. A. *Organometallics* **1990**, *9*, 226.

(2) Some representative examples: (a) Bianchini, C.; Meli, A.; Peruzzini, M.; Vizza, F.; Frediani, P.; Ramirez, J. A. *Organometallics* **1990**, *9*, 226. (b) Bianchini, C.; Meli, A.; Laschi, F.; Ramirez, J. A.; Zanello, P. *Inorg. Chem.* **1988**, *27*, 4429. (c) Bianchini, C.; Mealli, C.; Meli, A.; Peruzzini, M.; Zanobini, F. *J. Am. Chem. Soc.* **1988**, *110*, 8725. (d) Bianchini, C.; Meli, A.; Peruzzini, Vizza, F.; Fujiwara, Y.;

Jintoku, T.; Taniguchi, H. *J. Chem. Soc., Chem. Commun.* **1988**, 210. (e) DuBois, D. L.; Meek, D. W. *Inorg. Chim. Acta* **1976**, *19*, L29.

(3) (a) Brandt, K.; Sheldrick, S. *Chem. Ber.* **1996**, *129*, 1199-1206. (b) Rauscher, D. J.; Thaler, E. G.; Huffmann, J. C.; Caulton, K. G. *Organometallics* **1991**, *10*, 2209. (c) Thaler, E. G.; Folting, K.; Caulton, K. G. *J. Am. Chem. Soc.* **1990**, *112*, 2664-2672. Earlier evidence for phosphine-arm dissociation: (d) Bianchini, C.; Meli, A.; Peruzzini, M.; Vizza, F.; Albinati, A. *Organometallics* **1990**, *9*, 2283. (e) Thaler, E. G.; Caulton, K. G. *Organometallics* **1990**, *9*, 1871. (f) Johnston, G. G.; Baird, M. C. *J. Chem. Soc., Chem. Commun.* **1989**, 1008. (g) Johnston, G. G., Baird, M. C. *Organometallics* **1989**, *8*, 1894. References cited within as well.

(4) (a) Halpern, J. *Pure. Appl. Chem.* **1983**, *55*, 99-106. (b) Halpern, J. *Science* **1982**, *217*, 401-407.

(5) Ashby, M. T.; Halpern, J. *J. Am. Chem. Soc.* **1991**, *113*, 589-594.

(6) Ohta, T.; Takaya, H.; Noyori, R. *Tetrahedron Lett.* **1990**, *31*, 7189-7192.

(7) Yoshikawa, K.; Murata, M.; Yamamoto, N.; Inoguchi, K.; Achiwa, K. *Chem. Pharm. Bull.* **1992**, *40*, 1072-1074.

(8) Chan, A. S. C.; Chen, C. C.; Yang, T. K.; Huang, J. H.; Lin, Y. C. *Inorg. Chim. Acta* **1995**, *234*, 95-100.

(9) Yao, Y. *Heliphos and its Transition Metal Complexes*: M.Sc. Thesis; University of Alberta: Edmonton; 1997, Chapter 3.

(10) Burk, M. J.; Harlow, R. L. *Angew. Chem. Int. Ed. Engl.* **1990**, *29*, 1462.

(11) (a) Wiles, J. A.; Lee, C. E.; McDonald, R.; Bergens, S. H. *Organometallics* **1996**, *15*, 3782-3784. (b) Daley, C. J. A.; Wiles, J. A.; Bergens, S. H. *Can. J. Chem.* **1998**, *76*, 1447-1456.

(12) Rhodes, L. F.; Sorato, C.; Venanzi, L. M.; Bachechi, F. *Inorg. Chem.* **1988**, *27*, 604-610, and references therein.

(13) Methylation of the α-carbon to the phosphine (also benzylic carbon) may have occurred under these conditions but the products were never fully characterized.

(14) Yao, Y.; Daley, C. J. A.; McDonald, R.; Bergens, S. H. *Organometallics* **1997**, *16*, 1890-1896.

(15) Brändström, A.; Junggren, U. *Acta. Chem. Scand.* **1969**, *23*, 2536-2537.

(16) Rathke, M. W.; Cowan, P. J. *J. Org. Chem.* **1985**, *50*, 2622-2624.

(17) Some examples: (a) Muth, A.; Walter, O.; Huttner, G.; Asam, A.; Zsolnai, L.; Emmerich, Ch. *J. Organomet. Chem.* **1994**, *468*, 149-163. (b) Latour, S.; Wuest, J. D. *Synthesis* **1987**, 742. (c) Hewertson, W.; Watson, H. R. *J. Chem. Soc.* **1962**, 1490.

Chapter 4

Application of $[Ru((R)\text{-BINAP})(MeCN)(1\text{-}3{:}5,6\text{-}\eta\text{-}C_8H_{11})](BF_4)$ As a Catalyst Precursor For Enantioselective Hydrogenations.[†]

Introduction:

Asymmetric catalysis by chiral transition-metal complexes is among the most successful methods for the synthesis of optically active organic compounds.[1, 2a] Of the hundreds of chiral ligands reported, 2,2'-bis(diphenylphosphino)-1,1'-binaphthyl (BINAP) is among the most successful.[2] While rhodium-BINAP systems are highly enantioselective catalysts for the hydrogenation of certain prochiral olefins,[3] the development of ruthenium-BINAP systems has led to catalysts that hydrogenate a much wider range of prochiral olefins and ketones with high enantioselectivities.[4]

In the Bergens laboratories, the development of a new ruthenium-BINAP catalyst system was accomplished. The catalyst is a well-defined "(BINAP)Ru-H" species. The purpose of obtaining well defined ruthenium-hydride species is to have a well characterized system that we believe to be the "active" catalysts in ruthenium catalyzed

---

[†] A version of this chapter has been published in *Can. J. Chem.* **1998**, *76*, 1447-1456.

hydrogenation reactions.[5] The developed system used [Ru((*R*)-BINAP)(MeCN)(1-3:5,6-η-C_8H_{11})](BF_4) (**1**) as catalyst precursor. Its synthesis was first reported in 1996 along with its use as a catalyst precursor for several catalytic processes.[6] It was synthesized from $RuCl_3 \bullet xH_2O$ in four steps with an overall yield of approximately 45% (Scheme 4.1). Compound **1** reacts, within minutes, with dihydrogen gas at room temperature in acetone, tetrahydrofuran, or methanol solution to generate cyclooctane and [Ru((*R*)-BINAP)(H)$(MeCN)_n(Sol)_{3-n}$](BF_4) (**2**, Sol = acetone, tetrahydrofuran, or methanol; n= 0-3), which is believed to be the active catalyst species for the previously disclosed reactions.

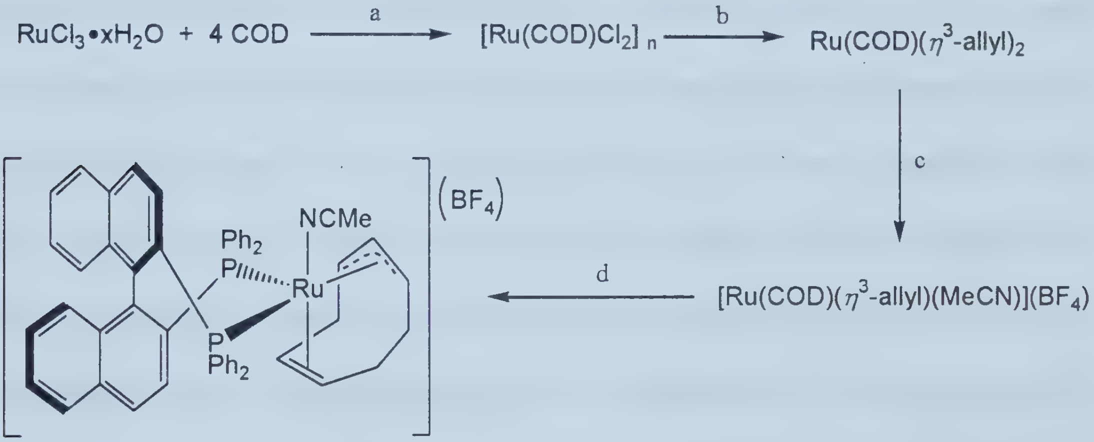

1

a) EtOH, 90°C, 20 h, 80% yield. b) 5 equiv $H_2C{=}CHCH_2MgCl$, Et_2O, r.t., 24 h, 85% yield. c) 0.9 equiv $HBF_4 \bullet OEt_2$, Et_2O:MeCN (1:1), 0°C, 73.5% yield. d) 1 equiv (*R*)-BINAP, acetone, 3 h, 92% yield.

Scheme 4.1: Synthesis of [Ru((*R*)-BINAP)(1-3;5,6-η-C_8H_{11})(MeCN)](BF_4) (1).

The catalyst system **2** is distinguished from other reported ruthenium-BINAP catalysts by the combination of the following three features. First, it is a reasonably well-defined system with an active ruthenium hydride species.[7] Second, the active catalyst is generated in high concentrations under mild conditions. In acetone, tetrahydrofuran, or

methanol solution, **1** reacts under 1-2 atm of dihydrogen gas at room temperature to generate **2** in minutes. Third, the system is not sterically hindered, it has at least two (three if acetonitrile ligand is displaced during catalysis) readily available coordination sites occupied by labile solvento ligands allowing easy access to the ruthenium center by substrates. This feature is essential for catalytic activity. Furthermore, the low-oxidation state of ruthenium and its tendency to undergo oxidative addition, insertion, and reductive elimination makes it a valuable catalyst system for the investigation of possible substrate-catalyst interactions.

The use of **2** as a catalyst system for the enantioselective catalytic hydrogenation of a representative series of prochiral substrates is reported. Further, the use of model protic and aprotic solvents was examined for the enantioselective hydrogenation of α,β-unsaturated acids and esters. This work was carried out to define the utility of **2** as a catalyst system relative to other ruthenium-BINAP catalyst systems reported in the literature, and to explore possible general trends in enantioselectivity by such catalysts. It is only through such trends that the general components of enantioselectivity by ruthenium-BINAP catalysts, if they exist, can be established.

Results and Discussion:

The nature of $[Ru((R)\text{-BINAP})(H)(MeCN)_n(Sol)_{3-n}](BF_4)$ (2, Sol = acetone, tetrahydrofuran, or methanol; n= 0-3). The acetonitrile ligand is rapidly exchanged between all the available vacant coordination sites in acetone solutions of **2** at room temperature. Static NMR spectra were observed upon cooling, showing a static mixture of eight hydrides ranging from $[Ru((R)\text{-BINAP})(H)(acetone)_3](BF_4)$ to $[Ru((R)\text{-BINAP})(H)(MeCN)_3](BF_4)$ (Scheme 4.2). From ^1H NMR studies in acetone-d_6, it was found that for all of the hydrides, the $^2J_{P\text{-}H}$ were approximately 25 to 30 Hz. These coupling constants correspond to *cis*- couplings between the hydride and phosphines, therefore, these species all contain the hydride ligand in a coordination site *cis*- to both phosphorus centers.[8] This mutually *cis*- disposition of the coordinated hydride and phosphorus centers presumably results from the high *trans*- influence of both of these types of ligands.[9] In tetrahydrofuran solution, the system exists mainly as one diastereomer of the monoacetonitrile complex $[Ru((R)\text{-BINAP})(H)(MeCN)(THF)_2](BF_4)$. In acetonitrile solution, **2** exists solely as $[Ru((R)\text{-BINAP})(H)(MeCN)_3](BF_4)$. To a first approximation, the system can be regarded sterically as a source of the fragment "$[Ru((R)\text{-BINAP})(H)]^+$." For example, the solvento and acetonitrile ligands can all be displaced by arene donors (e.g. benzene) to generate the corresponding $[Ru((R)\text{-BINAP})(H)(\eta^6\text{-arene})](BF_4)$ complexes. An example of this was observed on reaction of methyl α-acetamidocinnamate (MAC, **3b**)[10] with **2** (Equation 4.1). It is also noted that removal of acetonitrile from **1** resulted in no change in the enantioselectivity for the hydrogenation of MAC.

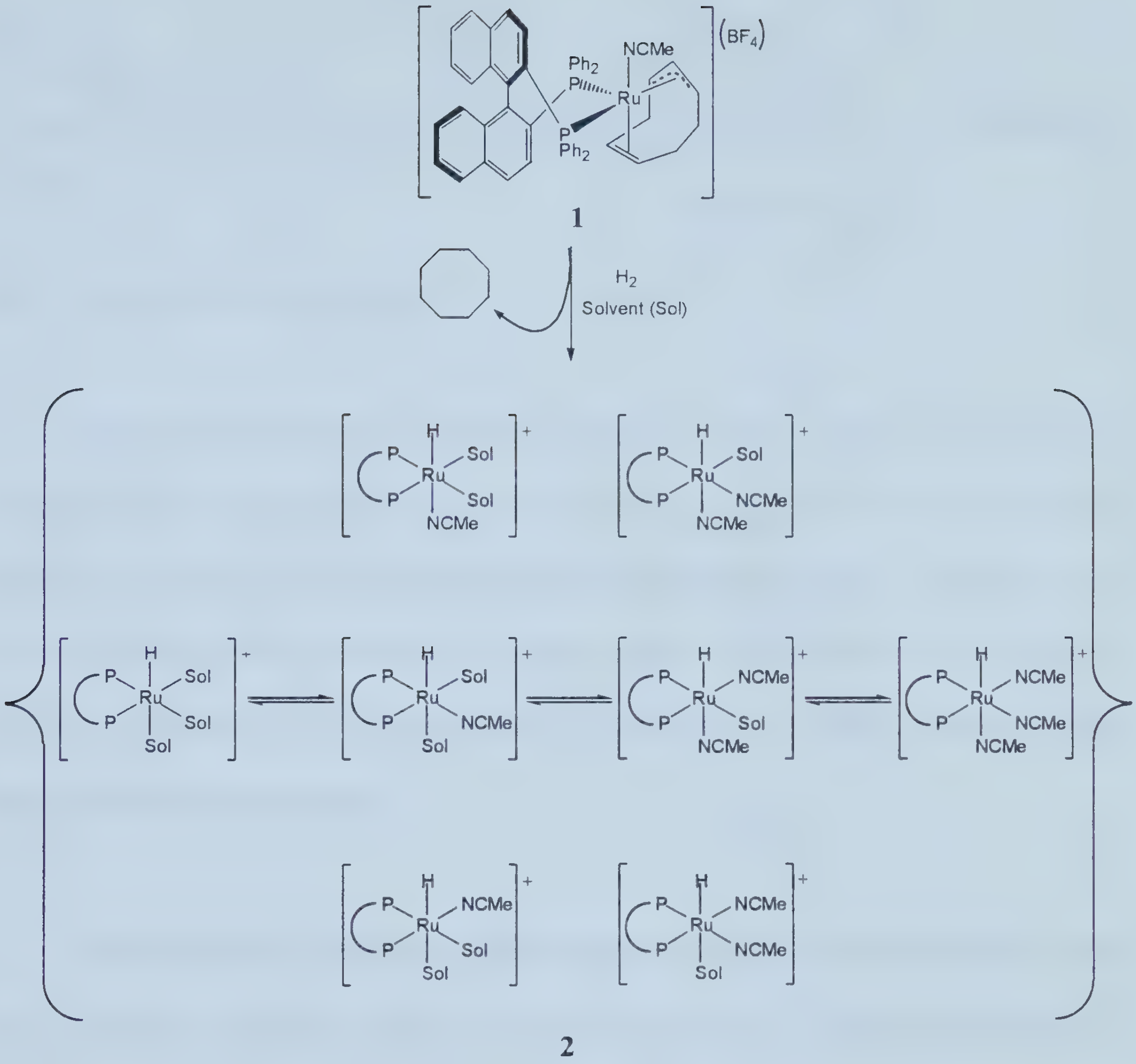
(BF4)
NCMe
Ph2
P
Ru
Ph2
1
H2
Solvent (Sol)
H
Sol
NCMe
+
2

Sol = acetone, THF, or MeOH

Scheme 4.2: Nature of 2 in solution.

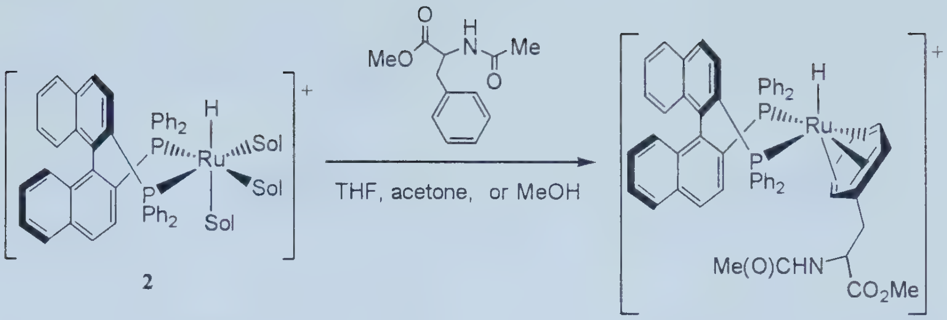

2

Equation 4.1

Sol = THF, acetone, MeOH, and/or MeCN

Hydrogenation using 2 as catalyst. Figures 4.1 and 4.2 show the representative substrates that were hydrogenated using **2** as the catalyst. These are the most commonly reported substrates for use in enantioselective hydrogenation reactions. Figures 4.1 and 4.2 also show the major enantiomer produced upon hydrogenation with **2** as catalyst. Tables 4.1, 4.2, 4.4 and 4.5 summarize the conditions and the results of these catalytic enantioselective hydrogenations.

***α,β*-Unsaturated carboxylic acid or ester substrates.** The hydrogenations were first performed in methanol solution as a model protic solvent. The hydrogenation of *α*-acetamidocinnamic acid (**3a**) under 4 atm of dihydrogen at 35 °C for 94 h resulted in only 10% conversion to *N*-acetylphenylalanine (**3a'**) (Table 4.1; entry 1). In order to obtain complete hydrogenation, it was necessary to increase the pressure of dihydrogen from 4 atm to 100 atm. Under these pressures and 40 °C, **3a'** was obtained in 100% yield after 20 h however, with only a moderate enantioselectivity of 46% ee (*R*) (Table 4.1; entry 2). Interestingly, the hydrogenation of the corresponding methyl ester of **3a**, (*Z*)-methyl *α*-acetamidocinnamate (MAC, **3b**), occurs under much milder conditions (Table 4.1; entry 3).[6] Hydrogenation of **3b** goes to completion under 4 atm of dihydrogen, 30 °C, in 30 h

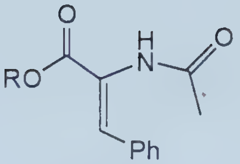
3a: R = H
3b: R = Me

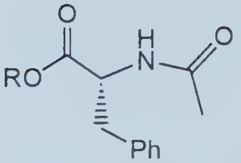
3a': R = H
3b': R = Me

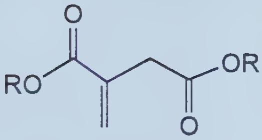
4a: R = H
4b: R = Me

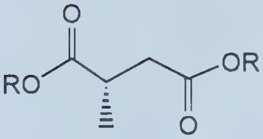
4a': R = H
4b': R = Me

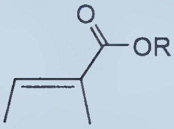
5a: R = H
5b: R = Me

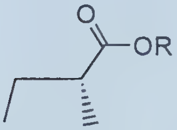
5a': R = H
5b': R = Me

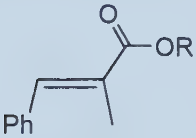
6a: R = H
6b: R = Me

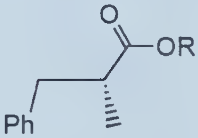
6a': R = H
6b': R = Me

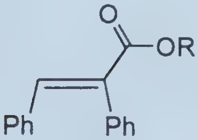
7a: R = H

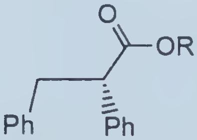
7a': R = H

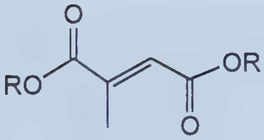
8a: R = H

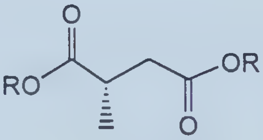
8a': R = H

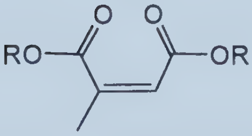
9a: R = H

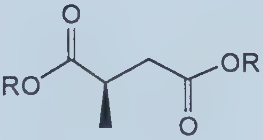
9a': R = H

Figure 4.1: *α, β*-Unsaturated acids and esters hydrogenated using 2 as catalyst.

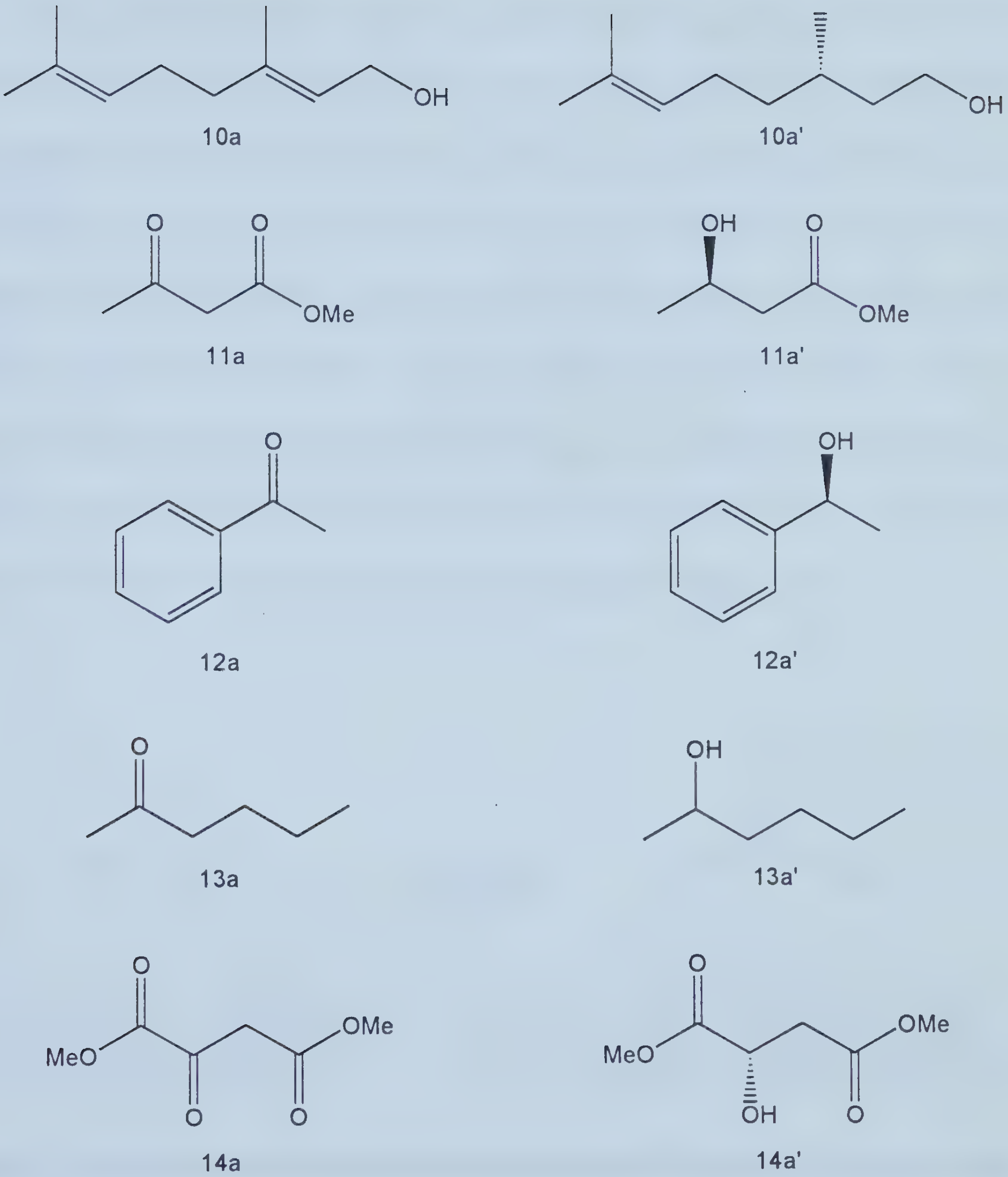
10a
10a'
11a
11a'
12a
12a'
13a
13a'
14a
14a'

Figure 4.2: Allylic alcohol and ketones hydrogenated with 2 as catalyst.

to yield *N*-acetylphenylalanine methyl ester (**3b'**) in much greater enantioselectivity (86% ee (*R*)) than observed with **3a'**.

Hydrogenation of itaconic acid (**4a**) proceeded smoothly under mild conditions (4 atm H_2, 25 °C, 20 h) giving methylsuccinic acid (**4a'**) with high enantioselectivity of 90% ee (*S*) (Table 4.1; entry 4). This result is in contrast to the structurally related acid **3a**, which required harsh conditions for complete conversion. The hydrogenation of the dimethyl ester of **4a**, dimethyl itaconate (**4b**), also proceeded under similar mild conditions (4 atm H_2, 25 °C, 20 h) yielding dimethyl methylsuccinate (**4b'**) with very high enantioselectivity (95 % ee (S)) (Table 4.1; entry 5). It should be noted that the net enantioface selection by the catalyst **2** towards the substrates **4a** and **4b** is the same as that observed for the structurally related substrates **3a** and **3b** (Figure 4.3).

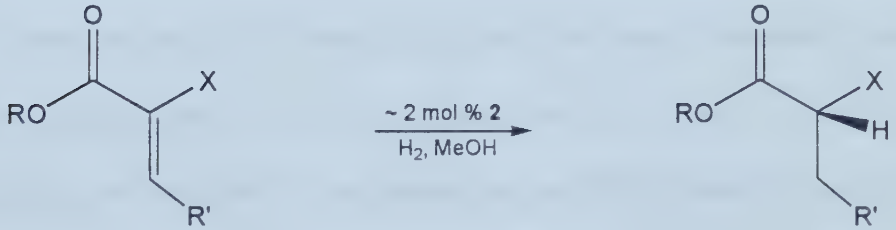

3a: R = H; R' = Ph; X = $N(H)CO_2Me$
3b: R = H; R' = Ph; X = $N(H)CO_2Me$
4a: R = H; R' = Ph; X = CH_2CO_2Me
4b: R = H; R' = Ph; X = CH_2CO_2Me

3a': R = H; R' = Ph; X = $N(H)CO_2Me$ (*R*) config.
3b': R = H; R' = Ph; X = $N(H)CO_2Me$ (*R*) config.
4a': R = H; R' = Ph; X = CH_2CO_2Me (*S*) config.
4b': R = H; R' = Ph; X = CH_2CO_2Me (*S*) config.

Figure 4.3: Net addition of hydrogen to substrates 3a, 3b, 4a, and 4b occurs through same face in the enantioselective hydrogenations catalyzed by 2.

The hydrogenation of tiglic acid (**5a**) (Table 4.1; entry 6) was quantitative under mild conditions giving 2-methylbutyric acid (**5a**') in high enantioselectivity (90% ee (*R*)). Unlike the success obtained in the hydrogenation of the methyl esters of both **3a** and **4a**, **3b** and **4b** respectively, the attempts to hydrogenate methyl tiglate (**5b**) were unsuccessful under 4 atm of dihydrogen (Table 4.1; entry 7). Furthermore, no hydrogenation was observed even under 100 atm of dihydrogen. This difference in reactivity between tiglic acid and methyl tiglate has been previously reported for another ruthenium-BINAP catalyst system.[11]

Attempts to hydrogenate α-methylcinnamic acid (**6a**) under conditions similar to those utilized for tiglic acid (4 atm H_2, 25 °C, 24 h) produced none of the expected 2-methyl-3-phenylpropionic acid (**6a**', Table 4.1; entry 8). In order to obtain 100% conversion, 100 atm of dihydrogen and 50 °C conditions were required. Under these conditions, **6a**' was produced in the moderate enantioselectivity of 40% ee (*R*) (Table 4.1; entry 9). As was the case for the ester of tiglic acid, **5b**, methyl α-methylcinnamate (**6b**) was not hydrogenated under 4 atm of dihydrogen over 90 h (Table 4.1; entry 10). Similar conditions and ee were reported for another ruthenium-BINAP catalyst system.[12]

Analogous to the observations of the hydrogenation of **6a**, α-phenylcinnamic acid (**7a**) was not hydrogenated under mild conditions (4 atm H_2, 25 °C, 24 h) but rather required 100 atm of dihydrogen and 50 °C. **7a** was completely hydrogenated under these conditions over 20 h to yield 2,3-diphenylpropionic acid in 46% ee (*R*) (Table 4.1; entry 11).

Investigations into the hydrogenations of mesaconic acid (**8a**) and citraconic acid (**9a**), structural isomers of itaconic acid (**4a**), were performed. It was determined that the

mild conditions used to hydrogenate **4a** were insufficient to hydrogenate both **8a** (0% conversion) and **9a** (10% conversion) (Table 4.1; entries 12 and 14, respectively). Complete conversion was obtained under 100 atm of dihydrogen and 50 °C yielding methylsuccinic acid from **8a** in 45% ee (*R*) and from **9a** in 30% ee (*S*) (Table 4.1; entries 13 and 15, respectively). This difference in enantioface selection with citraconic acid has been observed with another ruthenium-BINAP catalyst system.[13]

Table 4.1: Hydrogenation of substrates containing an α,β-unsaturated carboxylic acid or ester functionality in methanol using 2 as catalyst.[a]

Entry	Substrate	H_2 (atm)	Temp. (°C)	Time (h)	% Conv.	% ee
1	3a	4	35	94	10	---
2	3a	100	40	20	100	46 (*R*)
3[b]	3b	4	30	30	100	86 (*R*)
4	4a	4	25	20	100	90 (*S*)
5	4b	4	25	19	100	95 (*S*)
6	5a	3	25	9.5	100	90 (*R*)
7	5b	4	25	50	0	---
8	6a	4	25	24	0	---
9	6a	100	50	20	100	40 (*R*)
10	6b	4	25	24	0	---
11	7a	100	50	20	100	44 (*R*)
12	8a	4	25	24	< 1	---
13	8a	100	50	20	100	45 (*R*)
14	9a	4	25	24	< 5	---
17	9a	100	50	20	100	30 (*S*)

[a] Reaction conditions: 1 mol % catalyst, [Ru] = 3.0 mM. [b] Reaction conditions: 2 mol % catalyst, [Ru] = 2.6 mM (reference 6).

To investigate the use of an aprotic solvent, the hydrogenations were carried out in acetone solution. The results of these reactions are reported in Table 4.2. The hydrogenation of MAC (**3b**) proceeds smoothly under mild conditions to give *N*-acetylphenylalanine methyl ester in higher enantioselectivity (92% ee (*R*))[14] than does the hydrogenation in methanol solution (86% ee (*R*)) (Table 4.2; entry 3). The hydrogenation of dimethyl itaconate (**4b**) also proceeded under mild conditions in acetone solution (Table 4.2; entry 7) to yield dimethyl methylsuccinate with the same enantioselectivity (95% ee (*S*)) as that obtained from the hydrogenation in methanol solution (95% ee (*S*)). As was the case in methanol solvent, methyl tiglate (**5b**) did not undergo hydrogenation in acetone solution (Table 4.2; entry 10). The corresponding hydrogenations of α-acetamidocinnamic acid (**3a**), itaconic acid (**4a**), and tiglic acid (**5a**) were extremely slow under these conditions (4 atm H_2, 25 °C, acetone), giving low to moderate conversions ranging from 10% to 55% (Table 4.2; entries 1, 4, and 8 respectively). Even at 50 °C and 4 atm of dihydrogen the hydrogenation of **4a** proceeded to a maximum of approximately 65% conversion (Table 4.2; entry 5).

It has been reported that addition of an equivalent of base (e.g. amines) for every acid unit in the substrate often yields higher enantioselectivities and rates for the hydrogenation of acid substrates using both ruthenium and rhodium catalyst systems.[15] Examination of this effect on the hydrogenations of the acids (**3a**, **4a**, and **5a** show in Table 4.2) in acetone solution was undertaken. The hydrogenations of **4a** and **5a** (Table 4.2; entries 6 and 9, respectively) proceeded to completion in approximately 20 h under 4 atm of dihydrogen and 25 °C in the presence of one equivalent of triethylamine per acid group (NEt_3:**4a** = 2:1; NEt_3:**5a** = 2:1). Further, the enantiomeric excess improved from

90% ee (*R*) for **4a** and 90% ee (*S*) for **5a** in the absence of added base in methanol solution to 95% ee (*R*) and 95% ee (*S*) with added base in acetone solution. The addition of one equivalent of triethylamine did not enhance the rate of hydrogenation of **3a** yielding only approximately 10% conversion (Table 4.2; entry 2). It is noted that addition of base to the hydrogenation of the acids **6a**, **7a**, **8a**, and **9a** in acetone solution did not enhance the rate yielding essentially no product formation under 4 atm of dihydrogen.

Table 4.2: Hydrogenation of substrates containing an α,β-unsaturated carboxylic acid or ester functionality in acetone using 2 as catalyst.[a]

Entry	Substrate	N / S[b]	H_2 (atm)	Temp.(°C)	Time (h)	% Conv.	% ee
1	**3a**	0	4	25	20.5	<10	---
2	**3a**	1	4	25	20.5	<10	---
3[c]	**3b**	0	4	30	1	100	92 (*R*)
4	**4a**	0	4	25	18.5	~55	---
5	**4a**	0	4	50	18	~65	---
6	**4a**	2	4	25	18	100	95 (*S*)
7	**4b**	0	4	25	20.5	100	95 (*S*)
8	**5a**	0	4	25	20	<10	---
9	**5a**	1	4	25	18	100	95 (*R*)
10	**5b**	0	4	25	20	0	---

[a] Reaction conditions: 1 mol % catalyst, [Ru] = 3.0 mM. [b] N/S is defined as moles of NEt_3 added per mole of substrate. [c] Reaction conditions: 2 mol % catalyst, [Ru] = 2.6 mM (reference 14).

Table 4.3 compares these results to the best results reported in the literature for other ruthenium-BINAP systems. Apart from the hydrogenation of **3b**,[††] all the literature examples reported in Table 4.3 were performed in pure alcohol or binary alcohol-solvent solutions (solvent = tetrahydrofuran or methylene chloride), under mild temperatures (20-50 °C), and under low to moderate pressures of dihydrogen (1-5 atm). The results obtained with complex **1** as the catalyst precursor show it to be among the better ruthenium-BINAP systems examined to date for the hydrogenation of these substrates.

Inspection of Table 4.3 shows that while all the systems yield high enantioselectivities, no real trends in the enantioface selection, absolute configuration, of the major enantiomer produced by hydrogenation of tiglic acid (**5a**) using ruthenium-(*R*)-BINAP catalyst systems is observed. That methyl tiglate (**5b**) does not undergo hydrogenation but tiglic acid does suggests that substrates with one ester group that are not easily anchored by further chelation upon coordination to ruthenium will not undergo hydrogenation. Indeed, there was no evidence of interaction between the active catalyst species **2** and an up to 100-fold excess of methyl tiglate in acetone, tetrahydrofuran, methylene chloride, or methanol solution.[‡] The acids and other esters studied in this report all react stoichiometrically (1:1) with **2** to generate a variety of products. The structures of these ruthenium-BINAP-substrate complexes are under investigation.

[††] This is the only literature example we are aware of where **3b** is hydrogenated using a ruthenium-BINAP catalyst.

[‡] $[Ru((R)\text{-BINAP})(H)(MeCN)_n(acetone)_{3-n}](BF_4)$ (n = 0-3) was the only species detected by ^{31}P NMR spectroscopy.

Table 4.3: Comparison of Ru((*R*)-BINAP) catalyst systems in the hydrogenation of substrates containing an *α,β*-unsaturated carboxylic acid or ester functionality.

Catalyst System[a]	Substrates					Ref.
	3a	**3b**	**4a**	**4b**	**5a**	
1	46 (*R*)	92 (*R*)	95 (*S*)	95 (*S*)	95 (*R*)	6, 13
15	86 (*R*)	---	90 (*S*)	68 (*S*)	85 (*S*)	16, 17, 18
16	80 (*R*)	---	93 (*S*)	54 (*S*)	79 (*R*)	15a, 17, 18
17	---	---	94 (*S*)	---	88 (*R*)	15a
18	---	---	89 (*S*)	---	84 (*S*)	16
19	---	---	---	---	87 (*R*)	19
20	---	---	69 (*S*)	---	90 (*R*)	20
21	75 (*R*)	85 (*R*)[b]	98 (*S*)	---	---	21
22	---	---	---	---	94 (*R*)	22
23	---	---	---	---	92 (*R*)	23
24	---	---	---	---	89 (*R*)	24
25	---	---	---	---	89 (*R*)	25
26	63 (*R*)	69 (*R*)	---	32 (*S*)	---	26

[a] Catalyst systems; [Ru(BINAP)(C_8H_{11})(MeCN)](BF_4) (**1**); [Et_2NH_2](Ru_2Cl_5($BINAP)_2$) (**15**); Ru(BINAP)(H)(Cl) (**16**); [Ru$(BINAP)_2$(H)](PF_6) (**17**); Ru(BINAP)$(RCN)_2(Cl)_2$ (**18**, R = alkyl, aryl); [Ru(BINAP)(*p*-cymene)(I)](I) (**19**); Ru(BINAP)(2-methylallyl)$_2$ (**20**); Ru(BINAP)(2-methylallyl)$_2$ + 2 HBr (**21**); Ru(BINAP)($O_2CMe)_2$ (**22**); Ru(BINAP)($O_2CMe)_2$ + 2 HBF_4 (**23**); Ru(BINAP)(C_6H_6)(Cl)](Cl) (**24**); [Ru(BINAP)(C6H6)(Cl)](BF4) (**25**); Ru(BINAP)(MeOH)$_2$-(OC(O)$CF_3)_2$ (**26**). [b] Performed under 100 atm H_2.

Substrates **3a**, **3b**, **4a**, and **4b** were hydrogenated with good to excellent enantioselectivities and with the same enantioface selectivity. Figure 4.4 shows that these substrates all contain the same basic framework, a 1,4-dicarbonyl unit with the prochiral functionality at the 2-position (**27**). That hydrogenation of **3a**, **3b**, **4a**, and **4b**

all proceed with the same face selectivity for all reported ruthenium-(*R*)-BINAP systems (Table 4.3) under similar conditions, raises the possibility that they proceed through structurally related intermediates. Figure 4.4 illustrates one possible structure type (**28**) that may be an intermediate in ruthenium-BINAP catalyzed enantioselective hydrogenations. The structure proposed is based on the recently reported crystallographically characterized compound isolated from the reaction of MAC (**3b**) with **2** (Figure 4.4; **28**, R = OMe, R' = Me, R"= CHPh, Z = NH) performed in the Bergens laboratories.[10] Experimental investigations must be made to determine if such species form with these and other related substrates, and if these species contribute to the enantioselection of the catalytic hydrogenation.

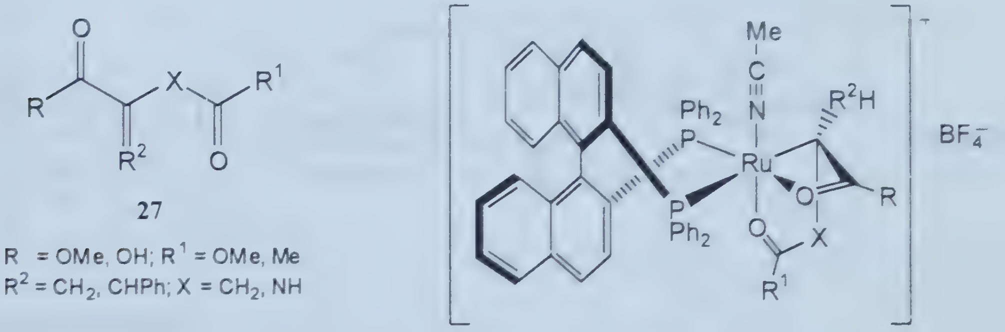

27

R = OMe, OH; R^1 = OMe, Me
R^2 = CH_2, CHPh; X = CH_2, NH

28

Figure 4.4: Model structure for a possible common catalytic intermediate.

The role of triethylamine as promoter for the hydrogenation of **4a** and **5a** in acetone solution is unknown. Investigations have found, however, that reaction of tiglic acid with **2** in acetone solution results in immediate protonolysis of the Ru-H bond of **2** and the generation of a Ru-tiglato complex (**29**, Equation 4.2).[27] Reaction of Ru-D, formed by deuterolysis of **1** with dideuterium gas, resulted in the formation of the Ru-tiglato complex and concomitant formation of H-D. Furthermore, reaction of tiglic acid

with one equivalent of triethylamine followed by reaction with **2** in acetone solution and reaction of tiglic acid with **2** in methanol solution yield the same species by ^1H and ^{31}P NMR. Isolation of **29** was complicated by the facile loss of acetonitrile *in vacuo*, and all attempts to obtain X-ray quality crystals were unsuccessful. It is postulated that the coordination geometry about the ruthenium center is in the Δ configuration on the basis of the X-ray structures and steric arguments previously reported for the related complexes Ru((*R*)-BINAP)($O_2CCMe{=}CHMe)_2$ and Ru((*S*)-BINAP)($O_2CC(Me)_3)_2$.[28] It is believed that the relative configuration of the phenyl rings on the phosphines of the BINAP ligand impose a steric environment that preferentially coordinates the tiglato ligands in a Δ configuration for (*R*)-BINAP and a Λ configuration for (*S*)-BINAP complexes.

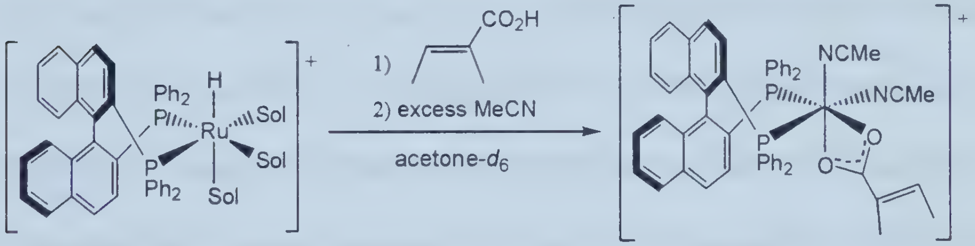

Equation 4.2

2

29

Sol = acetone and/or MeCN

One possible role of the triethylamine as promoter for hydrogenations of *α,β*-unsaturated acids may therefore be to enhance the rate of carboxylate exchange for such complexes. King and others have reported that triethylamine decomposes (perhaps via a *β*-hydride elimination)[29] upon reaction with $[RuCl_2(COD)]_n$ and BINAP, or similar bis(phosphines), from 110 to 140 °C to generate $[Et_2NH_2](Ru_2Cl_5(BINAP)_2)$.[30] It seems unlikely, however, that such a process occurs under a dihydrogen atmosphere at 25 °C using **2** as catalyst. The reason(s) why triethylamine is not required to promote these hydrogenations in methanol is unknown at present.

The allylic alcohol geraniol. The enantioselectivity for the hydrogenation of geraniol (**10a**) to citronellol (**10a'**) using **2** as catalyst depends inversely on the pressure of dihydrogen. In fact, the enantioface selection inverted as the pressure was increased (1 atm as = 21% ee (*R*); 4 atm = 70% ee (*S*)) and the magnitude of enantioselection also increased with pressure (Table 4.4, entries 1, 2, 3). The highest enantioselection occurred at 100 atm yielding **10a'** in 86% ee (*S*). These results were not unprecedented as Noyori has reported increases in enantioselectivities from 70% ee (*S*) to 98% ee (*S*) using Ru((*R*)-BINAP)(O_2CMe)$_2$ as the catalyst precursor when the pressure of dihydrogen was increased from 4 to 100 atm.[31] Detailed investigations reported by Sowa revealed that the isomerization of geraniol to γ-geraniol occurs at a rate comparable to that of its hydrogenation under low pressures, using [Et_2NH_2](Ru_2Cl_5((*S*)-Tol-BINAP)$_2$) as catalyst precursor.[32] Further, the enantioselectivity for the direct hydrogenation of geraniol was found to be opposite to that for the direct hydrogenation of γ-geraniol (Scheme 4.3). Increasing the pressure increases the rate of hydrogenation versus isomerization, and thereby inverts the enantioselectivity over the course of the catalytic hydrogenation. The hydrogenation of geraniol with **2** as catalyst showed similar behavior. Reaction of **2** with geraniol in the absence of dihydrogen gas, however, resulted in a complex mixture of olefin isomerization products, not the sole formation of γ-geraniol as reported with [Et_2NH_2](Ru_2Cl_5((*S*)-Tol-BINAP)$_2$). It is noted that a complex mixture of olefin isomerization products is formed using Ru(PPh_3)$_3$(Cl)$_2$ as catalyst in methanol solution in the absence of dihydrogen gas.[33]

Table 4.4: Hydrogenation of geraniol using 2 as catalyst.[a]

Entry	Substrate	H_2 (atm)	Temp. (°C)	Time (h)	% Conv.	% ee
1	**10a**	1	25	5	100	21 (*R*)
2	**10a**	4	25	5	100	70 (*S*)
3	**10a**	100	25	0.5	100	86 (*S*)

[a] Reaction conditions: 1 mol % **2**, [Ru] = 3.0 mM, 25C, MeOH, 100% conversion.

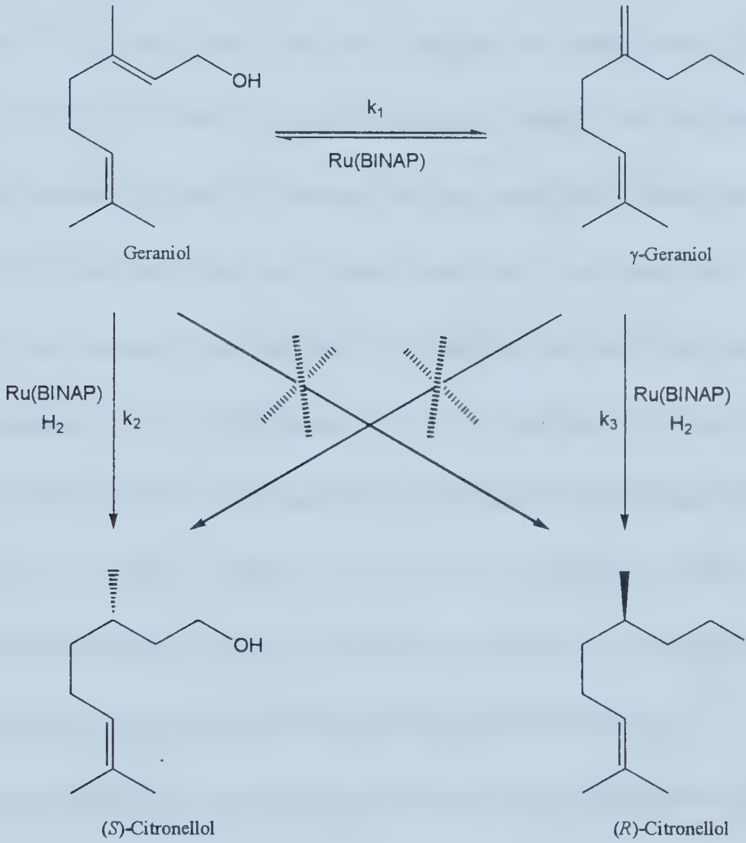
OH
k1
Ru(BINAP)
OH
Geraniol
γ-Geraniol
Ru(BINAP)
H2
k2
k3
Ru(BINAP)
H2
OH
OH
(S)-Citronellol
(R)-Citronellol

Low H_2 pressure: rate of isomerization is much greater than hydrogenation (k_1 and $k_3 >> k_2$), resulting hydrogenation favors (*R*)-citronellol

High H_2 pressure: rate of hydrogenation is much greater than isomerization (k_1 and $k_3 << k_2$), resulting hydrogenation favors (*S*)-citronellol

Scheme 4.3: Reaction scheme describing the competitive hydrogenation versus isomerization in the hydrogenation of geraniol.[32]

Ketone Substrates. The hydrogenation of ethyl acetoacetate (**11a**) to ethyl 3-hydroxybutyrate (**11a'**) (Table 4.5; entry 1) proceeded in a quantitative fashion under 100 atm of dihydrogen and 50 °C, but with low enantioselectivity (15% ee (*S*)). Takaya reported that addition of two equivalents of acid, specifically HX (e.g. X = Cl, Br), to Ru(BINAP)(O_2CMe)$_2$ followed by removal of all volatiles *in vacuo* gave rise to highly efficient catalysts that hydrogenate various β-keto esters with greater than 98% ee under similar conditions.[34] For this reason, the use of halide was examined by the addition of ten equivalents of LiCl to **1** (Table 4.5; entry 2). It was found that the presence of halide increased the enantioselectivity to 20% ee and in the opposite absolute configuration (*R*). The role of LiCl is unclear but the enantioselectivity of complex **2** towards the hydrogenation of **11a** remained low and further investigations were not performed.

The examination of the efficiency of **2** as catalyst for the enantioselective hydrogenation of simple aromatic ketones was performed with the commonly examined substrate acetophenone (**12a**). Hydrogenation of acetophenone with **2** as catalyst required 100 atm of dihydrogen, 50 °C, and 60 h to proceed to completion. Under these conditions, **12a'** was hydrogenated in 10% ee (*R*) (Table 4.5; entry 3).

To assess the ability of **2** as catalyst for the enantioselective hydrogenation of simple ketones (dialkyl ketones) the hydrogenation of 2-hexanone (**13a**) was performed. As with the other ketone substrates examined, complete hydrogenation of **13a** required 100 atm of dihydrogen, 50 °C, and 24 h. The hydrogenation yielded 2-hexanol (**13a'**) as racemic mixture (Table 4.5; entry 4).

It is noted, that in the case of the simple aromatic or alkyl ketones, there are very few reports of highly enantioselective hydrogenations occurring with ruthenium-BINAP

catalyst systems.[35] The conditions and selectivities observed with **2** as catalyst for the enantioselective hydrogenation of simple ketones were consistent with most ruthenium-BINAP catalyst systems reported. The investigation of these substrates was performed for completeness, to determine the net ability of **2** as catalyst. Overall, **2** appears to be less efficient than other reported ruthenium-BINAP systems that often yield greater than 95% ee for the hydrogenation of 1,3-dicarbonyl substrates.[36]

Examination of the structural framework of the highly successful olefinic substrates hydrogenated with **2** as catalyst (Figure 4.2, **27**) led to the investigation of dimethyl oxaloacetate (**14a**) as a ketone substrate. Dimethyl oxaloacetate has similar structural characteristics to dimethyl itaconate (**4b**) where the olefinic bond is replaced by a carbonyl functionality. The hydrogenation of **14a** proceeded to completion under similar conditions utilized with the previously investigated ketones (100 atm H_2, 50 °C, 28 h) yielding dimethyl hydroxysuccinate (**14a'**) in 74% ee (*S*) (Table 4.5; entry 5). The enantioselectivity is moderate, but it is a substantial increase from those observed with **11a** as substrate. This increased enantioselectivity suggests that the disposition of functional groups in a substrate, specifically as **27**, is required for high selectivity with **2** as catalyst and is also reflected in most other ruthenium-BINAP systems in general.

Table 4.5: Hydrogenation of simple and functionalized ketones using 2 as catalyst.[a]

Entry	Substrate	H_2 (atm)	Temp (°C)	Time (h)	% Conv.	% ee
1[b]	**11a**	100	50	24	100	15 (*S*)
2[b,c]	**11a**	100	50	24	100	20 (*R*)
3	**12a**	100	50	60	100	10 (*R*)
4	**13a**	100	50	20	100	~ 0
5[d]	**14a**	100	50	28	100	74 (*S*)

[a] Reaction conditions: 1 mol % catalyst, [Ru] = 2.6mM, MeOH. [b] [Ru] = 2.6 mM. [c] 10 equiv of LiCl added. [d] Reaction performed in acetone.

Conclusions:

Complex **2** is among the more effective ruthenium-BINAP catalysts reported for the enantioselective hydrogenation of substrates containing an α,β-unsaturated carboxylic acid or ester functionality. Its success in the asymmetric reduction of ketones was moderate. Prochiral substrates with the general structure **27** shown in Figure 4.4 were hydrogenated with the same enantioface selection. Extrapolations of these results from mechanistic investigations of one combination of substrate, catalyst, and reaction conditions are precarious in their nature because of the large number of variables involved in such reactions. That substrates of the general structure **27** were hydrogenated with the same enantioface selection raises the possibility that a general trend may exist in these catalyst systems. Further investigations into the true significance of this apparent general trend in enantioselection by ruthenium-BINAP catalysts are underway.

Experimental:

Materials and methods. All operations were performed under an argon atmosphere using standard Schlenk techniques. The solvents were dried and distilled under an argon atmosphere before use by standard methods.[37] The argon gas (Praxair, 99.998%) was passed through a drying train containing 3Å molecular sieves and P_4O_{10} before use. Trace quantities of oxygen were removed from the H_2 (Praxair, 99.99%) by passage through an Alltech Oxy-Trap. All commercial reagents (Aldrich) were recrystallized or distilled under an argon atmosphere before use. (*R*)-(+)-α-methoxy-α-

(trifluoromethyl)phenylacetylchloride,[38] $[Ru(COD)(Cl)]_n$,[39] $Ru(COD)(\eta^3\text{-allyl})_2$,[40] $[Ru(COD)(\eta^2\text{-allyl})(MeCN)](BF_4)$,[6] $[Ru((R)\text{-BINAP})(1\text{-}3;5,6\text{-}\eta\text{-}C_8H_{11})(MeCN)](BF_4)$,[6] $[Rh(\eta^4\text{-norbornadiene})(DIPHOS)](ClO_4)$,[41] and dimethyl oxaloacetate[42] were prepared using established procedures.

Unless stated otherwise, all ^1H, ^{13}C, and ^{31}P NMR spectra were measured with a Bruker AM-400 spectrometer operating at 400.1 MHz, 100.6 MHz, and 161.9 MHz respectively. ^1H and ^{13}C NMR chemical shifts are reported in ppm (δ) relative to TMS using the solvent as an internal reference. ^{31}P NMR chemical shifts are reported in ppm (δ) relative to an 85% H_3PO_4 external reference. All ^{13}C and ^{31}P NMR spectra are ^1H decoupled unless stated otherwise. Mass spectra were measured using a Kratos MS50 spectrometer. Microanalyses were performed at the University of Alberta Microanalysis Laboratory. Optical rotations were measured with a Perkin-Elmer 241 polarimeter at 589 nm using 1.0 dm cells. Specific rotations, $[\alpha]_D$, are reported in degrees per decimeter at 25 °C, and the concentration (*c*) is given in grams per 100 mL.

General hydrogenation procedure. A glass pressure reactor (Lab Glass) was employed for hydrogenation reactions where the pressure of dihydrogen gas was $\leq$ 4 atm. For reactions requiring elevated pressures, a Parr cell-disruption bomb was used. A typical hydrogenation procedure is described below.

Under an argon atmosphere, the catalyst precursor (**1**) (0.010 mmol), substrate (1.0 mmol), and triethylamine (1 equiv per acid unit as required, Table 4.2), were introduced into the reactor. The dry, deoxygenated solvent (methanol or acetone) was then added (3.8 mL) and the solution was stirred for 5 minutes. The atmosphere was then

replaced by dihydrogen gas and the solution was allowed to react under the prescribed conditions (Tables 4.1, 4.2, 4.4, and 4.5). On completion of the reaction, the solvent was removed under reduced pressure, and the products were worked-up as detailed below. Complete conversion and identification of the products were confirmed by CIMS and/or ^{1}H NMR analyses.

α-Acetamidocinnamic acid (3a) work-up. The absolute configuration of the product was determined by comparison of its optical rotation to that of the reported optical rotation of (*R*)-(-)-*N*-acetylphenylalanine (**3a'**) ($[\alpha]^{27}_D$ = -40.3°, *c* = 1.0, MeOH).[43] The product residue was converted to the corresponding diastereomeric amides of (*S*)-(-)-α-methylbenzylamine.[44] The enantiomeric excess was determined by ^{1}H NMR analysis (400 MHz, $CDCl_3$) of the resulting diastereomeric amides.[‡‡] NMR data of the diastereomeric amides: ^{1}H (400.1 MHz, $CDCl_3$): δ 1.21 (d, J = 7.0 Hz, 3H; (*R*, *R*) diastereomer), 1.40 (d, *J* = 7.0 Hz, 3H; (*R*, *S*) diastereomer), 1.88 (s, 3H; (*R*, *R*) diastereomer), 1.95 (s, 3H; (*R*, *S*) diastereomer), 2.92 (m, 2H; (*R*, *S*) diastereomer), 2.97 (dd, *J* = 13.4, 8.8 Hz, 1H; (*R*, *R*) diastereomer), 3.10 (dd, *J* = 13.4, 6.1 Hz, 1H; (*R*, *R*) diastereomer), 4.70 (m, 2H), 4.91 (apparent quintet, *J* = 7.0 Hz, 1H; (*R*, *R*) diastereomer), 4.97 (apparent quintet, *J* = 7.0 Hz, 1H; (*R*, *S*) diastereomer), 6.49 (d, *J* = 7.7 Hz, 1H), 6.72 (m, 3H), 7.00 - 7.45 (m, 20H). N*H* signals not observed.

[‡‡] The ratio of the acyl peaks at δ 1.94 (s, CH_3, *S*) and δ 1.78 (s, CH_3, *R*) was used to determine the enantiomeric excess. The ratio of these peaks was 1:1 for racemic *N*-acetyl phenylalanine.

Itaconic acid (4a) work-up. The product residue was converted directly to the dimethyl ester with CH_2N_2,[45] whereas the acetone/NEt_3 product was first worked-up in a manner similar to that described for tiglic acid (**5a**), and then treated with CH_2N_2. The product was then dissolved in CH_2Cl_2 and passed through a Florisil plug to remove the catalyst. The solvent was removed under reduced pressure to yield dimethyl methylsuccinate. The enantiomeric excess and absolute configuration were then determined as described in the dimethyl itaconate (**4b**) hydrogenation work-up.

Dimethyl itaconate (4b) work-up. The products of the MeOH and acetone reactions were treated in a similar manner. The product residue was dissolved in CH_2Cl_2 and passed through a Florisil plug to remove the catalyst. The solvent was removed under reduced pressure yielding dimethyl methylsuccinate. The enantiomeric excess was spectroscopically determined (^1H NMR, CD_2Cl_2)[‡‡‡] upon addition of chiral lanthanide shift reagent ((+)-Eu(tfc)$_3$)).[46] The absolute configuration of the product was determined by comparison of its optical rotation to that of authentic (*R*)-dimethyl methylsuccinate ($[\alpha]^{25}_D = +4.8°$, $c = 4.0$, $CHCl_3$).

Tiglic acid (5a) work-up. The product residue from the hydrogenation in MeOH was dissolved in CH_2Cl_2 and passed through a Florisil plug to remove the catalyst. The

---

[‡‡‡] The ratio of the methoxy signals (ca. δ 4.0) was used to determine the enantiomeric excess. The ratio of these peaks was 1:1 for racemic dimethyl methylsuccinate.

solvent was then removed under reduced pressure and the residue was converted to the corresponding diastereomeric amides of (*S*)-(-)-α-methylbenzylamine.

The enantiomeric excess and absolute configuration were determined by comparison of the ^{1}H NMR spectrum of the derivatized residue to that of the corresponding amide derivatives prepared from (±)-2-methylbutyric acid and authentic (*S*)-(+)-2-methylbutyric acid, respectively.

To the acetone/NEt$_3$ product residue was added 10% aq. HCl (10 mL). The solution was filtered and the filtrate extracted with Et$_2$O (5 x 40 mL). The combined organic layers were washed with 5% aq. HCl (3 x 8 mL), dried over MgSO$_4$, filtered, and concentrated under reduced pressure to give 2-methylbutyric acid. The enantiomeric excess and absolute configuration were then determined as described above. NMR data for the (*S*, *S*) diastereomer: ^{1}H (400.1 MHz, CDCl$_3$): δ 0.84 (t, *J* = 7.4 Hz, 3H), 1.13 (d, *J* = 6.9 Hz, 3H), 1.39 (m, 1H), 1.46 (d, *J* = 6.9 Hz, 3H), 1.64 (m, 1H), 2.10 (apparent sextet, *J* = 6.9 Hz, 1H), 5.14 (apparent quintet, *J* = 7.2 Hz, 1H), 5.89 (br s, 1H,), 7.15-7.40 (aromatic, 5H); NMR data for (*R*, *S*) diastereomer: ^{1}H (400.1 MHz, CDCl$_3$): δ 0.92 (t, *J* = 7.4 Hz, 3H), 1.10 (d, *J* = 6.9 Hz, 3H), 1.38 (m, 1H, overlapped with (*S*, *S*) diastereomer), 1.47 (d, *J* = 6.9 Hz, 3H), 1.64 (m, 1H, overlapped with (*S*, *S*) diastereomer), 2.09 (apparent sextet, *J* = 6.9 Hz, 1H, overlapped with (*S*, *S*) diastereomer), 5.13 (apparent quintet, *J* = 7.2 Hz, 1H, overlapped with (*S*, *S*) diastereomer), 5.89 (br s, 1H, overlapped with (*S*, *S*) diastereomer), 7.15-7.40 (m, 5H, aromatic, overlapped with (*S*, *S*) diastereomer).

***α*-Methylcinnamic acid (6a) work-up.** The product residue was dissolved in CH_2Cl_2 and passed through a Florisil plug to remove the catalyst. The product residue was then converted directly to the methyl ester with CH_2N_2. The enantiomeric excess was spectroscopically determined (^1H NMR, CD_2Cl_2)§ upon addition of chiral lanthanide shift reagent ((+)-Eu(tfc)$_3$)). The absolute configuration of the product was determined by comparison of its optical rotation to that of authentic (*R*)-methyl 2-methyl-3-phenylpropionate ($[\alpha]^{25}_D = +4.8°$, $c = 4.0$, $CHCl_3$).

***α*-Phenylcinnamic acid (7a) work-up.** The product residue was dissolved in EtOAc and passed through a Florisil plug to remove the catalyst. The product residue was then converted directly to the methyl ester with CH_2N_2. The enantiomeric excess and the absolute configuration of the product was determined by comparison of its optical rotation to that of authentic methyl-(*R*)-2,3-diphenylpropionate ($[\alpha]^{25}_D = +4.8°$, $c = 4.0$, $CHCl_3$).

Mesaconic acid (8a) work-up. The product residue was converted directly to the dimethyl ester with CH_2N_2. The product was then dissolved in EtOAc and passed through a Florisil plug to remove the catalyst. The solvent was removed under reduced pressure to yield dimethyl methylsuccinate. The enantiomeric excess and absolute configuration were determined as described in **4b** hydrogenation work-up.

---

§ The ratio of the methoxy signals (ca. δ 4.0) was used to determine the enantiomeric excess. The ratio of these peaks was 1:1 for racemic methyl 2-methyl-3-phenylpropionate.

Citraconic acid (9a) work-up. The product residue was converted directly to the dimethyl ester with CH_2N_2. The product was then dissolved in EtOAc and passed through a Florisil plug to remove the catalyst. The solvent was removed under reduced pressure to yield dimethyl methylsuccinate. The enantiomeric excess and absolute configuration were then determined as described in the dimethyl itaconate (**4b**) hydrogenation work-up.

Geraniol (10a) work-up. The product residue was purified by flash distillation and reacted with (*R*)-(+)-α-methoxy-α-(trifluoromethyl)phenylacetylchloride. The enantiomeric excess was determined by ^1H NMR spectroscopy of the diastereomeric esters.[§§] The absolute configuration of the product was determined by comparison of its rotation with the reported optical rotation of (*R*)-citronellol ($[\alpha]^{25}_D = +5.12°$, $c = 21.0$, $CHCl_3$).[47] NMR data for the diastereomeric esters: ^1H (400.1 MHz, $CDCl_3$): δ 0.90 (d, J = 6.3 Hz, 3H; (*R*, *S*) diastereomer), 0.91 (d, J = 6.3 Hz, 3H; (*R*, *R*) diastereomer), 1.19 (m, 2H), 1.33 (m, 2H), 1.51 (m, 4H), 1.59 (s, 6H), 1.68 (s, 6H), 1.74 (m, 2H), 1.95 (m, 4H), 3.50 (br s, 3H; (*R*, *S*) diastereomer), 3.56 (br s, 3H; (*R*, *R*) diastereomer), 4.37 (m, 4H), 5.06 (m, 2H), 7.35 - 7.70 (m, 10H, aromatic). ^1H NMR signals for individual diastereomers were assigned when overlap did not occur.

Ethyl acetoacetate (11a) work-up. The product residue was purified by flash distillation and reacted with (*R*)-(+)-α-methoxy-α-(trifluoromethyl)phenylacetylchloride.

[§§] The ratio of the methyl peaks at δ 0.91 (d, J = 6.4 Hz, CH_3, *R*) and δ 0.90 (d, J = 6.4 Hz, CH_3, *S*) was used to determine the ee. The ratio of these peaks was 1:1 for racemic β-citronellol.

The enantiomeric excess and absolute configuration were determined by comparison of the ^{1}H NMR of the derivatized residue to that of the diastereomeric Mosher's esters of (±)-3-hydroxybutyrate and authentic ethyl (*R*)-(-)-3-hydroxybutyrate, respectively. NMR data for the diastereomeric esters: ^{1}H NMR (400.1 MHz, $CDCl_3$): (*R*, *R*) diastereomer δ 1.23 (t, *J* = 7.1 Hz, 3H), 1.34 (d, *J* = 6.3 Hz, 3H), 2.57 (dd, *J* = 16.0, 4.7 Hz, 1H), 2.72 (dd, *J* = 16.0, 8.5 Hz, 1H), 3.49 (br s, 3H), 4.13 (qd, *J* = 7.1, 1.3 Hz, 2H), 5.57 (m, 1H), 7.3-7.7 (m, 5H, aromatic). (*R*, *S*) diastereomer δ 1.19 (t, *J* = 7.1 Hz, 3H), 1.43 (d, *J* = 6.3 Hz, 3H, 2.53 (dd, *J* = 16.0, 5.0 Hz, 1H), 2.68 (dd, *J* = 16.0, 8.3 Hz, 1H), 3.55 (br s, 3H), 4.06 (q, *J* = 7.1 Hz, 2H), 5.57 (m, 1H), 7.3-7.7 (m, 5H, aromatic).

Acetophenone (12a) work-up. The product residue was flash distilled under high vacuum to remove the catalyst. The product was then reacted with trifluoroacetic anhydride to form the trifluoroacetyl derivative of 2-methylbenzyl alcohol. The enantiomer excess and absolute configuration were determined by chiral GC analysis (60 °C, 0.5μL, retention time (*R*)-enantiomer 38.4 min., (*S*)-enantiomer 40.7 min) and comparison with chiral GC anaylsis of (*R*)-2-methylbenzyl alcohol.

2-Hexanone (13a) work-up. The product residue was flash distilled under high vacuum to remove the catalyst. The product was then reacted with trifluoroacetic anhydride to form the trifluoroacetyl derivative of 2-hexanol. The enantiomer excess and absolute configuration were determined by chiral GC analysis (40 °C, retention time (*R*)-enantiomer 14.4 min., (*S*)-enantiomer 20.7 min) and comparison with chiral GC analysis of (*R*)-2-hexanol.

Dimethyl oxaloacetate (14a) work-up. The product residue was dissolved in CH_2Cl_2 and passed through a Florisil plug to remove the catalyst. The solvent was removed under reduced pressure and the residue was then converted to the corresponding diastereomeric amides of (*S*)-(-)-α-methylbenzylamine. The enantiomeric excess was determined by comparison of the ^1H NMR spectrum of the derivatized residue to that of the amide derivative of (±)-dimethyl hydroxysuccinate (see achiral hydrogenation for NMR data). The absolute configuration was determined by comparison with the optical rotation of authentic (*S*)-(-)-dimethyl hydroxysuccinate ($[\alpha]^{25}_D = -8.85°$, $c = 5.2$, MeOH).

Achiral hydrogenation of dimethyl oxaloacetate (6a). A stainless steel autoclave was charged with [Rh(η^4-norbornadiene)(DIPHOS)](ClO_4) (6.9 mg, 0.01 mmol), dimethyl oxaloacetate (160.0 mg, 1.0 mmol), and acetone (3.8 mL). The solution was stirred for 5 min and the atmosphere was then replaced with H_2. The solution was allowed to react for 75 h at 50 °C and 100 atm H_2. The product was worked-up as described for the hydrogenation of dimethyl oxaloacetate with **1** as catalyst precursor and converted to the corresponding diastereomeric amides of (*S*)-(-)-α-methylbenzylamine. NMR spectroscopic data: ^1H (300.1 MHz, $CDCl_3$): (*R*, *R*) diastereomer δ 2.88 (dd, J = 16.7, 8.4 Hz, 1H), 2.96 (dd, J = 16.7, 5.0 Hz, 1H), 3.60 (s, 3H), 3.63 (br s, 3H), 3.81 (s, 3H), 5.72 (dd, J = 8.4, 5.0 Hz, 1H), 7.42 (m, 3H), 7.60 (m, 2H). (*R*, *S*) diastereomer δ 2.92 (dd, J = 16.9, 8.9 Hz, 1H), 3.02 (dd, J = 16.9, 4.0 Hz, 1H), 3.55 (br s, 3H), 3.70 (s, 3H), 3.76 (s, 3H), 5.71 (dd, J = 8.9, 4.0 Hz, 1H), 7.42 (m, 3H), 7.60 (m, 2H).

Hydrogenation of [Ru((*R*)-BINAP)(1-3:5,6-η-C_8H_{11})(MeCN)](BF_4) (1) in acetone-d_6. Compound **1** (19.5 mg, 2.03 x 10^{-5} mol) was partially dissolved in acetone-d_6 (0.6 mL) in an NMR tube under an argon atmosphere. At room temperature, the tube was flushed with H_2, pressurized (1-2 atm), and shaken until a deep orange-yellow solution was generated (~5 min). The H_2 atmosphere was replaced by argon gas and the resulting solution was analyzed by ^1H and ^{31}P NMR spectroscopy at -80 °C. NMR spectroscopic analysis indicated a mixture of eight ruthenium-hydrido species ([Ru((*R*)-BINAP)(H)$(MeCN)_n((CD_3)_2CO)_{3-n}$]($BF_4$), where n = 0-3) and cyclooctane were present. At -80 °C, D_2 (5.0 mL) was injected into the head-space of the tube. The tube was removed from the cooling bath, shaken for approximately 15 s, and then immediately placed in a pre-cooled (-80 °C) NMR probe. The ^{31}P NMR spectrum at -80 °C remained unchanged, while the ^1H NMR spectrum indicated that exchange of all ruthenium-hydrido species with D_2 (to form ruthenium-deutero species) had occurred with concomitant formation of HD. NMR spectroscopic data of the hydrides (A-H): ^1H (400.1 MHz, acetone-d_6, -80 °C): δ -19.87 (br, A), -19.60 (apparent t, $^2J_{H\text{-}P}$ = 30 Hz, B), -19.45 (br, C), -19.26 (apparent t, $^2J_{H\text{-}P}$ = 30 Hz, D), -13.50 (apparent t, $^2J_{H\text{-}P}$ = 25 Hz, E), -13.20 (apparent t, $^2J_{H\text{-}P}$ = 25 Hz, F), -13.15 (dd, $^2J_{H\text{-}P}$ = 28 Hz, $2J_{H\text{-}P}$ = 24 Hz, G), -12.88 (apparent t, $^2J_{H\text{-}P}$ = 27 Hz, H), 1.65 - 2.35 (12 s, Ru-NCCH_3), 6.00 - 8.50 (aromatic); ^{31}P (161.9 MHz, acetone-d_6, -80 °C): δ 59.4 (d, $^2J_{P\text{-}P}$ = 43.0 Hz, A), 60.8 (d, $^2J_{P\text{-}P}$ = 46.4 Hz, B), 63.2 (d, $^2J_{P\text{-}P}$ = 44.2 Hz, F), 63.6 (d, $^2J_{P\text{-}P}$ = 40.6 Hz, E), 66.0 (d, $^2J_{P\text{-}P}$ = 43.0 Hz, A), 68.2 (d, $^2J_{P\text{-}P}$ = 46.0 Hz, C),‡ 69.6 (d, $^2J_{P\text{-}P}$ = 40.6 Hz, E), 71.2 (d, $^2J_{P\text{-}P}$ = 49.6 Hz, D),

---

‡ The corresponding ^{31}P NMR signal was obscured by resonances attributed to hydrides D and G ca. δ 71.3.

71.5 (d, $^2J_{P\text{-}P}$ = 42.9 Hz, G), 74.2 (d, $^2J_{P\text{-}P}$ = 47.0 Hz, H), 75.4 (d, $^2J_{P\text{-}P}$ = 42.9 Hz, G), 76.5 (d, $^2J_{P\text{-}P}$ = 46.4 Hz, B), 79.3 (d, $^2J_{P\text{-}P}$ = 49.6 Hz, D), 80.3 (d, $^2J_{P\text{-}P}$ = 44.2 Hz, F), 82.7 (d, $^2J_{P\text{-}P}$ = 47.0 Hz, H). Approximate percentages of hydrido species present: A(3%), B(14%), C(5%), D(22%), E(15%), F(15%), G(11%), H(15%). Although the unambiguous assignment of the individual structures for each hydride could not be determined, *fac*-[Ru((*R*)-BINAP)(H)(MeCN)$_3$](BF$_4$) has been independently prepared and found to correspond to hydride E.

Stoichiometric reaction of [Ru((*R*)-BINAP)(H)(MeCN)$_n$ (Sol)$_{3\text{-}n}$](BF$_4$) (2, n = 0-3) with tiglic acid in acetone. A Schlenk flask was charged with **1** (40.0 mg, 4.18 x 10^{-5} mol), tiglic acid (4.2 mg, 4.18 x 10^{-5} mol), and acetone (4.0 mL) under an argon atmosphere. At room temperature, the flask was flushed with H_2, pressurized (1-2 atm), and shaken until a deep orange-yellow solution was generated (~5 min). The H_2 atmosphere was then replaced by argon gas. To this solution was added MeCN (2.6 μL, 4.98 x 10^{-5} mol) and the flask was shaken (~5 min) to ensure complete reaction. The solvent was removed under reduced pressure and the remaining orange solid was washed with hexanes (3 x 5 mL). The isolated solid was stored under an argon atmosphere at -30 °C. The product readily loses MeCN *in vacuo*. NMR spectroscopic data of the complex: ^{1}H (400.1 MHz, acetone-d_6): δ 1.45 (apparent t, CH$_3$CHC(C*H*$_3$)CO$_2$Ru, $^4J_{H\text{-}H}$ = 1.5 Hz, $^5J_{H\text{-}H}$ = 1.2 Hz), 1.56 (dd, C*H*$_3$CHC(CH$_3$)CO$_2$Ru, $^3J_{H\text{-}H}$ = 7.2 Hz, $^5J_{H\text{-}H}$ = 1.2 Hz), 2.01 (s, C*H*$_3$CN), 2.03 (s, C*H*$_3$CN), 6.45 (dq, CH$_3$C*H*C(CH$_3$)CO$_2$Ru, $^3J_{H\text{-}H}$ = 7.2 Hz, $^4J_{H\text{-}H}$ = 1.5 Hz), 6.58 - 7.89 (m, 32H, BINAP). ^{31}P (161.9 MHz, acetone-d_6): δ 52.6 (dd, $^2J_{P\text{-}P}$ = 37.5 Hz), 56.9 (d, $^2J_{P\text{-}P}$ = 37.5 Hz). ^{13}C (100.6 MHz, acetone-d_6): δ 2.4 (CH$_3$CN), 4.65

(CH_3CN), 10.72 & 13.90 ($CH_3CHC(CH_3)CO_2Ru$), 123.99 (CH_3CN), 124.14 (CH_3CN), 124.42 - 141.45 (BINAP and $CH_3CHC(CH_3)CO_2Ru$), 185.46 ($CH_3CHC(CH_3)CO_2Ru$).

Stoichiometric reaction of [Ru((*R*)-BINAP)(D)(MeCN)$_n$(Sol)$_{3-n}$](BF$_4$) (2, n = 0-3) with tiglic acid in acetone-*d*$_6$. Compound **1** (13.5 mg, 1.41 x 10^{-5} mol) was partially dissolved in acetone-d_6 (~0.8 mL) in an NMR tube under an argon atmosphere. At room temperature, the tube was flushed with D_2, pressurized (1-2 atm), and shaken until a deep orange-yellow solution was generated (~5 min). The D_2 atmosphere was replaced by argon gas and the solution was then transferred to an NMR tube containing tiglic acid (1.41 mg, 1.41x 10^{-5} mol) under an argon atmosphere. To this solution was added excess CD_3CN (2.0 μL, 3.83 x 10^{-5} mol) via a gas-tight syringe. The solution was immediately analyzed by ^1H NMR. The product was exclusively formed with concomitant formation of HD. ^1H (400.1 MHz, acetone-d_6): δ 1.45 (apparent t, $CH_3CHC(CH_3)CO_2Ru$, $^4J_{H\text{-}H}$ = 1.5 Hz, $^5J_{H\text{-}H}$ = 1.1 Hz), 1.46 - 1.52 (br m, partially deuterated cyclooctane), 1.56 (dd, $CH_3CHC(CH_3)CO_2Ru$, $^3J_{H\text{-}H}$ = 7.2 Hz, $^5J_{H\text{-}H}$ = 1.1 Hz), 1.99 (s, CH_3CN), 3.26 (br t, *HD*, $^1J_{H\text{-}D}$ = 240 Hz), 6.45 (dq, $CH_3CHC(CH_3)CO_2Ru$, $^3J_{H\text{-}H}$ = 7.2 Hz, $^4J_{H\text{-}H}$ = 1.6 Hz), 6.58 - 7.89 (m, 32H, BINAP). ^{31}P (161.9 MHz, acetone- d_6): δ 52.6 (dd, $^2J_{P\text{-}P}$ = 37.5 Hz), 56.9 (d, $^2J_{P\text{-}P}$ = 37.5 Hz).

Stoichiometric reaction of [Ru((*R*)-BINAP)(H)(MeCN)$_n$ (Sol)$_{3-n}$](BF$_4$) (2, n = 0-3) with tiglic acid in methanol-*d*$_4$. Compound **1** (20.0 mg, 2.09 x 10^{-5} mol) was partially dissolved in methanol-d_4 (~0.8 mL) in an NMR tube under an argon atmosphere. At room temperature, the tube was flushed with H_2, pressurized (1-2 atm), and shaken

until a deep orange-yellow solution was generated (~5 min). The H_2 atmosphere was replaced by argon gas and the solution was then transferred to an NMR tube containing tiglic acid (2.10 mg, 2.09 x 10^{-5} mol) under an argon atmosphere. To this solution was added excess CD_3CN (2.0 µL, 3.83 x 10^{-5} mol) via a gas-tight syringe The solution was immediately analyzed by ^{1}H NMR. The product was found to be identical to that formed upon stoichiometric reaction of tiglic acid with **2** in acetone solution.

Stoichiometric reaction of [Ru((*R*)-BINAP)(H)(MeCN)$_n$ (Sol)$_{3-n}$](BF$_4$) (2, n = 0-3) with tiglic acid and 1 equivalent of NEt$_3$ in acetone-*d*$_6$. Compound **1** (20.0 mg, 2.09 x 10^{-5} mol) was partially dissolved in acetone-*d*$_6$ (~0.6 mL) in an NMR tube under an argon atmosphere. At room temperature, the tube was flushed with H_2, pressurized (1-2 atm), and shaken until a deep orange-yellow solution was generated (~5 min). The H_2 atmosphere was replaced by argon gas and the solution was then transferred to an NMR tube containing tiglic acid (2.1 mg, 2.09 x 10^{-5} mol) and NEt_3 (2.9 µL, 2.1 mg, 2.09 x 10^{-5} mol) in acetone-*d*$_6$ (0.2 mL) under an argon atmosphere. To this solution was added excess CD_3CN (2.0 µL, 3.83 x 10^{-5} mol) via a gas-tight syringe. The solution was immediately analyzed by ^{1}H NMR. The product was found to be identical to that formed upon stoichiometric reaction of tiglic acid with **2** in the absence of added NEt_3 in acetone solution.

References and Notes:

(1) For general reviews on use of chiral metal complexes in asymmetric organic synthesis, see: (a) Noyori, R. *Asymmetric Catalysis in Organic Synthesis*, Wiley, New York 1994. (b) Ojima, I.; Clos, N.; Bastos, C. *Tetrahedron* **1989**, *45*, 6901-6939. (c) Morrison, J. D., (Ed.) *Asymmetric Synthesis*, Vol. 5, Chiral Catalysis, Academic Press, 1985, New York.

(2) For recent reviews on the use of BINAP in enantioselective catalysis, see: (a) Noyori, R. *Acta Chem. Scand.* **1996**, *50*, 380-390. (b) Kumobayashi, H. *Recl. Trav. Chim. Pays-Bas* **1996**, *115*, 201-210. (c) Akutagawa, S. *App. Catal. A.* **1995**, *128*, 171-207. (d) Noyori, R. *Tetrahedron* **1994**, *50*, 4259-4292. (e) Takaya, H.; Ohta, T.; Noyori, R. In *Catalytic Asymmetric Synthesis*. Ojima, I. (Ed.). VCH, New York, 1993. (f) Noyori, R. *CHEMTECH* **1992**, 360-367. (g) Noyori, R. *Science* **1990**, *248*, 1194-1199. (h) Noyori, R.; Takaya, H. *Acc. Chem. Res.* **1991**, *23*, 345.

(3) Some representative examples: (a) Ohta, T.; Ikegami, H.; Miyake, T.; Takaya, H. *J. Organomet. Chem.* **1995**, *502*, 169. (b) Kitamura, M.; Hsiao, Y.; Ohta, Y.; Tsukamoto, M.; Ohta, T.; Takaya, H.; Noyori, R. *J. Org. Chem.* **1994**, *59*, 297. (c) Inoue, S.; Osada, M.; Koyano, K.; Takaya, H.; Noyori, R. *Chem. Lett.* **1985**, 1007. (d) Miyashita, A.; Takaya, H.; Souchi, T.; Noyori, R. *Tetrahedron* **1984**, *40*, 1245. (e) Miyashita, A.; Yasuda, A.; Takaya, H.; Toriumi, K.; Ito, T.; Souchi, T.; Noyori, R. *J. Am. Chem. Soc.* **1980**, *102*, 7932.

(4) Some representative examples: (a) Monteiro, A. L.; Zinn, F. K.; de Souza, R. F.; Dupont, J. *Tetrahedron: Asymmetry* **1997**, *8*, 177. (b) Ohkuma, T.; Ikehira, H.; Ikariya, T.; Noyori, R. *SYNLETT* **1997**, 467. (c) Chan, A. S. C.; Chen, C. C.; Yang, T. K.; Huang, J. H.; Lin, Y. C. *Inorg. Chim. Acta* **1995**, *234*, 95. (d) Genêt, J. P.; Caño de Andrade, M. C.; Ratovelomanana-Vidal, V. *Tetrahedron Lett.* **1995**, *36*, 2063. (e) Ohkuma, T.; Ooka, H.; Hashiguchi, S.; Ikariya, T.; Noyori, R. *J. Am. Chem. Soc.* **1995**, *117*, 2675. (f) Kitamura, M.; Tokunaga, M.; Noyori, R. *J. Am. Chem. Soc.* **1995**, *117*, 2931. (g) Ohta, T.; Miyake, T.; Seido, N.; Kumobayashi, H.; Takaya, H. *J. Org. Chem.* **1995**, *60*, 357. (h) Kitamura, M.; Tokunaga, M.; Pham, T.; Lubell, W. D.; Noyori, R. *Tetrahedron Lett.* **1995**, *36*, 5769. (i) Kitamura, M.; Hsiao, Y.; Ohta, M.; Tsukamoto, M.; Ohta, T.; Takaya, H.; Noyori, R. *J. Org. Chem.* **1994**, *59*, 297. (j) Genêt, . P.; Pinel, C; Ratovelomanana-Vidal, V.; Mallart, S.; Pfister, X; Bischoff, L; Caño de Andrade, M. C.; Darses, S.; Galopin, C.; Laffitte, J. A. *Tetrahedron: Asymmetry* **1994**, *5*, 675. (k) Genêt, J. P.; Pinel, C.; Ratovelomanana-Vidal, V.; Mallart, S.; Pfister, X.; Caño de Andrade, M. C.; Laffitte, J. A. *Tetrahedron: Asymmetry* **1994**, *5*, 665. (l) Mashima, K.; Kusano, K.; Sato, N.; Matsumura, Y.; Nozaki, K.; Kumobayashi, H.; Sayo, N.; Hori, Y.; Ishizaki, T.; Akutagawa, S.; Takaya, H. *J. Org. Chem.* **1994**, *59*, 3064. (m) Kitamura, M.; Tokunaga, M.; Noyori, R. *J. Am. Chem. Soc.* **1993**, *115*, 144. (n) Hoke, J. B.; Hollis, L. S.; Stern, E. W. *J. Organomet. Chem.* **1993**, *455*, 193. (o) Manimaran, T.; Wu, T. C.; Kolbucar, W. D.; Kolich, C. H.; Stahly, G. P.; Fronczek, F. R.; Watkins, S. E. *Organometallics* **1993**, *12*, 1467. (p) Wan, K.; Davis, M. E.

Tetrahedron: Asymmetry **1993**, *4*, 2461. Early references: 1d, 1f, and references cited therein.

(5) Ruthenium-hydride species have been postulated as catalytic intermediates in a number of reaction. Examples are shown in reference 1a.

(6) Wiles, J. A.; Lee, C. E.; McDonald, R.; Bergens, S. H. *Organometallics* **1996**, *15*, 3782-3784.

(7) There are few well-defined ruthenium-hydride species: (a) Currao, A.; Feiken, N.; Macchioni, A.; Nesper, R.; Pregosin, P. S.; Trabesinger, G. *Helv. Chim. Acta* **1996**, *79*, 1587-1591. (b) Tsukahara, T.; Kawano, H.; Ishii, Y.; Takahashi, T.; Saburi, M.; Uchida, Y.; Akutagawa, S. *Chem. Lett.* **1988**, 2055-2058. (c) Kawano, H.; Ishii, Y.; Kodama, T.; Saburi, M.; Uchida, Y. *Chem. Lett.* **1987**, 1311-1314. (d) Ikariya, T.; Ishii, Y.; Kawano, H.; Arai, T.; Saburi, M.; Yoshikawa, S.; Akutagawa, S. *J. Chem. Soc., Chem. Commun.* **1985**, 922-924.

(8) Carty, A. J. In *Catalytic Aspects of Metal Phosphine Complexes*: Alyea, E. C.; Meek, D. W. Eds.; Advances in Chemical Series 196; American Chemical Society: Washington, 1982; pp. 181-183.

(9) Collman, J. P.; Hegedus, L. S.; Norton, L. S.; Finke, R. G. *Principles and Applications of Organotransition Metal Chemistry*: University Science Books: Mill Valley, CA, 1987.

(10) Wiles, J. A.; Bergens, S. H. *J. Am. Chem. Soc.* **1997**, *119*, 2940-2941.

(11) (a) Ohta, T.; Miyake, T.; Seido, N.; Kumobayashi, H.; Takaya, H. *J. Org. Chem.* **1995**, *60*, 357-363. (b) Ohta, T.; Takaya, H.; Kitamura, M.; Nagai, K.; Noyori, R. *J. Org. Chem.* **1987**, *52*, 3174.

(12) Similar reactivity has been observed with other ruthenium-BINAP systems: (a) Uemura, T.; Zhang, X.; Matsumura, K.; Sayo, N.; Kumobayashi, H.; Ohta, T.; Nozaki, K.; Takaya, H. *J. Org. Chem.* **1996**, *61*, 5510-5516. (b) Zhang, X.; Uemura, T.; Matsumura, K.; Sayo, N.; Kumobayashi, H.; Takaya, H. *SYNLETT* **1994**, 501-503.

(13) Kawano, H.; Ishii, Y.; Ikariya, T.; Saburi, M.; Yoshikawa, S.; Uchida, Y.; Kumobayashi, H. *Tetrahedron Lett.* **1987**, *28*, 1905-1987.

(14) Wiles, J. A.; Bergens, S. H. *Organometallics* **1998**, *17*, 2228-2240.

(15) (a) Saburi, M.; Takeuchi, H.; Ogasawara, M.; Tsukahara, T.; Ishii, Y.; Ikariya, T.; Takahashi, T.; Uchida, Y. *J. Organomet. Chem.* **1992**, *428*, 155. (b) Morimoto, T.; Chiba, M.; Achiwa, K. *Tetrahedron Lett.* **1988**, *29*, 4755. (c) Ojima, I.; Yoda, N. *Tetrahedron Lett.* **1980**, *21*, 1051. (d) Ojima, I.; Kogure, T.; Yoda, N. *Chem. Lett.* **1979**, 495. (e) Achiwa, K. *J. Am. Chem. Soc.* **1976**, *98*, 8265.

(16) Shao, L.; Takeuchi, K.; Ikemoto, M.; Kawai, T.; Ogasawara, M.; Takeuchi, H.; Kawano, H.; Saburi, M. *J. Organomet. Chem.* **1992**, *435*, 133.

(17) Kawano, H.; Ikariya, T.; Ishii, Y.; Saburi, M.; Yoshikawa, S.; Uchida, Y.; Kumobayashi, H. *J. Chem. Perkin Trans. 1* **1989**, 1571.

(18) Kawano, H.; Ishii, Y.; Ikariya, T.; Saburi, M.; Yoshikawa, S.; Uchida, Y.; Kumobayashi, H. *Tetrahedron Lett.* **1987**, *28*, 1905.

(19) Yamamoto, N.; Murata, M.; Morimoto, T.; Achiwa, K. *Chem. Pharm. Bull.* **1991**, *39*, 1085.

(20) Genêt, J. P.; Mallart, S.; Pinel, C.; Juge, S.; Laffitte, J. A. *Tetrahedron: Asymmetry* **1991**, *2*, 43.

(21) Noyori, R.; Ikeda, T.; Ohkuma, T.; Widhalm, M.; Kitamura, M.; Takaya, H.; Akutagawa, S.; Sayo, N.; Saito, T.; Taketomi, T.; Kumobayashi, H. *J. Am. Chem. Soc.* **1989**, *111*, 9134.

(22) Ashby, M. T.; Halpern, J. *J. Am. Chem. Soc.* **1991**, *113*, 589.

(23) Ohta, T.; Hidemasa, T.; Kitamura, M.; Nagai, K.; Noyori, R. *J. Org. Chem.* **1987**, *52*, 3176-3178.

(24) Mashima, K.; Kusano, K-h.; Sato, N.; Matsumura, Y-i.; Nozaki, K.; Kumobayashi, H.; Sayo, N.; Hori, Y.; Ishizaki, T.; Akutagawa, S.; Takaya, H. *J. Org. Chem.* **1994**, *59*, 3064-3076.

(25) Mashima, K.; Kusano, K-h; Ohta, T.; Noyori, R.; Takaya, H. *J. Chem. Soc. Chem. Commun.* **1989**, 1208-1210.

(26) Zanetti, N.; Spindler, F.; Spencer, J.; Togni, A.; Rihs, G. *Organometallics* **1996**, *15*, 860-866.

(27) Such species have been postulated as active catalytic intermediates in *α,β*-unsaturated carboxylic acids and two others have been crystallographically characterized: (a) Chen, C.-C.; Huang, T.-T.; Lin, C.-W.; Cao, R.; Chan, A. S. C.; Wong, W. T. *Inorg. Chim. Acta* **1998**, *270*, 247-251. (b) Ashby, M. T.; Khan, M. A.; Halpern, J. *Organometallics* **1991**, *10*, 2011-2015.

(28) Ashby, M. T.; Khan, M. A.; Halpern, J. *Organometallics* **1991**, *10*, 2011-2015.

(29) Fogg, D. E.; James, B. R. *Inorg. Chem.* **1995**, *34*, 2557.

(30) (a) King, S. A.; DiMichele, L. In *Catalysis of Organic Reactions*: Vol. 62, Scaros, M. G.; Prunier, M. L. Eds.; Marcel Dekker: New York, 1995; pp. 157-166. (b)

Ohta, T.; Tonomura, Y.; Nozaki, K.; Takaya, H.; Mashima, K. *Organometallics* **1996**, *15*, 1521.

(31) Takaya, T.; Ohta, T.; Inoue, S.; Tokunaga, M.; Kitamura, M.; Noyori, R. *Org. Synth.* **1993**, *72*, 74.

(32) Sun, Y.; LeBlond, C.; Wang, J.; Blackmond, D. G.; Laquidara, J.; Sowa, J. R. Jr. *J. Am. Chem. Soc.* **1995**, *117*, 12647.

(33) Sun. Y.; Wang, J.; LeBlond, C.; Reamer, R. A.; Laquidara, J.; Sowa, J. R. Jr.; Blackmond, D. G. *J. Organomet. Chem.* **1997**, *548*, 65-72, and references within.

(34) Mashima, K.; Hino, T.; Takaya, H. *J. Chem. Soc. Dalton Trans.* **1992**, 2099.

(35) Ruthenium catalyst systems: (a) Mikami, K.; Korenaga, T.; Terada, M.; Ohkuma, T.; Pham, T.; Noyori, R. *Angew. Chem. Int. Ed. Engl.* **1999**, *38*, 495-497 (aryl ketones). (b) Cao, P.; Zhang, X. *J. Org. Chem.* **1999**, *64*, 2127-2129 (aryl ketones). (c) Fehring, V.; Selke, R. *Angew. Chem. Int. Ed. Engl.* **1998**, *37*, 1827-1830 (alkyl ketones). (d) Nagel, U.; Roller, C. *Z. Naturforsch.* **1998**, *53b*, 267-270 (alkyl ketones). (e) Doucet, H.; Ohkuma, T.; Murata, K.; Yokozawa, T.; Kozawa, M.; Katayama, E.; England, A. F.; Ikariya, T.; Noyori, R. *Angew. Chem. Int. Ed. Engl.* **1998**, *37*, 1703-1707 (aryl and alkyl ketones). (f) Ohkuma, T.; Ooka, H.; Hashiguchi, S.; Ikariya, T.; Noyori, R. *J. Am. Chem. Soc.* **1995**, *117*, 2675-2676 (aryl ketones). Rhodium catalyst system: (g) Jiang, Q.; Jiang, Y.; Xiao, D.; Cao, P.; Zhang, X. *Angew. Chem. Int. Ed. Engl.* **1998**, *37*, 1100-1102 (aryl and alkyl ketones).

(36) (a) Ager, D. J.; Laneman, S. A. *Tetrahedron: Asymmetry* **1997**, *8*, 3327, and references cited therein. (b) Burk, M. J.; Harper, T. G. P.; Kalberg, C. S. *J. Am.*

Chem. Soc. **1995**, *117*, 4423. (c) Genêt, J. P.; Ratovelomanana-Vidal, V.; Caño de Andrade, M. C.; Pfister, X.; Guerreiro, P.; Lenoir, J. Y. *Tetrahedron Lett.* **1995**, *36*, 4801.

(37) Casey, M.; Leonard, J.; Lygo, B.; Procter, G. *Advanced Practical Organic Chemistry*: Chapman & Hall: London, 1990; pp. 28-42.

(38) Dale, J. A.; Dull, D. L.; Mosher, H. S. *J. Org. Chem.* **1969**, *34*, 2543.

(39) Bennett, M. A. *Chem. Ind.* **1959**, 1516.

(40) Schrock, R. R. *J. Chem. Soc., Dalton Trans.* **1974**, 951.

(41) Schrock, R. R.; Osborn, J. A. *J. Am. Chem. Soc.* **1971**, *93*, 2397.

(42) Sucrow, W.; Grosz, K. P. *Syn. Commun.* **1979**, *9*, 603.

(43) Fryzuk, M. D.; Bosnich, B. *J. Am. Chem. Soc.* **1977**, *99*, 6262.

(44) Shioiri, T.; Yokoyama, Y.; Kasai, Y.; Yamada, S. *Tetrahedron* **1976**, *32*, 2211.

(45) Casey, M.; Leonard, J.; Lygo, B.; Procter, G. *Advanced Practical Organic Chemistry*: Chapman & Hall: London. 1990; pp. 70-73.

(46) Parker, D. *Chem. Rev.* **1991**, *91*, 1441.

(47) Takaya, H.; Ohta, T.; Sayo, N.; Kumobayashi, H.; Akutagawa, S.; Inoue, S.; Kasahara, I.; Noyori, R. *J. Am. Chem. Soc.* **1987**, *109*, 1596.

Chapter 5

Mechanistic Insights into Ruthenium-BINAP Catalyzed Enantioselective Hydrogenation Reactions.

Introduction:

High enantioselectivities have been obtained for a number of reactions catalyzed by chiral transition metal complexes. Notably, the asymmetric hydrogenation of C=C, C=O, and C=N bonds has advanced through the development of new chiral ligands, primarily phosphines, over the past two decades.[1] It is interesting to note, however that most of these advances were made through an empirical approach. Systems are typically investigated by varying the reaction conditions (solvents, temperatures, pressures, and the catalyst complexes and ligands) until optimum rates and selectivities are obtained. The explanations of the origins of enantioselection have been mostly speculative in nature and were based on the consideration of the stereochemical environment around the metal catalyst center. However, as Noyori has said, “Asymmetric catalysis is in fact four-dimensional chemistry, and the three-dimensional stereochemical aspects of chiral catalysts must be combined with an understanding of the role that the fourth dimension, that of reaction kinetics, plays in determining enantioselectivity.”[2] The true

understanding of enantioselection can only come from detailed mechanistic investigations. These include the identification and complete structural determination of the intermediates formed throughout the catalytic cycle, specifically the diastereomers involved in enantioselection of the major product, the identification of the first irreversible step(s) proceeding through diastereomeric transition states in the catalytic cycle, termed the enantioselective step, and the complete investigation of the kinetics of the catalytic cycle. It remains that such studies are rare for catalytic enantioselective hydrogenation reactions, due to the required features that must exist for a mechanistic study to yield truly informative details. These features include a well-defined catalyst system that can be easily identified throughout the reaction and the requirement that the enantioselective step either be the turnover-limiting step or precede the turnover limiting step.

The most detailed mechanistic investigations into ruthenium(II)-bis(phosphine) catalyzed enantioselective hydrogenation reactions are the hydrogenation of prochiral α,β-unsaturated acids,[3-8] and the hydrogenation of α-aminoacrylic acid derivatives.[9] In this section the investigation into both these reactions will be reported with the studies using $[Ru((R)\text{-BINAP})(C_8H_{11})(MeCN)](BF_4)$ (**11**) as catalyst precursor and tiglic acid (**4**), angelic acid (**12**), and dimethyl itaconate (**9**) as substrates.

Results and Discussion:

Ruthenium-BINAP catalyzed enantioselective hydrogenation of α,β-unsaturated acids. Halpern[3] was the first to report on the kinetics of a ruthenium-

BINAP catalyzed enantioselective hydrogenation of α,β-unsaturated carboxylic acids. Halpern investigated the hydrogenation of tiglic acid (**4**) using the Ru((*R*)-BINAP)(O_2CCH_3)$_2$ catalyst developed by Noyori[10] that was shown to yield high enantioselectivities for a variety of α,β-unsaturated carboxylic acids. Furthermore, under atmospheric pressure of dihydrogen gas in methanol solution, hydrogenation begins immediately upon addition of **4** to the catalyst allowing for easy study of the system. From the investigations, Halpern proposed the catalytic cycle depicted in Scheme 5.1.

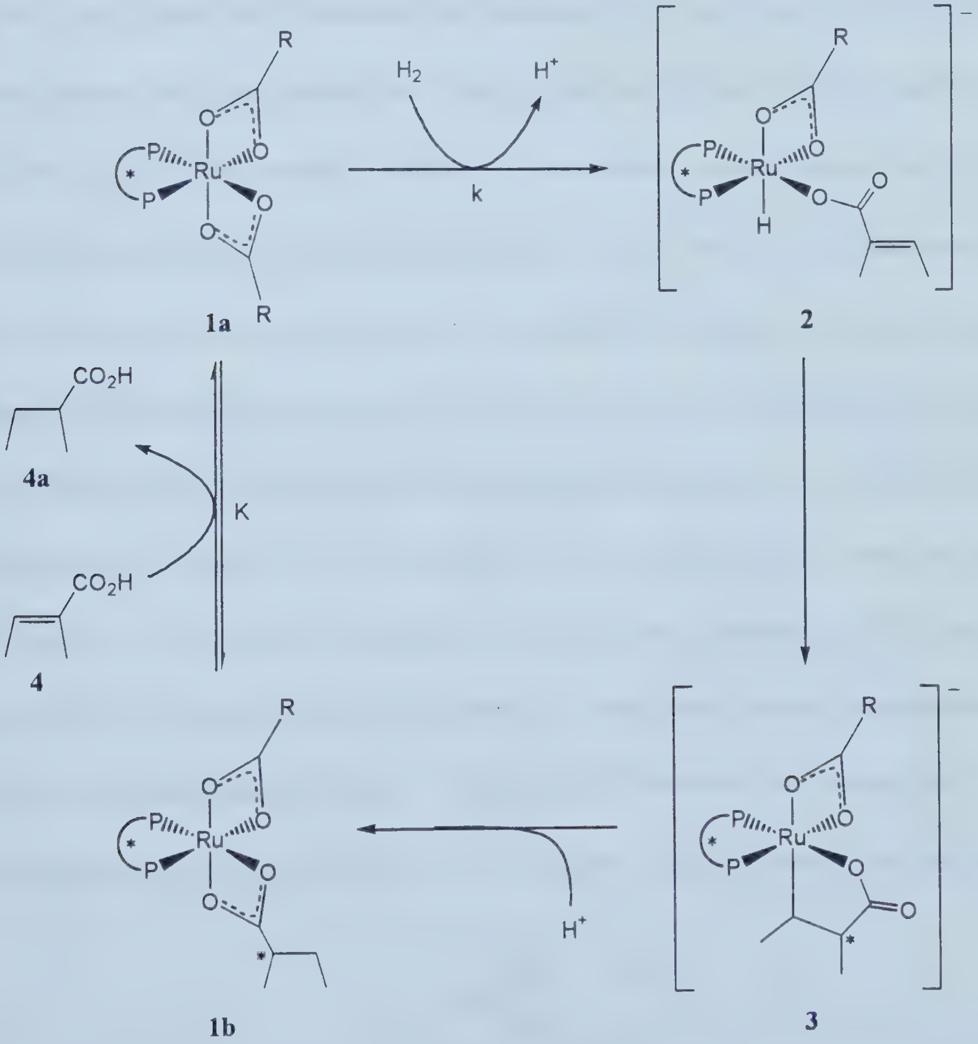

Scheme 5.1: Mechanism proposed by Halpern[3] for ruthenium-bis(phosphine) catalyzed hydrogenation. Key steps are heterolytic cleavage of H_2 and solvolysis to complete the catalytic cycle.

Halpern noted that the essential features of the cycle are (a) the rapid equilibrium between the catalyst precursor **1a** and the olefin substrate, (b) the heterolytic splitting of dihydrogen gas to give a ruthenium monohydride species (**2**), (c) insertion of the C=C bond of the olefin substrate into the ruthenium monohydride bond yielding a 5-membered heterometallacycle intermediate (**3**), and (d) the protonolysis (deuteronolysis) of the ruthenium-carbon bond to regenerate the ruthenium-dicarboxylate adduct (**1b**).

The analysis of the deuterium-labeling study of the catalytic hydrogenation reaction determined that the deuterium incorporation was found to be both regio- and stereoselective with the deuterium largely confined to one of the diastereotopic β-positions (H_{cis}) of the product, and only very minor incorporation into the other β-position (H_{trans}) and the α-position (H_c) (Figure 5.1). The lack of significant deuterium incorporation into the α-position (H_c) of 2-methylbutyric acid ruled out substantial H-D exchange between dihydrogen gas and the solvent prior to olefin-hydride insertion. This implied that, while H-D exchange was observed upon reaction of **1a** with dihydrogen gas in methanol-d_4, it must be slow compared with olefin-hydride insertion forming **2**. Furthermore, the essentially complete deuterium incorporation at H_{cis} indicated the reaction must proceed through a 5-membered heterometallacycle intermediate (**3**) and that solvolysis completes the cycle. To account for the solvolysis, heterolytic cleavage of dihydrogen gas was proposed (**1a** → **2**) to complete the mechanistic cycle pathway.

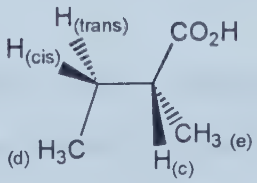

Figure 5.1: Assignment of protons for 2-methylbutyric acid.

Reports by Noyori,[4] on the deuterium-labeling studies of a number of α,β-unsaturated carboxylic acids, Achiwa,[5] on the hydrogenation of tiglic (**4**) and angelic (**12**) acids, and Chan,[7] on the deuterium-labeling investigations of itaconic acid and its ester derivatives, reaffirmed the Halpern mechanism. The results of all the studies revealed that hydrogen addition to the α-position (H_c) occurs from the dihydrogen gas and essentially complete regio- and stereochemical deuterium addition to the β-position (H_{cis}) occurs from the solvent solution. Brown's[8] deuterium-labeling investigations of the hydrogenation of the dimethyl itaconate methyl derivative **9**, however, indicated different deuterium patterns leading to the proposed pathway depicted in Scheme 5.2.

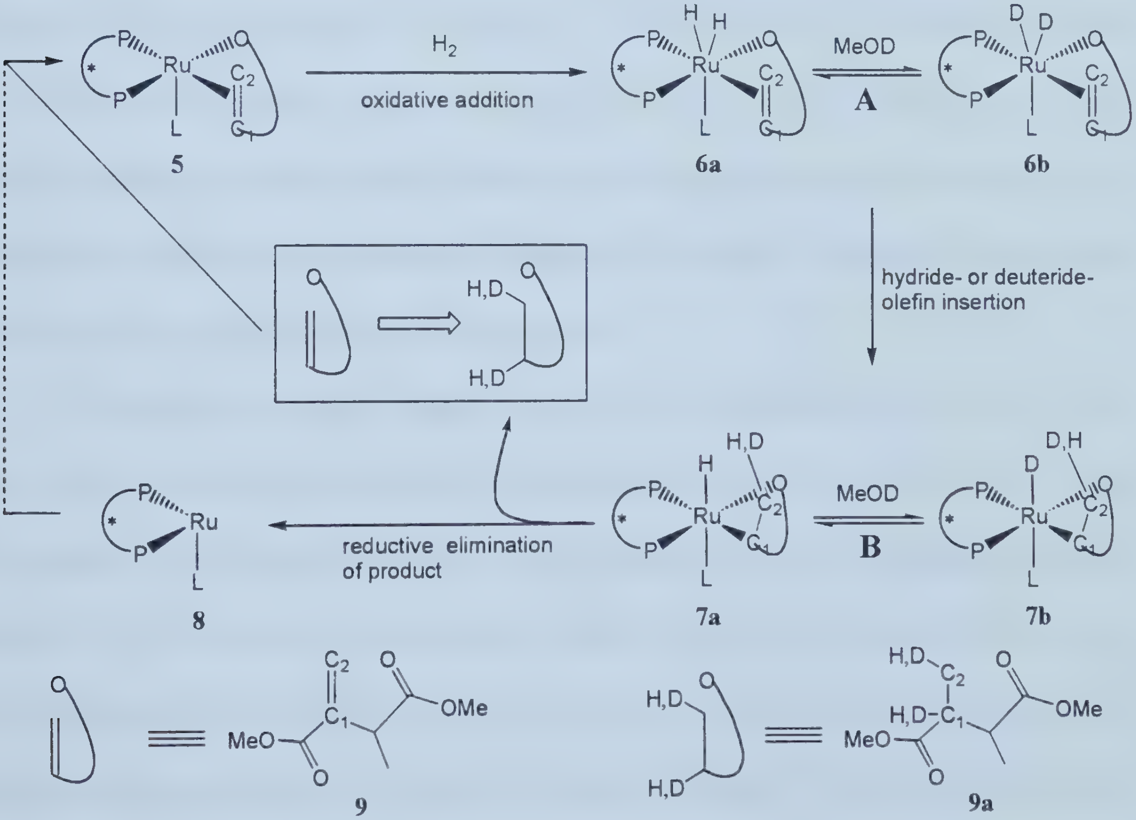
H₂
oxidative addition
MeOD
A
5
6a
6b
hydride- or deuteride-olefin insertion
H,D
H,D
reductive elimination of product
MeOD
B
8
7a
7b
MeO
OMe
9
H,D
H,D
9a
Ru
P
L
C₂
C₁

Scheme 5.2: Brown[8] mechanism for ruthenium-bis(phosphine) catalyzed hydrogenation. Predominant exchange process at step B for ruthenium-bis(phosphine) reductions of α,β-unsaturated acids. Predominant exchange process at step A for ruthenium-bis(phosphine) reductions of α,β-unsaturated esters.

Brown[8] observed that under similar conditions utilized in the deuterium studies of tiglic acid (**4**) by Halpern and Noyori (1 atm H_2, 25 °C, 24 h, methanol-d_4) the deuterium studies on **9** yielded essentially no deuterium incorporation into either the α- or β-positions of the hydrogenated product dimethyl 2,3-dimethylsuccinate (**9a**). This indicated that solvolysis did not occur for **9**. From these results, Brown suggested that a more likely reaction pathway was one in which oxidative addition of dihydrogen followed by H-D exchange with the solvent occurs (Scheme 5.2). The results observed with tiglic acid are accounted for by a slow rate of H-D exchange with solvent at **A** (**6a** → **6b**; Scheme 5.2) as compared to the rate of olefin-hydride insertion (**6** → **7**), and that the rate of reductive elimination of **9a** from **7** (**7** → **9a**; Scheme 5.2) is slow as compared to the rate of H-D exchange with solvent at **B** (**7a** → **7b**). It is important to note that a homolytic cleavage of dihydrogen yielding a ruthenium-dihydride intermediate (**7a**) is suggested, in contrast to the heterolytic cleavage of dihydrogen yielding the monohydride intermediate (**2**) suggested by Halpern and others.

With these differences in mechanism reported in the literature, deuterium-labeling studies were performed using $[Ru((R)\text{-BINAP})(H)(Sol)_{3-n}(MeCN)_n](BF_4)$ (**10**, n = 0-3, Sol = methanol or acetone) as catalyst for the enantioselective hydrogenation of tiglic acid (**4**).[11] **10** is formed from reaction of $[Ru((R)\text{-BINAP})(C_8H_{11})(MeCN)](BF_4)$ (**11**) with dihydrogen gas in methanol or acetone solution. Table 5.1 compares the results of the deuterium-labeling study to those of Takaya and Noyori.[4] Use of **10** as catalyst resulted in a greater degree of deuterium scrambling in **4a** than that reported by Halpern,[3]

Table 5.1: Pattern of deuterium incorporation in tiglic acid hydrogenation catalyzed by 1a and 10 under various conditions.

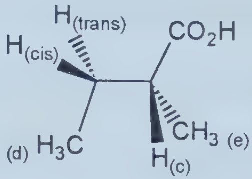

Catalyst, Conditions[a]	Percent Deuterium Incorporation				
	H_{cis}	H_{trans}	H_c	H_d	H_e
10 (H_2, CD_3OD)	85	---	70	---	---
10 (D_2, CH_3OH)	8	---	33	---	---
1a[b] (H_2, CD_3OD)	100	---	30	---	---
1a[b] (D_2, CH_3OH)	5	---	85	---	---

[a] Reaction conditions: catalyst **10**; 3 atm gas pressure, ambient temperature. Catalyst **1a**, 4 atm pressure, ambient temperature. [b] Reported by Takaya and Noyori (reference 4).

Takaya, and Noyori.[4] Under 3 atm of dihydrogen gas in methanol-d_4 solution, tiglic acid was hydrogenated to yield 2-methylbutyric acid (**4a**) in 90% ee (*R*), with an abundance of deuterium located at both the α-position (H_c) and the β-position (H_{cis}). The reaction performed under 3 atm of dideuterium gas in methanol solution showed the expected reversal of deuterium incorporation. The results from this system contrast those previously described in the literature.

The mechanistic pathway described by Halpern requires that the rate of H-D exchange between the solvent and dihydrogen gas be greater than the rate of olefin-hydride insertion (e.g., rate **1a** → **2** >> **2** → **3**; Scheme 5.1). It is noted, however, that unlike **1a**, **10** does not catalyze the H-D exchange between dihydrogen gas and methanol-d_4. To account for the exchange, the complex formed from the heterolytic cleavage of

dihydrogen gas (analogous to **2**, Scheme 5.1) must catalyze the exchange. The mechanism proposed by Brown, however, cannot be ruled out by these results. It may be that the rate of H-D exchange between dihydrogen gas and the solvent catalyzed by the complexes **6a** (step **A**) and **7a** (step **B**) is greater than the rates of olefin-hydride insertion (**6** → **7**) and reductive elimination (**7** → **9a**), respectively (slightly greater exchange in **A**, Scheme 5.2).

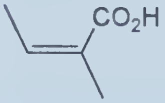

12

Figure 5.2: Structure of angelic acid (12), the thermodynamically less stable isomer of tiglic acid (4).

As the studies were inconclusive, examination of the hydrogenation of angelic acid[12] (**12**, Figure 5.2) was performed. Angelic acid is hydrogenated under 3 atm of dihydrogen gas in methanol solution, using **10** as catalyst, yielding 2-methylbutyric acid in 46% ee (*S*). Hydrogenation of **12** (Table 5.2) under 3 atm of dihydrogen gas in methanol-d_4 solution resulted in deuterium incorporation at the β-position (H_{cis} = 62%) and at the α-position (H_c = 43%) as well as at the other β-position (H_{trans} = 8%) and the β-methyl position (H_d = 43%, assuming CH_2D). The hydrogenation performed under 3 atm of dideuterium gas in methanol solution resulted in little deuterium incorporation at either the α-position (H_c = 30%) or the β-positions (H_{cis} = 7%). Small amounts of deuterium incorporation did, however, occur at the other β-position (H_{trans} = 8%) and at the β-methyl position (H_d = 5% of one H).

Table 5.2: Pattern of deuterium incorporation in angelic acid (12) hydrogenation catalyzed by 10 as catalyst under various conditions.

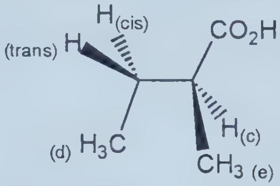

Catalyst, Conditions[a]	Percent Deuterium Incorporation H_{cis}	H_{trans}	H_c	H_d	H_e
10 (H_2, CD_3OD)	8	62	43	43	---
10 (D_2, CH_3OH)	5	8	30	5	---

[a] Reaction conditions: [Ru] = 2.6 mM, 3 atm gas pressure, ambient temperature.

The results of the labeling studies of **4** and **12** in methanol solution and the knowledge that the hydrogenations of **4** and **12** do not occur in aprotic solution in the absence of added base,[11] suggest that a mechanistic pathway, like that proposed by Halpern, is in operation (Scheme 5.3). While deuterium is scrambled more when using **10** than **1a** as catalyst, the evidence supports both the heterolytic cleavage of dihydrogen and a 5-membered heterometallacycle intermediate. That heterolytic cleavage is occurring and not dihydrogen oxidative addition is suggested by the observation that no hydrogenation of α,β-unsaturated carboxylic acids occurs in the absence of added base in aprotic solvent. Should the reaction proceed through the pathway proposed by Brown, with dihydrogen oxidative addition followed by insertion and reductive elimination of the hydrogenated product, one does not expect the use of aprotic solvents to suppress the reaction. That added base is required suggests that its role may be as the proton scavenger in the heterolytic cleavage of dihydrogen.

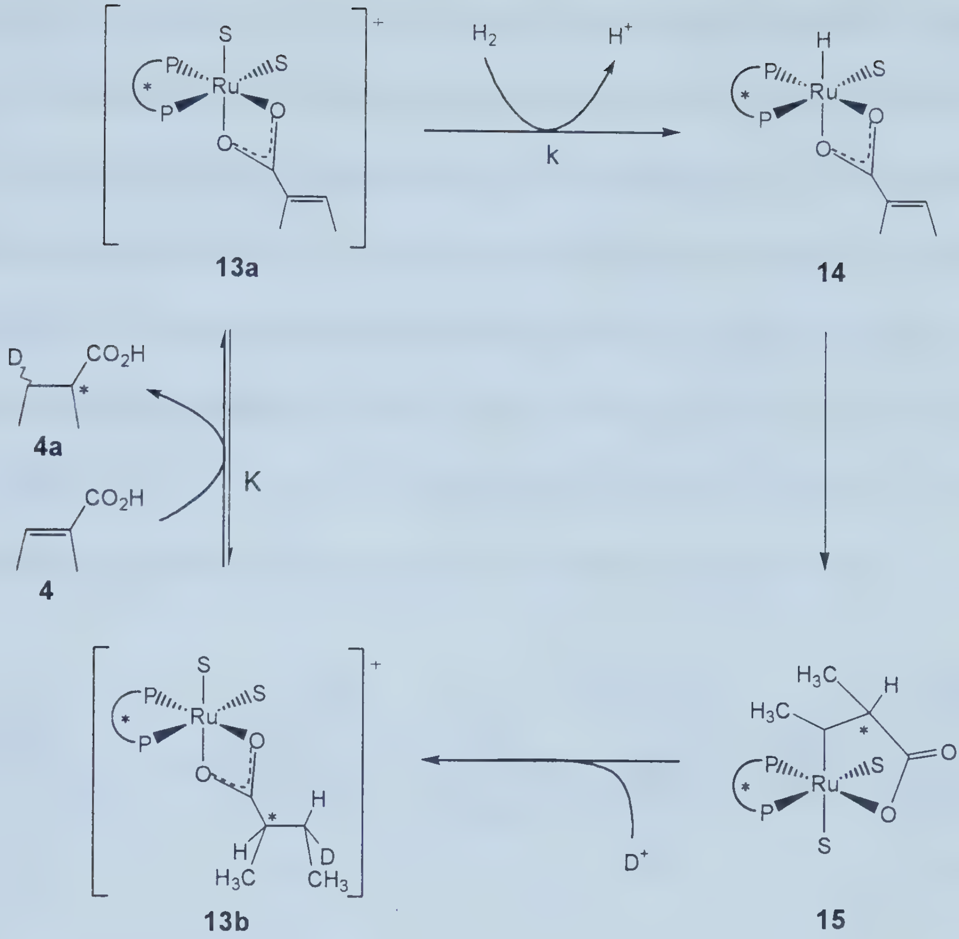

Scheme 5.3: Proposed general mechanistic pathway for ruthenium-bis(phosphine) catalyzed hydrogenation of α,β-unsaturated carboxylic acids.

The existence of 5-membered heterometallacycle intermediates is supported by the deuterium-labeling studies with angelic acid (**12**). That use of angelic acid (**12**) results in deuterium incorporation at the β-methyl position (H_d) of 2-methylbutyric acid (**4a**) suggests that olefin-hydride insertion occurs to form a 5-membered heterometallacycle species as this can be rationalized through the sequence of steps shown in Schemes 5.4 and 5.5. Heterolytic cleavage of dihydrogen leads to the species **14** (Scheme 5.4). From this intermediate, olefin-hydride insertion can occur through the

si-face to form the species (*R*)-**15**.[13] This species can undergo *β*-deuteride elimination from the *α*-position (H_a) or by *β*-hydride elimination from the *β*-methyl group (H_d). The removal of the deuteride at the *α*-position (H_a) is a moot issue as it is the reverse reaction of the olefin-deuteride insertion. Hydride abstraction from the *β*-methyl group (H_d) will produce (*R*)-**16**. H-D exchange with solvent would yield the deuteride (*R*)-**16-*d*₁**. (*R*)-**16-*d*₁** could then undergo insertion to form (*R*)-**15-*d*₁**, with deuterium now located at the *β*-methyl position (H_d) as observed (Scheme 5.4). Solvolysis, followed by exchange between the hydrogenated substrate and **4** would complete the catalytic cycle.

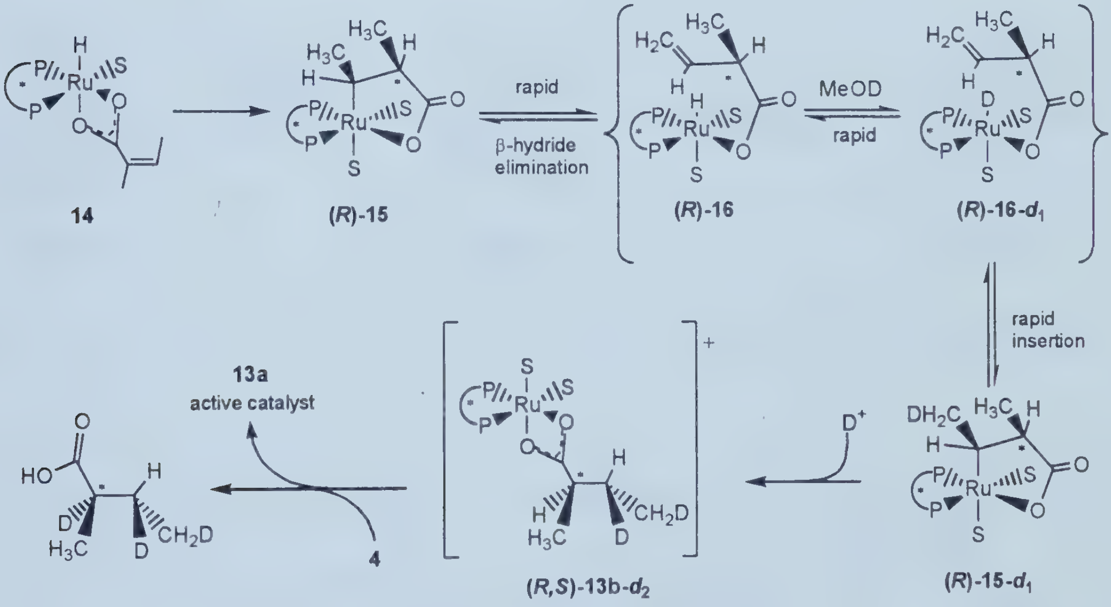

Scheme 5.4: Proposed mechanism to account for deuterium incorporation at H_a, H_{trans}, and H_d observed in angelic acid (12) hydrogenation with 10 as catalyst.

Deuterium incorporation into the *β*-methyl group can also occur from (*R*)-**16-*d*₁** as well. (*R*)-**16-*d*₁** can also undergo C_α-C_β bond rotation to form (*R*)-**17-*d*₁**. Olefin-deuteride insertion would form the 5-membered heterometallacycle (*R*)-**15a-*d*₁** resulting

in deuterium incorporation into the *β*-methyl group (H_d) also as observed (Scheme 5.5). Solvolysis, followed by exchange between the hydrogenated substrate and **4** would complete the catalytic cycle. It is noted that this pathway incorporates the isomerization of the C=C bond. The process of isomerization has precedent with a number of ruthenium-bis(phosphine) catalysts.[14] Isomerization of the C=C bond of angelic acid (**12**) is not surprising as its geometrical isomer, tiglic acid (**4**), is the thermodynamically more stable isomer.[12] All the above observations strongly support the Halpern type mechanism as depicted in Scheme 5.3.

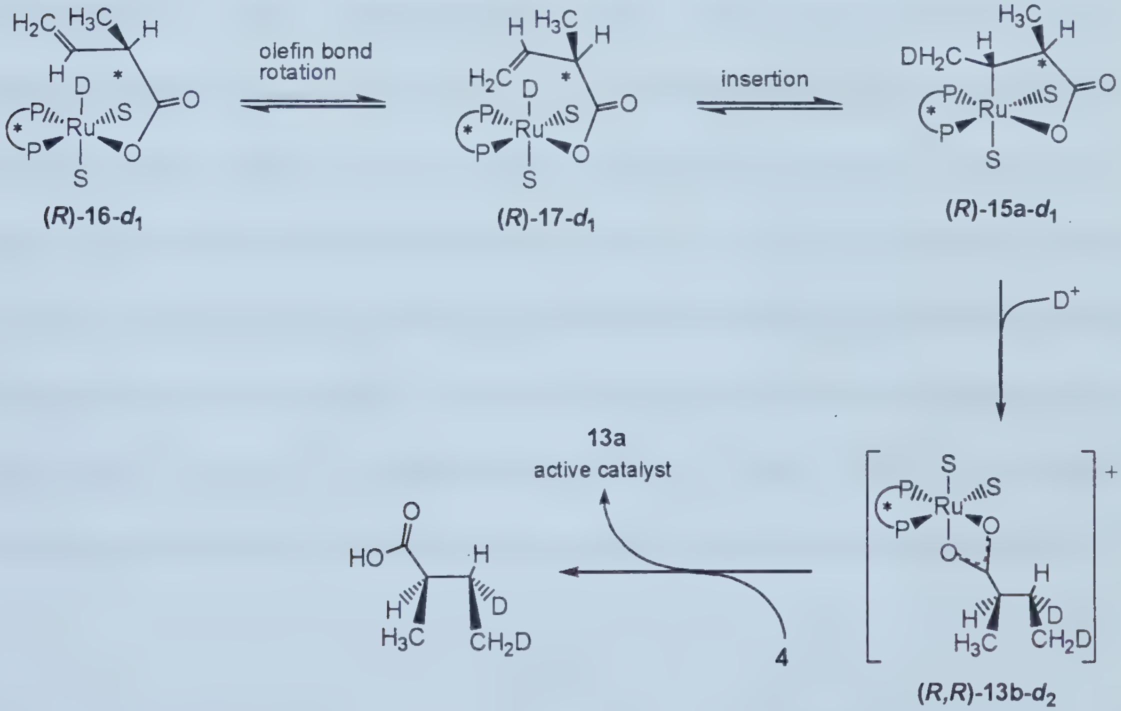

Scheme 5.5: Proposed mechanism to account for deuterium incorporation at H_a, H_{cis}, and H_d observed in angelic acid (12) hydrogenation with 10 as catalyst.

Corroboration of Brown mechanism. The substrate Brown examined was not an *α,β*-unsaturated acid, and therefore it likely goes through a different mechanistic pathway compared with the corresponding acids. As reported by Bergens,[9] the enantioselective hydrogenation of methyl *α*-acetamidocinnamate (MAC, **18**) proceeds through a different reaction mechanism from those of the *α,β*-unsaturated carboxylic acids (Scheme 5.7). MAC is hydrogenated in 92% ee (*R*) in acetone and 87% ee (*R*) in methanol solutions using **10** as catalyst.[11] In ^{31}P NMR spectroscopic studies of the operating catalytic reaction, only one ruthenium species was observed. Stoichiometric reaction of [Ru((*R*)-BINAP)(H)(Sol)$_n$(MeCN)$_{3-n}$](BF$_4$) (n = 0-3; Sol = acetone, **10**) and **18** resulted in a single species with identical NMR characteristics to those of the species observed in the catalytic reaction. Isolation and complete identification (solution NMR spectroscopic and X-ray crystallographic analyses) showed it to be the single diastereomer (**19**) formed via olefin-hydride insertion into the Ru-H bond (Figure 5.4).[9a]

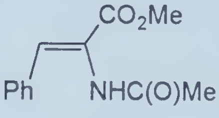

18

Figure 5.4: Structure of methyl *α*-acetamidocinnamate (18).

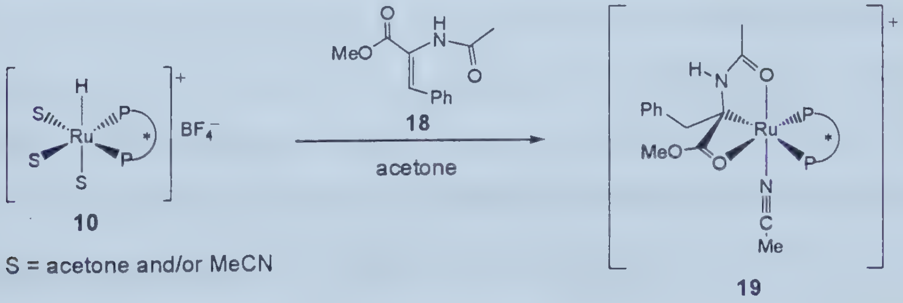

Figure 5.4: Structural identification of likely catalytic intermediate (19) in ruthenium-BINAP catalyzed enantioselective hydrogenation of MAC (18).

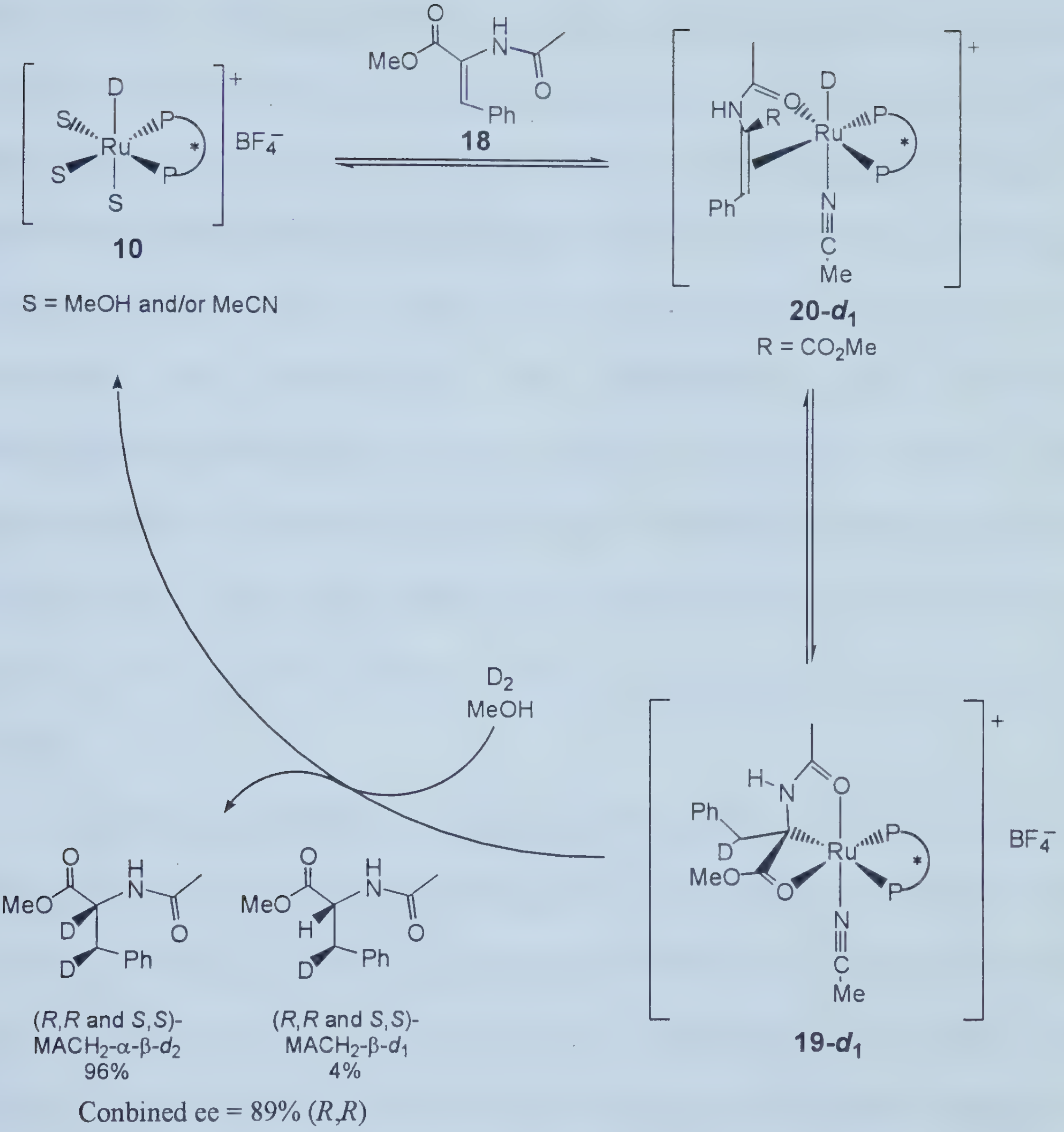
10
S = MeOH and/or MeCN
18
20-d_1
R = CO_2Me
19-d_1
BF_4^-
D_2
MeOH
(R,R and S,S)-
$MACH_2$-α-β-d_2
96%
(R,R and S,S)-
$MACH_2$-β-d_1
4%
Conbined ee = 89% (R,R)

Scheme 5.6: Proposed mechanism by Bergens for the ruthenium-BINAP catalyzed hydrogenation of MAC (18) with 10 as catalyst. Deuterium incorporation occurs at both centers with significant incorporation into the *α*-position as opposed to Halpern's observed incorporation (essentially only *β*-position) in ruthenium-BINAP catalyzed hydrogenation of *α*,*β*-unsaturated carboxylic acids.

The absolute configuration about the *α*-carbon center, assuming stereospecific replacement of ruthenium atom with hydrogen atom, is the same as that of the major

enantiomeric hydrogenation product formed ((*R*)-MAC(H)$_2$; Figure 5.4). Mechanistic studies showed **19** undergoes stoichiometric hydrogenolysis to yield the product in similar ee to the catalytic reaction using **10** as catalyst (87% ee (*R*) in MeOH).[9a] Additionally, deuterium-labeling studies identified that the olefin-hydride insertion step is reversible and is much faster than hydrogenolysis of the Ru-C bond.[9b] This corroborates the postulation made earlier by Saburi[15] on the reversibility of the insertion. The investigations also identified the first Ru(H)(Olefin) complex, [Ru((*R*)-BINAP)(H)(MAC)(MeCN)](BF$_4$) (**20**), from reaction of **10** with MAC at -40 °C.[9c] The proposed catalytic cycle (Scheme 5.6) includes the identification of a heterometallacycle intermediate (**19**). The resulting olefin-hydride insertion positions the hydride at the β-position, not the α-position as observed with many α,β-unsaturated carboxylic acid substrates.

Considering the similarity in structure of **9** to MAC, and of **9** to dimethyl itaconate (**21**), investigations of the hydrogenation of **21** using **10** as catalyst were undertaken. Dimethyl itaconate is hydrogenated in 95% ee (*S*) in both methanol and acetone solution using **11** as catalyst precursor.[11] Deuterium-labeling studies were performed and the results are listed in Table 5.3 along with the proton assignments. Under 3 atm of dihydrogen as and 25 °C in methanol-d_4 solution, deuterium incorporation occurred solely at the α-position (H$_\alpha$: ~ 30%). Under 3 atm of dideuterium and 25 °C in methanol solution the reaction yields deuterium incorporation at the α-position (H$_\alpha$: ~ 65%) and at the β-methyl position (H$_\beta$: ~ 80%, assuming formation of CH$_2$D).[16] These results are more in agreement with those observed by Brown, where deuterium incorporation from dideuterium gas is found at both the α-position (H$_\alpha$)

(Brown: 70% D; Here: 65% D) and *β*-methyl position (H_β) (Brown: 60%; Here: 80%, assuming formation of CH_2D).[16] The search for intermediates was undertaken to determine what information could be obtained on the mechanistic pathway in operation.

Table 5.3: Deuterium incorporation in hydrogenation of 9 and 21 with 22 (Brown's catalyst) and 10 as catalyst, respectively.

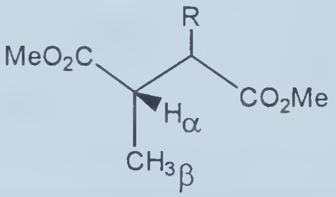

9 R = CH_3 **21** R = H

Catalyst, Conditions, Substrate[a]	H_α	H_β
10, (H_2, MeOD), **21**	30	---
10, (D_2, MeOH), **21**	65	80
22, (H_2, MeOD), **9**	10	10
22, (D_2, MeOH), **9**	70	60

[a] Reaction conditions: catalyst **10**, [Ru] = 2.6 mM, 3 atm gas pressure, ambient temperature. Catalyst **22** (Brown; Ru(BINAP)(η^2-MeC(O)CHC(O)Me)$_2$(η^2-allyl), 1 atm gas pressure, ambient temperature.

^{31}P NMR analysis of the operating catalytic hydrogenation of **21** showed only two species. Stoichiometric reaction of **21** with **10** yielded a ^{31}P NMR spectrum with consistent NMR signals as those observed in the catalytic hydrogenation. The analysis of the NMR data and comparison with the NMR data of **19** allowed for the identification of the species as two diastereomers of opposite absolute configuration (**23a/23b**). These species are structurally related to **19**. (Figure 5.5 depicts major species). Furthermore, the stereochemistries of the stoichiometric hydrogenolysis reactions of the isolated intermediates (**23a, 23b**) are similar to those of the catalytic hydrogenations (92% ee (*S*) and 95% ee (*S*), respectively). Thus far all investigations have shown parallel

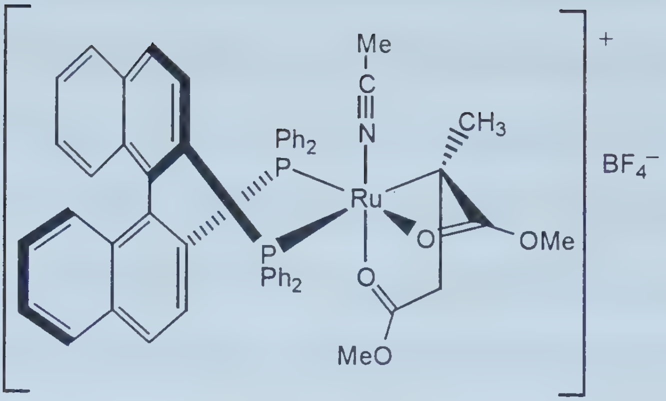

23a

Figure 5.5: Isolation and structural identification of likely catalytic intermediate (major species 23a) in ruthenium-bis(phosphine) catalyzed enantioselective hydrogenation of 21.

results to those for the hydrogenation studies of MAC, yielding strong evidence for **23a** and **23b** as catalytic intermediates. The investigations support homolytic cleavage of dihydrogen gas (deuterium-labeling studies) and olefin-hydride insertion yielding a 4-membered heterometallacycle (deuterium-labeling studies and isolation and characterization of **23a/23b**) with the Ru-C bond formed with C_1 of **21** (Scheme 5.2). Thus, the studies have yielded strong evidence supporting the mechanistic pathway proposed by Brown and Bergens for the catalytic enantioselective hydrogenation of **21**.

Conclusions:

The investigation into the mechanism of the ruthenium-BINAP catalyzed enantioselective hydrogenation of olefins is complicated by discrepancies in deuterium-labeling studies reported in the literature. Here, it has been shown that two mechanisms

can account for the observed differences in the reported deuterium-labeling studies. It can be concluded that the nature of the substrate will significantly affect the choice of mechanistic pathway utilized. It has been shown that tiglic and angelic acid likely proceed with heterolytic cleavage of dihydrogen gas while the diester dimethyl itaconate has evidence of proceeding with homolytic cleavage of dihydrogen gas. The favored pathway may result from electronic factors, from the disposition of the functional group in the substrate, or from a combination of both. A complete investigation using a wide variety of olefins must be performed in order to determine which factors prejudice which mechanistic pathway.

Experimental:

Methods and materials. The solvents tetrahydrofuran (K, Ph_2CO), diethyl ether (K, Ph_2CO), triethylamine (CaH_2), acetone (3 Å sieves), and methanol (MeOMg) were distilled from drying agents under argon gas. The argon and dinitrogen gases were passed through a bed of Drierite drying agent. Unless stated otherwise, commercial reagents were used without further purification, except dimethyl itaconate (distilled under argon atmosphere), and all operations were performed under an inert atmosphere of argon or dinitrogen gas. The compounds $[Ru((R)\text{-BINAP})(1\text{-}3;5,6\text{-}\eta\text{-}C_8H_{11})(MeCN)](BF_4)$[14a] (**11**) and angelic acid[17] (**12**) were synthesized via literature procedures.

All ^1H, ^{13}C, and ^{31}P NMR spectra were measured with a Bruker AM-400 NMR spectrometer operating at 400.13 MHz, 100.61 MHz, and 161.97 MHz respectively. ^1H and ^{13}C NMR chemical shifts are reported in parts per million (δ) relative to

tetramethylsilane using the solvent as an internal reference. ^{31}P NMR chemical shifts are reported in parts per million (δ) relative to an 85% H_3PO_4 external reference. All ^{13}C and ^{31}P NMR spectra are ^1H decoupled unless stated otherwise. Mass spectra were measured using Kratos MS50. Microanalyses were performed at the University of Alberta Microanalysis Laboratory. Optical rotations were measured with a Perkin-Elmer 241 polarimeter at 589 nm (sodium D line) using 1.0 dm cells. Specific rotations, $[\alpha]_D$, are reported in degrees per decimeter at 25 °C, and the concentration (c) is given in grams per 100 mL.

Hydrogenations of tiglic acid with D_2 in methanol or H_2 in methanol-*d*$_4$ using 11 as catalyst precursor. The catalyst precursor **11** (10.0 mg, 1.04×10^{-5} mol) was transferred to a glass bomb along with 100 equiv of tiglic acid (**4**) (104.1 mg, 1.04×10^{-3} mol) in the glove box. The dry, deoxygenated methanol, or methanol-*d*$_4$, was then added (4.0 mL) and the solution was stirred for 5 minutes. The atmosphere was then flushed with dihydrogen gas, or dideuterium gas, and once flushed the bomb was sealed under 3 atm of dihydrogen or dideuterium. The solution was stirred for 20 h at 25 °C to complete hydrogenation. Once completed, the solvent was removed under reduced pressure, and the product was dissolved in CH_2Cl_2 and passed through a Florisil plug to remove the catalyst. The solvent was then removed under reduced pressure and the product analyzed by NMR.

Residue from hydrogenation with H_2 in methanol-*d*$_4$: ^1H (400.1 MHz, acetone-*d*$_6$): δ 0.9('d', H_d, 0% D incorp.), 1.10 ('s', H_e, 0% D incorp.), 1.43 (m, H_{trans}, 0% D incorp.), 1.62 (m, H_{cis}, 85% D incorp.), 2.34 (m, H_c, 70.5% D incorp.), 10.45 (br s, H_{acid}).

Residue from hydrogenation with D_2 in methanol: ^{1}H (400.1 MHz, acetone-d_6): δ 0.9 ('t', H_d, 0% D incorp.), 1.10 ('d', H_e, 0% D incorp.), 1.43 (m, H_{trans}, 0% D incorp.), 1.62 (m, H_{cis}, 7.5% D incorp.), 2.34 (m, H_c, 33% D incorp.), 10.45 (br s, H_{acid}).

Hydrogenations of angelic acid with D_2 in methanol or H_2 in methanol-d_4 using 11 as catalyst precursor. The catalyst precursor **11** (12.0 mg, 1.25 x 10^{-5} mol) was transferred to a glass bomb along with 100 equiv of angelic acid (**12**) (125.5 mg, 1.25 x 10^{-3} mol). The dry, deoxygenated methanol, or methanol-d_4, was then added (4.8 mL) and the solution was stirred for 5 minutes. The atmosphere was then flushed with dihydrogen gas, or dideuterium gas, and once flushed the bomb was sealed under 3 atm of dihydrogen or dideuterium. The solution was stirred for 20 h at 25 °C to complete hydrogenation. Once completed, the solvent was removed under reduced pressure, and the product was dissolved in CH_2Cl_2 and passed through a Florisil plug to remove the catalyst. The solvent was then removed under reduced pressure and the product analyzed by NMR.

Residue from hydrogenation with H_2 in methanol-d_4: ^{1}H (400.1 MHz, acetone-d_6): δ 0.9 ('d', H_d, 43% D incorp.), 1.10 ('s', H_e, 0% D incorp.), 1.43 (m, H_{trans}, 62% D incorp.), 1.62 (m, H_{cis}, 8% D incorp.), 2.34 (m, H_c, 43% D incorp.), 10.45 (br s, H_{acid}).

Residue from hydrogenation with D_2 in methanol: ^{1}H (400.1 MHz, acetone-d_6): δ 0.9 ('d', H_d, 5% D incorp.), 1.10 ('s', H_e, 0% D incorp.), 1.43 (m, H_{trans}, 7.5% D incorp.), 1.62 (m, H_{cis}, 5% D incorp.), 2.34 (m, H_c, 30% D incorp.), 10.45 (br s, H_{acid}).

Hydrogenations of dimethyl itaconate (21) with D_2 in methanol or H_2 in methanol-d_4 using 11 as catalyst precursor. The catalyst precursor **11** (11.5 mg, 1.20 x 10^{-5} mol) was transferred to a glass bomb along with 75 equiv of dimethyl itaconate **21** (126 μL, 9.00 x 10^{-4} mol) via gas-tight syringe. The methanol, or methanol-d_4, was then added (4.6 mL) and the solution was stirred for 5 minutes. The atmosphere was then flushed with dihydrogen gas, or dideuterium gas, and once flushed the bomb was sealed under 3 atm of dihydrogen or dideuterium. The solution was stirred for 20 h at 25 °C to complete hydrogenation. Once completed, the solvent was removed under reduced pressure, and the product was dissolved in CH_2Cl_2 and passed through a Florisil plug to remove the catalyst. The solvent was then removed under reduced pressure and the product analyzed by NMR.

Residue from hydrogenation with H_2 in methanol-d_4: ^1H (400.1 MHz, CD_2Cl_2): δ 1.18 (d, H_β, 0% D incorp.), 2.46 (dd, 0% D incorp.), 2.68 (dd, 0% D incorp.), 2.88 (m, H_α, 30% D incorp.), 3.62 (s, OCH_3, 0% D incorp.), 3.63 (s, OCH_3, 0% D incorp.).

Residue from hydrogenation with D_2 in methanol: ^1H (400.1 MHz, CD_2Cl_2): δ 1.18 (d, H_β, 80% D incorp. assuming CH_2D), 2.46 (dd, 0% D incorp.), 2.68 (dd, 0% D incorp.), 2.88 (m, H_α, 65% D incorp.), 3.62 (s, OCH_3, 0% D incorp.), 3.63 (s, OCH_3, 0% D incorp.). Actual amounts of product were determined by ^{13}C NMR chemical shifts based on reported assignments: **21** (5%), **21-*α-d*₁** (15%), **21-*β-d*₁** (30%), **21-*α,β-d*₂** (50%).[15]

Synthesis of [Ru((*R*)-BINAP)(MeCN)(C[CH_3][CO_2CH_3][$CH_2CO_2CH_3$])](BF_4) (23a/23b). To a 50 mL solvent Schlenk flask was added **11** (102.2 mg, 1.07 x 10^{-4} mol).

The Schlenk flask was placed under reduced pressure and purged with argon gas several times to remove traces of oxygen. To the Schlenk flask was added acetone (7.5 mL) via gas-tight syringe. The solution was stirred for 5 min then dihydrogen gas was bubbled through the solution until complete hydrogenation of **11** was achieved (2 min). The solution was then bubbled with argon gas to remove all traces of excess dihydrogen gas (5 min). Once all traces of dihydrogen gas were removed, dimethyl itaconate (**21**) was added (17.4 μL, 1.23 x 10^{-4} mol) via gas-tight syringe. The golden orange solution turned bright orange-yellow immediately. The flask was shaken for 5 min, then it was placed under reduced pressure to remove the solvent. The residue was dissolved in a minimal amount of acetone (~1.0 mL) and then precipitated out of solution with Et_2O (40 mL). The solution was filtered to dryness, the solid washed with Et_2O (3 x 10 mL), dried under a stream of argon gas (20 min), and finally dried under high vacuum overnight. The sample was then transferred to a vial and stored at -30 °C in the glove box: yield = 75.6 mg (70.2%). Attempts to obtain X-ray quality crystals by slow diffusion of a variety of solvents (CH_2Cl_2/Et_2O, CH_2Cl_2/pentane, CH_2Cl_2/*n*-Bu_2O, acetone/Et_2O, acetone/*n*-Bu_2O, MeOH/Et_2O, MeCN/Et_2O, benzene/Et_2O) were unsuccessful. ^1H NMR of major product (85%) **(*R*)-23a** (400 MHz, 25 °C, acetone-d_6): δ 0.56 (d, 1H, Ru-$C(CH_3)(CO_2CH_3)(CH_2CO_2CH_3)$, $^2J_{H\text{-}H}$ = 19.5 Hz), 1.49 (d, 3H, $RuC(CH_3)(CO_2CH_3)(CH_2CO_2CH_3)$, $^4J_{H\text{-}Pa}$ = 5.8 Hz), 1.95 (s, 3H, CH_3CN), 2.28 (dd, 1H, $RuC(CH_3)(CO_2CH_3)(CH_2CO_2CH_3)$, $^2J_{H\text{-}H}$ = 19.5 Hz, $^4J_{H\text{-}Pa}$ = 6.0 Hz), 3.83 (s, 3H, OCH_3), 4.00 (s, 3H, OCH_3), 6.45 - 8.15 (m, 32H, BINAP, overlap with minor). ^{13}C (400 MHz, 25 °C, CD_2Cl_2): δ 4.6 (s, CH_3CN), 20.7 (s, $RuC(CH_3)(CO_2CH_3)(CH_2CO_2CH_3)$), 38.4 (dd, $RuC(CH_3)(CO_2CH_3)(CH_2CO_2CH_3)$), $^2J_{C\text{-}P}$ = 42.0 Hz, $^2J_{C\text{-}P}$ = 3.0 Hz), 40.8 (d,

RuC(CH_3)(CO_2CH_3)($CH_2CO_2CH_3$), ${}^3J_{C\text{-}P}$ = 4.0 Hz), 52.8 (s, OCH_3), 55.8 (s, OCH_3), 126.4 - 142.8 (m, BINAP and CH_3CN), 167.2 (s, CO_2CH_3, ${}^3J_{C\text{-}P}$ = 3 Hz), 190.0 (d, CO_2CH_3, ${}^3J_{C\text{-}P}$ = 6.5 Hz). ^{31}P (MHz, 25 °C, acetone-d_6): δ 34.64 (d, 1P_a, ${}^2J_{P\text{-}P}$ = 21.5 Hz)*, 56.65 (d, 1P_b, ${}^2J_{P\text{-}P}$ = 21.5 Hz). Note, P_a is *trans* to the Ru-C and P_b is *cis* to the Ru-C. Complete identification of ^{1}H and ^{13}C of minor complex (15%, **(*S*)-23b**) could not be performed due to lack of concentration and overlap with major product signals. ^{31}P (MHz, 25 °C, acetone-d_6): δ 40.8 (d, ${}^2J_{P\text{-}P}$ = 36.5 Hz), 63.6 (d, ${}^2J_{P\text{-}P}$ = 36.5 Hz). ESIMS. Calcd for $C_{53}H_{46}O_4NP_2Ru$ (M - BF_4)$^+$: 924.194. Found: 924.1. Anal. Calcd for $C_{53}H_{46}O_4NP_2Ru$: C, 62.98; H, 4.59; N, 1.39. Found: C, 62.47; H, 4.67; N, 1.31.

Stoichiometric hydrogenation of [Ru((*R*)-BINAP)(MeCN)(C[CH_2(D)]-[CO_2CH_3][$CH_2CO_2CH_3$])](BF_4) (23a-*d*$_1$/23b-*d*$_1$). To a glass bomb was added **23a-*d*$_1$/23b-*d*$_1$** (100.8 mg, 9.96 x 10^{-5} mol), made exactly like **23a/23b** only with dideuterium gas replacing dihydrogen gas. The bomb was flushed with argon gas for 20 min to ensure no oxygen gas was present. To the bomb was added acetone (7.5 mL) via gas-tight syringe. The bomb was then flushed with dihydrogen gas for 2 min, then it was sealed under 4 atm of dihydrogen gas. The reaction was stirred at room temperature for 10 min and then the bomb was depressurized. The solution was transferred to a flask and the solvent was removed under reduced pressure. The residue was then dissolved in CH_2Cl_2 (0.2 ml) and passed through a Florisil plug with Et_2O (~5 mL) to remove the catalyst. NMR analysis showed complete conversion to dimethyl methylsuccinate in 93% ee (*S*), with D-H exchange (~35%) occurring at the *β*-methyl position corresponding to reversibility of formation of **23a/23b** on time-scale of irreversible hydrogenolysis of

Ru-C_α bond. Similar reversibility was observed in the studies with **18** as substrate and **10** as catalyst.

References and Notes:

(1) For reviews on these advances, see: (a) Noyori, R.; *Asymmetric Catalysis in Organic Synthesis*: Wiley-Interscience: New York, 1994; chapter 5. (b) Willoughby, C. A.; Buchwald, S. L. *J. Am. Chem. Soc.* **1994**, *116*, 8592. (d) Pfaltz, A. *Acc. Chem. Res.* **1993**, *26*, 339. (e) Brunner, H. *Topics Stereochemistry* **1988**, *18*, 129. (f) Asymmetric Synthesis, vol. 5, Chiral Catalysis, Morrison, J. D. (Ed.); Academic Press, Orlando, 1985. (g) Knowles, W. S. *Acc. Chem. Res.* **1983**, *16*, 106.

(2) Noyori, R.; *Asymmetric Catalysis in Organic Synthesis*: Wiley-Interscience: New York, 1994; Chapter 1, pp. 2.

(3) Ashby, M. T.; Halpern, J. *J. Am. Chem. Soc.* **1991**, *113*, 589-594.

(4) Ohta, T.; Takaya, H.; Noyori, R. *Tetrahedron Lett.* **1990**, *31*, 7189-7192.

(5) Yoshikawa, K.; Murata, M.; Yamamoto, N.; Inoguchi, K.; Achiwa, K. *Chem. Pharm. Bull.* **1992**, *40*, 1072-1074.

(6) Saburi, M.; Takeuchi, H.; Ogasawara, M.; Tsukahara, T.; Ishii, Y.; Ikariya, T.; Takahashi, T.; Uchida, Y. *J. Organomet. Chem.* **1992**, *428*, 155-167.

(7) Chan, A. S. C.; Chen, C. C.; Yang, T. K.; Huang, J. H.; Lin, Y. C. *Inorg. Chim. Acta* **1995**, *234*, 95-100.

(8) Brown, J. M.; Rose, M.; Knight, F. I.; Wienland, A. *Recl. Trav. Chim. Pays-Bas* **1995**, *114*, 242-251.

(9) (a) Wiles, J. A.; Bergens, S. H. *J. Am. Chem. Soc.* **1997**, *119*, 2940-2941. (b) Wiles, J. A.; Bergens, S. H. *Organometallics* **1998**, *17*, 2228-2240. (c) Wiles, J. A.; Bergens, S. H. *Organometallics* **1999**, *18*, 3709-3714.

(10) Ohta, T.; Takaya, H.; Kitamura, M.; Nagai, K.; Noyori, R. *J. Org. Chem.* **1987**, *52*, 3174.

(11) **10** is efficient catalyst precursor for enantioselective hydrogenation of α,β-unsaturated carboxylic acids and ester derivatives, and is comparable in efficiency to other ruthenium-BINAP catalyst systems reported. It is also noted that hydrogenation of α,β-unsaturated carboxylic acids in acetone solution did not proceed unless 1 equiv of triethylamine per acid unit was added. These studies have been reported: Daley, C. J. A.; Wiles, J. A.; Bergens, S. H. *Can. J. Chem.* **1998**, *76*, 1447-1456.

(12) Thermodynamically less stable than tiglic acid: (a) Buckles, R. E.; Mock, G. V. *J. Am. Chem. Soc.* **1950**, *72*, 680-684. (b) The Merck Index: Budavari, S.; O'Neil, J.; Smith, A.; Heckelman, P. E. Eds.; 11th ed; Merck & Co., Inc.: New Jersey, 1989; pp. 102 (angelic acid), pp. 1486 (tiglic acid).

(13) Defined as *R* configuration assuming replacement of ruthenium atom by hydrogen atom as in final hydrogenation product.

(14) Examples of isomerizations of olefinic substrates: (a) Wiles, J. A.; Lee, C. E.; McDonald, R.; Bergens, S. H. *Organometallics* **1996**, *15*, 3782-3784. (b) Saburi *et al*, reference 6. Examples of isomerizations with allylic alcohols: (c) Sun, Y.; Wang, J.; LeBlond, C.; Reamer, R. A.; Laquidara, J.; Sowa, J. R. Jr.; Blackmond, D. G. *J. Organomet. Chem.* **1997**, *548*, 65-72. (d) Sun, Y.; LeBlond, C.;Wang, J.;

Blackmond, D. G.; Laquidara, J.; Sowa, J. R. Jr. In *Catalysis of Organic Reactions*: Malz, R. E. Jr. Ed.; Marcel Dekker: New York, 1996; pp. 167-176. (e) Trost, B. M.; Kulawiec, R. J. *J. Am. Chem. Soc.* **1993**, *115*, 2027-2036. (f) Takaya, T.; Ohta, T.; Inoue, S.; Tokunaga, M.; Kitamura, M.; Noyori, R. *Org. Synth.* **1993**, *72*, 74. (g) Takaya, H.; Ohta, T.; Sayo, N.; Kumobayashi, H.; Akutagawa, S.; Inoue, S.; Kasahara, I.; Noyori, R. *J. Am. Chem. Soc.* **1987**, *109*, 1596-1597. (h) Inoue, S.; Osada, M.; Koyano, K.; Takaya, H.; Noyori, R. *Chem. Lett.* **1985**, 1007-1008.

(15) Kawano, H.; Ikariya T.; Ishii, Y.; Saburi, M.; Yoshikawa, S.; Ucida, Y.; Kumobayashi, H. *J. Chem. Soc. Perkin Trans 1* **1989**, 1571-1575.

(16) The assumption of only CH_2D being formed is appears to be correct. The ^{13}C NMR data show that there is solely formation of CH_2D based on the ^{13}C chemical shift data reported: Hardick, D. J.; Blagbrough, I. S.; Potter, V. L. *J. Am. Chem. Soc.* **1996**, *118*, 5897-5903.

(17) Buckles, R. E.; Mock, G. V. *J. Org. Chem.* **1950**, *15*, 680-684.

Chapter 6

The First Identified Diastereomeric Catalyst-Alkoxide Species in Enantioselective Ketone Hydrogenation.

Introduction:

The enantioselective catalytic hydrogenation of ketones is an area of great research interest that has been extensively studied as the facile conversion of achiral ketones to enantiomerically pure alcohols is widely desired in pharmaceuticals, industry, and academia.[1] Although early catalyst systems were successful for a limited number of functionalized ketones, these systems generally required high pressures and high temperatures to proceed. For these reasons, the isolation and/or identification of catalytic intermediates has remained difficult resulting in little evidence to support proposed catalytic cycles.[2]

In the last decade, the field has undergone some major advances that have led to innumerable ruthenium and rhodium catalyst systems yielding high enantioselectivities.[3] These systems most often effect the catalytic hydrogenation of functionalized ketones while a few newer ones also hydrogenate aryl-alkyl[3a, b, i-k] and dialkyl ketones.[3c-e, i-k] Traditionally, the latter two ketone substrate types have been difficult to hydrogenate

with high enantioselectivity. Another great advance is that many of the newer catalyst systems perform hydrogenations under mild reaction conditions.[3b, f-h, j] Despite these advances and the many published reports on enantioselective ketone hydrogenation, no report describing the conclusive structural characterization of a diastereomeric catalyst-ketone complex exists.[4] As a result, the nature of the steric interactions between the catalyst core and the ketone substrate for this scientifically and economically important enantioselective catalytic reaction was, to date, interpreted with little direct experimental evidence.

Chiral ruthenium-bis(phosphine) complexes are among the most active catalysts for enantioselective ketone hydrogenation.[3] Some have effected the reaction with high turnover frequencies and turnover numbers under near-ambient conditions. In the Bergens group, the use of $[Ru((R)\text{-BINAP})(1\text{-}3;5,6\text{-}\eta\text{-}C_8H_{11})(MeCN)](BF_4)$ (**1**) as catalyst precursor has resulted in the isolation and structural elucidation of a number of possible catalytic intermediates in ruthenium-bis(phosphine) catalyzed enantioselective hydrogenations of olefins.[5, 6] These discoveries led to the successful investigation of catalytic enantioselective ketone hydrogenation reactions using **1** as catalyst precursor.[6] The objective of this study was to utilize **1** as catalyst system for a detailed mechanistic investigation of enantioselective ketone hydrogenation.

Results and Discussion:

The catalyst system **1** was utilized previously for the catalytic enantioselective hydrogenation of ketones.[6] Dimethyl oxaloacetate (**2**) was hydrogenated using **1** as

catalyst precursor in 74 % ee under 100 atm of dihydrogen gas and 50 °C (Figure 6.1). This previously unexplored ketone substrate[7] was used because it has structural similarities with the *α,β*-unsaturated olefins methyl *α*-acetamidocinnamate (MAC, **3**) and dimethyl itaconate (**4**), both of which are hydrogenated in high ee (92% ee (*R*) and 95% (*S*), respectively) using **1** as catalyst precursor.[6] **3** and **4** have the same disposition of carbonyl groups about the olefin unit to be hydrogenated (one *α*-carbonyl group and one *β*-carbonyl group; Figure 6.1). Dimethyl oxaloacetate (**2**) has this same disposition of carbonyl groups about the ketone carbonyl unit that is to be hydrogenated (Figure 6.1). The use of catalyst system **1** has resulted in a great deal of catalytic mechanistic information as detailed in the reports on the enantioselective hydrogenation of **3**,[5] and of those found with **4** and tiglic acid (**5**).[6]

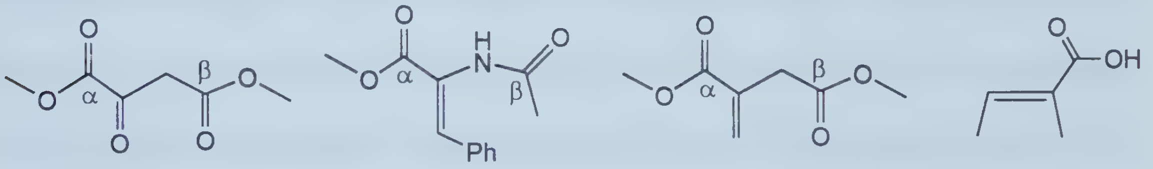

2 **3** **4** **5**

Figure 6.1: Substrates hydrogenated in high ee using 1 as catalyst precursor.

The stoichiometric reaction between the active catalyst species, [Ru((*R*)-BINAP)(H)(Sol)$_{3-n}$(MeCN)$_n$](BF$_4$) (**6**, Sol = acetone, THF, or methanol, n = 0-3), and **2** resulted in an immediate solution color change from golden yellow to bright green, followed moments later (~5 s) by a change to orange-yellow.[8] ^{1}H and ^{31}P NMR analysis were complicated by the presence of several species in solution with overlapping signals or broad signals indicative of fluxional species. Addition of excess acetonitrile, a strong binding ligand that will occupy any labile coordination sites and yield a static species, did

not simplify the spectrum to any useful degree. Reexamination of the ^{1}H NMR, however, revealed a pattern of interest. The pattern consisted of three distinct sets of doublets of doublets at δ 2.4 (1H, H_b or H_c, $^2J_{H\text{-}H}$ = 14 Hz, $^3J_{H\text{-}H}$ = 4 Hz) and δ 2.65 (1H, H_b or H_c, $^2J_{H\text{-}H}$ = 14 Hz, $^3J_{H\text{-}H}$ = 8 Hz) and at δ 4.0 (1H, H_c, $^3J_{H\text{-}H}$ = 4 Hz, $^3J_{H\text{-}H}$ = 8 Hz). The pattern was consistent with a catalyst-alkoxide complex formed by the C=O bond of the ketone inserting into the ruthenium-hydride bond. Figure 6.2 depicts one possible structure for the catalyst-alkoxide complex. Metal-alkoxides are believed to be intermediates in the enantioselective transition-metal catalyzed hydrogenation of ketones,[2] but have never been directly observed during such a process, and thus the isolation and characterization of this species was of utmost importance. The complex, however, was present in limited quantity (~40 %) and it could not be separated from the other species in solution. NMR data showed that the other species in solution were likely ruthenium-acac type complexes (Figure 6.2). These complexes almost certainly formed from reaction between **6** and the enol of **2**. The enolic proton is highly acidic and, as observed with acid substrates (e.g. tiglic acid (5)),[6] acidic protons react with the ruthenium-hydrido complex **6** to form a

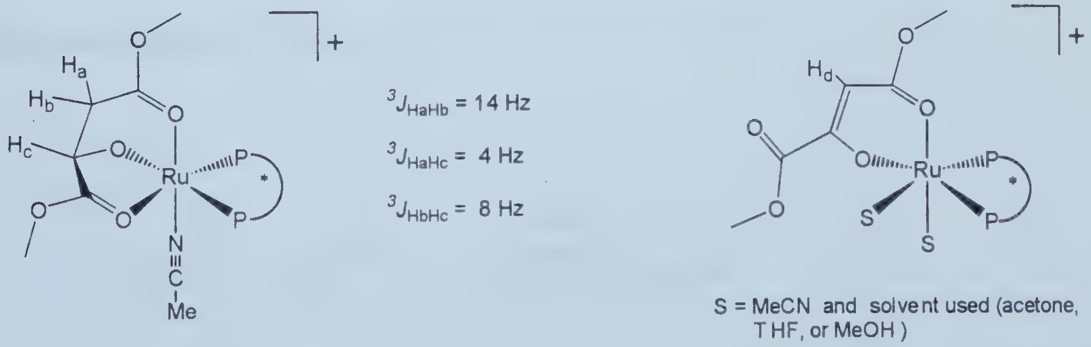

S = MeCN and solvent used (acetone, THF, or MeOH)

Possible catalyst-alkoxide species

Ruthenium-acac type complex (enolate of **2**)

Figure 6.2: Possible ruthenium species formed via stoichiometric reaction of 6 and 2 where P-P* is (*R*)-BINAP.

ruthenium-carboxylate complex with concomitant formation of dihydrogen gas. In order to eliminate competing reaction from the enolic proton, it was decided that the enolizable sites of the ketone would be removed.

Conversion of dimethyl oxaloacetate (**2**) to a non-enolizable ketone was accomplished by methylating the CH_2-carbon center (Scheme 6.1). The reaction of **2** with excess methyl iodide in the presence of two equivalents of potassium carbonate yielded the desired product dimethyl 3,3-dimethyloxaloacetate (7) in 90% yield. The question remained, would non-enolizable ketone substrates undergo hydrogenation with **5** as catalyst, or was enolization a prerequisite for successful conversion to the desired alcohol product? Hydrogenation of 7 was successful, under similar conditions used for the hydrogenation of **2**, yielding dimethyl 3,3-dimethyl-2-hydroxysuccinate (7') in 59% ee (*R*). The stoichiometric reaction between the active catalyst (**6**) and dimethyl-3,3-dimethyloxaloacetate (7) was performed to determine if ketone-hydride insertion occurred. The reaction resulted in an immediate solution color change from golden yellow to deep orange-yellow. Examination of both the ^1H and ^{31}P NMR spectra showed the formation of only two distinct non-fluxional species upon immediate addition of 7 to the active catalyst **6**.

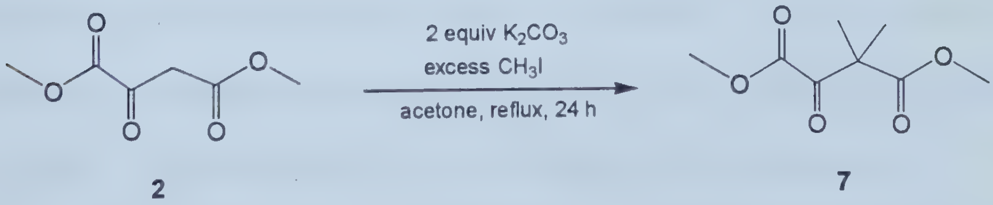

Scheme 6.1: Synthesis of non-enolizable ketone 7 from 2.

Structural characterization of ruthenium-BINAP-alkoxide complexes.

The stoichiometric reaction between 7 and the active catalyst **6** at room temperature in tetrahydrofuran or in methanol solution resulted in the immediate loss of the hydride ^{1}H NMR signal with concomitant formation of two species (**8a** and **8b**).[10] ^{31}P NMR analysis showed that the complexes formed in an ~80:20 ratio. Analysis of the ^{1}H and ^{13}C APT data showed that the products were diastereomeric ruthenium-alkoxide complexes.

Assignment of substrate signals. The structural features of the coordinated substrate were easily identified in the ^{1}H NMR spectrum. The backbone methyl groups are diastereotopic, resulting in two distinct singlets (two for major complex and two for minor complex) and the methoxy signals of the major and minor complexes were found in the appropriate region (ca. δ 3.6-3.8). Both ester groups in each of **8a** and **8b** were bonded to ruthenium as shown by the observed ^{13}C-^{31}P coupling in the ^{13}C NMR spectra. The coupling constants were similar and ranged from 2 to 3 Hz, making it impossible to determine with certainty if one or both ester groups were *trans* to a phosphorus center.[10] The signals in the ^{31}P NMR spectra of the ^{15}N-labeled isotopomers (prepared by exchange between ^{15}N-labeled acetonitrile and **8a** and **8b**) of **8a** and **8b** had small ^{15}N-^{31}P coupling ($^2J_{P\text{-}N} \approx 2.8$ Hz), showing that the acetonitrile ligands occupied coordination sites mutually cis to both phosphorus centers in **8a** and **8b**.[11] ^{1}H NMR analysis also showed the newly formed alkoxy carbon proton at δ 3.9 (br s, overlap of both major and minor complex). The identification of the alkoxide unit was confirmed by ^{13}C APT NMR analysis of the complexes synthesized by reaction of 7 with both the hydrido catalyst (**6**) and deuterido catalyst (**6-d_1**). The ^{13}C APT NMR analysis showed inversion

of the ^{13}C signal at δ 89.0 in comparing the spectra of the complexes formed with **6** and those formed with **6-d_1**.[12] This observation is proof positive that insertion had occurred via hydride/deuteride addition to the carbon of the C=O bond and ruthenium addition to the oxygen. Hydride/deuteride addition to the oxygen cannot result in inversion of this signal (Scheme 6.2).

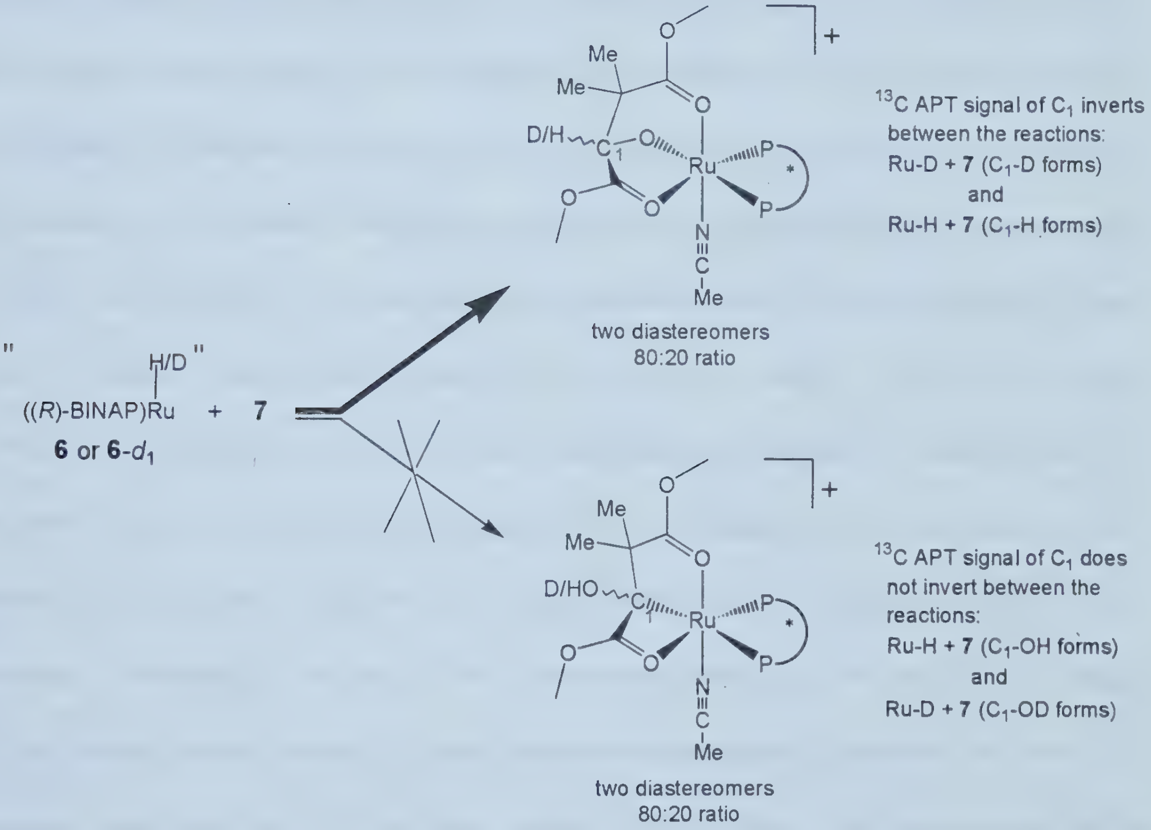

6 or 6-d_1

two diastereomers
80:20 ratio

^{13}C APT signal of C_1 inverts between the reactions:
Ru-D + **7** (C_1-D forms)
and
Ru-H + **7** (C_1-H forms)

two diastereomers
80:20 ratio

^{13}C APT signal of C_1 does not invert between the reactions:
Ru-H + **7** (C_1-OH forms)
and
Ru-D + **7** (C_1-OD forms)

Scheme 6.2: ^{13}C APT experiment to determine how ketone-hydride insertion occurred between 6 and 7 (P-P* is (*R*)-BINAP).

The remaining ^1H NMR signals were those of acetonitrile (δ 1.9 (s, 3H)) and the aromatic protons from the (*R*)-BINAP ligand (δ 6.5 - 8.02). Attempts to separate the two complexes via crystallization were unsuccessful. Nevertheless, these results determined

that reaction between **6** and 7 produced two ruthenium-alkoxide intermediates (**8a** and **8b**) from the insertion of the C=O bond of 7 into the ruthenium-hydride bond of **6**.

Absolute configuration about the alkoxy carbon center. X-ray crystallographic analysis could not be performed to determined whether the complexes were diastereomers that differ by the absolute configuration about the alkoxy carbon center. Isotopic labeling was employed to determine the absolute stereochemistry about the alkoxy carbon centers. The synthesis and isolation of the ruthenium-alkoxide complexes with deuterium labels at the alkoxy carbon (**8a-d_1** and **8b-d_1**) were carried out by reaction of 7 with **6-d_1**. The goal was to react these deuterium labeled complexes with a strong, non-hydronium, acid such that the acid would cleave the ruthenium-alkoxy bond (Ru-O) without causing epimerization at the alkoxide center. In order for direct conclusions to be drawn about the absolute configuration of the alkoxy carbon center, one property must be maintained: there must be no D-H exchange at the alkoxy carbon. D-H exchange would show a side reaction occurred other than the ruthenium-alkoxide bond cleavage. Furthermore, the ratio of the diastereomers must equal the ratio of enantiomers of the alcohol product formed, if indeed the ruthenium-alkoxide complexes are related by opposite facial selectivity at the alkoxy carbon. If the ratios of the ruthenium-alkoxide complexes equals that of the alcohol product enantiomers, the absolute configuration of the major alcohol enantiomer produced must correspond to the major ruthenium-alkoxide intermediate. Consequently, the minor alcohol enantiomer would correspond to the minor ruthenium-alkoxide intermediate (Scheme 6.3).

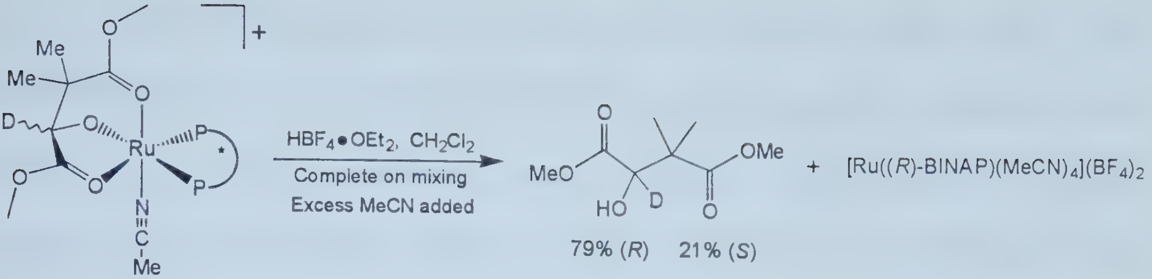

8a-d_1/8b-d_1

7'

Scheme 6.3: Reaction scheme to determine absolute configuration about alkoxy carbon center of 8a and 8b (P-P* is (*R*)-BINAP).

The reaction between **8-*d*₁** and HBF_4•OEt_2 in methylene chloride solution was completed upon addition. NMR analysis of the reaction mixture indicated that the alcohol product was still coordinated to the ruthenium center after the protonation was complete. Addition of excess acetonitrile resulted in the displacement of the alcohol product, and formation of the known ruthenium complex [Ru((*R*)-BINAP)$(MeCN)_4](BF_4)_2$.[13] ^{1}H and ^{2}H NMR analyses proved that protonolysis did not cause D-H exchange at the alkoxy carbon center.[14] Further, the diastereomeric ratio of **8a-*d*₁** and **8b-*d*₁** was maintained in the enantiomeric ratio of the product alcohols as determined by ^{1}H NMR analysis of the displaced 7' with added chiral shift reagent.[15] The major diastereomer of **8** was therefore of *R* absolute configuration at the alkoxy carbon center ((*R*)-**8a**). Consequently, the minor diastereomer was of *S* absolute configuration ((*S*)-**8b**). Thus, the complexes formed are a result of the facial selectivity of the ketone substrate (**7**) by the active catalyst (**6**) with the *si*-face being favored.

Stereochemistry of the substrate about ruthenium metal center in [Ru((*R*)-BINAP)(7(H))(MeCN)](BF_4) ((*R*)-8a/(*S*)-8b). It remained that the stereochemistry about the ruthenium center had to be determined. From the analysis of the data to this

point, it had been determined that the diastereomers (*R*)-**8a** and (*S*)-**8b** contain **7** as an alkoxide tridentate ligand bonded to ruthenium in a *fac*-arrangement through the ester carbonyl groups and the alkoxide group. Therefore, there were three possible configurations that may have formed for each diastereomer. Considering the major diastereomer (Figure 6.3), the configurations of (*R*)-**8a-1** and (*R*)-**8a-2** have the alkoxy group coordinated *trans* to one phosphine, *cis* to the other, and *cis* to the acetonitrile ligand. The third configuration ((*R*)-**8a-3**) has the alkoxy group coordinated *cis* to both phosphines and *trans* to the acetonitrile ligand. The use of two-dimensional NMR experiments to elucidate the structure was hampered by overlap of ^{1}H NMR signals from the products and thus a new approach was taken.[16]

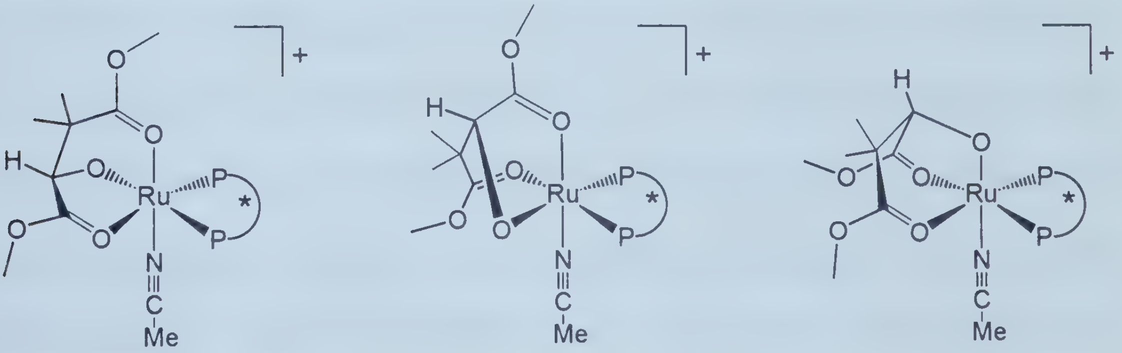

(*R*)-**8a-1** (*R*)-**8a-2** (*R*)-**8a-3**

Figure 6.3: Possible structures of major diastereomer (*R*)-8a (P-P* is (*R*)-BINAP).

Examining the diastereomers (major (*R*)-**8a** and minor (*S*)-**8b**) using molecular models indicated the diastereomeric ratio could likely be enhanced by increasing the steric bulk of the ester groups. This theory led to the testing of both the di-*iso*-propyl 3,3-dimethyloxaloacetate (**9**) and di-*tert*-butyl 3,3-dimethyloxaloacetate (**10**) substrates.[17] The ketones were catalytically hydrogenated (68% ee (*R*) and 82% ee (*R*), respectively)

Table 6.1: Enantioselective hydrogenation of ketones 7, 9, and 10 using 6 as catalyst.[a]

Substrate	Solvent	% ee
7	THF MeOH	59 (*R*)[b] 59 (*R*)[b]
9	THF MeOH	66 (*R*)[b] 68 (*R*)[b]
10	THF MeOH	80 (*R*)[c] 82 (*R*)[c]

[a]Reaction conditions: [Ru] = 2.6 mM, 5.0 mL solvent, 50 °C, 50 h. [b] The ee was determined by ^{1}H NMR with added chiral shift reagent. [c] The ee was determined by chiral GC analysis.

under the conditions used for 7 as substrate (Table 6.1). The stoichiometric reaction between **6** and **9** yielded two species by ^{31}P NMR analysis in an approximate 90:10 ratio (**11a** and **11b**). ^{31}P NMR analysis of the stoichiometric reaction of **6** with **10** showed the presence of only a single complex (**12**) in solution. X-ray quality crystals could not be obtained. As observed with (*R*)-**8a**/(*S*)-**8b**, ruthenium-oxygen cleavage by HBF_4•OEt_2 of the labeled alkoxides (**11a-*d*₁**/**11b-*d*₁** and **12-*d*₁**, performed separately) resulted in no D-H exchange and the observed enantiomeric ratio of the alcohol product equaled the diastereomeric ratio of the ruthenium-alkoxide complexes. The absolute configuration of the major diastereomers (**11a** and **12**) was identified as (*R*) and the minor diastereomer (**11b**) was (*S*). It is noteworthy to mention that only the (*R*)-enantiomer of the alcohol **10'** was observed by chiral GC analysis, as expected by the exclusive formation of only one diastereomer (**12**).

Unambiguous characterization of the major ruthenium-BINAP-alkoxide diastereomer. As discussed earlier, the diastereomers (*R*)-**11a** and (*S*)-**11b** formed in an approximate 90:10 ratio on stoichiometric reaction between **6** and **9**. As the minor

diastereomer was present in such a relatively small amount, overlap of signals in the ^{1}H NMR spectrum did not complicate the structural analysis.

Substrate Signals. Analysis of the COSY and selective ^{1}H{^{1}H} decoupling data connected the signals from the protons in each *iso*-propyl group (*iso*-propyl A: δ 0.76 and 1.15 - 2 methyl groups, and δ 4.76 - methyne proton; *iso*-propyl B: δ 1.09 and 1.23 - 2 methyl groups, and δ 5.42 - methyne proton). The analysis of the HMQC data identified the ^{13}C signals that corresponded to the *iso*-propyl methyne carbons, the alkoxy carbon, and the methyl groups on the backbone of the coordinated substrate. With these assignments, the analysis of the HMBC data showed that the alkoxide methyne proton coupled to both ester carbonyl carbon signals at δ 182 and δ 190. Further, the backbone methyl groups coupled with only the ester carbonyl carbon signal at δ 182, assigning it to the ester carbonyl group *beta* to the alkoxide unit. The remaining carbonyl carbon signal at δ 190 must therefore correspond to that of the *alpha* ester carbonyl group. HMBC analysis also indicated that the methyne proton signal from *iso*-propyl group A (δ 4.76) coupled to the *alpha* ester carbonyl carbon.[18] Therefore *iso*-propyl group B is that of the *beta* ester group. These assignments are shown in Table 6.2. Similar assignments were made for the substrate unit in both the dimethyl major diastereomer (*R*)-**8a** and di-*tert*-butyl diastereomer (*R*)-**12** except that for (*R*)-**12** the HMBC experiments could not distinguish the *tert*-butyl group ^{1}H NMR signals to the *alpha* or *beta* ester groups do to the limits of detection of the NMR technique.[19]

Table 6.3: Assignments of substrate ^1H and ^{13}C NMR signals of (*R*)-11a along with key HMBC correlations (shown by arrows to structure).

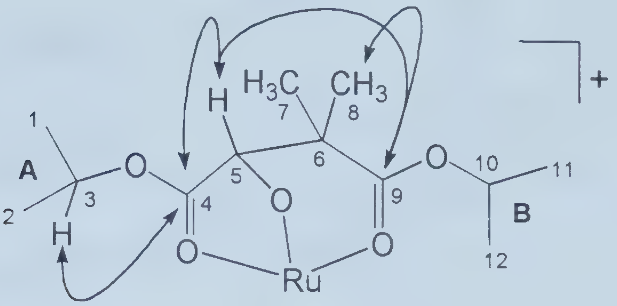

Assignment	^1H NMR (δ)	^{13}C NMR (δ)
1 or 2	0.76	20 (overlap)
1 or 2	1.15	21 (overlap)
3	4.76	73
4	---	190
5	3.82	87
6	---	46
7 or 8	0.8	24
7 or 8	0.98	21 (overlap)
9	---	182
10	5.42	72
11 or 12	1.09	18
11 or 12	1.23	20 (overlap)

BINAP Signals. Having assigned the signals for the substrate group the attention shifted to the C_2-symmetric (*R*)-BINAP ligand. Figure 6.4 shows the conformation of coordinated (*R*)-BINAP and the spatial distribution of its components relative to the *cis*-coordinated acetonitrile ligand. The relative tilt of the naphthyl rings forces one phenyl ring on each phosphorus axial and the other equatorial. With the acetonitrile ligand in the *cis* coordination site shown in Figure 6.4, the P_2 axial phenyl (P_2-Ph_{ax}) ring is on the opposite side of the P-Ru-P plane as the acetonitrile ligand, and the backbone naphthyl group (P_2-Naph) is on the same side as the acetonitrile ligand. Consequently, P_1-Ph_{ax} is

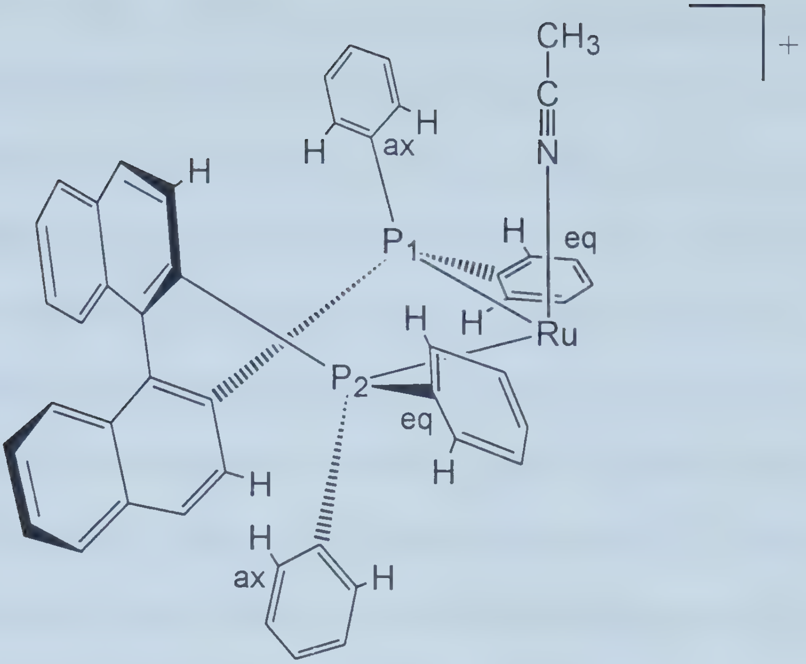

Figure 6.4: Depiction of the (*R*)-BINAP and acetonitrile ligands about the ruthenium metal center in (*R*)-11a and the *ortho*-phenyl and naphthyl protons (ones shown) identified from variable temperature ^{31}P-^{1}H HETCOR studies.

on the same side of the P-Ru-P plane as the acetonitrile ligand and P_1-Naph is opposite. As (*R*)-BINAP is C_2-symmetric it is of no consequence which side of the P-Ru-P plane the acetonitrile ligand is placed. The choice shown in Figure 6.4 was arbitrary. Variable temperature ^{31}P-^{1}H HETCOR experiments were utilized to assign the ^{1}H NMR signals of the *ortho* protons on the phenyl and naphthyl rings bonded to P_1 and P_2. Each ^{31}P signal is expected to show three to five ^{1}H NMR correlations corresponding to two axial *ortho*-phenyl proton signals, two equatorial *ortho*-phenyl proton, and one *ortho*-naphthyl proton signal. Consider the case where the phenyl rings of both P_1 and P_2 are rotating about the phosphorus-phenyl bond at a much greater rate than the NMR time-scale. The *ortho*-phenyl proton ^{1}H NMR signals of each individual phenyl ring (P_1-Ph_{ax}, P_1-Ph_{eq}, P_2-Ph_{ax},

and P_2-Ph_{eq}) will coalesce. Therefore, in this case one would expect to observe three correlations for each the P_1 and P_2 ^{31}P NMR signals (one for P-*ortho*-Naph, one for both P-*ortho*-Ph_{ax}, and one for both P-*ortho*-Ph_{eq}). Now, consider the case where the phenyl rings are all rotating a much slower rate than the NMR time-scale. All of the individual *ortho*-phenyl protons will be observed in different magnetic environments resulting in different ^1H NMR signals for all the *ortho*-phenyl protons. Thus, in this case one would expect to observe five correlations for each the P_1 and P_2 ^{31}P NMR signals (one for P-*ortho*-Naph, two for both P-*ortho*-Ph_{ax}, and two for both P-*ortho*-Ph_{eq}). In the case where only one of the phenyl rings is rotating faster than the NMR time-scale (e.g. Ph_{ax}) and the other slower (e.g. Ph_{eq}), one would expect to observe four correlations (one for the P-*ortho*-Naph, one for both P-*ortho*-Ph_{ax}, and two for both P-*ortho*-Ph_{eq}).

Ambient temperature studies identified only two ^1H NMR correlations to the ^{31}P NMR signal of P_2 and only one ^1H NMR correlation to the signal P_1. That less than the expected number of correlations were observed indicated first, that essentially unrestricted rotation about many of the phosphorus-phenyl bonds was likely occurring at ambient temperature and second, that some of the *ortho*-phenyl proton ^1H NMR signals must be in the baseline of the spectrum.[20] Variable temperature investigations (-40 °C, -80 °C, and -100 °C) showed all of the *ortho*-phenyl proton correlations, some of which did only grow out of the baseline of the ^1H NMR spectrum at low temperatures.

Substrate-BINAP and BINAP-BINAP correlations. Analysis of the ambient temperature ROESY experiments showed an ROE contact between the methyl proton ^1H NMR signal of acetonitrile (CH_3CN) and the *ortho*-naphthyl signal at δ 8.02.[21] This *ortho* proton therefore, had to be on the naphthalene ring bonded to P_2, on the same side

of the ruthenium-phosphine plane close to the acetonitrile ligand (Figure 6.5, P_2-*ortho*-Naph). This P_2-*ortho*-Naph ^{1}H NMR signal (δ 8.02) also showed ROE contacts to the ^{1}H NMR signal at δ 7.64 corresponding to two *ortho*-phenyl protons associated with P_2. This signal (δ 7.64) was therefore unambiguously assigned to the equatorial P_2 *ortho*-phenyl protons as they are the only *ortho*-phenyl protons close in space to the P_2-*ortho*-Naph proton. Finally, the ^{1}H NMR signal for P_1-*ortho*-Naph proton was found at δ 7.02.[22]

Assignment	^{1}H NMR (δ)
P_1-*ortho*-Naph	7.02 (r.t.)
P_1-*ortho*-Ph_{ax}	9.15/6.19 (-100 °C)
P_1-*ortho*-Ph_{eq}	7.15/7.95 (-40 °C)
P_2-*ortho*-Naph	8.02 (r.t.)
P_2-*ortho*-Ph_{ax}	8.76/7.05 (-40 °C)
P_2-*ortho*-Ph_{eq}	7.64 (r.t)

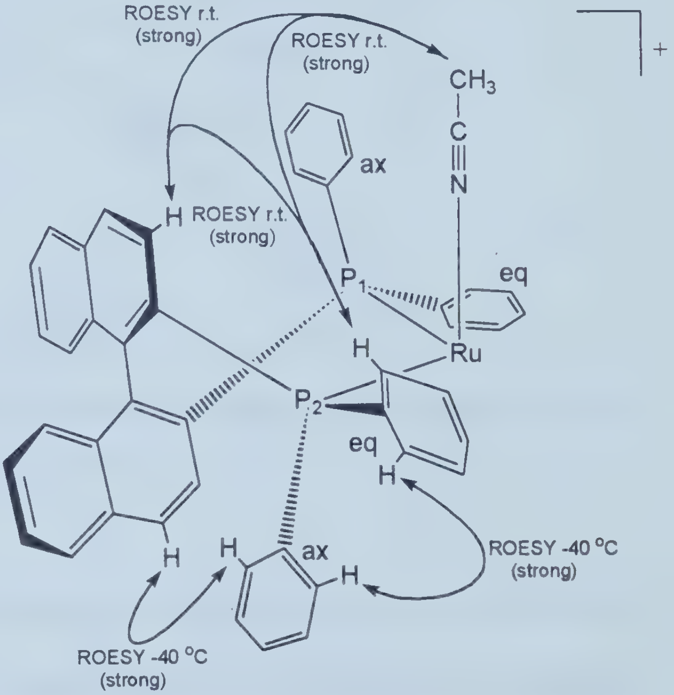
ROESY r.t.
(strong)
ROESY r.t.
(strong)
+
CH3
C
N
ax
H
ROESY r.t.
(strong)
P1
eq
H
Ru
P2
eq
H
H
H
ax
H
ROESY -40 °C
(strong)
ROESY -40 °C
(strong)

Figure 6.5: Assignment of quadrant of space about ruthenium center from variable temperature ROESY data.

Examination of the ROESY data from the -40 °C, -80 °C, and -100 °C yielded further information. At ambient temperature, the ^{1}H NMR signal (δ 0.8, CH_3 (a); Figure 6.6) of one of the backbone methyl groups showed an ROE contact to the P_2-*ortho*-Ph_{eq}

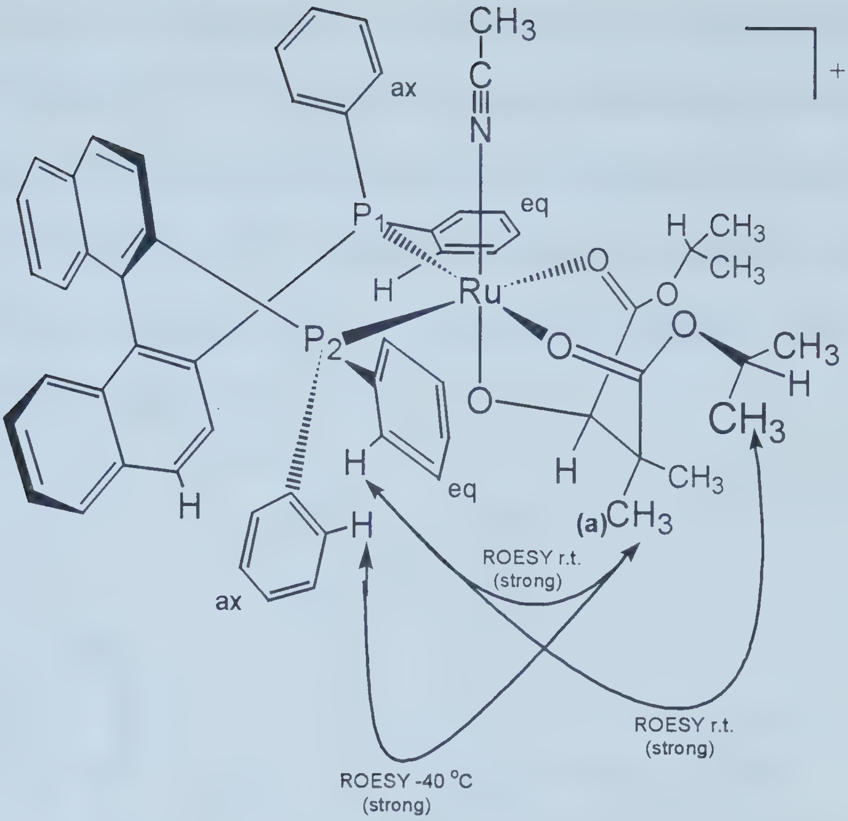
CH3
C
N
ax
eq
P1
H
Ru
O
H CH3
CH3
O
O
CH3
H
P2
O
CH3
H
eq
H
CH3
(a)CH3
H
ax
ROESY r.t.
(strong)
ROESY r.t.
(strong)
ROESY -40 °C
(strong)
+

Figure 6.6: Important ROE contacts observed between the substrate and (*R*)-BINAP ligand (ambient temperature to -40 °C).

proton signal (δ 7.64) and at -40 °C it showed another ROE contact to the P_2-*ortho*-Ph_{ax} proton signal (δ 8.76).[23] These ROE contacts show that one backbone methyl group is close in space to both the P_2 axial and equatorial phenyl rings. Further, the methyne proton and one of the methyl group proton signals of *iso*-propyl group B showed ROE contacts to the P_2 equatorial *ortho*-phenyl proton signal (P_2-Ph_{eq}; δ 7.64) at ambient temperature and -40 °C. Analysis of the ROESY data obtained at -80 °C determined that the alkoxy methyne proton signal (δ 3.85) had ROE contacts to the P_2 axial *ortho*-phenyl protons (P_2-Ph_{ax}; δ 8.76) and to a signal at δ 9.15 (Figure 6.7). Furthermore, the P_2 axial *ortho*-phenyl proton signal (δ 8.76) also showed an ROE contact to the same signal at δ

9.15. The signal at δ 9.15 was shown to correlate to P_1 by ^{31}P-^1H HETCOR NMR analysis performed at -100 °C. The only *ortho*-phenyl proton signals that are remotely close in space to the P_2 axial *ortho*-phenyl protons are those of the P_1 and P_2 equatorial *ortho*-phenyl protons. As the P_2 equatorial *ortho*-phenyl protons had already been assigned (δ 7.64) the signal at δ 9.15 was unambiguously assigned to the P_1 equatorial *ortho*-phenyl protons (Figure 6.9).

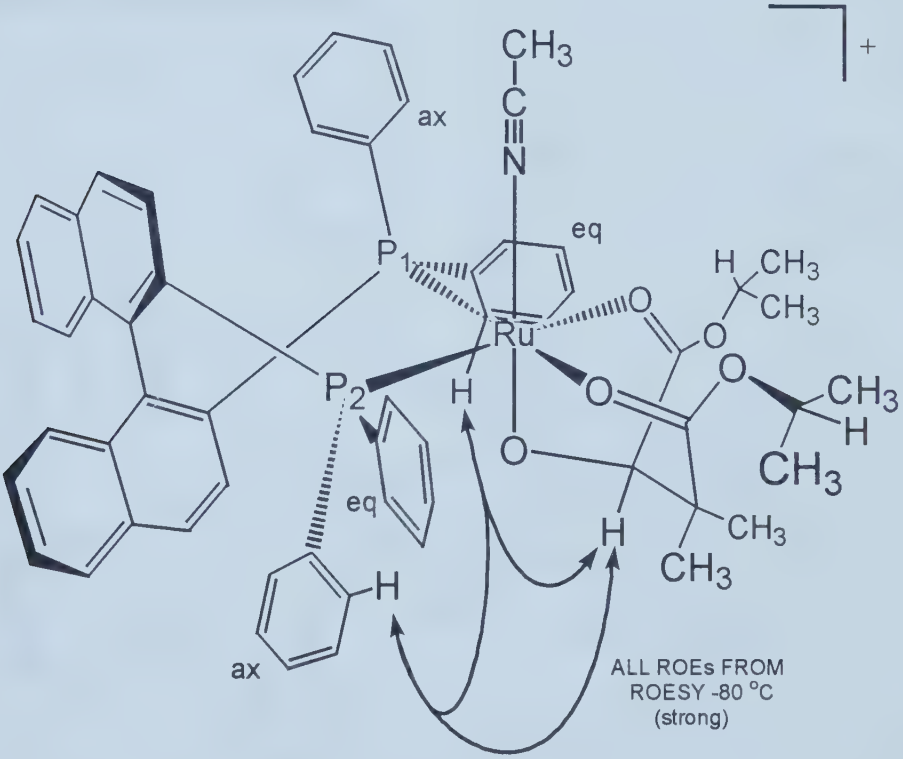
CH3
C
N
+
ax
eq
P1
Ru
O
H
CH3
CH3
O
O
CH3
H
CH3
P2
H
O
O
eq
H
CH3
CH3
H
ax
ALL ROEs FROM
ROESY -80 °C
(strong)

Figure 6.7: The key ROE contacts (at -80 °C) that conclusively identified the structure of (*R*)-11a.

The structure (*R*)-**8a-3** (Figure 6.3) is unambiguously assigned as it is the only structure that agrees with all the observed NMR data. Reexamination of variable temperature ROESY NMR data of (*R*)-**12** also showed similar correlations and showed

that (*R*)-**12** has a structure analogous to (*R*)-**11a**. While such a structure determination of (*R*)-**8a** is complicated by overlap with ^{1}H NMR signals from (*S*)-**8b**, the resulting patterns also correspond to those observed with the complexes of (*R*)-**11a** and (*R*)-**12**. The major diastereomers formed from reaction of 7, **9**, or **10** with **6** therefore have the structure of that shown in Figure 6.8. This is the first isolation and complete, unambiguous, structure identification of diastereomeric catalyst-alkoxide species formed during an enantioselective ketone hydrogenation.

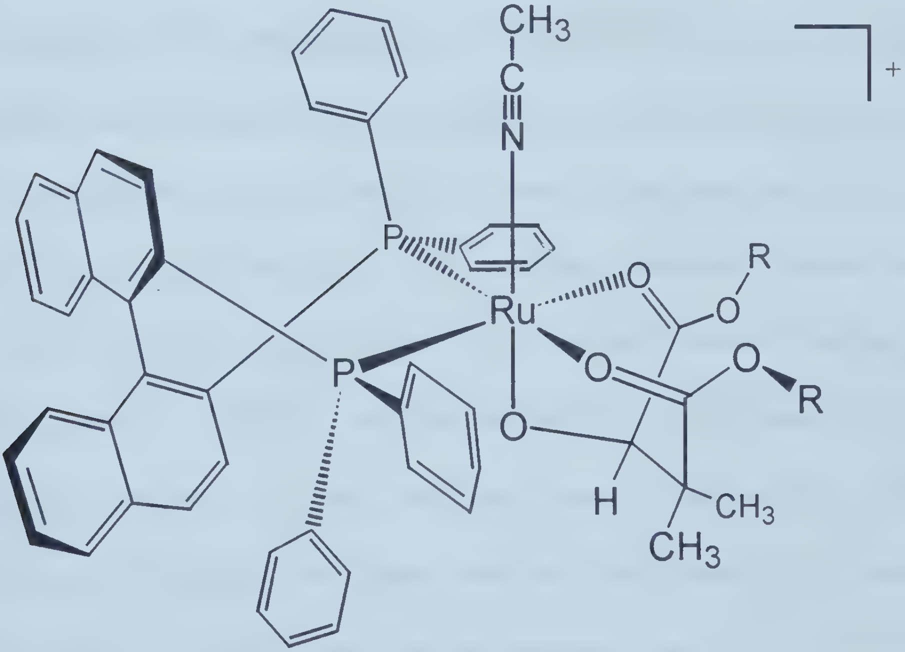

R = Me, *i*-Pr, or *t*-Bu

Figure 6.8: Unambiguously characterized structures of (*R*)-8a, (*R*)-11a, (*R*)-12.

Low-temperature investigations for pre-insertion complexes. It has been reported that coordination of a ketone group to the metal center in rhodium and ruthenium systems was observed.[4a, b] In order to determine if such a pre-insertion

complex forms with these substrate-catalyst combinations, low temperature studies were performed on the stoichiometric reaction between **6** and the ketone substrates 7, **9**, and **10**. The active catalyst was prepared by reaction of **1** with dihydrogen gas in tetrahydrofurane-d_8 in an NMR tube and the sample was cooled in an acetone/dry ice bath to -80 °C. A stoichiometric amount of the ketone substrate was added at -80 °C and the sample placed in the pre-cooled NMR probe (-80 °C). For the substrates 7, **9**, and **10**, analysis of both the ^{1}H and ^{31}P NMR spectra from -80 °C to -30 °C showed that no net reaction occurred as only the active catalyst **6** and the free ketone substrate were present. At approximately -30 °C, new peaks in the ^{1}H and ^{31}P NMR spectra appeared that corresponded to the previously characterized ruthenium-alkoxide complexes ((*R*)-**8a** and (*S*)-**8b** with **7** as substrate, (*R*)-**11a** and (*S*)-**11b** with **9** as substrate, and (*R*)-**12** with **10** as substrate). Furthermore, warming the probe to ambient temperature resulted in the same ratio of ruthenium-alkoxide complexes observed in the stoichiometric reaction performed at ambient temperature. At no time was there evidence of any other species being formed (e.g. η^2-ketone complexes). It was determined that, in this catalytic cycle, ketone-hydride insertion is very fast, even faster than prior coordination of the ketone group (assuming ketone coordination is required for insertion to occur). It is evident that the insertion step is not the turnover-limiting step of the catalytic cycle but that it was very facile. As even with highly encumbered ketone substrates like **10**, insertion still occurred at -30 °C and it is therefore likely that insertion is facile in most catalytic ketone hydrogenation systems. The turnover-limiting step must be after the insertion step, and is likely the hydrogenolysis of the ruthenium-alkoxide bond. These arguments assume that

the isolated complexes are incorporated in the main catalytic cycle of the hydrogenation. It was necessary to investigate the system further to provide proof of this assumption.

Isolated ruthenium-alkoxide complexes as catalytic intermediates. As mentioned earlier, commonly proposed mechanisms for the enantioselective transition-metal catalyzed hydrogenation of ketones invoke the insertion of the C=O bond of the ketone into the active metal-hydride bond forming a metal-alkoxide intermediate.[2] The investigations into the enantioselective ketone hydrogenation with **6** as catalyst has resulted in the isolation and complete characterization of such metal-alkoxide complexes. In order for these species to be considered catalytic intermediates, the following must be true:

(a) The species itself acts as catalyst for the enantioselective hydrogenation of ketones

(b) The species must react at the same rate as the active catalyst **6** and yield similar enantioselectivity

(c) The enantiomeric excess obtained on stoichiometric hydrogenolysis of the ruthenium-alkoxide complexes must equal that of the catalytic hydrogenation

(d) A full kinetic study must corroborate the presence of the species as an active catalyst complex and not as a ruthenium sink.

The ruthenium-alkoxide complexes were first examined as catalysts for the enantioselective hydrogenation of the ketone substrates. It was determined that all the isolated ruthenium-alkoxides ((*R*)-**8a**/(*S*)-**8b**, (*R*)-**8a**/(*S*)-**8b**, and (*R*)-**12**) catalyzed the

hydrogenation of the ketones at comparable rate and enantioselectivity as the hydrogenations performed using **6** as catalyst (Table 6.3). Therefore, the reactivity of the ruthenium-alkoxide complexes was in accordance with the criteria of points (a) and (b).

Table 6.3: Hydrogenation of ketones 7, 9, and 10 with isolated ruthenium-alkoxide intermediates (8a/8b, 11a,11b, and 12, respectively).[a]

Substrate	Catalyst	Solvent	%ee
7	**8a/8b**	MeOH	60 (*R*)
9	**11a/11b**	MeOH	68 (*R*)
11	**12**	MeOH	80 (*R*)

[a] Reaction conditions: [Ru] = 2.6 mM, 5.0 mL MeOH, 50 equiv substrate, 50 °C, and 50 atm H_2. [b] The ee was determined by ^{1}H NMR with added chiral shift reagent. [c] The ee was determined by chiral GC analysis.

The isolated ruthenium-alkoxide-*d* complexes were stoichiometrically hydrogenated under catalytic conditions over the time period required for one turnover to occur in the catalytic hydrogenation. In each case, the reactions went to completion yielding the alcohol products in an enantiomeric excess that corresponded, within experimental error, to those obtained in the catalytic hydrogenation with **6** as catalyst (Table 6.4). The stoichiometric hydrogenolysis of the complexes was found to react at the same rate and with the same enantioselectivity as in the catalytic hydrogenation as required by criteria (c). The stoichiometric hydrogenolyses were performed with the deuterium labeled complexes to try to determine the extent of reversibility of the ketone-hydride insertion step (extent of *β*-deuteride elimination) on the time-scale of hydrogenolysis of the ruthenium-alkoxide bond. It was shown that only partial D-H

Table 6.4: Stoichiometric hydrogenation of deuterium labeled ruthenium-alkoxide complexes (8a-d_1/8b-d_1, 11a-d_1/11b-d_1, and 12-d_1).[a]

Complex	Solvent	% ee (cat. % ee)[b]	% D-H exchange[c]
8a/8b	THF	58 (59)[d]	~ 40
	MeOH	60 (59)[d]	~ 25
11a/11b	THF	69 (66)[d]	~ 20
	MeOH	70 (68)[d]	~ 15
12	THF	84 (80)[e]	~ 20
	MeOH	84 (82)[e]	~ 10

[a] Reaction conditions: [Ru] = 2.6 mM, 25 mL solvent, 50 °C, and 50 atm H_2. [b] Absolute configuration of major enantiomer is (*R*). [c] Percent D-H exchange determined by ^1H NMR analysis and mass spectroscopy. [d] Ee determined by ^1H NMR with added chiral shift reagent. [e] Ee determined by chiral GC analysis.

exchange was observed in the produced alcohol products. Therefore, *β*-hydride/deuteride elimination must be occurring during the operating catalytic reaction. However, the extent of reversibility (and rate compared with hydrogenolysis of the ruthenium-alkoxide bond) could not be determined. The complexes may undergo *β*-deuteride elimination at a faster rate than hydrogenolysis of the ruthenium-alkoxide bond but may not be shown in the analysis of the extent of D-H exchange. It may be that D-H exchange between the de-inserted catalyst species (**6•ketone** complex formed via *β*-deuteride elimination) and dihydrogen gas (or solvent) proceeds at a slower rate than re-insertion. Therefore, only in the case of complete D-H exchange would a definitive conclusion have been obtained (i.e. the process of *β*-hydride/deuteride elimination, D-H exchange between catalyst and dihydrogen gas, and olefin-hydride re-insertion would be much faster than hydrogenolysis).

All of the above reactivity studies have provided further evidence that strongly supported the notion that the isolated ruthenium-alkoxide complexes were catalytic

intermediates in the enantioselective hydrogenation of ketones with **6** as catalyst. It is believed that while the putative intermediates were isolated at ambient temperature and ambient pressure of dihydrogen gas (1 atm), they are likely the active intermediates of the operating catalytic reaction performed under 50 atm of dihydrogen and 50 °C. We believe that it is unlikely that higher pressures and temperatures would result in the formation of different ruthenium-alkoxide intermediates with the same corresponding facial selectivity and reactivity as those isolated at ambient temperature. However, a final kinetic study of the system must be performed to further confirm the identification of the isolated ruthenium-alkoxide complexes as active catalytic intermediates in the catalytic enantioselective hydrogenation of ketones with ruthenium-BINAP catalysts.

Conclusions:

The [Ru((*R*)-BINAP)(1-3;5,6-η-C_8H_{11})(MeCN)](BF_4) (**1**) catalyst system developed in the Bergens laboratories behaves similarly to the other ruthenium-BINAP catalyst systems reported. The catalyst system **1** has allowed for a detailed investigation into the reaction mechanism of the ketone hydrogenation and has led to the first isolation and complete solution structural characterization of diastereomeric ruthenium-alkoxide complexes commonly believed to be active catalytic intermediates in these reactions. Investigations of the isolated complexes have yielded strong support that favor the identification of these ruthenium-alkoxide species as active catalytic intermediates in the ruthenium-BINAP catalyzed enantioselective hydrogenation of ketones.

Experimental:

Materials and methods. All operations were performed under an argon atmosphere using standard Schlenk techniques. The solvents were dried and distilled under an argon atmosphere by standard methods before use.[24] The argon gas (Praxair, 99.998%) was passed through a drying train containing 3Å molecular sieves and P_4O_{10} before use. Trace quantities of oxygen were removed from the dihydrogen gas (Praxair, 99.99%) by passage through an Alltech Oxy-Trap. All commercial reagents (Aldrich or Fluka) were recrystallized or distilled under an argon atmosphere before use. [Ru((*R*)-BINAP)(MeCN)(1-3:5,6-η-C_8H_{11})](BF_4) was prepared using established procedures.[25]

Unless stated otherwise, all ^{1}H, ^{13}C, and ^{31}P NMR spectra were measured with a Bruker AM-200 or AM-400 spectrometers. ^{1}H and ^{13}C NMR chemical shifts are reported in parts per million (δ) relative to TMS using the solvent as an internal reference. ^{31}P NMR chemical shifts are reported in parts per million (δ) relative to an 85% H_3PO_4 external reference. All ^{13}C and ^{31}P NMR are ^{1}H decoupled unless stated otherwise. Mass spectra were measured using a Kratos MS50 spectrometer. Microanalyses were performed at the University of Alberta Microanalysis Laboratory. Optical rotations were measured with a Perkin-Elmer 241 polarimeter at 589 nm using 1.0 dm cells. Specific rotations, $[\alpha]_D$, are reported in degrees per decimeter at 25 °C, and the concentration (*c*) is given in grams per 100 mL.

Di-*iso*-propyl acetylenedicarboxylate. To a 100 mL flask was transferred acetylene dicarboxylic acid (20.0242 g, 1.756×10^{-1} mol), concentrated H_2SO_4 (2.5 mL),

and 150 mL of *iso*-propanol. The solution was stirred and heated to reflux (80 °C) for 5 h. The solution was cooled to room temperature and then concentrated under reduced pressure. The remaining clear-colorless liquid was taken up in Et_2O (100 mL) and sequentially washed with a 2 N solution of NaOH until aqueous layer is basic (2 x 20 mL) and with distilled H_2O (4 x 25 mL). The organic layer was then dried over $MgSO_4$ for 24 h, filtered, washed with Et_2O (3 x 100 mL), and then the solvent was removed under reduced pressure yielding the clear-colorless liquid product (30.2 g, 86.8 %). The product was used without further purification. ^1H NMR (400.1 MHz, CD_2Cl_2, 25 °C): δ 1.28 (d, 12H, $^3J_{H\text{-}H} = 6.5$ Hz, RC≡CR, R = $CO_2C(\mathit{CH}_3)_2(H)$), 5.12 (quint, 2H, $^3J_{H\text{-}H} = 6.5$ Hz, RC≡CR, R = $CO_2C(CH_3)_2(\mathit{H})$). ^{13}C NMR (100.6 MHz, CD_2Cl_2, 25 °C): δ 21.58 (4C, RC≡CR, R = $CO_2C(\mathit{C}H_3)_2(H)$), 71.34 (2C, RC≡CR, R = $CO_2\mathit{C}(CH_3)_2(H)$), 74.68 (2C, R*C*≡*C*R, R = $CO_2C(CH_3)_2(H)$), 151.45 (2C, RC≡CR, R = $\mathit{C}O_2C(CH_3)_2(H)$).

Dimethyl 3,3-dimethyloxaloacetate (7). To a dry 100 mL flask was transferred potassium carbonate (1.76 g, 12.8 mmol). The flask was flushed with dry argon gas for 20 min and then to the flask was transferred dimethyl oxaloacetate (1.02 g, 6.38 mmol) and acetone (30 mL, distilled). A condenser was added to the flask and the system remained under an argon atmosphere. The solution was stirred for 5 min and then methyl iodide (2.4 mL, 38.3 mmol) was added down the condenser. The mixture was then heated and stirred under reflux for 20 h. The solution was then cooled and the solvent removed under reduced pressure. The solid residue was washed with CH_2Cl_2 (20 mL) and passed through a column of alumina (10 cm long, 1 cm diameter). The column was further washed with CH_2Cl_2 (20 mL) and the solvent was then removed under reduced

pressure to yield a clear pale yellow liquid (0.97 g, 80.8 % yield). ^{1}H NMR (400 MHz, CD_2Cl_2, 25 °C): δ 1.39 (s, 6H, C(C*H*$_3$)$_2$), 3.67 (s, 3H, CO_2C*H*$_3$), 3.82 (s, 3H, CO_2C*H*$_3$). ^{13}C NMR (400 MHz, CD_2Cl_2, 25 °C): δ 21.94 (2C, C(*C*H$_3$)$_2$), 52.76 (1C, CO_2*C*H$_3$), 52.92 (1C, *C*(CH$_3$)$_2$), 53.33 (1C, CO_2*C*H$_3$), 160.94 (1C, *C*O$_2$CH$_3$), 173.24 (1C, *C*O$_2$CH$_3$); 191.77 (1C, *C*(O)CO$_2$CH$_3$). CI-MS (pos) *m/z* 206.1 ((M + NH_4^+), exact mass calcd for $C_8H_{12}O_5$ + NH_4^+ = 206.2). *Anal.* Calcd for $C_8H_{12}O_5$: C, 51.06; H, 6.43. Found: C, 50.89; H, 6.58.

Di-*iso*-propyl 3,3-dimethyloxaloacetate (9). Performed using similar procedure as in the synthesis of dimethyl-3,3-dimethyloxaloacetate. ^{1}H NMR (400 MHz, $CDCl_3$, 25 °C): δ 1.19 (d, 6H, $^{3}J_{H\text{-}H}$ = 6.5 Hz, CO_2C(C*H*$_3$)$_2$(H)), 1.33 ((d, 6H, $^{3}J_{H\text{-}H}$ = 6.5 Hz, CO_2C(C*H*$_3$)$_2$(H)), 1.42 (s, 6H, C(C*H*$_3$)$_2$), 5.03 (quint, 1H, $^{3}J_{H\text{-}H}$ = 6.5 Hz, CO_2C(CH$_3$)$_2$(*H*)), 5.11 (quint, 1H, $^{3}J_{H\text{-}H}$ = 6.5 Hz, CO_2C(CH$_3$)$_2$(*H*)).

Di-*tert*-butyl 3,3-dimethyloxaloacetate (10). Performed using similar procedure as in the synthesis of dimethyl-3,3-dimethyloxaloacetate. ^{1}H NMR (400 MHz, $CDCl_3$, 25 °C): δ 1.39 (s, 6H, C(C*H*$_3$)$_2$), 1.43 (s, 9H, CO_2C(C*H*$_3$)$_3$); 1.55 (s, 9H, CO_2C(C*H*$_3$)$_3$). FT-IR (CH_2Cl_2, 22 °C): 1744 cm^{-1} (shoulder, $\nu_{C=O}$); 1725 cm^{-1} (s, $\nu_{C=O}$).

2,2-Dimethylbutan-1,3,4-triol. $LiAlH_4$ (0.122 g, 3.21 x 10^{-3} mol) was transferred to a 3-necked flask that had an addition funnel and septa. To the addition funnel was transferred the hydrogenated product di-*tert*-butyl-3,3-dimethyl-2-hydroxysuccinate (90.0 mg, 3.28 x 10^{-4} mol) and Et_2O (5 mL). To the flask was

transferred Et_2O (15 mL) via canula. The system was flushed with argon gas for 10 min and then left under an argon atmosphere. The flask was cooled to -5 °C and, after 5 min, the alcohol Et_2O solution was added dropwise over 10 min. The addition funnel was rinsed with Et_2O and the solution was allowed to react for 1.5 h at ambient temperature. The flask was then cooled back to -5 °C and distilled water (125 μL) was added slowly over 30 s. Then 0.1 N HCl (125 μL) was added dropwise and finally more distilled water (375 μL) was added dropwise. The solution was allowed to react for 30 min then it was filtered and the solid washed with Et_2O (4 x 10 mL). The solvent was then removed under reduced pressure yielding the clear colorless liquid product (38.2 mg, 86.8% yield). A similar procedure was utilized for the reduction of di-*iso*-propyl 3,3-dimethyl-2-hydroxysuccinate (85.5% yield). ^1H and ^{13}C NMR correspond to literature data.[26]

[Ru((*R*)-BINAP)(OC(H)(CO$_2$CH$_3$)(C(CH$_3$)$_2$(CO$_2$CH$_3$))](BF$_4$) (8a/8b). To a 20 mL solvent Schlenk was transferred [Ru((*R*)-BINAP)(1-3;5,6-η-C811)(MeCN)](BF4) (100.5 mg, 1.05×10^{-4} mol). The flask was placed under vacuum and refilled with argon gas (x 3) to remove all traces of oxygen. To a side-arm flask was transferred dimethyl 3,3-dimethyloxaloacetate (21.7 mg, 1.15×10^{-4} mol) in the glove box. Solvent (1.5 mL; acetone, THF, or methanol) was then added to the flask via gas-tight syringe. The solution was then transferred to the solvent Schlenk via canula. The flask was rinsed with solvent (8.5 mL) and transferred to the solvent Schlenk. The tube was then flushed with dihydrogen gas for 2 min and then pressurized to 20 psig. The tube was then shaken vigorously until all catalyst precursor was in solution, and then for a further 5 min. The tube was then depressurized to atmospheric pressure under argon gas. The solution was

then transferred to a side-arm flask and the solvent removed under reduced pressure. The solid residue was then re-dissolved in THF (2.0 mL) and precipitated with pentane (25 mL). The solution was filtered, the solid washed with pentane (3 x 5 mL), and the solid dried under high vacuum for 2 h (96.3 mg, 88.7% yield). The ratio of products observed by ^{31}P NMR analysis when synthesized in acetone is (64:36), in THF it is (79:21), and in methanol it is (75:25). To obtain ^{15}N enriched complexes, the compounds were dissolved in acetone and excess ^{15}NCMe was added. The solution was stirred for 2 hours and ^{31}P NMR analysis indicated > 95% exchange of ^{14}NCMe with ^{15}NCMe had occurred. FT-IR (CH_2Cl_2, 22 °C): 1608 cm^{-1} (w, $\nu_{C=O}$), 1636 cm^{-1} (s, $\nu_{C=O}$). ESI-MS (pos) *m/z* 954.1 $(M)^+$, exact mass calcd for $C_{54}H_{48}O_5NP_2Ru^+$ = 954.2. *Anal.* Calcd for $C_{54}H_{48}O_5NP_2Ru$-BF_4: C, 62.32; H, 4.65; N, 1.35. Found: C, 61.97; H, 4.44; N, 1.37. (*R*)-**8a**: ^{1}H NMR (400 MHz, acetone-*d*$_6$, 25 °C): δ 0.94 (s, 3H, $C(CH_3)_2$), 1.03 (s, 3H, $C(CH_3)_2$), 1.93 (s, 3H, CH_3CN), 3.41 (s, 3H, Ru-O-C(H)(C(O)OCH_3)-(C(CH_3)$_2$(C(O)OCH_3))), 3.62 (s, 3H, Ru-O-C(H)(C(O)OCH_3)(C(CH_3)$_2$(C(O)OCH_3))), 3.84 (br s, 1H, Ru-O-C(*H*), overlapped with minor), 6.45 - 7.95 (m, 32H, BINAP, overlapped with minor). ^{13}C NMR (400 MHz, acetone-*d*$_6$, 25 °C): δ 4.09 (1C, CH_3CN), 21.04 (1C, $C(CH_3)_2$), 25.35 (1C, $C(CH_3)_2$), 46.98 (1C, $C(CH_3)_2$), 55.0 (1C, CO_2CH_3), 55.1 (1C, CO_2CH_3), 86.7 (1C, Ru-O-*C*(H), overlapped with minor), 126.8 (1C, CH_3CN), 127 - 142.5 (BINAP, overlapped with minor), 183.5 (1C, Ru-O-C(H)(CO_2CH_3)-(C(CH_3)$_2$(CO_2CH_3))), 190.2 (1C, Ru-O-C(H)(CO_2CH_3)(C(CH_3)$_2$(CO_2CH_3)), overlapped with minor). ^{31}P NMR (400 MHz, acetone-*d*$_6$, 25 °C): δ 58.9 (d, 1P, $^2J_{P-P}$ = 45.5 Hz), 62.3 (d, 1P, $^2J_{P-P}$ = 45.5 Hz). ^{31}P NMR (400 MHz, acetone-*d*$_6$, 25 °C) of ^{15}NCMe enriched compound: δ 58.9 (dd, 1P, $^2J_{P-P}$ = 45.0 Hz, $^2J_{P-N}$ = 2.8 Hz), 62.3 (dd, 1P, $^2J_{P-P}$ = 45.0 Hz, $^2J_{P-N}$ = 2.8 Hz).

(*S*)-**8b**: ^{1}H NMR (400 MHz, acetone-d_6, 25 °C): δ 1.12 (br s, 3H, $C(C\mathit{H}_3)_2$), 1.19 (br s, 3H, $C(C\mathit{H}_3)_2$), 1.89 (s, 3H, $C\mathit{H}_3CN$), 3.37 (br s, 3H, $Ru\text{-}O\text{-}C(H)(C(O)OC\mathit{H}_3)\text{-}(C(CH_3)_2(C(O)OCH_3))$), 3.52 (br s, 3H, $Ru\text{-}O\text{-}C(H)(C(O)OCH_3)(C(CH_3)_2(C(O)OC\mathit{H}_3))$), 3.84 (br s, 1H, Ru-O-C(H), overlapped with major), 6.45 - 7.95 (m, 32H, BINAP, overlapped with major). ^{13}C NMR (400 MHz, acetone-d_6, 25 °C): δ 4.3 (1C, $\mathit{C}H_3CN$), 22.0 (1C, $C(\mathit{C}H_3)_2$), 23.2 (1C, $C(\mathit{C}H_3)_2$), 49.2 (1C, $\mathit{C}(CH_3)_2$), 53.1 (1C, $CO_2\mathit{C}H_3$), 55.0 (1C, $CO_2\mathit{C}H_3$), 86.7 (1C, Ru-O-*C*(H), overlapped with major), 126.8 (1C, $CH_3\mathit{C}N$, overlapped with major), 127 - 142.5 (BINAP, overlapped with major), 190.5 (1C, $Ru\text{-}O\text{-}C(H)(CO_2CH_3)(C(CH_3)_2(\mathit{C}O_2CH_3))$), 191.2 (1C, $Ru\text{-}O\text{-}C(H)(\mathit{C}O_2CH_3)(C(CH_3)_2(CO_2CH_3)$ overlapped with major). ^{31}P NMR (400 MHz, acetone-d_6, 25 °C): δ 57.4 (br d, 1P, $^{2}J_{P\text{-}P}$ = 45.0 Hz), 63.7 (br d, 1P, $^{2}J_{P\text{-}P}$ = 45.0 Hz). ^{31}P NMR (400 MHz, acetone-d_6, 25 °C) of ^{15}NCMe enriched compound: δ 57.4 (dd, 1P, $^{2}J_{P\text{-}P}$ = 45.5 Hz, $^{2}J_{P\text{-}N}$ = 2.9 Hz), 63.7 (dd, 1P, $^{2}J_{P\text{-}P}$ = 45.5 Hz, $^{2}J_{P\text{-}N}$ = 2.9 Hz).

[Ru((*R*)-BINAP)(OC(H)(CO$_2$(CH$_3$)$_2$(H))(C(CH$_3$)$_2$(CO$_2$(CH$_3$)$_2$(H)))](BF$_4$) (11a/11b). Synthesized in the similar manor as (**8a/8b**) in THF. FT-IR (CH_2Cl_2, 22 °C): 1610 cm^{-1} (w, $\nu_{C=O}$), 1638 cm^{-1} (s, $\nu_{C=O}$). ESI-MS (pos) *m/z* 1038.3 $(M)^+$, exact mass calcd for $C_{58}H_{56}O_5NP_2Ru^+$ = 1038.298. *Anal.* Calcd for $C_{58}H_{56}O_5NP_2RuBF_4$: C, 64.06; H, 5.38; N, 1.25. Found: C, 63.32; H, 5.44; N, 1.54. (*R*)-**11a**: ^{1}H NMR (400 MHz, THF-d_8, 25 °C): δ 0.76 (d, 3H, $^{3}J_{H\text{-}H}$ = 5.5 Hz, $Ru\text{-}O\text{-}CH(CO_2(CH(C\mathit{H}_3)_2)(C(CH_3)_2\text{-}CO_2(CH(CH_3)_2))$), 0.80 (2, 3H, $Ru\text{-}O\text{-}CH(CO_2(CH(CH_3)_2)\text{-}(C(C\mathit{H}_3)_2CO_2(CH(CH_3)_2))$), 0.98 (s, 3H, $Ru\text{-}O\text{-}CH(CO_2(CH(CH_3)_2)(C(C\mathit{H}_3)_2CO_2.(CH(CH_3)_2))$), 1.09 (d, 3H, $^{3}J_{H\text{-}H}$ = 5.5 Hz, $Ru\text{-}O\text{-}CH(CO_2(CH(CH_3)_2)(C(CH_3)_2CO_2.(CH(C\mathit{H}_3)_2))$), 1.15 (d, 3H, $^{3}J_{H\text{-}H}$ = 5.5

Hz, Ru-O-CH(CO$_2$(CH(C*H*$_3$)$_2$)(C(CH$_3$)$_2$CO$_2$-(CH(CH$_3$)$_2$)), 1.23 (d, 3H, $^3J_{\text{H-H}}$ = 5.5 Hz, Ru-O-CH(CO$_2$(CH(CH$_3$)$_2$)(C(CH$_3$)$_2$CO$_2$-(CH(C*H*$_3$)$_2$)), 1.89 (s, 3H, NCC$\underline{\mathrm{H}}$3), 3.82 (s, 1H, Ru-O-C*H*(CO$_2$(CH(CH$_3$)$_2$)(C(CH$_3$)$_2$-CO$_2$(CH(CH$_3$)$_2$)), 4.76 (quint, 1H, $^3J_{\text{H-H}}$ = 5.5Hz, Ru-O-CH(CO$_2$(C*H*(CH$_3$)$_2$)(C(CH$_3$)$_2$-CO$_2$(CH(CH$_3$)$_2$)), 5.42 (quint, 1H, $^3J_{\text{H-H}}$ = 5.5Hz, Ru-O-CH(CO$_2$(CH(CH$_3$)$_2$)(C(CH$_3$)$_2$-CO$_2$(C*H*(CH$_3$)$_2$)), 6.40 - 8.02 (m, 32H, BINAP). ^{13}C NMR (400 MHz, THF-d_8, 25 °C): δ 3.9 (1C, *C*H$_3$CN), 20-21 (3C, CH(*C*H$_3$)$_2$, 2 from *α*-ester group and 1 from *β*-ester group), 25.0 (1C, CH(*C*H$_3$)$_2$, from *β*-ester group), 46.0 (1C, Ru-O-CH(CO$_2$(CH(CH$_3$)$_2$)(*C*(CH$_3$)$_2$CO$_2$(CH(CH$_3$)$_2$)), 72.0 (1C, Ru-O-CH(CO$_2$-(CH(CH$_3$)$_2$)(C(CH$_3$)$_2$CO$_2$(*C*H(CH$_3$)$_2$)), 73.0 (1C, Ru-O-CH(CO$_2$(*C*H(CH$_3$)$_2$)-(C(CH$_3$)$_2$CO$_2$(CH(CH$_3$)$_2$)), 87.0 (1C, Ru-O-*C*H), 124-142 (46C, BINAP carbons), 182 (1C, Ru-O-CH(CO$_2$(CH(CH$_3$)$_2$)(C(CH$_3$)$_2$*C*O$_2$(CH(CH$_3$)$_2$)), 190 (1C, Ru-O-CH(*C*O$_2$(CH(CH$_3$)$_2$)(C(CH$_3$)$_2$CO$_2$(CH(CH$_3$)$_2$)). ^{31}P NMR (400 MHz, THF-d_8, 25 °C): δ 56.0 (d, 1P, $^2J_{\text{P-P}}$ = 47.0 Hz, P$_1$ of minor complex), 60.4 (d, 1P, $^2J_{\text{P-P}}$ = 45.0 Hz, P$_1$ of major complex), 64.1 (d, 1P, $^2J_{\text{P-P}}$ = 45.0 Hz, P$_2$ of major complex), 66.4 (d, 1P, $^2J_{\text{P-P}}$ = 47.0 Hz, P$_2$ of minor complex). ^{31}P NMR (400 MHz, acetone-d_6, 25 °C) of ^{15}NCMe enriched compound: δ 56.0 (dd, 1P, $^2J_{\text{P-P}}$ = 47.0 Hz, $^2J_{\text{P-N}}$ = 3.0 Hz, P$_1$ of minor complex), 60.4 (dd, 1P, $^2J_{\text{P-P}}$ = 45.0 Hz, $^2J_{\text{P-N}}$ = 2.7 Hz, P$_1$ of major complex), 64.1 (dd, 1P, $^2J_{\text{P-P}}$ = 45.0 Hz, $^2J_{\text{P-N}}$ = 2.7 Hz, P$_2$ of major complex), 66.4 (dd, 1P, $^2J_{\text{P-P}}$ = 47.0 Hz, $^2J_{\text{P-N}}$ = 3.0 Hz, P$_2$ of minor complex).

[Ru((*R*)-BINAP)(OC(H)(CO$_2$(CH$_3$)$_3$)(C(CH$_3$)$_2$(CO$_2$(CH$_3$)$_3$))](BF$_4$) (12).

Synthesized in the same manor as (**8a/8b**) in THF. FT-IR (CH$_2$Cl$_2$, 22 °C): 1608 cm^{-1} (w, $\nu_{\text{C=O}}$), 1644 cm^{-1} (s, $\nu_{\text{C=O}}$).ESI-MS (pos) *m/z* 1038.3 (M)$^+$, exact mass calcd for

$C_{58}H_{56}O_5NP_2RuBF_4$ = 1038.298. *Anal.* Calcd for $C_{58}H_{56}O_5NP_2RuBF_4$: C, 64.06; H, 5.38; N, 1.25. Found: C, 63.32; H, 5.44; N, 1.54. (*R*)-**12**: ^{1}H NMR (400 MHz, THF-d_8, 25 °C): δ 0.86 (s, 3H, C(CH_3)$_2$), 1.07 (s, 3H, C(CH_3)$_2$), 1.17 (s, 9H, α-$CO_2C(CH_3)_3$); 1.50 (s, 9H, β-$CO_2C(CH_3)_3$); 1.92 (s, 3H, CH_3CN), 3.98 (s, 1H, Ru-O-C(H)); 6.5 - 8.04 (m, 32H, BINAP). ^{13}C NMR (400 MHz, THF-d_8, 25 °C): δ 3.78 (1C, CH_3CN), 22.24 (1C, C(CH_3)$_2$), 24.97 (1C, C(CH_3)$_2$), 28.30 (3C, OC(CH_3)$_3$), 28.78 (3C, OC(CH_3)$_3$), 48.20 (1C, *C*(CH_3)$_2$), 87.32 (1C, O*C*(CH_3)$_3$), 88.23 (1C O*C*(CH_3)$_3$), 89.48 (1C, Ru-O-*C*(H)), 126.5 - 142.6 (42C, aromatics, BINAP), 183.41 (1C, β-C(O)OC(CH_3)$_3$), 190.20 (α-C(O)OC(CH3)3). ^{31}P NMR (400 MHz, THF-d_8, 25 °C): δ 59.5 (d, 1P, P_1, $^2J_{P\text{-}P}$ = 45.5 Hz), 63.5 (d, 1P, P_2, $^2J_{P\text{-}P}$ = 45.5 Hz). ^{31}P NMR (400 MHz, acetone-d_6, 25 °C) of ^{15}NCMe enriched compound: δ 59.5 (dd, 1P, P_1, $^2J_{P\text{-}P}$ = 45.0 Hz, $^2J_{P\text{-}N}$ = 2.8 Hz), 63.5 (dd, 1P, P_2, $^2J_{P\text{-}P}$ = 45.0 Hz, $^2J_{P\text{-}N}$ = 2.8 Hz). For details on assignment of BINAP signals refer to *Results and Discussion* section in text.

Low temperature NMR investigation of catalyst and substrate interactions. Compound [Ru((*R*)-BINAP)(C_8H_{11})(MeCN)](BF_4) (19.5 mg, 2.03 x 10^{-5} mol) was partially dissolved in THF-d_8 (0.6 mL) in an NMR tube under an argon atmosphere. At room temperature, the tube was flushed with dihydrogen gas, pressurized (1-2 atm), and shaken until a golden orange solution was generated (~5 min). The dihydrogen atmosphere was replaced by argon and the resulting solution was analyzed by ^{1}H and ^{31}P NMR spectroscopy at -80 °C. NMR spectroscopic analysis indicated a mixture of 2 ruthenium-hydrido species ([Ru((*R*)-BINAP)(H)(THF-d_8)$_n$(MeCN)$_{3-n}$](BF_4) (n = 0-3, with n = 2 as major species (75%)), and cyclooctane were present. At -80 °C, dimethyl

3,3-dimethyloxaloacetate (4.0 mg, 1.15 x 10^{-4} mol) was injected into the NMR tube via gas-tight syringe. The tube was removed from the cooling bath, shaken for ~15 s, and then immediately placed in a pre-cooled (-80 °C) NMR probe. The ^{31}P NMR spectrum at -80 °C remained unchanged, as did the ^{1}H NMR spectrum except for the introduction of dimethyl 3,3-dimethyloxaloacetate. Upon warming the NMR probe, the ^{31}P and ^{1}H NMR remained unchanged until the temperature reached -30 °C. At -30 °C, the ^{31}P NMR slowly showed the signs of (*R*)-**8a** and (*S*)-**8b** peaks growing in and no other peaks were observed. Once warmed to ambient temperature, the ^{31}P NMR showed only the presence of (*R*)-**8a** and (*S*)-**8b** in the same ratio observed with the stoichiometric reaction at room temperature. ^{31}P (162.0 MHz, THF-d_8, -80 °C to -40 °C): δ 72.2 (d, $^{2}J_{P\text{-}P}$ = 42.5 Hz, A), 72.4 (d, $^{2}J_{P\text{-}P}$ = 49.5 Hz, B), 77.1 (d, $^{2}J_{P\text{-}P}$ = 43.5 Hz, A), 81.4 (d, $^{2}J_{P\text{-}P}$ = 49.5 Hz, B). Approximate percentages of hydrido species present: A(25%) and B(75%). ^{31}P (162.0 MHz, THF-d_8, -30 °C): δ 59.8 (d, 1P, $^{2}J_{P\text{-}P}$ = 45.5 Hz, (*R*)-**8a**), 63.0 (d, 1P, $^{2}J_{P\text{-}P}$ = 45.5 Hz, (*R*)-**8a**), 56.4 (br d, 1P, $^{2}J_{P\text{-}P}$ ~ 45 Hz, (*S*)-**8b**), 63.7 (br d, 1P, $^{2}J_{P\text{-}P}$ ~ 45 Hz, (*S*)-**8b**).

Similar results were observed upon low temperature investigation of both di-*iso*-propyl 3,3-dimethyloxaloacetate (**9**) and di-*tert*-butyl 3,3-dimethyloxaloacetate (**10**). The only observable species upon warming were the alkoxide intermediates (*R*)-**11a** and (*S*)-**11b** for **9** (in the same ratio observed in stoichiometric reaction of **6** with the ketone at room temperature) and solely (*R*)-**12** for **10**.

Typical procedure for hydrogenation of dialkyl 3,3-dimethyloxaloacetate (alkyl = Me, *iso*-Pr, *tert*-Bu) with [Ru((*R*)-BINAP)(1-3;5,6-η-C_8H_{11})(MeCN)](BF_4) as catalyst precursor. To a 25 mL side-arm flask was transferred **1** (10.0 mg, 1.04 x 10^{-5}

mol) and the 50 equiv of the corresponding ketone (5.21 x 10^{-4} mol) in a glove box. Solvent (methanol or THF, 5.0 mL) was added to the sealed flask via gas-tight syringe. The flask was then transferred to a pre-flushed, argon gas, stainless-steel bomb. The bomb was flushed for a further 15 min with argon gas then with dihydrogen gas for 10 min and finally it was pressurized to 50 atm. Once stabilized, the bomb was placed in a 50 °C oil bath and reacted for 50 h. The bomb was then cooled to ambient temperature, depressurized, and the flask placed under reduced pressure to remove the solvent. The residue was then passed through a Florisil plug with Et_2O (~10 mL) to remove the catalyst. The Et_2O was then removed under reduced pressure and the clear-colorless liquid products were analyzed by ^1H NMR. The enantiomeric excess was determined by either ^1H NMR ,with added chiral shift reagent (tris[3-(heptafluoropropylhydroxy-methylene)-(+)-camphorato]europium(III)) and its comparison to that of the racemic alcohol and added shift reagent (used for dimethyl 3,3-dimethyloxaloacetate and di-*iso*-propyl 3,3-dimethyloxaloacetate products)[†] or by chiral GC analysis (di-*tert*-butyl 3,3-dimethyloxaloacetate product).[‡] The absolute configuration of the major enantiomeric product for dimethyl 3,3-dimethyl-2-hydroxysuccinate was determined by comparison to the reported optical rotation of (*S*)-dimethyl 3,3-dimethyl-2-hydroxysuccinate ($[\alpha]_D$ = +33°, c = 1.42, $CHCl_3$).[27] The absolute configuration of the major enantiomeric product for di-*iso*-propyl 3,3-dimethyl-2-hydroxysuccinate and di-*tert*-butyl 3,3-dimethyl-2-

---

[†] Dimethyl 3,3-dimethyl-2-hydroxysuccinate: The ratio of the methoxy signals (ca. δ 4.0) was used to determine the ee. The ratio of these peaks was 1:1 for racemic alcohol. Di-*iso*-propyl 3,3-dimethyl-2-hydroxysuccinate: The ratio of the backbone methyl signals (ca. δ 1.2 and δ 1.1) was used to determine the ee. The ratio of these peaks was 1:1 for racemic alcohol.

[‡] Performed on Beta Dex 120 column in acetone solution. Initial oven temperature was 120 °C for 45 min then it was increased at a rate of 10 °C/min to 200 °C. The enantiomers were eluted at ~ 45 min for (*S*)-enantiomer and at ~ 46 min for (*R*)-enantiomer.

hydroxysuccinate were determined by reduction of the products with $LiAlH_4$ to the corresponding triol, 2,2-dimethylbutan-1,3,4-triol, and comparison to the reported optical rotation of (3*R*)-(-)- 2,2-dimethylbutan-1,3,4-triol ($[\alpha]_D$ = -16°, c = 1.06, EtOH).[26] ^1H NMR of dimethyl 3,3-dimethyl-2-hydroxysuccinate (400.1 MHz, $CDCl_3$, 25 °C): δ 1.12 (s, 3H, $C(CH_3)_2$), 1.21 (s, 3H, $C(CH_3)_2$), 3.23 (br d, 1H, $^3J_{H\text{-}H}$ ~ 6 Hz, C(H)(O*H*)), 3.66 (s, 3H, OCH_3), 3.72 (s, 3H, OCH_3), 4.30 (br d, 1H, $^3J_{H\text{-}H}$ ~ 6 Hz, C(*H*)(OH)).

^1H NMR of di-*iso*-propyl 3,3-dimethyl-2-hydroxysuccinate (400.1 MHz, $CDCl_3$, 25 °C): δ 1.12 (s, 3H, $C(CH_3)_2$), 1.22 (s, 3H, $C(CH_3)_2$), 1.23 (d, 6H, $^3J_{H\text{-}H}$ = 6.5 Hz, $CO_2C((CH_3)_2(H))$), 1.24 (d, 6H, $^3J_{H\text{-}H}$ = 6.5 Hz, $CO_2C((CH_3)_2(H))$), 3.19 (d, 1H, $^3J_{H\text{-}H}$ = 6.5 Hz, C(H)(O*H*)), 4.30 (d, 1H, C(*H*)(OH)), 4.99 (quint, 1H, $^3J_{H\text{-}H}$ = 6.5 Hz, $CO_2C((CH_3)_2(H))$), 5.08 (quint, 1H, $^3J_{H\text{-}H}$ = 6.5 Hz, $CO_2C((CH_3)_2(H))$).

^1H NMR of di-*tert*-butyl 3,3-dimethyl-2-hydroxysuccinate (400.1 MHz, $CDCl_3$, 25 °C): δ 1.14 (s, 3H, $C(CH_3)_2$), 1.68 (s, 3H, $C(CH_3)_2$), 1.44 (s, 9H, $CO_2C(CH_3)_3$), 1.48 (s, 9H, $CO_2C(CH_3)_3$), 3.19 (d, 1H, C(H)(O*H*)), 4.17 (d, C(*H*)(OH)).

Stoichiometric hydrogenolysis of $[Ru((R)\text{-BINAP})(OC(D)(CO_2CH_3)\text{-}(C(CH_3)_2(CO_2CH_3))](BF_4)$ (8a-d_1/8b-d_1). In the glove box, the mixture of complexes **8a-d_1** and **8b-d_1** (105.0 mg, 1.01 x 10^{-4} mol) was transferred to a 100 mL side-arm. The flask was sealed and had the solvent (MeOH or THF, 48.6 mL) added via gas-tight syringe. The side-arm was then placed in a pre-flushed stainless-steel bomb, the bomb was further flushed for 15 min with argon gas. The bomb was then flushed with dihydrogen gas for 10 min and then pressurized to 50 atm. The bomb was then allowed to react for 1 h (the time, on average, for a single turnover in the operating catalytic

reaction) in a 50 °C oil bath. The bomb was then depressurized, the flask removed and bubbled with oxygen to destroy the catalyst. The flask was then placed under reduced pressure to remove the solvent. The residue was then passed through a Florisil plug with Et_2O (5 mL) to remove the catalyst, the solvent removed under reduced pressure, and the product analyzed by NMR. ^1H NMR of THF reaction (400.1 MHz, $CDCl_3$, 25 °C): δ 4.3 (0.4 H as compared to 3H methoxy signals at ca. δ 3.8). The ee was determined to be 58% (*R*). ^1H NMR of MeOH reaction (400.1 MHz, $CDCl_3$, 25 °C): δ 4.3 (0.25 H as compared to 3H methoxy signals at ca. δ 3.8). The ee was determined to be 60% (*R*). The stoichiometric hydrogenations of the complexes $[Ru((R)\text{-BINAP})(OC(D)\text{-}(CO_2C(CH_3)_2(H))(C(CH_3)_2(CO_2C(CH_3)_2(H)))](BF_4)$ (**11a-*d*₁/11b-*d*₁**) and $[Ru((R)\text{-BINAP})(OC(D)(CO_2C(CH_3)_3)(C(CH_3)_2(CO_2C(CH_3)_3))](BF_4)$ (**12-*d*₁**) were performed in a similar manner. ^1H NMR of THF reaction of **11a-*d*₁/11b-*d*₁** (400.1 MHz, $CDCl_3$, 25 °C): δ 4.3 (0.2 H as compared to 3H methoxy signals at ca. δ 3.8). The ee was determined to be 69% (*R*). ^1H NMR of MeOH reaction of **11a-*d*₁/11b-*d*₁** (400.1 MHz, $CDCl_3$, 25 °C): δ 4.3 (0.15 H as compared to 3H methoxy signals at ca. δ 3.8). The ee was determined to be 70% (*R*). ^1H NMR of THF reaction of **12-*d*₁** (400.1 MHz, $CDCl_3$, 25 °C): δ 4.2 (0.2 H as compared to 3H methoxy signals at ca. δ 3.8). The ee was determined to be 84% (*R*). ^1H NMR of MeOH reaction of **12-*d*₁** (400.1 MHz, $CDCl_3$, 25 °C): δ 4.3 (0.1 H as compared to 3 H methoxy signals at ca. δ 3.8). The ee was determined to be 84% (*R*).

Reaction of $[Ru((R)\text{-BINAP})(OC(D)(CO_2CH_3)(C(CH_3)_2\text{-}(CO_2CH_3))](BF_4)$ (8a-*d*₁/8b-*d*₁) with HBF_4•OEt_2. The ruthenium-alkoxide complexes (**8a-*d*₁/8b-*d*₁**)

(150.4 mg, 1.44 x 10^{-4} mol) were transferred to a 50 mL side-arm. The flask was sealed, placed under reduced pressure and refilled (x 3) to remove all traces of oxygen. To the flask was added CH_2Cl_2 (5.0 mL) via gas-tight syringe. The solution was stirred under argon atmosphere for 2 min. To this solution was added 1 equiv of $HBF_4•OEt_2$ via gas-tight syringe. The solution turned from a deep orange color to a pale yellow upon immediate addition of the HBF_4. The solution was stirred for 5 min then the flask was placed under reduced pressure to remove the solvent. The residue was analyzed by ^1H, ^2H, and ^{31}P NMR and determined to have produced the desired alcohol product, with complete retention of deuterium at the alkoxy position, and the [Ru((*R*)-BINAP)$(MeCN)_4](BF_4)_2$ byproduct. The sample was then passed through a Florisil plug with Et_2O, the solvent removed, and the residue analyzed for the enantiomeric excess. The dimethyl 3,3-dimethyl-2-hydroxysuccinate yielded 58% ee (*R*). Similar reactions were performed with the ruthenium-alkoxides **11a-*d*₁/11b-*d*₁** and with the ruthenium-alkoxide **12**. Reaction with **11a-*d*₁/11b-*d*₁** yielded 79% ee (*R*), and reaction with **12-*d*₁** yielded > 99% ee (*R*).

References and Notes:

(1) Examples of use in pharmaceuticals, industry, and academia: (a) *Chirality in Industry*: Collins, A. N.; Sheldrake, G. N.; Crosby, J. Eds.; John Wiley & Sons: New York, 1997. (b) *Reductions in Organic Chemistry*: Abdel-Magid, A. F. Ed.; Advances in Chemistry Series 641; American Chemical Society: Washington, 1996. (c) Noyori, R. *Asymmetric Catalysis in Organic Synthesis*, Wiley, New York 1994. (d) *Catalytic Asymmetric Synthesis*: Ojima, I. Ed.; VCH Publishers: New York, 1993.

(2) Investigations into mechanism of rhodium and ruthenium catalyzed enantioselective hydrogenation of ketone reaction. Rhodium: (a) Agbossou, F.; Carpentier, J.-F.; Mortreux, A.; Surpateanu, G.; Welch, A. J. *New J. Chem.* **1996**, *20*, 1047-1060. (b) Mezzetti, A.; Tschumper, A.; Consiglio, G. *J. Chem. Soc., Dalton Trans.* **1995**, 49-55. (b) Pasternak, H.; Pruchnik, F. P. *Polish J. Chem.* **1992**, *66*, 865-871. (c) Hatat, C.; Karim, A.; Kokel, N.; Mortreux, A.; Petit, F. *New J. Chem.* **1990**, *14*, 141-152. (d) Chiba, M.; Takahashi, H.; Takahashi, H.; Morimoto, T.; Achiwa, K. *Tetrahedron Lett.* **1987**, *28*, 3675. (e) Tani, K.; Tanigawa, E.; Tatsuno, Y.; Otsuka, S. *J. Organomet. Chem.* **1985**, *279*, 87-101. (f) Torös, S.; Heil, B.; Kollar, L.; Marko, L. *Acta Chim. Hung.* **1985**, *119*, 135. (g) Ojima, I.; Kogure, T. *J. Organomet. Chem.* **1980**, *195*, 239. Ruthenium: (h) King, S. A.; DiMichele, L. In *Catalysis of Organic Reactions*: Scaros, M. G.; Prunier, M. L. Eds.; Vol 62; Marcel-Dekker: New York, 1995; pp. 157-166. (i) Geraty, S. M.; Harkin, P.; Vos, J. G. *Inorg. Chim. Acta* **1987**, *131*, 217-220.

(3) Selected examples of advances in enantioselective ketone hydrogenations. Ruthenium catalysts: (a) Mikami, K.; Korenaga, T.; Terada, M.; Ohkuma, T.; Pham, T.; Noyori, R. *Angew. Chem. Int. Ed. Engl.* **1999**, *38*, 495-497. (b) Cao, P.; Zhang, X. *J. Org. Chem.* **1999**, *64*, 2127-2129. (c) Fehring, V.; Selke, R. *Angew. Chem. Int. Ed. Engl.* **1998**, *37*, 1827-1830. (d) Nagel, U.; Roller, C. *Z. Naturforsch.* **1998**, *53b*, 267-270. (e) Doucet, H.; Ohkuma, T.; Murata, K.; Yokozawa, T.; Kozawa, M.; Katayama, E.; England, A. F.; Ikariya, T.; Noyori, R. *Angew. Chem. Int. Ed. Engl.* **1998**, *37*, 1703-1707. (f) Ager, D. J.; Laneman, S. A. *Tetrahedron: Asymmetry* **1997**, *8*, 3327-3355, and references within. (g) Genêt, J. P.; Ratovelomanana-Vidal, V.; Caño de Andrade, M. C.; Pfister, X.; Guerreiro, P.; Lenoir, J. Y. *Tetrahedron Lett.* **1995**, *36*, 4801-4804. (h) Burk, M. J.; Harper, T. G. P.; Kalberg, C. S. *J. Am. Chem. Soc.* **1995**, *117*, 4423-4424. (i) Ohkuma, T.; Ooka, H.; Ikariya, T.; Noyori, R. *J. Am. Chem. Soc.* **1995**, *117*, 10417-10418. (j) Ohkuma, T.; Ooka, H.; Hashiguchi, S.; Ikariya, T.; Noyori, R. *J. Am. Chem. Soc.* **1995**, *117*, 2675-2676. Rhodium catalyst: (k) Jiang, Q.; Jiang, Y.; Xiao, D.; Cao, P.; Zhang, X. *Angew. Chem. Int. Ed. Engl.* **1998**, *37*, 1100-1102.

(4) Some partial characterization of identifications have been made: two examples for rhodium systems: references 2c and 2e. Two examples in ruthenium systems: references 2h and 2i.

(5) (a) Wiles, J. A.; Bergens, S. H. *J. Am. Chem. Soc.* **1997**, *119*, 2940-2941. (b) Wiles, J. A.; Bergens, S. H. *Organometallics* **1998**, *17*, 2228-2240. (c) Wiles, J. A.; Bergens, S. H. *Organometallics* **1999**, *18*, 3709-3714.

(6) Daley, C. J. A.; Wiles, J. A.; Bergens, S. H. *Can. J. Chem.* **1998**, *76*, 1447-1456.

(7) To our knowledge, there are no reports in the literature on the use of dimethyl oxaloacetate (**2**) as substrate in enantioselective ketone hydrogenation.

(8) When green solutions are normally encountered, it usual indicates the active catalyst has been destroyed with O_2 or H_2O therefore, the reaction was performed several times. The reaction mixture proceeded to the green color followed by the orange-yellow color in all cases. It is therefore believed that the green color is not an indication of decomposition.

(9) Similar observations were reported by King *et al* for reaction between α-keto esters and the partially characterized hydrides obtained from hydrogenation of $Ru(BINAP)(Cl)_2/NEt_3$ in CH_2Cl_2. The products reported by King were the corresponding α-hydroxy ester and unidentified ruthenium complexes: reference 2h.

(10) Generally, *trans* coordination to phosphine yields greater observed couplings that *cis* coordination to phosphines. However, larger coupling constant does not ensure *trans* coordination versus *cis*, see reference 5c.

(11) It was shown in the related complex $[Ru((R)\text{-BINAP})(^{15}N\text{-MeCN})_3(H)](BF_4)$ that only when MeCN is coordinated *trans* to phosphorus in these complexes does it show significant ^{31}P-^{15}N coupling ($^2J_{P\text{-}N} \geq 8$ Hz; reference 5c).

(12) HMQC analysis showed the proton with ^1H NMR signal at δ 3.9 as being attached to the carbon atom with ^{13}C NMR signal at δ 89.0.

(13) Mashima, K.; Hino, T.; Takaya, H. *J. Chem. Soc. Dalton Trans.* **1992**, 2099-2107.

(14) There was no ^1H NMR signal observed at δ 3.9 and the only ^2H NMR signal was observed at δ 3.9.

(15) Addition of ((+)-Eu(tfc)$_3$)) to the isolated "free alcohol" from reaction in CDCl$_3$ showed 58% ee (*R*) corresponding to 79% (*R*)-**7'** and 21% (*S*)-**7'**. The observed ratio is equal, within experimental error, to the observed ratio of diastereomers **8a** and **8b** (80:20).

(16) A number of solution NMR experiments were employed (ambient temperature and -40 °C: ^{1}H, ^{13}C, ^{31}P, ^{31}P-^{1}H HETCOR, HMQC, HMBC, COSY, and ROESY). Significant information as to the exact identification of many of the backbone BINAP ligand signals was obtained but the COSY and ROESY experiments were complicated by signal overlap from the presence of the minor diastereomer. Concrete evidence as to the structure was not obtained from these investigations alone.

(17) The compounds **9** and **10** were synthesized in an analogous manner as **7**.

(18) The methyne proton signal of *iso*-propyl group B (δ 5.42) did not show any correlation to either ester carbonyl carbon signal (by HMBC experiments). That the methyne proton signal of *iso*-propyl group A (δ 4.76) did is sufficient proof of assignments.

(19) The experimental limits of detection of the HMBC NMR experiment are generally 3-bond correlations. The *tert*-butyl methyl protons are 4 bonds away from their respective ester carbonyl carbon atoms and thus correlations were not observed.

(20) If the ^{1}H NMR signals are too broad and/or in the baseline, the transfer of magnetization information from the proton to the phosphorus of interest will be lost, as the proton relaxes too quickly for the ^{31}P-^{1}H HETCOR experiment.

(21) The identification of the P_2 *ortho*-Naph proton (^{1}H δ 8.02 ('t', $^3J_{P\text{-}H} = {^3J_{H\text{-}H}} = 9$ Hz)) was confirmed by the analysis of the COSY data that identified only a single coupling to another proton group (^{1}H δ 7.92 (d, $^3J_{H\text{-}H}= 9$ Hz)). There are only three possible protons that could appear as doublets in the ^{1}H NMR for BINAP. The possibilities are all naphthalene protons (H(4), H(5), and H(8) where the numbers in brackets represent the IUPAC numbering system of the P_2 bonded naphthyl ring). Therefore, the only P_2 coupled protons would be the P_2 *ortho*-Naph proton. Furthermore, the proton with the ^{1}H NMR signal at δ 7.92 (d) cannot be H(5) or H(8), as they would not have coupling to a proton that had coupling to P_2. Therefore, H(5) and H(8) were eliminated as possibilities. The proton with the ^{1}H NMR signal at δ 7.92 must be H(4) of P_2.

(22) From the analyses of the COSY and ROESY experiments, the P_1 *ortho*-Naph proton signal (δ 7.02) was identified, again, due to the coupling to the doublet H(4) (H(4), H(5), and H(8) where the number in brackets represent the IUPAC numbering system of the P_1 bonded naphthyl ring). H(4) was identified from its coupling to the region where the analysis of the ^{31}P-^{1}H HETCOR showed correlation to the ^{31}P NMR signal of P_1 as well as, the observed ROE contact to the ^{1}H signal at δ 6.96 (d, $^3J_{H\text{-}H} = 8$ Hz). The only doublets that would show ROE contacts to other protons appearing as doublets in the ^{1}H NMR are the H(4) and H(5) protons of either naphthyl ring. Having identified H(4) of P_2 already, it remained that the signals must correspond to the protons H(4) and H(5) of P_1. Unequivocal identification of the exact position of P_1 *ortho*-Naph proton was hampered by overlap with other ^{1}H NMR signals.

(23) Identified by ROE contact to equatorial *ortho*-phenyl proton signal at -40 °C (Figure 6.7), as well as it is the last remaining type of P_2 *ortho*-phenyl protons not previously identified.

(24) Casey, M.; Leonard, J.; Lygo, B.; Procter, G. *Advanced Practical Organic Chemistry*: Chapman & Hall: London, 1990; pp. 28-42.

(25) Wiles, J. A.; Lee, C. E.; McDonald, R.; Bergens, S. H. *Organometallics* **1996**, *15*, 3782-3784.

(26) Matsuo, T.; Mori, K.; Matsui, M. *Tetrahedron Lett.* **1976**, *23*, 1979-1982.

(27) Seebach, D.; Wasmuth, D. *Helv. Chim. Acta* **1980**, *63*, 197-200.

Chapter 7

Conclusions

Helical chiral tripodal tris(phosphine) ligand investigations. Early empirical investigations of chiral ligands led to the proposal that higher symmetry ligands may yield catalyst systems having greater enantioselectivity. The design, synthesis, and characterization of the *pseudo*-C_3 symmetric ligand heliphos (**1**; Figure 7.1) yielded a well-defined, tris(phosphine) ligand. Heliphos was determined to lock into one helical conformation upon tripodal coordination to a rhodium(I) metal center as designed (Figure 7.2). This conformation is held in solution as well as in the solid state as determined by solution NMR spectroscopic and X-ray crystallographic studies. Furthermore, the synthetic pathway utilized led to the isolation of a number of enantiopure phosphine

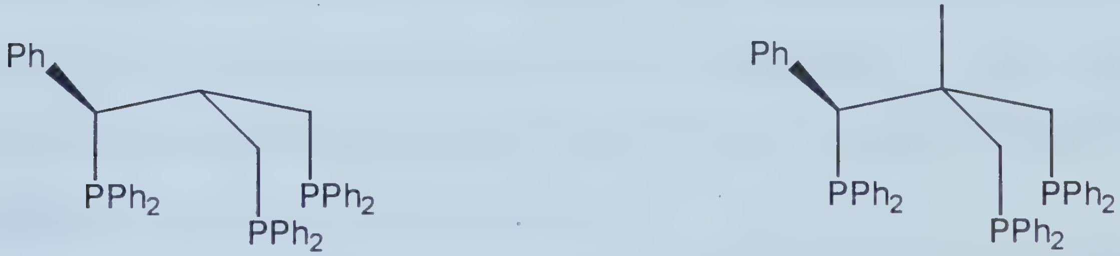

(*R*)-heliphos

(*R*)-Me-heliphos

Figure 7.1: Structure of (*R*)-heliphos (1) and (*R*)-Me-heliphos (2).

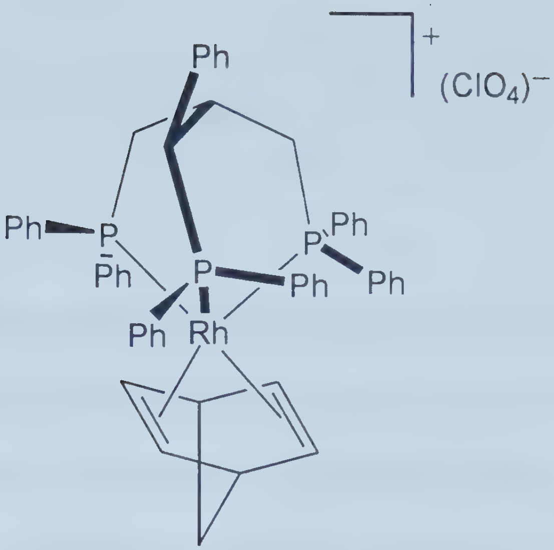

Figure 7.2: Coordination of (R)-heliphos in [Rh((R)-heliphos)(NBD)](ClO_4).

ligands without the requirement of the resolution of enantiomers with costly chiral metal resolving agents. The pathway allows for a general synthetic route to be utilized to obtain a number of new enantiopure phosphines. Thus, the development of heliphos not only resulted in the successful synthesis of the desired heliphos ligand, but it has opened a pathway to enantiopure chiral phosphines that can be tested for use as chiral ligands in transition-metal catalyzed enantioselective reactions.

Coordination of heliphos to ruthenium(II) metal complexes yielded incomplete coordination of the ligand. Analysis of molecular models suggested that the absence of a central neopentyl unit might favor phosphine arm dissociation over the crowding of the metal center upon tripodal coordination. The theory was to be tested by the use of Me-heliphos (**2**; Figure 7.1) as ligand. While the synthesis is incomplete at this time, the recently developed Ru((*R*)-BINAP)(pyridine)$_2$(Cl)$_2$ catalyst system of the Bergens group has led to the successful catalytic hydrogenation of the ketone **3** to yield the key alcohol diester compound ($CH_3C(H)(OH)(C(CH_3)(CO_2CH_3)_2)$) (**4**; Equation 7.1). This discovery,

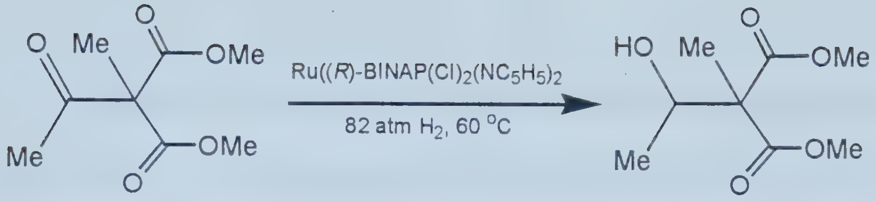

3 4

Equation 7.1

along with the successful syntheses of a couple of triol precursors of Me-heliphos, has led to a number of synthetic pathways that are expected to yield Me-heliphos without difficulty. Once completed, coordination to ruthenium(II) metal complexes should be performed to determine if tridentate coordination of the ligand is favored as compared with phosphine arm dissociation, as postulated. Furthermore, a study of both steric and electronic effects should be performed with a number of synthetic derivatives of both heliphos and Me-heliphos to obtain a more complete understanding of the nature of the properties required in tridentate coordination of such ligands.

With the anticipated tripodal locked helical coordination of Me-heliphos to ruthenium(II) metal centers, the complexes should be further investigated as possible catalysts in enantioselective catalysis reactions (e.g. hydrogenations, isomerizations, etc.). A full investigation and comparison to less symmetric chiral ligands, where appropriate, should also be undertaken to yield further information on the effects of increased symmetry in chiral ligand systems.

Overall, the successful synthesis of the chiral tris(phosphine) ligand heliphos yielded the desired locked helical coordination upon coordination to a metal center. As well, the synthetic pathway utilized has led to a general pathway that can be used to generate innumerable enantiopure chiral phosphine compounds that may find success as chiral ligands in enantioselective catalysis.

Studies utilizing [Ru((*R*)-BINAP)(1-3;5,6-*η*-C_8H_{11})(MeCN)](BF_4) as catalyst precursor. The development of [Ru((*R*)-BINAP)(1-3;5,6-*η*-C_8H_{11})(MeCN)](BF_4) (**5**) in the Bergens group has led to the most detailed mechanistic study of an enantioselective catalytic reaction, specifically in the enantioselective hydrogenation of methyl-*α*-acetamidocinnamate (MAC).[1] The investigation of the enantioselective hydrogenation of *α*,*β*-unsaturated carboxylic acids reported in this thesis (protic/aprotic solvent analysis and deuterium labeling studies) has resulted in the isolation and characterization of the likely catalytic intermediate [Ru((*R*)-BINAP)($O_2CC(CH_3)=C(CH_3)(H)$)$(Sol)_{2-n}(MeCN)_n$]-(BF_4) (**6**; n = 0-2; Sol = methanol or acetone; Figure 7.3) and provided strong evidence to further corroborate the catalytic cycle mechanism proposed by Halpern.[2]

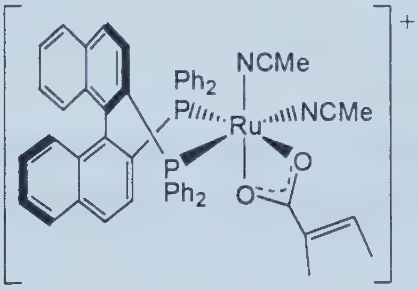

6

Figure 7.3: Isolated putative catalytic intermediate in ruthenium-BINAP catalyzed enantioselective hydrogenation of *α*,*β*-unsaturated carboxylic acid.

Kinetic studies remain to corroborate **6** as catalytic intermediate and the proposed catalytic cycle. Unfortunately the kinetic studies are not expected to yield further information on the nature of the proposed 5-membered catalytic intermediate as the turnover-limiting step occurs prior to the enantioselective step. However, as heterolytic cleavage is believed to be occurring and given that reaction does not proceed in aprotic

solvent without added base, the reactivity of the isolated complex **6** should be investigated. In particular, the reaction of **6** with a hydride source (e.g. KH) should be investigated, as the species Ru((*R*)-BINAP)(H)($O_2CC(CH_3)=C(CH_3)(H)$)(MeCN) (**7**) is proposed as catalytic intermediate. Should reaction occur to form either the ruthenium-hydrido species **7**, or the proposed 5-membered ring intermediate **8** (formed via olefin-hydride insertion of **7**; Figure 7.4), the isolation of such complexes may be possible in aprotic solvent as solvolysis will not occur. The isolation and characterization of these complexes would yield further information into the nature of enantioselection in the reaction as well as yield information on the mechanism of catalytic enantioselective hydrogenation of α,β-unsaturated carboxylic acids. Further, analysis of a wide variety of α,β-unsaturated carboxylic acids, with different electronic and steric properties, should be investigated to determine the effects of these properties on the net enantioselective catalytic hydrogenation reaction.

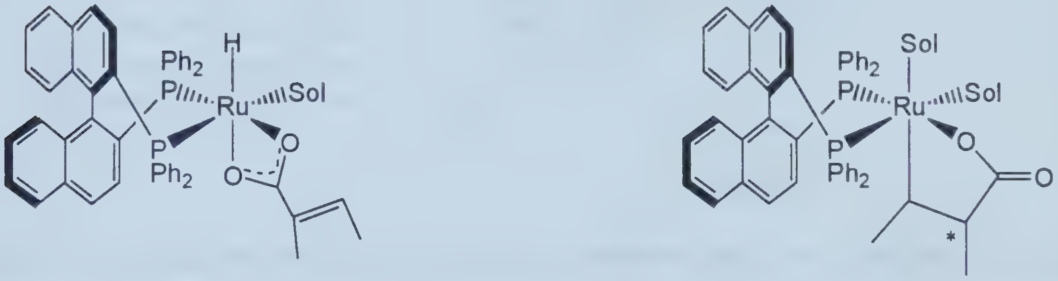

7

8

Figure 7.4: Possible catalytic intermediates in ruthenium-BINAP catalyzed enantioselective hydrogenation of α,β-unsaturated acids.

Investigations into the catalytic enantioselective hydrogenation of dimethyl itaconate (**9**) led to the isolation and characterization of the putative catalytic

intermediates [Ru((*R*)-BINAP)(**9**(H))(MeCN)](BF_4) (diastereomers **10a**:**10b**; 80:20), formed via olefin-hydride insertion. These intermediates are analogous in structure to the isolated and completely structurally characterized complex, [Ru((*R*)-BINAP)-(MAC(H))(MeCN)](BF_4) (**11**), observed in the operating catalytic hydrogenation of (*Z*)-methyl α-acetamidocinnamate (**12**, MAC; Figure 7.5)).[1] These studies, along with

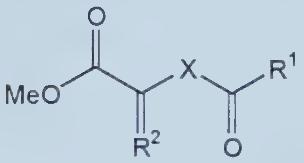

9 R^1 = OMe; R^2 = CH_2; X = CH_2
12 R^1 = OMe; R^2 = CHPh; X = NH
13 R^1 = OMe; R^2 = CH_2; X = $CHCH_3$

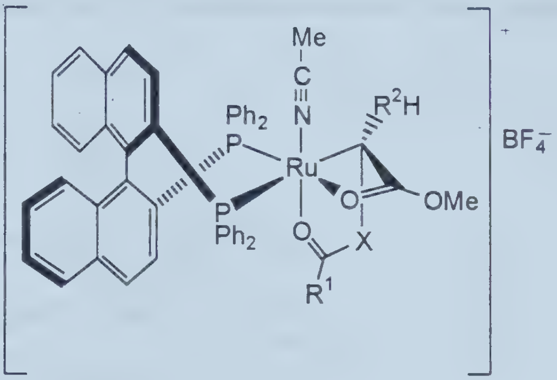

10a, 11

Figure 7.5: Structures of putative catalytic intermediates (10a (major), 11) in the ruthenium-BINAP catalyzed enantioselective hydrogenation of 9 and 12, respectively.

the MAC investigations performed in the Bergens group, have yielded strong evidence that agree with the mechanism of the catalytic cycle, similar to that proposed by Brown, in the enantioselective hydrogenation of **13** using Ru((*R*)-BINAP)(η^2-MeC(O)CHC(O)Me)$_2$(η^2-allyl) as catalyst.[3] In all cases, kinetic studies remain to further corroborate if the isolated complexes are catalytic intermediates or if they are simply ruthenium sinks that are in equilibrium with the true catalytic intermediates.

The use of [Ru((*R*)-BINAP)(1-3;5,6-η-C_8H_{11})(MeCN)](BF_4) (**5**) as catalyst precursor was also successful in the investigation of catalytic enantioselective

hydrogenation of ketones. Studies on the enantioselective hydrogenation of dialkyl 3,3-dimethyoxaloacetate ketone substrates (alkyl = methyl (**14**), *iso*-propyl (**15**), *tert*-butyl (**16**)) led to the first isolation and complete structural characterization (solution) of diastereomeric catalyst-alkoxide complexes that are proposed as catalytic intermediates in enantioselective ketone hydrogenation reactions (Figure 7.6). The isolated ruthenium-alkoxide complexes were found to act as catalyst in the enantioselective hydrogenation of

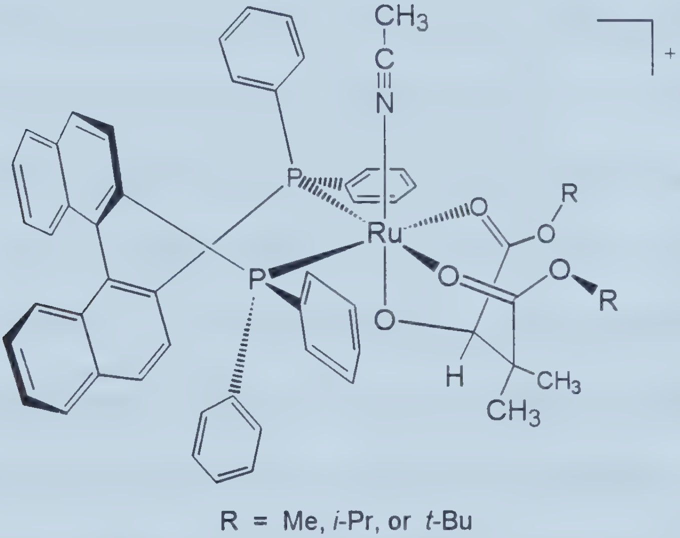

Figure 7.6: Unambiguously characterized putative catalytic intermediates in ruthenium-BINAP catalyzed enantioselective ketone hydrogenation.

the dialkyl 3,3-dimethyloxaloacetate ketones (DAMO) and yielded similar ee as compared with those observed using **5** as catalyst precursor. Furthermore, the results from the deuterium labeling studies of the complexes demonstrate that the stereoselectivity and regioselectivity of the rapid and reversible formation of [Ru((*R*)-BINAP)(DAMO(H))(MeCN)](BF_4) (**17**) complexes and the conversion of **17** to DAMO$(H)_2$ (the completed hydrogenation product formed via irreversible hydrogenolysis of the ruthenium-oxygen bond) summate to yield the stereoselectivity and

regioselectivity of the catalytic hydrogenation. These data, along with the observation that the rate of hydrogenolysis of ruthenium-alkoxide complexes is no slower than the catalytic hydrogenation under similar conditions, strongly support the identification of the isolated complexes as active catalytic intermediates in the operating catalytic reaction. Although the rate requirement is strong proof for such an argument, it is not conclusive, as the proposed intermediates may be in equilibrium with the true intermediate(s) that react(s) to generate the product. Complete kinetic studies of the catalytic hydrogenation are required to further corroborate the identification of **17** as active catalytic intermediates. The high pressures required to perform the necessary reactions complicate these studies. The use of sapphire NMR tubes that are capable of withstanding high pressures could be utilized to circumvent this problem. The observation, via ^{1}H and ^{31}P NMR, of the operating catalytic reaction should yield detailed information as to the nature of the ruthenium-alkoxide complexes as catalytic intermediates. As an example, such a reaction would determine if the complexes are the only species observed throughout the operating catalytic reaction or if they are transients that convert to other "catalytically active" ruthenium complexes.

Overall, this work has resulted in the isolation and complete characterization of the complexes **17** that constitute the second examples of putative ruthenium-BINAP catalytic intermediates that contain a substrate that is bonded to the ruthenium center through the prochiral group of the substrate.[4] Further, **17** are the first diastereomeric ruthenium-ketone intermediates to be fully characterized in catalytic enantioselective hydrogenation of ketones. Finally, this study has yielded the most complete information

into the ruthenium-BINAP catalyzed enantioselective hydrogenation of ketones reported to date.

References and Notes:

(1) (a) Wiles, J. A.; Bergens, S. H. *J. Am. Chem. Soc.* **1997**, *119*, 2940-2941. (b) Wiles, J. A.; Bergens, S. H. *Organometallics* **1998**, *17*, 2228-2240. (c) Wiles, J. A.; Bergens, S. H. *Organometallics* **1999**, *18*, 3709-3714.

(2) Ashby, M. T.; Halpern, J. *J. Am. Chem. Soc.* **1991**, *113*, 589-594.

(3) Brown, J. M.; Rose, M.; Knight, F. I.; Wienland, A. *Recl. Trav. Chim. Pays-Bas* **1995**, *114*, 242-251.

(4) The first characterization of putative ruthenium-BINAP catalytic intermediates that contain a substrate that is bonded to the ruthenium center through the prochiral group of the substrate were also reported by the Bergens group (See references 1a and 1c).

University of Alberta Library
0 1620 1250 6414

B45363